



University of Zagreb

FACULTY OF ELECTRICAL ENGINEERING AND COMPUTING

Josip Ćesić

**MULTIPLE MOVING OBJECTS TRACKING  
BASED ON RANDOM FINITE SETS AND  
LIE GROUPS**

DOCTORAL THESIS

Zagreb, 2017



University of Zagreb

FACULTY OF ELECTRICAL ENGINEERING AND COMPUTING

Josip Ćesić

**MULTIPLE MOVING OBJECTS TRACKING  
BASED ON RANDOM FINITE SETS AND  
LIE GROUPS**

DOCTORAL THESIS

Supervisor: Professor Ivan Petrović, PhD

Zagreb, 2017



Sveučilište u Zagrebu

FAKULTET ELEKTROTEHNIKE I RAČUNARSTVA

Josip Ćesić

**PRAĆENJE VIŠE GIBAJUĆIH OBJEKATA  
ZASNOVANO NA SLUČAJNIM KONAČNIM  
SKUPOVIMA I LIEVIM GRUPAMA**

DOKTORSKI RAD

Mentor: prof. dr. sc. Ivan Petrović

Zagreb, 2017.

Doctoral thesis was written at the University of Zagreb, Faculty of Electrical Engineering and Computing, Departement of Control and Computer Engineering.

Supervisor: Professor Ivan Petrović, PhD

Thesis contains 140 pages

Thesis no.:

Date of doctoral thesis defence: September 29, 2017.





---

## ABOUT THE SUPERVISOR

IVAN PETROVIĆ received B.Sc., M.Sc. and Ph.D. degrees in electrical engineering from the University of Zagreb, Faculty of Electrical Engineering and Computing (FER), Zagreb, Croatia, in 1983, 1989 and 1998, respectively.

For the first ten years after graduation he was with the Institute of Electrical Engineering of Končar Corporation in Zagreb, where he had been working as a research and development engineer for control and automation systems of electrical drives and industrial plants. From 1994 he has been working at the Department of Control and Computer Engineering at FER, where he is currently a Full Professor with tenure. He has actively participated as a collaborator or principal investigator on more than 30 national and 20 international scientific projects, where from them six are funded from FP7 and Horizon 2020 framework programmes. He is also co-director of the Centre of Research Excellence for Data Science and Cooperative Systems. He published more than 50 papers in scientific journals and more than 180 papers in proceedings of international conferences in the area of control engineering and automation applied to control mobile robots and vehicles, power systems, electromechanical systems and other technical systems.

Professor Petrović is a member of IEEE, Croatian Academy of Engineering (HATZ), chair of the Technical committee on Robotics of the International Federation of Automatic Control (IFAC), a permanent board member of the European Conference on Mobile Robots, an executive committee member of the Federation of International Robot-soccer Association (FIRA), and a founding member of the iSpace Laboratory Network. He is also a member of the Croatian Society for Communications, Computing, Electronics, Measurements and Control (KoREMA) and Editor-in-Chief of the *Automatika* journal. He received the award "Professor Vratislav Bedjanić" in Ljubljana for outstanding M.Sc. thesis in 1990 and silver medal "Josip Lončar" from FER for outstanding Ph.D. thesis in 1998. For scientific achievements he received the award "Rikard Podhorsky" from the Croatian Academy of Engineering (2008), "National Science Award of the Republic of Croatia" (2011), the gold plaque "Josip Lončar" (2013) and "Science Award" from FER (2015).

---

## O MENTORU

IVAN PETROVIĆ diplomirao je, magistrirao i doktorirao u polju elektrotehnike na Sveučilištu u Zagrebu Fakultetu elektrotehnike i računarstva (FER), 1983., 1989. odnosno 1998. godine.

Prvih deset godina po završetku studija radio je na poslovima istraživanja i razvoja sustava upravljanja i automatizacije elektromotornih pogona i industrijskih postrojenja u Končar - Institutu za elektrotehniku. Od svibnja 1994. radi u Zavodu za automatiku i računalno inženjerstvo FER-a, gdje je sada redoviti profesor u trajnome zvanju. Sudjelovao je ili sudjeluje kao suradnik ili voditelj na više od 30 domaćih i 20 međunarodnih znanstvenih projekata, od čega šest projekata iz programa FP7 i Obzor 2020. Nadalje, suvoditelj je Znanstvenog centra izvrsnosti za znanost o podacima i kooperativne sustave. Objavio je više od 50 znanstvenih radova u časopisima i više od 180 znanstvenih radova u zbornicima skupova u području automatskog upravljanja i estimacije s primjenom u upravljanju mobilnim robotima i vozilima te energetskim, elektromehaničkim i drugim tehničkim sustavima.

Prof. Petrović član je stručne udruge IEEE, Akademije tehničkih znanosti Hrvatske (HATZ), predsjednik tehničkog odbora za robotiku međunarodne udruge IFAC, stalni član upravnog tijela European Conference of Mobile Robots, član izvršnog odbora međunarodne udruge FIRA, suutemeljitelj međunarodne udruge „The iSpace Laboratory Network”. Član je i upravnog odbora Hrvatskog društva za komunikacije, računarstvo, elektroniku, mjerenja i automatiku (KoREMA) te glavni i odgovorni urednik časopisa *Automatika*. Godine 1990. primio je u Ljubljani nagradu „Prof. dr. Vratislav Bedjanić” za posebno istaknuti magistarski rad, 1998. srebrnu plaketu "Josip Lončar" FER-a za posebno istaknutu doktorsku disertaciju, a za znanstvena je postignuća dobio 2008. godine nagradu „Rikard Podhorsky” Akademije tehničkih znanosti Hrvatske, 2011. godine „Državnu nagradu za znanost”, 2013. godine zlatnu plaketu "Josip Lončar" FER-a te 2015. godine nagradu za znanost FER-a.

---

## ZAHVALA

*You can't connect the dots looking forward;  
you can only connect them looking backwards.  
So you have to trust that the dots will somehow  
connect in your future*

— Steven Paul Jobs

Gledajući unatrag, putovanje kroz istraživanje koje je rezultiralo ovim doktoratom bilo je prepuno neočekivanih puteljaka s mnoštvom točkica koje je trebalo povezati. Veliko hvala mome mentoru Profesoru Ivanu Petroviću što mi je tijekom cijelog tog perioda, nesebično u maniri prijatelja, ukazivao na raspored točkica prije nego što sam sâm to bio u stanju, te što mi je pružio priliku i davao podršku u radu i razvoju u okviru LAMOR grupe.

Hvala cimeru Docentu Ivanu Markoviću na mnogobrojnim plodnim raspravama te na njegovu neposrednom doprinosu radu koji je rezultirao ovom disertacijom.

Docent Mario Bukal pomogao mi je rušiti barijere u bespućima matematičkih formalizama i zamršene matematičke terminologije te mu na tome hvala.

Hvala Profesorici Dani Kulić, voditeljici Adaptive Systems Laboratory grupe sa Sveučilišta u Waterloou, Kanada, na prilici za suradnjom i njenom osobnom doprinosu zajedničkom radu.

Hvala svim prijateljima i kolegama iz LAMOR-a te sa ZARI-a na zajedničkim kavama, ručkovima i raspravama na najrazličitije stručne i nestručne teme tijekom ovih godina. Ne bi bilo fer ovdje ih ne spomenuti poimence; Kruno, Ivan, Mario, Igor, Fule, Juraj, Tamara, Murky, Domagoj, Srećko, Vasko, Marija, Andrej, Goran, Luka, Petky, Borna, Branac, Vinko, Nikola, Tomislav, Marko, Vedran, Haus, Edin, Vrano, Anita, Goca, Đalac, Hrvoje.

Hvala mojim prijateljima Ivanu, Mati, Bruni, Domagoju i Hrvoju što godinama dijele životne radosti samnom.

*Najveće hvala mojoj supruzi, mami, tati i sestri,  
bez čije ljubavi ovo ne bi bilo moguće.*

U Zagrebu, 29. rujna 2017. godine.

---

## ABSTRACT

Autonomous navigation of an agent strongly relies on the capability of tracking multiple moving objects using various on-board sensing technologies. In the thesis we first consider a type of application arising when multiple objects are tracked using a microphone array as a single on-board sensor system. Both objects and measurements state space in this application arise as directional value represented either as a vector belonging to a unit sphere or equivalently as an angle. The thesis presents a method for multiple moving objects tracking on the unit sphere based on the von Mises distribution defined directly on this space of interest, and probability hypothesis density filter based on random finite sets.

The state of objects in the agent's surrounding are typically determined with their position and orientation which evolve on a non-Euclidean geometry. The orientation of such object can be described using a special orthogonal group, while full pose, including translation vector and orientation information, can be given with a special Euclidean group employing either their 2 or 3 dimensional counterparts. The thesis further proposes several methods for estimating motion evolving on the special Euclidean group based on the extended Kalman filter on Lie groups, and accounting for the statistics of concentrated Gaussian distribution. It also describes approaches for performing full body human motion estimation using marker position measurements or inertial measurement units, accounting for the full kinematic chain of the body.

As an alternative to the extended Kalman filter on Lie groups, the thesis proposes the estimation method relying on an information form for states evolving on matrix Lie groups. A trivial example of suitable application is when the number of measurements is larger than the size of the state space, while other examples include any filter constructed such that the information form can be exploited in terms of computational complexity.

As an extension of the multiple moving objects tracking algorithm limited exclusively to the space of a unit circle, the thesis proposes two methods suitable for applications when states evolve on matrix Lie groups. The first one relies on joint integrated probabilistic data association filter modified such that it can operate with variables on matrix Lie groups, while the second one employs the probability hypothesis density filter on matrix Lie groups. In the thesis we propose an approach to reduction of mixture of concentrated Gaussian distributions, which is an essential part of the probability hypothesis density filter.

**KEY WORDS:** multiple moving objects tracking, Lie groups, directional statistics, concentrated Gaussian distribution, extended Kalman filter, extended information filter, random finite sets, probability hypothesis density, joint integrated probabilistic data association

---

## SAŽETAK

### PRAĆENJE VIŠE GIBAJUĆIH OBJEKATA ZASNOVANO NA SLUČAJNIM KONAČNIM SKUPOVIMA I LIEVIM GRUPAMA

Autonomna navigacija predstavlja radikalnu tehnologiju koja će zasigurno izmijeniti ljudsko društvo transformirajući navike i djelovanje ljudi i povećavajući djelotvornost i sigurnost izvršenja različitih vrsta poslova. Ta je tehnologija zasnovana na sposobnostima percepcije i predikcije inherentno nepredvidljivih dinamičkih okruženja, što autonomnom objektu omogućava dijeljenje radnoga prostora s drugim objektima. Tek pošto razumije uzorke ponašanja i karakteristike gibanja objekata oko sebe, autonomni sustav može započeti s autonomnom operacijom. Praćenje više gibajućih objekata u tome smislu predstavlja fundamentalni problem. Naime, autonomni sustav akciju mora izvršiti oslanjajući se na nesavršene senzorske podatke, a razina nesigurnosti tih podataka značajno ovisi o tipu dinamičkog okruženja pa tako u proizvodnim pogonima ona može biti poprilično mala, dok primjerice u prometnom sustavu ili općenito u urbanim okruženjima ona može biti vrlo velika. Vjerojatnosni pristupi u području autonomnih sustava i navigacije mobilnih robota koriste se već dugi niz godina u svrhu percepcije i modeliranja prostora te lokalizacije i upravljanja gibanjem mobilnih robota, ali se sve donedavno tome problemu pristupalo s pretpostavkom da su sve razmatrane varijable takvih sustava Euklidske te da je njihova statistika dobro opisana Gaussovom razdiobom. Istraživanje prikazano u ovoj disertaciji bavi se problemom praćenja više gibajućih objekata u vjerojatnosnom smislu, tako što je gibanje pažljivo modelirano uzimajući u obzir ne-Euklidsku geometriju prostora. Varijable stanja sustava u ovome su radu opisane Lievim grupama koje se često pojavljuju u fizikalnim znanostima i inženjerstvu.

U nastavku je obrazložen naslov disertacije. Problem praćenja više gibajućih objekata važno je razmatrati drugačije od estimacije stanja jednoga objekta. Naime, osim potrebe za vjerojatnosnim pristupom procjeni stanja sustava, u slučaju praćenja više gibajućih objekata potrebno je voditi računa o njihovom promjenjivom broju tijekom vremena. Pretpostavka ovoga rada jest da su podaci prikupljeni sa senzora obrađeni u koraku predprocesiranja, dok algoritam praćenja kao ulazne informacije koristi skup točkastih mjerenja. Elementi skupa mjerenja stoga mogu odgovarati mjerenjima stvarnih ili lažnih objekata, gdje lažni objekti mogu biti uzrokovani ograničenjima senzora ili algoritma predobrade. Dakle, osim procesnog i mjernog šuma, algoritam praćenja više gibajućih objekata mora voditi računa i o pojavama kao što su (i) nesigurnost uzroka mjerenja, (ii) nastajanje i nestajanje objekata,

(iii) lažna mjerenja, (iv) propuštena mjerenja te (v) pridruživanje mjerenja objektima. Naslov disertacije nadalje sadrži pojam slučajnih konačnih skupova koji su privukli značajnu pažnju u području praćenja više gibajućih objekata tijekom posljednjih 15-ak godina. Razlog je taj što su skup stanja objekata i skup mjerenja prirodno opisani kao slučajni konačni skupovi umjesto da je svaki objekt opisan kao nezavisna varijabla.

Sljedeći važan element disertacije razmatra mogućnost opisivanja prostora stanja sustava koristeći ne-Euklidske varijable. Donedavno se u statističkim pristupima u inženjerskim aplikacijama u pravilu zanemarivala potencijalno ne-Euklidska geometrija prostora, dok se u posljednje vrijeme sve više tehnika bavi statističkim pristupima koji omogućavaju da se geometrija prostora uzima u obzir. Na taj je način moguće izbjeći teorijske i implementacijske probleme koji se tipično pojavljuju u primjenama u kojima se prostorna ograničenja ne uzimaju u obzir na odgovarajući način. Najjednostavniji je primjer ne-Euklidskog prostora stanja prostor jedinične kružnice. Primjerice, takav se prostor javlja u primjenama u kojima se koristi polje mikrofona. Kako bi se opisalo stanje sustava u statističkom smislu, moguće je koristiti von Misesovu razdiobu koja je definirana izravno nad prostorom jedinične kružnice te je kao takva u mogućnosti uzeti u obzir globalnu geometriju ovog ne-Euklidskog prostora. Zbog svojih karakteristika ta se razdioba može koristiti u okviru Bayesovog filtra. Međutim, ako se razmatra kompleksnija vrsta prostora stanja, kao što je položaj objekta u 2D ili 3D okruženju, pridruživanje nesigurnosti takvome stanju nije jednostavno provesti. Iz toga se razloga često koristi vektorski zapis stanja te pridruživanje nesigurnosti oblika Gaussove razdiobe. Ipak, umjesto toga moguće je koristiti pridruživanje nesigurnosti stanju prikazanom Lievom grupom. Takav pristup omogućava veću fleksibilnost u opisu nesigurnosti sustava, nego kada se isto opisuje elipsoidalnim Gaussovim komponentama, dok sam zapis u prostoru Lievih grupa pruža veću robusnost algoritama te izbjegava pojavu singulariteta. Nesigurnost je u ovome radu pridružena stanju opisanom Lievim grupama korištenjem koncentrirane Gaussove razdiobe (engl. *concentrated Gaussian distribution* - CGD), gdje je srednja vrijednost  $\mu \in G$  opisana elementom na grupi, a nesigurnost je opisana matricom kovarijanci  $\Sigma$  pridruženoj pomaku u tangencijalnom prostoru grupe. Slučajna varijabla  $X$  koja je na taj način definirana zapisuje se kao  $X \sim \mathcal{G}(\mu, \Sigma)$  te vrijedi

$$X = \mu \exp_G^\wedge(\xi), \text{ i } \xi \sim \mathcal{N}(0, \Sigma),$$

gdje je  $\exp_G^\wedge$  preslikavanje iz tangencijalnog prostora grupe  $g$ , koji se često naziva Lievom algebrom (odgovara Euklidskom prostoru), na Lievu grupu  $G$ .

Von Misesova razdioba uzima u obzir globalnu geometriju prostora, no zbog različitih ograničavajućih elemenata za kompleksnije tipove prostora to nije uvijek moguće. S druge strane, pristupi zasnovani na CGD-u mogu barem lokalno uzeti u obzir geometriju prostora te tako povećati točnost i robusnost algoritama estimacije u kojima se susreće ne-Euklidska geometrija. Primjer primjene analiziran u ovome radu praćenje je većega broja gibajućih objekata čija stanja nisu Euklidske veličine, već su opisana Lievim grupama.

Disertacija je podijeljena u sedam poglavlja. Prvo poglavlje prikazuje uvod u disertaciju. Drugo i treće poglavlje daju opširan pregled pozadine rada. Četvrto poglavlje prikazuje glavne rezultate disertacije. Peto poglavlje donosi zaključak rada i pruža pregled mogućeg budućeg istraživanja. U poglavljima šest i sedam prikazan je popis objavljenih radova koji čine disertaciju te doprinos autora disertacije svakome od njih. Na poslijetku, nakon popisa

bibliografije priloženi su radovi koji prikazuju rezultate disertacije. Disertacija je izrađena po skandinavskom modelu te je sačinjena od po četiri časopisna i konferencijska članka. U nastavku su ukratko prikazani i opisani glavni doprinosi disertacije.

*#1 Metoda praćenja više gibajućih objekata na jediničnoj sferi na temelju mjerenja smjera zasnovana na von Misesovoj razdiobi i slučajnim konačnim skupovima.*

Većina algoritama praćenja više gibajućih objekata zasniva se na Bayesovom filtru, a s obzirom na potrebu korištenja ne-Euklidskog stanja sustava, evaluacija Bayesove rekurzije može biti vrlo zahtjevna. U prvom je redu izazovno riješiti Chapman-Kolmogorovu jednadžbu Bayesove predikcije (konvolucijski integral) u zatvorenoj formi tako da rezultirajuća razdioba ima isti oblik razdiobe kao i početna. Nadalje je potrebno integrirati informaciju o mjerenju evaluirajući Bayesovo pravilo i zadržavajući se u prostoru iste razdiobe. Von Misesova razdioba je primjer u kojemu konvolucijski integral ne rezultira egzaktno novom von Misesovom komponentom, ali rezultirajuća razdioba može biti dobro opisana von Misesovom razdiobom. S druge strane, korekcija rezultira izravno von Misesovom razdiobom bez aproksimacija.

Disertacija se bavi problemom praćenja više gibajućih objekata na prostoru jedinične kružnice primjenom filtra vjerojatnosti gustoće hipoteza koji predstavlja aproksimaciju optimalnog Bayesova filtra definiranog korištenjem teorije slučajnih konačnih skupova. U radu [Pub1] prikazan je izvod rekurzivnog filtra vjerojatnosti gustoće hipoteza korištenjem mješavine von Misesovih razdioba te je uspoređen s filtrom vjerojatnosti gustoće hipoteza zasnovanom na Gaussovoj razdiobi na simuliranom i stvarnom skupu podataka. Filtar zasnovan na von Misesovoj razdiobi ostvario je smanjenje pogreške od 10, 5%, odnosno 2, 8% s obzirom na mjeru optimalnog pridruživanja uzoraka.

*#2 Metoda praćenja objekta u prostoru specijalne euklidske grupe zasnovana na proširenom Kalmanovu filtru na Lievim grupama.*

Lieove su grupe prirodan prostor stanja za opis položaja i gibanja krutoga tijela. Položaj krutoga tijela, što uključuje njegovu poziciju i orijentaciju, može se opisati korištenjem specijalne Euklidske grupe  $SE(2)$  ili  $SE(3)$ , ovisno o tome radi li se o 2D ili 3D prostoru. Istraživanja o razdiobama koje mogu opisati nesigurnosti izravno na specijalnoj Euklidskoj grupi vrlo su intenzivna, međutim do sada nije pronađen način na koji se to može činiti, a da se pritom zadrže neka od svojstava razdiobe korisna za integraciju u Bayesov filter. Iz toga je razloga pristup estimaciji ovdje zasnovan na lokalnom pristupu korištenjem CGD-a čiji se parametri djelomično oslanjaju na oba prostora – srednja je vrijednost definirana na Lieovoj grupi, dok je kovarijanca pridružena tangencijalnom prostoru, tj. Lieovoj algebri.

Provedena istraživanja u okviru disertacije započela su razmatranjem specijalne ortogonalne grupe  $SO(2)$  uz korištenje modela konstantne akceleracije u okviru proširenog Kalmanova filtra na Lievim grupama (engl. *extended Kalman filter on Lie groups* - LG-EKF) u svrhu praćenja govornika poljem mikrofona [Pub2]. Zaključeno je da zbog komutativnosti grupe  $SO(2)$  njezina primjena rezultira istim odzivom kao i u slučaju korištenja pretpostavke Euklidskog prostora uz prošireni Kalmanov filter (engl. *extended Kalman filter*



- EKF) s dodanom heuristikom za zatvaranje prostora u točkama  $-\pi$  i  $\pi$ . Nadalje, razmatrano je korištenje specijalne Euklidske grupe  $SE(2)$  uz pretpostavku svesmjernog gibanja, korištenjem modela konstantne brzine u okviru LG-EKF-a [Pub3]. Tim je pristupom moguće inherentno uzeti u obzir spregnutost rotacije i translacije sadržane u stanju opisanom grupom  $SE(2)$ . Osim toga, pridruživanje nesigurnosti grupi  $SE(2)$  pruža veću fleksibilnost, nego što je to slučaj s izravnim pridruživanjem vektorskom zapisu. Tako, primjerice, osim elipsoidalnih krivulja nesigurnosti ovakav opis omogućuje ostvarivanje kontura oblika banane. U radu je uspoređen predloženi filter s nekoliko standardnih filterskih pristupa iz čega je vidljivo da filter zasnovan na LG-EKF-u postiže veću točnost za slučaj svesmjernog gibanja približno konstantne brzine. Konačno, u okviru rada razvijen je filter za estimaciju stanja zglobova cijeloga čovjekova tijela zasnovan na LG-EKF-u koristeći grupe  $SO(2)$ ,  $SO(3)$  i  $SE(3)$ , a koji se oslanja na mjerenja pozicija markera [Pub4] i inercijalnih mjernih jedinica [Pub5]. Za oba su slučaja izvedene jednadžbe rekurzije LG-EKF-a. Izvod jednadžbi za osvježavanje stanja zglobova na temelju mjerenja akcelerometra prikazan je u prilogu [\*Pub5]. Usporedba performansi predloženoga algoritma s pristupom zasnovanim na Eulerovim kutovima i EKF-u provedena je nad simuliranim i stvarnim podacima te se pokazalo da predloženi algoritam ostvaruje manju pogrešku.

### #3 *Prošireni informacijski Kalmanov filter za estimaciju stanja na matričnim Lievim grupama.*

Informacijski je filter dualni filter klasičnom Kalmanovu filtru. On se oslanja na isti skup pretpostavki kao i Kalmanov filter, ali koristi drukčiju parametrizaciju. Informacijski filter umjesto srednje vrijednosti i kovarijance koristi informacijsku matricu i informacijski vektor. Najvažnija je prednost informacijskog filtra manja računska složenost u slučajevima kada je broj mjerenja velik ili općenito kada struktura estimacijskog problema može biti dobro iskorištena u takvoj alternativnoj parametrizaciji. Istodobna lokalizacija mobilnog robota i kartiranje nepoznatog prostora (engl. *simultaneous localization and mapping* - SLAM) primjer je primjene u kojoj informacijski oblik filtra može biti dobro iskorišten. Nadalje, SLAM je također primjer primjene gdje je važno uzeti u obzir geometriju prostora u svrhu povećanja točnosti izvođenja algoritama. Rješenja SLAM-a donedavno su bila gotovo isključivo zasnovana na filterskim pristupima, točnije proširenom informacijskome filtru (engl. *extended information filter* - EIF). Najvažnije inačice filtera za korištenje u SLAM-u su prošireni informacijski filter s rijetkom strukturom (engl. *sparse extended information filter* - SEIF) te egzaktno rijedak filter s odgođenim stanjem (engl. *exactly sparse delayed state filter* - ESDSF).

Položaj mobilnog robota u SLAM-u najčešće je opisan elementom  $SE(3)$  pa je stoga u novijim pristupima čest slučaj da algoritmi pokušavaju uzeti u obzir geometriju prostora. Ipak, ti su pristupi zasnovani su na optimizacijskim metodama budući da donedavno nisu postojali filterski pristupi koji bi mogli uzeti u obzir geometriju prostora stanja. Kao treći doprinos ovoga rada predložen je prošireni informacijski filter na Lievim grupama (engl. *extended information filter on Lie groups* - LG-EIF) [Pub6]. U radu je prikazana teorijska podloga LG-EIF rekurzije i primjena predloženog filtra za praćenje orijentacije krutoga tijela korištenjem velikog broja senzora. Provedena je i usporedba s EIF-om zasnovanim na

Eulerovim kutovima te je analizirana računska složenost s obzirom na osvježavanje stanja filtra korištenjem velikog broja senzora. Rezultati prikazuju da predloženi filter postiže bolju konzistentnost performansi i manju pogrešku estimacije te da istovremeno zadržava manju računsku složenost informacijskog oblika u slučaju većeg broja mjerenja.

#### #4 *Metoda praćenja više gibajućih objekata na Lievim grupama zasnovana na koncentriranoj Gaussovoj razdiobi i slučajnim konačnim skupovima.*

Potreba za zapisom sustava korištenjem ne-Euklidskog prostora stanja uz praćenje gibajućih objekata javlja se u (i) različitim tradicionalnim inženjerskim disciplinama (sigurnost i nadzor, kontrola zračnog prometa, praćenje svemirskih objekata i sl.) te u (ii) modernim inženjerskim poljima (autonomni sustavi i robotika). Ne-Euklidski prostor stanja javlja se uvijek kada je stanje objekta predstavljeno položajem u kojemu je uključena i informacija o orijentaciji kao ne-Euklidskoj veličini oslanjajući se primjerice na grupu  $SE(2)$  ili  $SE(3)$ .

Prvi dio doprinosa koji je predložen u ovome radu zasnovan je na filtru združenog integriranog vjerojatnosnog pridruživanja podataka (engl. *joint integrated probabilistic data association* - JIPDA) na matičnim Lievim grupama koji predstavlja specijalan slučaj algoritma zasnovanog na slučajnim konačnim skupovima [Pub7]. Vjerojatnost svakog mogućeg događaja ne evaluira se izravno u prostoru Lieve grupe  $G$ , već u prostoru Lieve algebre  $g$  pridružene propagiranom stanju razmatranoga objekta. Predloženi je pristup testiran korištenjem stvarnoga podatkovnog skupa prikupljenog u urbanom prometnom okruženju s višesenzorskim sustavom stereo kamere i dvaju radara. Nesigurnosti senzora modelirane su na Lievim grupama dok je stanje sustava prikazano grupom  $SE(2)$ .

Drugi je dio doprinosa novi aproksimacijski filter vjerojatnosti gustoće hipoteza za praćenje više gibajućih objekata na Lievim grupama (LG-PHD). Taj je filter zasnovan na statističkom modelu CGD-a te kao i svaki filter vjerojatnosti gustoće hipoteza ima karakteristiku da mu se eksponencijalno povećava broj komponentata kroz vrijeme. Broj komponentata stoga se mora kontrolirati korištenjem metoda smanjenja mješavine komponentata. U okviru disertacije predložen je pristup smanjenju broja komponentata u mješavini CGD-ova [Pub8]. U radu su analizirane mogućnosti odgovarajuće reparametrizacije komponentata CGD-a koja omogućuje evaluaciju Kullback-Leiblerove udaljenosti te strategiju odabira i spajanja komponentata. Budući da reparametrizacija dviju komponentata uključuje izbor tangencijalnog prostora za reparametrizaciju, u radu je detaljnije analiziran upravo taj korak smanjenja broja komponentata. Detaljan izvod LG-PHD-a prikazan je u dodatnom materijalu [\*Pub8].

**KLJUČNE RIJEČI:** praćenje više gibajućih objekata, Lieve grupe, usmjerena statistika, koncentrirana Gaussova razdioba, prošireni Kalmanov filter, prošireni informacijski filter, slučajni konačni skupovi, filter gustoće vjerojatnosti hipoteza, združeno integrirano vjerojatnosno pridruživanje podataka

---

## CONTENTS

1	INTRODUCTION	1
1.1	Motivation and problem statement	1
1.1.1	Multiple moving objects tracking	1
1.1.2	Motion modelling on Lie groups	2
1.2	Original contributions	4
1.3	Outline of the thesis	5
2	PROBABILISTIC STATE ESTIMATION ON MANIFOLDS	6
2.1	Introduction	6
2.1.1	Probabilistic state estimation	6
2.1.2	Estimation on manifolds	7
2.1.3	Application significance	9
2.1.4	Organization of the chapter	12
2.2	Bayesian filtering	13
2.2.1	Model of the system	13
2.2.2	Statistical inference	13
2.2.3	Validation gate	14
2.3	Traditional probabilistic state estimation	14
2.3.1	Extended Kalman filter	14
2.3.2	Extended Information filter	15
2.4	Directional estimation	16
2.4.1	Von Mises distribution	16
2.5	Estimation on Lie groups	16
2.5.1	Mathematical preliminaries	16
2.5.2	Concentrated Gaussian distribution	18
2.5.3	Extended Kalman filter on Lie groups	18
3	MOVING OBJECTS TRACKING BASED ON RANDOM FINITE SETS	20
3.1	Introduction	20
3.1.1	Overview of traditional methods	21
3.1.2	Overview of RFS-based methods	23
3.1.3	Organization of the chapter	25
3.2	Random finite sets based multi-object Bayes filter	25
3.3	Probability Hypothesis Density Filter	25

3.3.1	Gaussian Mixture PHD filter	27
3.4	Mixture component reduction	28
3.4.1	Component distance measure	29
3.4.2	Symmetrized Kullback-Leibler divergence	30
3.4.3	Component picking strategy	30
3.4.4	Component merging equations	31
3.5	Metrics for evaluation	31
3.5.1	Metric definition	33
3.5.2	Optimal subpattern assignment	33
4	THE MAIN SCIENTIFIC CONTRIBUTIONS OF THE THESIS	35
5	CONCLUSIONS AND FUTURE WORK	39
5.1	The main conclusions of the thesis	39
5.2	Further research directions	41
6	LIST OF PUBLICATIONS	42
7	AUTHOR'S CONTRIBUTION TO PUBLICATIONS	43
	BIBLIOGRAPHY	46
	PUBLICATIONS	62
	Publication 1 - Von Mises Mixture PHD Filter	62
	Publication 2 - On wrapping the Kalman filter and estimating with the SO(2) group	68
	Publication 3 - Moving object tracking employing rigid body motion on matrix Lie groups	75
	Publication 4 - Full Body Human Motion Estimation on Lie Groups Using 3D Marker Position Measurements	83
	Publication 5 - Human motion estimation on Lie groups using IMU measurements	92
	Publication 5 - Supplementary material	101
	Publication 6 - Extended information filter on matrix Lie groups	104
	Publication 7 - Radar and stereo vision fusion for multitarget tracking on the special Euclidean group	114
	Publication 8 - Mixture Reduction on Matrix Lie Groups	126
	Publication 8 - Supplementary material	132
	CURRICULUM VITAE	137
	ŽIVOTOPIS	140

## Introduction

**A**UTONOMOUS navigation relies on the ability to perceive and anticipate inherently unpredictable dynamic environments based on imperfect sensor data. The degree of uncertainty significantly varies in different environments, and while in assembly lines it may appear small, environments such as traffic systems or urban areas emerge being highly unpredictable. The probabilistic approaches in the field of autonomous systems and mobile robotics have already paid tribute to the uncertainty in perception and action [1], but until recently they used to rely on the assumption that the considered variables are Euclidean and the statistics of uncertainty is well described using Gaussian distribution. The research conducted in this thesis deals with the task of multiple moving objects tracking performed in a probabilistic manner, while the motion modeling is carefully performed relying on non-Euclidean state description. In particular, the system variables are described by Lie groups, which is a type of manifold often encountered in physical sciences and engineering.

### 1.1 MOTIVATION AND PROBLEM STATEMENT

#### 1.1.1 *Multiple moving objects tracking*

Multiple objects tracking (MOT) is an essential problem in the field of autonomous systems and mobile robotics. In any environment, where an autonomous system operates sharing its workspace with humans or other subjects, it has to be able to perceive the environment, recognize obstacles including static and moving objects, and anticipate their future behavior. Finally, only when understanding the characteristics and motion patterns of objects in the surrounding, and after being able to predict the future progress of those objects, an autonomous system can continue reasoning about safe continuation of operation. An illustration of an autonomous system operating in a dynamic environment is shown in Fig. 1.1.

Let us continue now by decomposing the title of the thesis. The problem of *multiple objects tracking* needs to be considered as opposed to the problem of a single object state estimation. After set into a probabilistic framework, estimation of a state of a single object deals with the problem of determining the best guess about the true object state following the process and measurement models which are respectively affected by the process and measurement noise. Determining the best guess about the true object state is as well the main goal of a MOT application, while it aims at accurately determining the state of multiple objects concurrently, being aware that the number of objects varies in time due to appearing

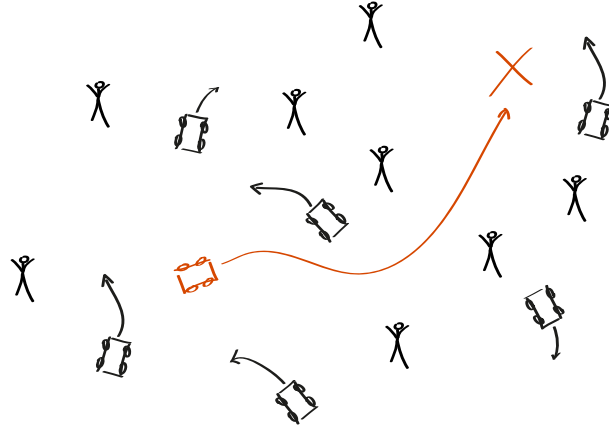


Figure 1.1: An illustration of an autonomous system operating in a dynamic environment populated with other moving objects.

and disappearing of objects. Furthermore, when referred to a standard MOT setting, it is typically assumed that the set of measurements at each instance is preprocessed into a set of points or detections. Some of the set members correspond to true objects, while some appear as false alarms due to a limited sensor system used for data acquisition and/or an imperfect preprocessing algorithm. To summarize, apart from process and measurement models uncertainty, typical for general probabilistic estimation applications, in MOT applications one has to contend with much more complex sources of uncertainty, such as (i) the measurement origin uncertainty, (ii) births and deaths of objects, (iii) false alarm, (iv) missed detections, and (v) data association [2].

Next, the title continues by denoting that the underlying MOT approach is *based on random finite sets* (RFS). This concept gained a great deal of attention in the tracking community during the last 15 years [3] since it arises naturally from the reasoning that the set of objects and set of measurements are described as random sets, rather than multiple independent random variables. The RFS paradigm in MOT applications is developed upon the theory of finite-set statistics (FISST) [4], and formal extension of conventional Bayesian state estimation algorithms to general multiple objects–multiple sensors tracking.

### 1.1.2 Motion modelling on Lie groups

The field of probabilistic estimation has experienced a rapid upturn in the early 1960s with the development of a Kalman filter (KF) [5]. Since the KF is originally designed for linear Gaussian systems, during the next several decades research community mostly focused on dealing with different types of non-linearities in the motion and measurement models, while the variables were mostly assumed to be Euclidean. However, in the last few years, the formalism exploiting the non-Euclidean (manifold) geometry of the state space was extensively employed in a wide range of applications, due to theoretical and implementation difficulties that may show up by treating a constrained problem naively employing classical Euclidean space tools [6].

Probably the most trivial example of a non-Euclidean manifold is the unit circle. The subject matter of the statistics considered when the observations arise on the sample space

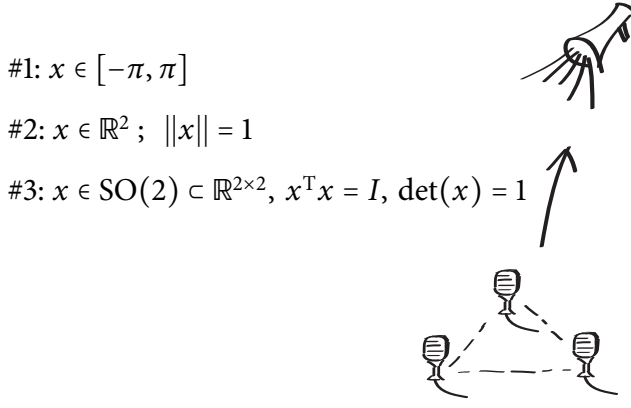


Figure 1.2: An illustration of the sound source tracking using microphone array and the list of several possible representations of the space of unit circle.

of a circle is usually referred to as directional statistics [7]. An example where such problem appears is the tracking by employing a microphone array. This is illustrated in Fig. 1.2, where several different ways of representing the state of a circular variable are also provided. In order to describe the state of such directional variable one can employ the von Mises distribution (vM) which is defined directly on the unit circle [8], and captures the global geometry of this space. Due to some useful properties, this distribution is applicable for manipulation within a Bayesian probabilistic framework.

Lets further consider two more complex examples involving typical robotic platforms, respectively operating in 2D and 3D environments. We firstly consider the example of a mobile platform operating in 2D, where the associated state space can be considered using the traditional position-orientation vector  $x = [t_x \ t_y \ \theta]^T$  and the Gaussian uncertainty associated to it. Unfortunately, it has been observed that already a simple differential drive mobile robot exhibits more complex shape of uncertainty contours than the flexibility of standard elliptical Gaussians supports. Alternatively, it is possible to exhibit more flexible uncertainty contours by associating uncertainty to the state described by the special Euclidean group  $X \in \text{SE}(2)$ . In particular, the uncertainty can be associated to this state through the pertaining tangent space with 3 degrees-of-freedom (dof), thus gaining more flexibility and possibly boosting the performance of estimation algorithms [9].

Secondly, we consider the example of an areal vehicle operating in 3D, where traditionally the state space is considered using the position-orientation vector  $x = [t_x \ t_y \ t_z \ \phi \ \psi \ \theta]^T$  and the Gaussian uncertainty associated to it. In this case, the pose and its associated uncertainty can be alternatively described using the special Euclidean group  $X \in \text{SE}(3)$  which is, in contrast to the Euler-angle based representation, free of singularities and avoids the need to enforce constraints when solving optimal estimation problems [10]. The uncertainty can be considered in the pertaining tangent space and stored using the zero-mean 6 dof perturbation vector with an associated covariance matrix. This approach to uncertainty association is called the concentrated Gaussian distribution (CGD), and can be applied for any member of a matrix Lie group. We emphasize that both  $\text{SE}(2)$  and  $\text{SE}(3)$  groups belong to the family of matrix Lie groups.

A random variable  $X$  has a CGD of mean  $\mu \in G$  and covariance matrix  $\Sigma$ , written

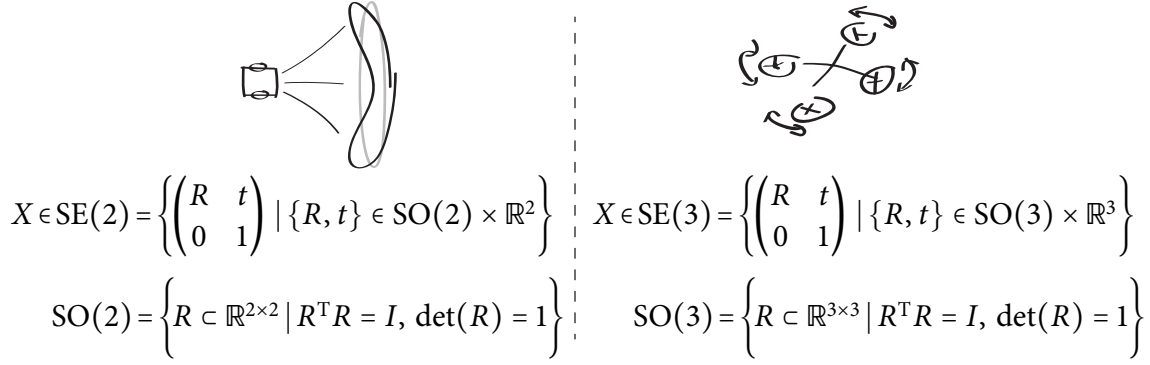


Figure 1.3: Lie group representation of the state of a differential drive mobile robot considered in 2D ( $X \in \text{SE}(2)$ ), left, with accompanied uncertainty contours illustrated in grey for Gaussian and black for CGD) and an aerial vehicle considered in 3D ( $X \in \text{SE}(3)$ ), right).

$X \sim \mathcal{G}(\mu, \Sigma)$ , if

$$X = \mu \exp_G^\wedge(\xi) \quad \text{and} \quad \xi \sim \mathcal{N}(0, \Sigma) \quad (1.1)$$

where  $\exp_G^\wedge$  performs mapping from the Euclidean space (tangent space of the Lie group referred to as Lie algebra) to Lie group  $G$ . Other important examples of Lie groups of interest are special orthogonal group  $\text{SO}(2)$  and  $\text{SO}(3)$ , special unitary group  $\text{SU}(2)$ , invertible matrices, homographies, similarity transformations, etc [11]. The two previously discussed examples involving differential drive mobile robot and an aerial vehicle are illustrated in Fig. 1.3.

The vM captures the geometry of the unit circle in a global manner, but due to various limiting factors such global approach may not be possible for an arbitrary manifold. On the other hand, the approaches relying on CGD can at least locally account for the state space geometry and thus boost the performance of estimation algorithms regarding both ease and stability of implementation and the overall accuracy. This thesis questions if the world in the surrounding of an autonomous system can be assumed to be Euclidean, and develops approaches for dealing with eventually non-Euclidean nature of state space for various types of objects, but also different measurements which arise on non-Euclidean manifolds including microphone arrays, radar units or camera systems.

## 1.2 ORIGINAL CONTRIBUTIONS

Four original contributions of the thesis essentially revolve about probabilistic estimation methods suitable for operating on variables arising on Lie groups rather than the Euclidean space. The scientific contributions of this thesis resulting from the performed research are:

- #1 Method for multiple moving objects tracking on the unit sphere based on the von Mises distribution and the random finite sets.
- #2 Method for moving object tracking in the space of the special Euclidean group based on the extended Kalman filter on Lie groups.
- #3 Extended information Kalman filter for state estimation on matrix Lie groups.



- #4 Method for multiple moving objects tracking on Lie Groups based on the concentrated Gaussian distribution and the random finite sets.

A more detailed discussion on the scientific contributions of the thesis is given in Sec. 4.

### 1.3 OUTLINE OF THE THESIS

The thesis is organized into seven chapters. Among them, two chapters particularly provide the background material of the thesis. After discussing the main results of the thesis and providing some concluding remarks, contributing publications are included in the thesis. Hereafter, we present the outline of the thesis with a short summary of the contents.

- Ch 2 This chapter presents the general mathematical background and sets up the context of the problem of probabilistic estimation on manifolds. The introductory part of the chapter reveals the problematic of (i) computational potential of filtering methods in forms of Kalman and information filters, and (ii) discusses the potential of global vs. local approaches to accounting for the non-Euclidean geometry of considered variables. Afterwards, some basic background material including the Bayesian recursion, extended Kalman and extended information filter is provided. Finally, the basics on global circular statistics and local approach to estimation on Lie groups is presented.
- Ch 3 This chapter comprises the methods for multiple moving objects tracking, by providing an extensive overview of both traditional and widely accepted methods, as well as recent approaches. Afterwards, it provides some underlying ideas of the probabilistic hypothesis density (PHD) filter and provides an approximation of this filter for nonlinear systems based on the Gaussian mixture and the extended Kalman filter. Since manipulation with mixtures of distributions represents an essential task in many multiple objects tracking applications, here we provide a brief recapitulation of techniques for component number reduction. Finally, we describe the optimal subpattern assignment (OSPA) metric for evaluation of the multiple objects tracking algorithms.
- Ch 4 A description of the main scientific contributions of the thesis is given here.
- Ch 5 This chapter brings the conclusions of the thesis and presents some ideas for future work from the viewpoint of open theoretical questions, application perspective and evaluation challenges.
- Ch 6 Here we include the list of publications contributing the main results of the thesis.
- Ch 7 This chapter gives a statement on the author's contribution to each of the included publications.

After the seven chapters follows the list of referenced bibliography. Finally, the publications giving the main results of the thesis which were previously published in peer-reviewed journals or in proceedings of international scientific conferences are included.

## Probabilistic state estimation on manifolds

PROBABILISTIC state estimation has been widely accepted approach in a variety of engineering problems and scenarios in both traditional application domains including tracking and surveillance, aerospace engineering, telecommunications and medicine, as well as in some modern fields such as computer vision, speech recognition and many others. Probabilistic approaches pay tribute to the uncertainty in perception, by relying on a key idea of representing the uncertainty in an explicit manner using the calculus of probability theory [1]. A long history of research in this field experienced appearance of many different estimation methods, designed for different use-cases depending on the (i) (non)linearity of system model, (ii) the characteristics of underlying statistics as well as (iii) the state space geometry of the variables of an estimation interest that are possibly non-Euclidean.

### 2.1 INTRODUCTION

#### 2.1.1 Probabilistic state estimation

The nature of applications of our interest cover such cases where the full or partial observations of the system occur sequentially at time instants  $k \in \mathbb{N}$ , while in the meantime the system is assumed to follow some motion model. Hence we aim to consider estimation approaches which recursively apply (i) the prediction/propagation step relying on the assumed motion/propagation model and (ii) the correction/update step employing measurements once they become available. In this thesis, the processes will follow either continuous or discrete motion models, while the update will usually be given with measurements at some discrete time instant. The background idea of the overall random variable estimation of our interest is called Bayesian since its implementation is grounded in the Bayes theorem [12]. This enables us to build-in some (i) prior knowledge on the value of the considered random variable, (ii) the uncertain motion model which the variable is expected to follow, and (iii) the uncertain measurement model which the sensor is expected to follow.

▷ KALMAN FILTERING. Probably the most important application of the Bayesian recursion is the Kalman filter (KF), and majority of Bayesian approaches used nowadays are somehow built upon the similar assumptions used in the KF's original derivation. In particular, the KF was presented in seminal works of Kalman [5], and Kalman and Bucy [13], originally developed for linear systems described with Gaussian statistics and evolving on Euclidean space. Although it was originally derived for a linear problem, the Kalman filter is

habitually applied with impunity and considerable success to many nonlinear problems [14]. These extensions are introduced in [15] and are generally called the extended Kalman filter (EKF). Over time, many other methods designed following the basic concepts of KF have also appeared. Some prominent examples are iterative extended Kalman filter (IEKF) [16], unscented Kalman filter (UKF) [17, 18, 19], cubature Kalman filter (CKF) [20, 21], quadrature Kalman filter (QKF) [22, 23], and many others. Also, if the underlying distribution is not Gaussian and if it is possibly multimodal then different approaches relying on particle [24] and mixture filters [25, 26] need to be utilized. However, since the thesis focuses on unimodal EKF-like approaches, we do not provide the exhaustive overview of other filtering methods.

▷ **INFORMATION FILTERING.** From the viewpoint of processing complexity, another important aspect of Bayesian filtering is the information filter (IF), which is the dual of the KF. It is as well relying on the state representation by a Gaussian distribution [27] and is the subject of the same assumptions underlying the KF. While the KF is represented by the first two moments, i.e., mean and covariance, the IF relies on the canonical parametrization consisting of an information matrix and information vector [28]. As well as KF, IF operates cyclically in two steps: the prediction and update step. The main characteristics which make significant difference between the two parameterizations lie in the complexity of the prediction and update steps. The advantage of the IF lies in the update step when the number of measurements is larger than the size of the state space, since in this case the update step is additive. In contrast, when the opposite applies, the prediction step is additive and computationally less complex for the KF. Hence, what is computationally complex in one parameterization turns out to be simple in the other (and vice-versa) [1]. The most common extension of the linear IF to non-linear systems is following similar linearization approach as in the vein of EKF. The resulting filter is called the extended information filter (EIF) [27]. Respecting different applications and different types of non-linearity, various strategies have been developed within the information form framework over time. This includes sigma-point information filter [29], square-root information filter [30, 31, 32], unscented information filter (UIF) [33], sparse extended information filter (SEIF) [34], exactly sparse delayed-state filter (ESDSF) [35], etc.

### 2.1.2 Estimation on manifolds

Apart from the non-linearity of the motion and measurement models, for the overall estimation performance it is important to account for the state space geometry and the association of uncertainty when the underlying space is not Euclidean. This is motivated by theoretical and implementation difficulties caused by treating a constrained problem naively with Euclidean tools. Hence recently, many works have been dedicated to associating uncertainty to, and estimating the state of, non-Euclidean systems.

▷ **ESTIMATION OF CIRCULAR VARIABLES.** Working with directional data, especially under uncertainty, imposes a problem on how to represent them in a probabilistic framework. This subject matter is usually referred to as directional statistics [7], since it mainly

studies the observations which are unit vectors either in the plane where the sample space will be a circle, or in the three dimensional space where the sample space will be a sphere. The robotics community has already recognized the benefits of the directional distributions applied for modeling directional data. Although the approaches which rely on wrapped distributions were still recently successfully used in different applications [36, 37], the desire for globally capturing the entire geometry of the state space influenced more intensive employment of directional distributions. Some early applications of the  $\nu\text{M}$  distribution defined on the unit circle [8] were presented in [38] where it was used for odometry evaluation in order to deal with the heading changes for topological model learning. Later, in [39] authors proposed a solution for solving large-scale partially observable Markov decision processes applying the same distribution. In [40, 41, 42, 43], the same distribution was used in the context of a single speaker localization and tracking in order to model the state and the microphone array measurements as a  $\nu\text{M}$  mixture and evaluated in the context of Bayesian estimation framework. This distribution has also been successfully applied for people trajectory shape analysis [44], radar processing [45], and a multitarget tracking application [46].

The von Mises-Fisher distribution [47] is defined on a unit hypersphere, and hence  $\nu\text{M}$  is also sometimes considered only as its special case. It was already utilized in applications like single target tracking [48], as well as in multitarget tracking applications [49]. Another distribution which can be considered as directional is a Bingham distribution used for describing the inference directly on the space of quaternions. It actually models variables with  $180^\circ$  symmetry, and was used in [50, 51, 52] and in [53] where, furthermore, a second-order filter was derived which included also the rotational velocity. These approaches, advocating the unit hypersphere as the appropriate filtering space, showed better performance of the Bingham filter and the underlying global estimation approach with respect to the EKF.

From the engineering perspective, distributions defined directly over the entire space of interest seem to be attractive since they are able to globally capture the state space geometry, but unfortunately their practical applicability is often very limited. An important question arises regarding the possibility of evaluating the pdf normalization constants in closed form. This issue makes the Bayes prediction and correction hard to evaluate in the closed form as well. However, the  $\nu\text{M}$  distribution contains some properties that could be easily exploited within the Bayesian framework, which make it applicable for practical use. In this thesis we analyze the directional multitarget application for 2D case, relying on the  $\nu\text{M}$  distribution, which is hence more formally introduced in Sec. 2.4.1.

▷ **ESTIMATION ON LIE GROUPS.** Some of the most prominent examples of the non-Euclidean geometries are the orientation and the pose of a rigid body mechanical systems. Lie groups are natural ambient (state) spaces for description of such systems. The orientation of a rigid body is often described using special orthogonal groups  $\text{SO}(2)$  or  $\text{SO}(3)$  as 2- and 3-dimensional counterparts. The pose is often represented with special Euclidean groups  $\text{SE}(2)$  or  $\text{SE}(3)$ , where again they represent 2- and 3-dimensional counterparts [54, 55]. Respecting the field of robotics, the SE groups have been used from the very early days, while associating the uncertainty came into focus later [56]. The most often used concept for associating the uncertainty to Lie groups is the concept of CGD, which assumes that the

eigenvalues of covariance are small, hence almost all the mass of distribution is contained around the mean value [57, 58].

From the application perspective, an early example of error propagation on the  $SE(3)$  group with applications to manipulator kinematics was presented in [59]. Therein the authors developed a closed-form solution for the convolution of the CGDs on  $SE(3)$ . In [57] the authors proposed a solution to Bayesian fusion on Lie groups by assuming conditional independence of observations on the group, thus setting the fusion result as a product of CGDs, and finding the single CGD parameters which are closest to the beginning product. One of the first significant works which combines both, uncertainty propagation and fusion on the group, was presented in [10], where authors exclusively deal with the  $SE(3)$  group. A more general approach proposed for dealing with any matrix Lie groups in the vein of the ‘classical’ EKF was proposed in [60]. Therein authors derived a nonlinear continuous-discrete extended Kalman filter on Lie groups (LG-EKF), meaning that the prediction step is presented in the continuous domain, while the update step is discrete. In an earlier publication [61], the authors presented a discrete version of the LG-EKF. Another approach to a nonlinear KF on manifolds was presented in [62]. It is designed to operate on a wider range of manifolds than LG-EKF, and is following the ideas of the unscented transform and the UKF itself.

Some works have also addressed the uncertainty on the  $SE(2)$  group proposing new distributions [52, 63], but these approaches still do not provide a closed-form Bayesian recursion framework for both the prediction and update that can include non-linear models. Additionally, in [64] authors use Gaussian process kernels for estimating the 6 dof motion of an UAV, while in [65] authors study the appearance of multi-modal pdfs on  $SO$  and  $SE$  groups and propose an approach relying on mixtures of projected Gaussians.

Another important group is a 3D similarity transform  $Sim(3)$  which represents an extension of  $SE(3)$ , but includes an additional parameter referred as scaling factor. Such group may be appropriately employed in mono-vision SLAM tasks when the scale is not known [66]. The quaternions have also been previously mentioned in the context of circular variables, and it was also noted that the Bingham distribution can globally capture the nature of this space. However, quaternions are also members of Lie groups and can be represented in matrix form as they are isomorphic to the special unitary group  $SU(2)$  [11]. Alongside circular variables and Lie groups which are in the focus of the thesis, there also exist a variety of manifolds significant for the engineering community, and alongside this idea several approaches for filtering on such manifolds were developed. This includes Grassmann manifolds [67, 68], Riemannian Manifolds [69, 70], Stiefel manifolds [71], and other specific types of manifolds [72, 73].

### 2.1.3 Application significance

▷ POSE ESTIMATION. Pose and ego-motion estimation represent some of the most prominent examples of employment of manifold approaches. In [74] authors studied the problem of registering local relative pose estimates to produce a global consistent trajectory of a moving robot relying on probabilistic uncertainties associated to Lie groups. Authors in [9] specifically study the uncertainty of a motion of a two-wheeled robot and discuss the significance of associating the uncertainty to variables on the groups, rather than the

Euclidean space. In [75] authors study error growth in position estimation from noisy relative pose measurements by carefully accounting for the geometry of the  $SE(2)$  and  $SE(3)$  groups. In [62] authors demonstrate the filter on a synthetic dataset addressing the problem of trajectory estimation by posing the system state to reside on the manifold combining Euclidean space with an  $SO(3)$  group, while in the end they also demonstrate their approach on SLAM application relying on graph optimization.

In [76] authors perform fusion of optical flow and inertial measurements for robust egomotion estimation modifying the UKF by following the similar approach as was proposed by [62], and applying it for a legged robot application. The same application was developed in [77], and the same estimation approach was used, although different sensor setup was employed. Alongside the estimation algorithm, in [77] the authors proposed a careful observability analysis by employing the concept of Lie derivatives [78]. In [79] authors use only IMU and contact information for estimating the state of the leg of a humanoid robot and use quaternion representation and an EKF implementation. In [60], the authors have demonstrated the efficiency of the filter on a synthetic camera pose filtering problem by forming the system state to reside on the direct product of an  $SO(3)$  group with a Euclidean space vector representing sequentially camera orientation, object position, angular and radial velocities. A problem of an estimation of a complex kinematic chain has also recently been observed, and although several Euler angles-based solutions exists [80], an approach employing Lie groups have recently been proposed [81].

A tracking task can be seen as an extension of a pose estimation problem in terms of sources of uncertainty of a measurements. A pioneer work on tracking on manifolds was presented in [82] where authors perform fleet tracking by modeling the target motion as a particle describing the motion on  $SE(3)$  and employing the particle filtering approach. Another particle filtering based approach applies a first-order autoregressive state dynamics and use coordinate-invariant particle filter on the  $SE(3)$  group in a single-target visual tracking application [83].

▷ **ATTITUDE ESTIMATION.** Attitude also represents an important manifold from the estimation perspective. Although suitability of Euler angle-based representation was proven in many practical application, the presence of singularities and non-orthogonality of components caused these algorithms to experience different disadvantages. Hence, recent filtering approaches relying on  $SO$  or quaternion-based setting managed to significantly outperform the traditional Euler angle-based approaches, and have become standard in different application fields. In particular, in [84] author presented real-time estimation of a rigid body orientation from measurements of acceleration, angular velocity and magnetic field strength by using quaternions and is one of the first authors who carefully treats the inherent properties of unit quaternions. Later, in [85] authors used a similar approach to attitude estimation by employing the same sensor setup. In [86] the authors also built upon similar ideas, and particularly derived the so-called manifold-constrained UKF. Recently, in [87] the authors have proposed an invariant EKF applied for attitude estimation, where they managed to systematically exploit the invariance properties to design stochastic filters on  $SO(3)$ . Although majority of approaches rely on local techniques, some approaches have also tempted to globally account for the geometry of  $SO(3)$  group. Hence in [88] authors



have used numerical parametric uncertainty techniques, noncommutative harmonic analysis, and geometric numerical integration for obtaining the global uncertainty propagation scheme for the attitude dynamics of a rigid body. In [89] author numerically solved the Fokker-Planck equation on the  $SO(3)$  group via noncommutative harmonic analysis to obtain computational tools to propagate a pdf over the attitude kinematics, and finally uses it for attitude motion planning and estimation. The more in-depth survey of nonlinear attitude estimation approaches is available in [90].

▷ **MANIPULATOR KINEMATICS AND CONTROL.** An early application of associating the uncertainty to  $SE(3)$  group was presented in [91], and later in [56]. Therein, the constant position motion model was assumed, and the uncertainty is assumed to be small. This pioneering systematic methodology of propagating and fusing spatial uncertainties was applied for actions in an assembly task. A more careful treatment of error propagation was later presented in [59] where more general propagation model was used. While in [59] a first-order error propagation on the  $SE(3)$  group was presented, the same authors have later extended the approach to second-order error propagation [92].

There has also been several control applications where a manifold geometry was exploited. In [93, 94] authors used the  $SE(3)$  group representation for describing the state of steerable needle which is in the focus of their control application. They particularly derived the equations for parametrically propagating the uncertainty accounting for the geometry of the  $SE(3)$  state space. Another approach relying on Lie group representation of highly articulated robot and applied in invasive surgery was presented in [95]. The position and orientation of every robot link evolves in  $SE(3)$ , while authors used the EKF implementation such that the state vector is defined using elements of Lie algebra representation.

▷ **CALIBRATION.** A popularity of quaternion based approaches has risen via time, and many authors have tried to exploit the geometry of a quaternion state space by employing the nonlinear propagation functions. However, in the update step majority of the approaches relied on the post-normalization, and hence forced the mean to preserve the unit constraint. Calibration is a ‘classic’ application of such quaternion based EKF or UKF approaches. In [96, 97] authors used a quaternion based EKF formulation which fuses different measurements with inertial sensors and does not only estimate pose and velocity of an UAV, but also estimates sensor biases, scale of the position measurement and self (inter-sensor) calibration. Similarly, in [98] authors combined visual and inertial sensing for navigation, with an emphasis on the ability to self-calibrate the camera-IMU transformation, but use UKF filtering approach. In [99] authors developed a framework for fusion of different sensors allowing for their self-calibration by relying on an IEKF implementation. Alternatively to quaternion approaches, in [100] authors performed an extrinsic calibration between two sensors mounted rigidly on a moving body by describing the 6 dof state using  $SE(3)$  group.

A more general approach to calibration in terms of state space geometry was proposed in [101]. Therein authors use non-linear optimization on constraint graphs and combine it with a principled way of handling non-Euclidean spaces (class of box-plus spaces as in the vein of [62]) making it particularly easy to solve non-trivial multi-sensor calibration problems. Their developed Matlab framework is available as open source toolkit.

▷ **SLAM.** An early SLAM application accounting for the state space geometry was presented in [102], where the state is given as a group element, while the estimation error is represented locally by a differential location vector. The authors refer to this concept as the symmetries and perturbations map (SPmap), while they use the EKF implementation. Another EKF-based SLAM using the quaternion-based approach and accounting for the state space geometry was presented in [103], and relies on the quaternion normalization in the update step. A direct approach to visual EKF-based SLAM which uses the  $SE(3)$  representation is presented in [104]. In [105] the authors preintegrated a large number of inertial measurement unit measurements for visual-inertial navigation into a single relative motion constraint by respecting the structure of the  $SO(3)$  group and defining the uncertainty thereof in the pertaining tangent space.

A quite prominent example of an application where the need arises for computational benefits of the IF and the geometric accuracy of Lie groups is SLAM. SLAM is of great practical importance in many robotic and autonomous system applications since it represents a problem of acquiring a map of an unknown environment, and simultaneously localizing itself within the map. The earliest SLAM solutions were based on an EKF implementation and in practice they could handle maps that contain a few hundred features, while in many applications maps are orders of magnitude larger [34]. Therefore, the EIF is often employed and widely accepted for SLAM [106]. The EIF based approaches reached its zenith with sparsification techniques resulting with SEIF [34] and ESDSF [35]. However, the localization component of SLAM conforms the pose estimation problem as arising on Lie groups. Furthermore, the mapping part of SLAM consists of landmarks whose position, as well, arises on  $SE(3)$ . Therefore, some recent SLAM solutions approached the problem by respecting the geometry of the state space [107, 108, 109], since significant cause of error in such application was determined to stem from the state space geometry approximations. However, these SLAM solutions, although able to account for the geometry of the state space, exclusively rely on graph optimization [66, 110, 111], but still not on filtering approaches (although filtering approaches have still recently been successfully used for plain odometry applications [112, 113]).

#### 2.1.4 Organization of the chapter

The rest of the chapter is organized as follows. The underlying background estimation theory in the form of a Bayesian filtering is presented in Sec. 2.2. The traditional solution to the Bayes filtering problem in the form of an extended Kalman filter and an extended information filter, suitable for operation with Euclidean variables is given in Sec. 2.3. A basic overview of the  $\mathfrak{vM}$  distribution is given in Sec. 2.4. The last section of this chapter provides directions for evaluation of the LG-EKF including (i) mathematical preliminaries useful for understanding the necessary mappings between the triplet including Lie group, Lie algebra and Euclidean space, (ii) basics on the concept of CGD, and (iii) equations for the LG-EKF Sec. 2.5.



## 2.2 BAYESIAN FILTERING

The Bayesian filter has a recursive form and operates in two steps. Firstly, based on the prior knowledge and motion model, the prediction can be performed. Secondly, once the measurement becomes available, the update step is executed.

### 2.2.1 Model of the system

To define the filtering problem, we consider the evolution of the discrete system from time instant  $k - 1$  to  $k$  following the motion model given as

$$x_k = f(x_{k-1}, u_{k-1}) + w_{k-1}, \quad k \in \mathbb{N}, \quad (2.1)$$

where  $f$  is a nonlinear function of the system state  $x$  and control actions  $u$  at time step  $k - 1$ , while  $w$  is process noise. The objective of estimation is to recursively estimate  $x_k$  from measurements given via another non-linear function

$$z_k = h(x_k) + v_k, \quad k \in \mathbb{N}, \quad (2.2)$$

where  $h$  is possibly a nonlinear function in the system state and  $v$  is a measurement noise.

### 2.2.2 Statistical inference

From a Bayesian perspective, the estimation problem is to recursively calculate some degree of belief in the state  $x$  at time instant  $k$ , i.e.,  $x_k$ , given the measurement data  $z_k$  [24].

From the perspective of the pdf, we are striving to estimate the density  $p(x_k | z_{1:k})$ , i.e., the pdf of the state  $x_k$  given the history of all measurements  $z_{1:k}$ , often referred as posterior at time instant  $k$ . This may be obtained recursively applying the prediction and update steps. Assuming that the posterior  $p(x_{k-1} | z_{1:k-1})$  is available, the prediction step particularly involves calculating the prior pdf via the Chapman–Kolmogorov equation [24]

$$p(x_k | z_{1:k-1}) = \int p(x_k | x_{k-1}) p(x_{k-1} | z_{1:k-1}) dx_{k-1}, \quad (2.3)$$

where  $p(x_k | x_{k-1})$  is the probabilistic model of the state evolution.

In the update step, once the measurement  $z_k$  becomes available, it can be used to update the prior via the Bayes rule

$$p(x_k | z_{1:k}) = \frac{p(z_k | x_k) p(x_k | z_{1:k-1})}{p(z_k | z_{1:k-1})}, \quad (2.4)$$

where the pdf  $p(z_k | x_k)$  represents our likelihood function defined by the sensor model (2.2) and  $p(z_k | z_{1:k-1})$  represents a normalization constant. For implementation purposes, the three probability distributions are required; (i) the initial belief  $p(x_0)$ , (ii) the measurement probability  $p(z_k | x_k)$ , (iii) state transition probability  $p(x_k | x_{k-1})$ . This recursive propagation of the posterior density is only a conceptual solution, while in general it cannot be determined analytically. However, solutions do exist in a restrictive set of cases which will be briefly introduced in the thesis [24]. Furthermore, one should note that there is nothing intrinsic in the Bayesian filter propagation and update steps that would limit this concept to operating on Euclidean spaces only. This thesis shows several applications of this concept in various non-Euclidean problems.

### 2.2.3 Validation gate

The normalization constant  $p(z_k | z_{1:k-1})$  results from applying the marginalization of the state  $x_k$  from the nominator of (2.4) as

$$p(z_k | z_{1:k-1}) = \int p(z_k | x_k) p(x_k | z_{1:k-1}) dx_k. \quad (2.5)$$

This probability can further be used for validation gate purposes, so as to reject highly unlikely measurements/outliers. In particular, the validity of a measurement  $z_k$  is directly evaluated through (2.5) [114].

## 2.3 TRADITIONAL PROBABILISTIC STATE ESTIMATION

Since the concept of Kalman filtering represents an important aspect of this thesis, the EKF is briefly presented in the sequel.

### 2.3.1 Extended Kalman filter

Let us assume that the system is given with motion (2.1) and measurement models (2.2), and process and measurement noises are Gaussian given as  $w_k \sim \mathcal{N}(0, Q_k)$ ,  $v_k \sim \mathcal{N}(0, R_k)$ . We also assume the system state and measurement spaces are Euclidean, i.e.,  $x_k \in \mathbb{R}^n$ ,  $z_k \in \mathbb{R}^m$ ,  $\forall k \in N$ . If the posterior at time instance  $k-1$  is a Gaussian distribution  $x_{k-1} \sim \mathcal{N}(\mu_{k-1}, \Sigma_{k-1})$ , the predicted state  $x_{k|k-1}$  is given with parameters

$$\begin{aligned} \mu_{k|k-1} &= f(\mu_{k-1}, u_{k-1}) \\ \Sigma_{k|k-1} &= F_{k-1} \Sigma_{k-1} F_{k-1}^T + Q_{k-1}, \end{aligned} \quad (2.6)$$

where  $F$  is state transition matrix defined to be the Jacobian

$$F_{k-1} = \left. \frac{\partial f}{\partial x} \right|_{x=\mu_{k-1}}. \quad (2.7)$$

Having the estimated prior  $x_{k|k-1} \sim \mathcal{N}(\mu_{k|k-1}, \Sigma_{k|k-1})$ , once having the measurement  $z_k$  available, the updated state of the system is evaluated as

$$\begin{aligned} K_k &= \Sigma_{k|k-1} H_k^T (H_k \Sigma_{k|k-1} H_k^T + R_k)^{-1} \\ \mu_k &= \mu_{k|k-1} + K_k (z_k - H_k \mu_{k|k-1}) \\ \Sigma_k &= (I - K_k H_k) \Sigma_{k|k-1}, \end{aligned} \quad (2.8)$$

where  $H$  is measurement matrix defined to be the Jacobian

$$H_k = \left. \frac{\partial h}{\partial x} \right|_{x=\mu_{k|k-1}}. \quad (2.9)$$

A complete and intuitive derivation of KF is available in [1].

When considering the validation gating, the validity of a measurement is determined from its residual (or innovation) with the predicted observation, which results from (2.5) producing a Gaussian distribution of the innovation as [106]

$$\mathcal{N}(z_k - H_k \mu_{k|k-1}, H_k \Sigma_{k|k-1} H_k^T + R_k). \quad (2.10)$$

Validation is computed by gating the normalized innovation squared (NIS; also commonly known as the Mahalanobis distance) as

$$(z_k - H_k \mu_{k|k-1})^T (H_k \Sigma_{k|k-1} H_k^T + R_k)^{-1} (z_k - H_k \mu_{k|k-1}) \leq \chi_d^2, \quad (2.11)$$

where  $\chi^2$  is a chi-square pdf, and  $d$  is innovation dimension.

The above recursion results from the first-order Taylor series expansion of nonlinear motion and measurement models, and although higher-order EKF [115] exist, its practical usage is not nearly as often as first-order based approximation [27].

### 2.3.2 Extended Information filter

While KF relies on moment representation of Gaussian distributions using mean  $\mu$  and covariance  $\Sigma$  parameters, the IF replaces them with canonical parameters called information vector  $y$  and information matrix  $Y$ . The relation between the two set of parameters are given as

$$\mathcal{N}_c(y, Y) = \mathcal{N}_c(\Sigma^{-1}\mu, \Sigma^{-1}), \quad \mathcal{N}_m(\mu, \Sigma) = \mathcal{N}_m(Y^{-1}y, Y^{-1}), \quad (2.12)$$

where index  $m$  denotes the moment representation, while  $c$  represents the canonical representation. Since moment representation is considered ‘classical’, in the rest of the thesis we omit specifically using index  $m$  when referring to it.

Given the same assumptions as in the EKF case about motion and measurement models, and if the posterior at time instance  $k-1$  is a Gaussian distribution given with canonical parameters  $x_{k-1} \sim \mathcal{N}_c(y_{k-1}, Y_{k-1})$ , the predicted state  $x_{k|k-1}$  is calculated as

$$\begin{aligned} \mu_{k|k-1} &= f(Y_{k-1}^{-1}y, u_{k-1}) \\ Y_{k|k-1} &= (F_{k-1}Y_{k-1}^{-1}F_{k-1}^T + Q_{k-1})^{-1} \\ y_{k|k-1} &= Y_{k|k-1}\mu_{k|k-1}, \end{aligned} \quad (2.13)$$

where  $F$  is state transition matrix defined as in the EKF case. Having the estimated prior  $x_{k|k-1} \sim \mathcal{N}_c(y_{k|k-1}, Y_{k|k-1})$ , once having the measurement  $z_k$  available, the updated state of the system is calculated as

$$\begin{aligned} y_k &= y_{k|k-1} + H_k^T R_k^{-1} (z_k - h(\mu_{k|k-1}) + H_k \mu_{k|k-1}) \\ Y_k &= Y_{k|k-1} + H_k^T R_k^{-1} H_k, \end{aligned} \quad (2.14)$$

where  $H$  is measurement matrix defined as in the EKF case. Furthermore, if  $N$  measurements are available at time step  $k$  through different measurement models  $h_i$  and measurement noise  $r_k^i \sim \mathcal{N}(0, R_{i,k})$ , the updated information vector and matrix become

$$\begin{aligned} y_k &= y_{k|k-1} + \sum_{i=1}^N H_{i,k}^T R_{i,k}^{-1} (z_{i,k} - h_i(\mu_{k|k-1}) + H_{i,k} \mu_{k|k-1}), \\ Y_k &= Y_{k|k-1} + \sum_{i=1}^N H_{i,k}^T R_{i,k}^{-1} H_{i,k}. \end{aligned} \quad (2.15)$$

## 2.4 DIRECTIONAL ESTIMATION

### 2.4.1 Von Mises distribution

The vM distribution is a continuous parametric probability distribution defined on the unit circle  $S^1$ , or equivalently on interval  $[0, 2\pi)$ , i.e. the 1-dimensional sphere with unit radius and center at the origin. A unit random vector  $x$  is said to have a vM distribution  $vMF(\mu, \kappa)$  if its probability density function (pdf) is of the following form [8]

$$p(x; \mu, \kappa) = \frac{1}{2\pi I_0(\kappa)} \exp(\kappa \cos(x - \mu)), \quad x \in S^2, \quad (2.16)$$

where  $0 \leq x < 2\pi$ ,  $\mu \in [0, 2\pi)$  denotes the mean angle,  $\kappa \geq 0$  is the concentration parameter and  $I_0$  is the modified Bessel function of the first kind and of order zero [7]. The modified Bessel function of the first kind and of order  $n \in \mathbb{N}$  is defined by the following expression

$$I_n(\kappa) = \frac{1}{2\pi} \int_0^{2\pi} \exp(\kappa \cos \xi) \cos(n\xi) d\xi. \quad (2.17)$$

The vM distribution is often referred as the circular analogue of the normal distribution on the real line: it is unimodal, symmetric around mean angle  $\mu$ , and the concentration parameter  $\kappa$  is analogous to the inverse of the variance. Several examples of the vM distribution are given in Fig. 2.1.

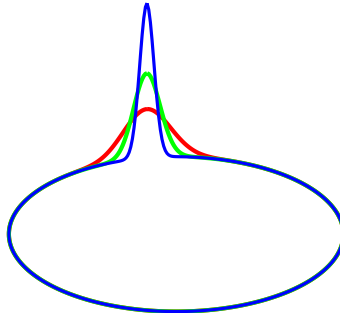


Figure 2.1: Examples of the vM distribution on the unit 1-sphere, with equal mean directions and concentration parameters of 50 (red), 150 (green), and 500 (blue), which correspond approximately to standard deviations of  $8.2^\circ$ ,  $4.7^\circ$  and  $2.6^\circ$ , respectively [116].

## 2.5 ESTIMATION ON LIE GROUPS

### 2.5.1 Mathematical preliminaries

A Lie group  $G$  is a group which has the structure of a smooth manifold with the smooth group operators of composition and inversion. Moreover, each point  $X \in G$  has an associated tangent space  $T_X(G)$ , called the Lie algebra of  $G$  and denoted  $\mathfrak{g}$ , which almost completely captures a curved object like  $G$  [117]. The Lie algebra  $\mathfrak{g}$ , which is of the same dimension as  $G$ , admits a binary operation  $[\cdot, \cdot]$  called the Lie bracket, which reflects the non-commutative content of the group operation, and we usually consider this space being placed at the group identity. Furthermore, if the group  $G$  is a matrix Lie group, then  $G \subset \mathbb{R}^{n \times n}$  and group

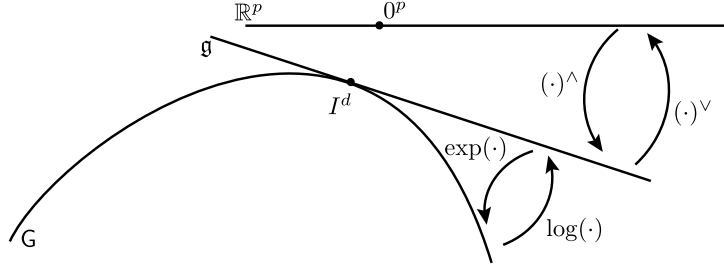


Figure 2.2: An illustration of mappings within the triplet of Lie group  $G$  – Lie algebra  $\mathfrak{g}$  – Euclidean space  $\mathbb{R}^p$  [121].

operations are simply matrix multiplication and inversion. Although not all Lie groups are matrix groups, the majority of them has an equivalent matrix representation—especially the ones considered in physical sciences [60]. Moreover, the theorem [118] says that every Lie algebra is isomorphic to a matrix Lie algebra, thus we will simply say ‘Lie algebra’ rather than ‘matrix Lie algebra’.

The Lie algebra  $\mathfrak{g} \subset \mathbb{R}^{n \times n}$  associated to a  $p$ -dimensional matrix Lie group  $G \subset \mathbb{R}^{n \times n}$  is a  $p$ -dimensional vector space defined by a basis consisting of  $p$  real matrices  $E_r$ ,  $r = 1, \dots, p$ , often referred to as generators [119]. In particular, a Lie algebra is an open neighbourhood around  $\mathbf{0}^p$  in the tangent space of  $G$  at the identity  $I^n$ . The matrix exponential  $\exp_G$  and matrix logarithm  $\log_G$  establish a local diffeomorphism between  $G$  and  $\mathfrak{g}$  as

$$\exp_G : \mathfrak{g} \rightarrow G \text{ and } \log_G : G \rightarrow \mathfrak{g}. \quad (2.18)$$

Furthermore, a natural relation exists between the  $p$ -dimensional Lie algebra  $\mathfrak{g}$  and the Euclidean space  $\mathbb{R}^p$ , and is given through a linear isomorphism

$$[\cdot]_G^\vee : \mathfrak{g} \rightarrow \mathbb{R}^p \text{ and } [\cdot]_G^\wedge : \mathbb{R}^p \rightarrow \mathfrak{g}. \quad (2.19)$$

For brevity, we will use the notation in the vein of [120]

$$\exp_G^\wedge(x) = \exp_G([\cdot]_G^\wedge(x)) \text{ and } \log_G^\vee(X) = [\log_G(X)]_G^\vee, \quad (2.20)$$

where  $x \in \mathbb{R}^p$  and  $X \in G$ . An illustration of these concepts is given in Fig. 2.2.

Lie groups are generally non-commutative, i.e.,  $XY \neq YX$ . However, the non-commutativity can be captured by the so-called adjoint representation of  $G$  on  $\mathfrak{g}$  [58]

$$X \exp_G^\wedge(y) = \exp_G^\wedge(\text{Ad}_G(X)y)X, \quad (2.21)$$

which can be seen as a way of representing the elements of the group as a linear transformation of the group’s algebra. The adjoint representation of  $\mathfrak{g}$ ,  $\text{ad}_G$ , is in fact the differential of  $\text{Ad}_G$  at the identity. Another important result for working with Lie group elements is the Baker-Campbell-Hausdorff (BCH) formula, which enables representing the product of Lie group members as a sum in the Lie algebra. We will use the following BCH formulae [122, 58]

$$\log_G^\vee(\exp_G^\wedge(x) \exp_G^\wedge(y)) = y + \varphi_G(y)x + O(\|y\|^2), \quad (2.22)$$

$$\log_G^\vee(\exp_G^\wedge(x+y) \exp_G^\wedge(-x)) = \Phi_G(x)y + O(\|y\|^2), \quad (2.23)$$

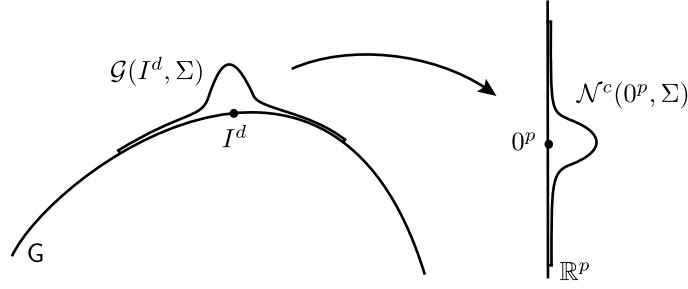


Figure 2.3: An illustration of the CGD  $\mathcal{G}(I^d, \Sigma)$ . The mean value  $I^d$  resides on the group  $G \subset GL(d; \mathbb{R})$  while the covariance matrix  $\Sigma$  belongs to  $GL(p; \mathbb{R})$ . On the right we depict the corresponding  $\mathcal{N}^c$  Gaussian in  $\mathbb{R}^p$  with mean value  $0^p$  and covariance matrix  $\Sigma$  [121].

where  $\varphi_G(y) = \sum_{n=0}^{\infty} \frac{B_n \text{ad}_G(y)^n}{n!}$ ,  $B_n$  are Bernoulli numbers, and  $\Phi_G(x) = \varphi_G(x)^{-1}$ . For many common groups used in engineering and physical sciences closed form expressions for  $\varphi_G(\cdot)$  and  $\Phi_G(\cdot)$  can be found [10, 58]; otherwise, a truncated series expansion is used.

### 2.5.2 Concentrated Gaussian distribution

Let us assume that a random variable  $X$  taking values in  $G$  has the probability distribution with the probability density function (pdf) of the following form [59]

$$p(X; \Sigma) = \beta \exp \left( -\frac{1}{2} (\log_G^\vee(X))^T \Sigma^{-1} \log_G^\vee(X) \right), \quad (2.24)$$

where  $\beta$  is a normalizing constant such that (2.24) integrates to unity, and  $\Sigma$  is a positive definite  $p \times p$  matrix. Seemingly, in notation  $\xi = \log_G^\vee(X) \in \mathbb{R}^p$ , density (2.24) has the structure of a zero mean Gaussian with covariance matrix  $\Sigma$ . However, observe that the normalizing constant  $\beta$  differs from  $(2\pi)^{-p/2} (\det \Sigma)^{-1/2}$  and, in the sense of  $\mathbb{R}^p$ , it is only defined on an open neighborhood of the origin. Additionally, we will assume that all eigenvalues of  $\Sigma$  are small, thus, almost all the mass of the distribution is concentrated in a small neighborhood around the mean value, and such a distribution is called a CGD [59]. Furthermore, we say that a random variable  $X$  has a CGD of mean  $\mu \in G$  and covariance matrix  $\Sigma$ , written  $X \sim \mathcal{G}(\mu, \Sigma)$ , if  $M^{-1}X$  has the CGD of mean  $I^d$  and covariance  $\Sigma$  [59], i.e., the density of  $\mathcal{G}(\mu, \Sigma)$  is given by

$$p(X; \mu, \Sigma) = \beta \exp \left( -\frac{1}{2} (\log_G^\vee(\mu^{-1}X))^T \Sigma^{-1} \log_G^\vee(\mu^{-1}X) \right). \quad (2.25)$$

Correspondingly, a random variable  $X$  can be seen as

$$X = \mu \exp_G^\wedge(\xi), \text{ with } X \sim \mathcal{G}(\mu, \Sigma). \quad (2.26)$$

An illustration of the CGD is provided in Fig. 2.3.

### 2.5.3 Extended Kalman filter on Lie groups

For the general filtering approach on matrix Lie groups, the system is assumed to be modeled as satisfying the following equation [61]

$$X_k = f(X_{k-1}, \omega_{k-1}) = X_{k-1} \exp_G^\wedge(\hat{\Omega}_{k-1} + \omega_{k-1}), \quad (2.27)$$

where  $X_k \in G$  is the state of the system at time  $k$ ,  $G$  is a  $p$ -dimensional Lie group,  $\omega \sim \mathcal{N}_{\mathbb{R}^p}(\mathbf{0}^{p \times 1}, Q)$  is white Gaussian noise and  $\hat{\Omega} = \Omega(X) : G \rightarrow \mathbb{R}^p$  is a non-linear  $\mathcal{C}^2$  function.

The prediction step of the LG-EKF, based on the motion model (2.27), is governed by the following formulae

$$\mu_{k|k-1} = \mu_{k-1} \exp_G^\wedge(\hat{\Omega}_{k-1}) \quad (2.28)$$

$$\Sigma_{k|k-1} = \mathcal{F}_{k-1} \Sigma_{k-1} \mathcal{F}_{k-1}^T + \Phi_G(\hat{\Omega}_{k-1}) Q_{k-1} \Phi_G(\hat{\Omega}_{k-1})^T, \quad (2.29)$$

where  $\mu \in G$  and  $\Sigma \in \mathbb{R}^{p \times p}$  are predicted mean value and the covariance matrix, respectively, hence the state remains  $\mathcal{G}$ -distributed  $X_{k|k-1} \sim \mathcal{G}(\mu_{k|k-1}, \Sigma_{k|k-1})$ . The operator  $\mathcal{F}$ , a matrix Lie group equivalent to the Jacobian of  $f(X, n)$ , and  $\Phi_G$  are given as follows

$$\mathcal{F}_{k-1} = \text{Ad}_G(\exp_G^\wedge(-\hat{\Omega}_{k-1})) + \Phi_G(\hat{\Omega}_{k-1}) C_{k-1} \quad (2.30)$$

$$\Phi_G(a) = \sum_{m=0}^{\infty} \frac{(-1)^m}{(m+1)!} \text{ad}_G(\mathbf{v})^m, \quad a \in \mathbb{R}^p \quad (2.31)$$

$$C_{k-1} = \frac{\partial}{\partial \xi} \Omega(\mu_{k-1} \exp_G^\wedge(\xi))|_{\xi=0}. \quad (2.32)$$

The discrete measurement model on the matrix Lie group is modelled as

$$Z_k = h(X_k) \exp_{G'}^\wedge(m_k), \quad (2.33)$$

where  $Z_k \in G'$ ,  $h : G \rightarrow G'$  is a  $\mathcal{C}^1$  function and  $m_k \sim \mathcal{N}_{\mathbb{R}^q}(\mathbf{0}^{q \times 1}, R_k)$  is white Gaussian noise.

The update step of the filter, based on the measurement model (2.33), strongly resembles the standard EKF update procedure, relying on the Kalman gain  $K_k$  and innovation vector  $v_k$  calculated as follows

$$\begin{aligned} K_k &= \Sigma_{k|k-1} \mathcal{H}_k^T (\mathcal{H}_k \Sigma_{k|k-1} \mathcal{H}_k^T + R_k)^{-1} \\ v_k &= K_k (\log_{G'}^\vee(h(\mu_{k|k-1})^{-1} Z_k)). \end{aligned} \quad (2.34)$$

The matrix  $\mathcal{H}_k$  can be seen as the measurement matrix of the system, i.e., a matrix Lie group equivalent to the Jacobian of  $h(X_k)$ , and is given as

$$\mathcal{H}_k = \frac{\partial}{\partial \xi} [\log_{G'}^\vee(h(\mu_{k|k-1})^{-1} h(\mu_{k|k-1} \exp_G^\wedge(\xi)))]|_{\xi=0}. \quad (2.35)$$

Finally, having defined all the constituent elements, the update step is calculated via

$$\mu_k = \mu_{k|k-1} \exp_G^\wedge(v_k) \quad (2.36)$$

$$\Sigma_k = \Phi_G(v_k) (I^{p \times p} - K_k \mathcal{H}_k) \Sigma_{k|k-1} \Phi_G(v_k)^T. \quad (2.37)$$

As in the case of the prediction step, the state  $X_{k+1} \sim \mathcal{G}(\mu_k, \Sigma_k)$  remains  $\mathcal{G}$ -distributed after the correction as well. For a more formal derivation of the LG-EKF, the interested reader is referred to [61] and [121].

## Moving objects tracking based on random finite sets

MULTIPLE objects tracking has a long history spanning over 50 years referring to the problem of jointly estimating the trajectories, e.g., position and orientation as well as their respective velocities and accelerations, and the number of objects in the space, relying on the observations from sensor data. Driven by aerospace applications in the 1960's, it finds its application in diverse traditional engineering disciplines such as intelligence, surveillance and reconnaissance, radar/sonar applications, air traffic control, etc. During the last decade, advances in MOT techniques along with sensing and computing technologies, have opened up numerous research venues such as robotics and autonomous systems, computer vision, biomedical research, agriculture and forestry, epidemiology and public health, communications networks, oceanography, remote sensing, etc [123].

### 3.1 INTRODUCTION

From the viewpoint of the several sources of uncertainty appearances (described in Ch.1) among whom each appears challenging itself, data association attracted probably the most significant attention of the overall research community. The reasoning might lie in the fact that all other sources of uncertainty can be considered as special cases of the data association task. For example, one can contend with the recognition of births and deaths only once the data association task figures out that the existing list of recognized objects does not match the evolving observations well. Furthermore, false positive and false negative observations, i.e., false alarms and missed detections, can also be considered only after the data association task figures out that the list of existing objects does not overlap with the observations well.

Given the previous discussion, the MOT application can be considered as a task which aims at tracking a random number of objects receiving a random number of measurements. Among all the existing MOT approaches, the most popular are naive global nearest neighbor approaches (GNN) [124], the joint probabilistic data association (JPDA) [125, 126], the multiple hypothesis tracking (MHT) [127, 128], and commonly referred to as RFS based multi-object filters [129, 130]. Although recent developments in RFS have yielded a variety of tracking methods that claim to avoid data association (often referred to as data association-free approaches), it was proven that both MHT and JPDA can be derived within the RFS framework [131], thus representing only special cases of RFS approaches. The research community often intentionally follows the terminology which inherently abuses the true relation between data



association based approaches and data association-free approaches, by referring to MHT and JPDA as non-RFS. Herein we emphasize that although they were not intentionally developed through the theory of RFS, the data association is still implicitly present in majority of RFS-based filters, and hence the distinction between the traditional and RFS approaches is obvious only from the viewpoint of the theoretical background.

The traditional data association-based approaches explicitly formulate and reason over association hypotheses describing the correspondence of measurements and objects. In contrary, the RFS-based approaches data association is implicitly present. As such, the RFS-based algorithms, introduced by Mahler, have gained a great deal of attention in the tracking community during the last 15 years. This paradigm is developed upon an *engineering friendly* version of point process theory called finite-set statistics (FISST) [4, 132]. The summary of motivations, concepts, techniques, and applications of FISST, and description on how conventional single-sensor, single-object formal Bayesian modeling is carefully extended to general data fusion problems, is given in the tutorial “Statistics101” [129]. Although the background theory of FISST may appear involved, after years of research the optimal multi-sensor–multi-object recursive Bayes filter was successfully used to derive principled statistical approximations in the form of PHD filters [3, 133], cardinalized PHD (CPHD) filters [134, 135], multi-Bernoulli (MB) filters [136], etc. The basic ideas of these approximations are summarized in another tutorial by Mahler called “Statistics102” [137].

In the subsequent part of this introduction section, an overview of the traditional MOT methods including (i) MHT and (ii) JPDAF, and the RFS-based methods including (i) PHD, (ii) CPHD and (iii) MB, are provided.

### 3.1.1 Overview of traditional methods

▷ **MHT.** The underlying idea of the MHT algorithm is the hypothesis generation process which considers different phenomena of measurement origin uncertainty since (i) it is unknown if a measurement is from an object or due to clutter, (ii) it is unknown which measurement originates from which object, (iii) it is unknown if missed detection events have occurred due to less than unity probability of detection [138]. Each possible combination of the previous phenomena generates a hypothesis, which can be limited by performing gating. GNN in this context can be seen as MHT which keeps only the hypothesis with the maximum total track score or the minimum total cost, while MHT uses a deferred decision logic [124].

There exist two types of MHT algorithms, the hypothesis-oriented (HOMHT) [127, 139] and the track-oriented (TOMHT) [140] algorithm. The original idea of MHT, presented in [127], was the HOMHT, where a number of global hypotheses between consecutive scans were kept, whereas the number of association hypotheses or tracks grew exponentially. Since this issue was shown to be easily handled by TOMHT, these approaches were utilized significantly more often than HOMHT. TOMHT can then be further divided into tree based [140, 141] and non-tree based [142, 139] approaches. The HOMHT keeps a number of global hypotheses between consecutive scans whereas tree based TOMHT only maintains a number of ‘target’ trees, each containing a number of tracks which are not compatible. In tree based TOMHT, the best global hypothesis is formed from the existing set of tracks and the  $N$ -scan pruning

[124] and track-score based pruning are used to limit the number of tracks from growing exponentially [138]. An early efficient implementation of the tree based TOMHT algorithm in which the  $N$ -best hypotheses are determined in polynomial time is presented in [143]. On the other hand, a number of different non-tree TOMHT variants were proposed [123], but due to the intuitive interpretation and the clarity of the tree based TOMHT, the non-tree methods never attracted such significant attention as tree based methods. Several different varieties of the probabilistic MHT (PMHT), relying on soft a posteriori probability associations were also developed, but they never attracted significant attention [144, 145, 146, 147]. and since this is not in the focus of the thesis we do not consider them any further. A general motivation for MHT, its basic principles and the alternative implementations in common use are summarized in [128].

▷ **JPDAF.** The early research on probabilistic data association approaches was exclusively focused on single object tracking applications, accounting for some basic phenomena related to the measurement origin uncertainty. The seminal paper by Yaakov Bar-Shalom and Edison Tse [125] proposed the probabilistic data association PDA approach which grounded the basis for the entire research on probabilistic MOT research. The PDA algorithm calculates the association probabilities to the object being tracked for each validated measurement at the current time. The joint probabilistic data association JPDA approach is a multi-object extension of the PDA [126], relying on the assumption that the number of tracked objects is known. The key feature of the JPDA is that it evaluates the conditional probabilities of the joint association events, where each event represents one combination of measurements-to-object associations. Typically the state estimation algorithm, which is carried out upon events evaluation is calculation of marginal association probabilities. These marginal probabilities are obtained from the joint probabilities by summing over all joint association events in which the marginal event of interest (respecting each object separately) occurs [148]. The state estimation equations are then decoupled among the objects and exactly the same as in PDA. For this purpose, JPDA shows tendency that tracks of closely spaced objects become overlapped due to the shared measurements across tracks, when this sharing lasts for many frames or scans [148]. Alternatively, more realistic assumption accounts for possible correlations between states of two objects after sharing some measurements, yielding a covariance matrix with off-diagonal blocks which reflect the correlation between the state estimation errors of the objects. This approach is called JPDA coupled filter (JPDAC). This problem is well-known as a problem of track coalescence, and some improvements on this topic are available in [149]. Over time, some approximations of JPDA designed for circumventing the combinatorial complexity for large number of objects have also been developed [150]. A tutorial on PDA and JPDA techniques is available in [148].

Mušicki et al. managed to rederive PDA without an initial assumption of track existence which was an important relaxation of the original PDA assumptions, and called the algorithm integrated probabilistic data association IPDA [151]. As such, this algorithm simultaneously provides expressions for both probability of track existence and data association. Later, Mušicki and Evans managed to extend the JPDA with the concept of object existence probability for individual track [152] and called the algorithm joint integrated PDA (JIPDA). This concept easily allows for track management in terms of false track discrimination or

newly birth tracks confirmation. Recently, some directions for performance/computation resources trade-off for JPDA were discussed in [153].

The main difference in the overall ideas of MHT and JPDA is that MHT uses a Gaussian posterior of the object states at the rear end of its sliding window, conditioned on the chosen hypothesis up to that point in time while it ignores all other association hypotheses. JPDA on the other hand relies on a soft decision since it averages over all the possibilities, which is never totally correct but never totally wrong [148]. However, it is interesting to note that although the RFS approaches have recently attracted a significant attention, some PDA-based approaches are still the focus of ongoing research [154].

### 3.1.2 Overview of RFS-based methods

FISST enables formal extension of conventional single-sensor, single-object Bayesian probabilistic modeling to general data fusion problems relying on the Bayesian convolution and fusion defined over random sets, rather than random variables. Such definition of Bayesian prediction and correction suited well with the nature of the multi-sensors–multi-object detection and tracking problems. In particular, the concept of a random set is defined to contain an uncertain number of random variables, i.e., each of the objects' state is presented as random variable, while the size of the set is presented with a random number. Hence, the multi-object filtering algorithm tempts at estimating states of objects as well as the number of objects existing in space. An intuitive interpretation of FISST-based MOT is given in [155].

One of the first significant RFS-based filters was developed by Mahler in 2003 [3], where author proposes the filter which propagates a first-order statistical moment of a random set, rather than the entire distribution, and called the approach PHD filter. Early PHD applications were mostly relying on particle filtering approaches based on the work presented in [156], and referred to as a generic particle PHD filter. Some interesting applications of such filter are multisensor vehicle tracking presented in [157] and an exclusive vision-based application presented in [158]. It is also worth mentioning that the estimation for the particle PHD filter requires clustering of particles into groups, which involves additional processing, relying on techniques such as the auxiliary particle PHD filter [159], or measurement driven particle PHD filter [160]. A seminal work on a derivative of the PHD is presented in [133], where authors present the closed form solution for the Bayesian recursion of the PHD filter under the 'linear Gaussian multitarget model' assumption, and refer to it as Gaussian mixture probability hypothesis density GM-PHD filter. Therein, the authors also provide directions for the similar algorithms employed for nonlinear propagation and measurement models following the ideas of EKF and UKF for general state estimation (as given in Sec. 2), referring to the PHD alternatives as EK-PHD and UK-PHD, respectively. Further research related to the GM-PHD was dealing with different topics related to this filter such as convergence analysis [161] as well as other issues regarding initiating, propagating and terminating tracks [162] that are not specifically referenced in the original GM-PHD paper [133].

In 2007 [134], a filter which propagates not only the PHD but also the entire probability distribution on objects number was derived in closed form and called the cardinalized probability hypothesis density (CPHD). Again, In the vein of the GM-PHD, under the assumption of 'linear Gaussian multitarget model', the Gaussian mixture cardinalized probability

hypothesis density GM-CPHD filter was derived [163, 135], while it was first applied for a ground moving object tracking application with jointly employing digital road maps for road constraint [164].

At this time, large part of the research community have also dealt with the problems of estimating or learning the parameters typical for MOT applications and usually used in both traditional and RFS approaches, such as unknown clutter intensity [165, 166, 167, 168], object birth intensity [160], and detection profile [167]. Also, since both PHD and CPHD have been originally developed such that the newly birth components were induced via a mixture of components, it was significant to provide a relaxation of this assumption supporting the uniform object birth model over the entire space of interest [169]. They have also been extended to multiple models [170], extended objects [171, 172], multiple sensors, superpositional measurements, distributed multi-object filtering, etc. [138].

Already at this early theoretical stages of development of RFS approaches, they have attracted a significant attention in practical applications, such as information fusion in automotive engineering [173]. A performance comparison of PHD and CPHD versus JIPDA was presented in [174].

In addition to the PHD and CPHD filters, Mahler has proposed the multi-object multi-Bernoulli (MeMBer) recursion as a tractable approximation to the Bayes multi-object recursion under low clutter density scenarios [130], which approximately propagates the complete multi-object posterior density rather than only the moments and cardinality distributions. In particular, MeMBer propagates the parameters of a multi-Bernoulli RFS that approximates the posterior multi-object RFS. Since the original MeMBer overestimates the cardinality hence generating bias in the number of objects, cardinality-balanced multi-object multi-Bernoulli (CBMeMBer) filter was proposed by [136]. The first particle filtering implementation as well as GM implementation for ‘linear Gaussian multitarget models’ were presented in [136]. A robust version of an MB filter for adaptive learning of non-homogeneous clutter intensity and detection probability while filtering was proposed in [175]. An early tutorial on Bernoulli filters including the theory, implementation and applications is available in [176].

Afterwards, Vo and Vo [177] claim that the conjugacy is highly desirable in multi-object inference, and hence introduce the conjugate priors for the standard multi-object likelihood function, which are closed under RFS Bayes prediction (Chapman-Kolmogorov equation) and correction (Bayes rule), and refer to the filter as generalized labeled multi-Bernoulli GLMB filter. In particular, if starting with the proposed conjugate initial prior, then all subsequent predicted and posterior distributions have the same form as the initial prior. Some directions and details for efficient implementations were chronologically presented in [178, 179, 180] and [181]. Although in this thesis we do not specifically consider the labeling task, the general MOT algorithms can also involve labels joint to each tracked object. An example which inherently accounts for this possibility is GLMB. It is also worth mentioning that the research on MB filters was also significant from the viewpoint of the practical applications, whereas one of the most advanced autonomous driving-related projects, i.e., autonomous driving at Ulm University, was relying on a GLMB filter implementation [182].

It is also important to mention also that many different SLAM approaches have been developed upon the theory of RFS, including PHD-based [183, 184, 185, 186, 187, 188, 189] and MB-based [190] SLAM approaches.

### 3.1.3 Organization of the chapter

The rest of the chapter is organized as follows. The underlying description of the multi-object Bayes filtering definition with an illustration of the set integral is given in Sec. 3.2. Section 3.3 provides the background of the PHD filter which was as well used in the thesis, and provides the equations for the example of a finite mixture approximation of the PHD in the form of GM-PHD. In Sec. 3.4 we deal with the problem of mixture component number reduction, which appears due to the nature of the PHD correction step when the number of components geometrically increases in each step of the filter. For this purpose several topics such as (i) component distance measure, (ii) component picking strategy and (iii) component merging equations are discussed. The last section (Sec. 3.5.1) represents the overview of existing metrics suitable for a MOT applications.

## 3.2 RANDOM FINITE SETS BASED MULTI-OBJECT BAYES FILTER

In an MOT scenario, at time  $k-1$  the scene might consist of  $N_{k-1}$  objects,  $X_{k-1}^1, \dots, X_{k-1}^{N_{k-1}} \in \mathbb{R}^n$ , whose number is a subject to change due to births and deaths. In turn, the objects give rise to  $M_k$  measurements,  $Z_k^1, \dots, Z_k^{M_k} \in \mathbb{R}^m$ , whose origin is unknown; some objects might not have been detected while some measurements are false alarms. The multi-object approach of [130] addresses this problem by modeling the states and measurements as RFS, which consist of random variables where the set cardinality is also a random variable. More formally at time  $k$

$$\begin{aligned}\mathcal{X}_k &= \{X_k^1, \dots, X_k^{N_k}\} \in \mathcal{F}_{\mathcal{X}} \\ \mathcal{Z}_k &= \{Z_k^1, \dots, Z_k^{M_k}\} \in \mathcal{F}_{\mathcal{Z}},\end{aligned}\tag{3.1}$$

where  $\mathcal{F}_{\mathcal{X}}$  and  $\mathcal{F}_{\mathcal{Z}}$  denote spaces of all finite subsets  $\mathcal{X}$  and  $\mathcal{Z}$ , respectively. The final goal of the multi-object Bayes filtering [130] is to estimate the multi-object posterior probability distribution  $p(\mathcal{X}_k | \mathcal{Z}_k)$  via ‘classical’ Bayes filter form

$$\begin{aligned}p(\mathcal{X}_k | \mathcal{Z}_{1:k-1}) &= \int p(\mathcal{X}_k | \mathcal{X}_{k-1}) p(\mathcal{X}_{k-1} | \mathcal{Z}_{1:k-1}) \delta \mathcal{X}_{k-1} \\ p(\mathcal{X}_k | \mathcal{Z}_{1:k}) &= \frac{p(\mathcal{Z}_k | \mathcal{X}_k) p(\mathcal{X}_k | \mathcal{Z}_{1:k-1})}{\int p(\mathcal{Z}_k | \mathcal{X}_k) p(\mathcal{X}_k | \mathcal{Z}_{1:k-1}) \delta \mathcal{X}_k},\end{aligned}\tag{3.2}$$

where  $\mathcal{Z}_{1:k} = \{\mathcal{Z}_1, \dots, \mathcal{Z}_k\}$  is the history of all the measurements,  $p(\mathcal{X}_k | \mathcal{X}_{k-1})$  is the multi-object Markov transition density which is equivalent to the single state propagation pdf given in (2.3),  $p(\mathcal{Z}_k | \mathcal{X}_k)$  is the multisource likelihood function equivalent to single source measurement model pdf appearing in (2.4) and the integrals in (3.2) are set integrals as defined by the multi-object calculus in [130]. Analytic solution to (3.2) is derived in [177, 178] with generalization to general multi-object densities presented in [180]. However, often utilized are principled approximations among which the PHD filter is an example.

## 3.3 PROBABILITY HYPOTHESIS DENSITY FILTER

The idea of the PHD filter is to propagate the intensity function  $D_k$ , i.e. the first order statistical moment of the multi-object density, in lieu of the multi-object density  $p(\mathcal{X}_k | \mathcal{Z}_{1:k})$



itself. Although there is information loss due to this step, it is outweighed by the gain in alleviating the computational intractability of the multi-object Bayes filter. Function  $D_k$  is not a density function, but is uniquely characterized by the property that given a region  $S$  of single-object space  $\mathcal{X}$  the integral  $\int_S D_k(X) dX$  yields the expected number of objects in  $S$ . Hence, the PHD filter reasons first on the level of group behavior and then attempts to detect and track individual objects only as the quantity and quality of data permits [130].

To present the PHD filter, the following assumptions also need to be used [133, 130]

- Each object evolves and generates independent observations.
- Clutter is Poisson distributed with the corresponding intensity  $\lambda_z$  and independent of object-originated measurements.
- The predicted multi-object  $p(\mathcal{X}_k | \mathcal{Z}_{1:k-1})$  in (3.2) is distributed according to the multi-object Poisson distribution.

Under these assumptions, it can be shown that the posterior intensity can be propagated in time via the PHD recursion, i.e., by evaluating two successive steps — prediction and correction. The prediction is governed by the following equation [130]

$$D_{k+1|k}(X) = b_{k+1}(X) + \int_{\mathcal{X}} p_{S,k+1}(\zeta) p_{k+1|k}(X | \zeta) D_k(\zeta) d\zeta, \quad (3.3)$$

where  $p_{k+1|k}(X | \zeta)$  is single-object Markov transition density,  $p_{S,k}(X)$  is the probability of survival of existing objects given their previous state and  $b_k(X)$  is the object birth intensity. In conjunction, the PHD correction is governed by

$$D_{k+1}(X) = [1 - p_{D,k+1}(X)] D_{k+1|k}(X) + \sum_{Z_{k+1} \in \mathcal{Z}_{k+1}} \frac{p_{D,k+1}(X) p_{k+1}(Z | X) D_{k+1|k}(X)}{\lambda_Z c(Z) + D_{k+1|k}[p_{D,k+1}(X) p_{k+1}(Z | X)]}, \quad (3.4)$$

where  $D_{k+1|k}[f(X)] = \int_{\mathcal{X}} f(X) D_{k+1|k}(X) dX$ ,  $\lambda_Z$  is clutter intensity with its spatial distribution  $c(Z)$ ,  $p_k(Z | X)$  is single-source likelihood function and  $p_{D,k}(X)$  is probability of object detection given its current state. We also make further assumptions that do not necessarily restrict the method just to such scenarios, but serve only for the purposes of the clarity of presentation. For example, note that we have omitted spawning from existing objects, thus (3.3) does not represent a general form of the PHD filter prediction, and we shall also assume that  $p_{D,k}(X) = p_D$  and  $p_{S,k}(X) = p_S$  are constant and independent of the previous object state. We also assume that the spatial distribution of clutter  $c(Z)$  is uniform over the whole measurement space  $\mathcal{Z}$ , since no additional assumptions on the design of the space is induced.

The PHD recursion does not admit closed-form solutions in general [130], however sequential Monte Carlo (SMC) approximations [156] and the Gaussian multi-object model approach based on Gaussian mixtures (GM) [133] render the aforementioned problem soluble. In this thesis, in the vein of [133], we propose an MOT approach as in the vein of [133] and hence for the completeness of the thesis we provide the equations for GM-PHD.

### 3.3.1 Gaussian Mixture PHD filter

We now continue by providing equations of the PHD recursion. Under certain assumption which is in the literature referred to as ‘linear Gaussian multi-target model’ [133], the PHD recursion (3.3)-(3.4) admits a closed form solution. However, for the completeness of presentation of the background material of the thesis here we consider an extension to nonlinear object models in the vein of a single-object EKF filter denoted EK-PHD. In particular, the ‘linear Gaussian multi-target model’ assumes each object follows a motion following the linear Gaussian dynamical model and the linear Gaussian measurement model given as

$$f(x_{k|k-1}) = \mathcal{N}(F_{k-1}x_{k-1}, Q_{k-1}) \quad (3.5)$$

$$h(z_k|x_k) = \mathcal{N}(H_k x_k, R_k), \quad (3.6)$$

where  $F$  is a state transition matrix, while  $H$  is the observation matrix of a linear system. However, we use a relaxed version appropriate for more general nonlinear model where

$$x_k = f(x_{k-1}, w_{k-1}) \quad (3.7)$$

$$z_k = h(x_k, v_k), \quad (3.8)$$

where  $f$  and  $h$  are nonlinear propagation and measurement functions, respectively, while  $w$  and  $v$  are process and measurement noises.

Lets assume that the posterior intensity at time  $k$  is a GM of the form

$$D_{k-1}(X) = \sum_{i=1}^{J_{k-1}} w_{k-1}^i \mathcal{N}_{k-1}^i(X), \quad (3.9)$$

where  $w_{k-1}^i$  is the weight of the  $i$ -th component of the mixture joint to distribution  $\mathcal{N}_{k-1}^i = \mathcal{N}(\mu_{k-1}^i, \Sigma_{k-1}^i)$ . Given this assumption, and after employing (3.3) and (3.7), the predicted intensity  $D_{k|k-1}(X)$  is under linearization given as GM

$$D_{k|k-1}(X) = \sum_{i=1}^{J_k^b} w_k^{b,i} \mathcal{N}_k^{b,i}(X) + \sum_{i=1}^{J_{k|k-1}^s} w_{k|k-1}^{s,i} \mathcal{N}_{k|k-1}^i(X), \quad (3.10)$$

where  $w_{k|k-1}^{s,i} = p_s w_{k-1}^i$  and  $J_{k|k-1}^s = J_{k-1}$ . The first sum of the term (3.10) brings in the newly born components, while the second one describes the survived objects. A component  $\mathcal{N}_{k|k-1}^i$  represents the component resulting after applying the EKF prediction on  $\mathcal{N}_{k-1}^i$ . The predicted number of objects can be calculated by taking the integral of (3.10) over the entire state space  $\mathcal{X}$

$$N_{k|k-1} = \sum_{i=1}^{J_k^b} w_k^{b,i} + \sum_{i=1}^{J_{k|k-1}^s} w_{k|k-1}^{s,i}. \quad (3.11)$$

At this point we have finished the less complex prediction step, whereas now we shall move on to the correction which appears to be slightly more involved. The key steps of the prediction of EK-PHD filter are summarized in Alg. 1, where the function  $\text{PRED}(\cdot)$  denotes the EKF prediction.

---

**Algorithm 1:** The prediction step of the EK-PHD filter
 

---

**Require:**  $\{w_{k-1}^i, \mathcal{N}_{k-1}^i\}_{i=1}^{J_{k-1}}, \{w_k^{b,i}, \mathcal{N}_k^{b,i}\}_{i=1}^{J_k^b}, p_S$

- 1:  $j \leftarrow 0$  (*initialization*)
- 2: **for**  $i := 1$  to  $J_k^b$  (*# of newly born components*) **do**
- 3:    $w_{k|k-1}^j \leftarrow w_k^{b,i}; \mathcal{N}_{k|k-1}^j \leftarrow \mathcal{N}_k^{b,i}; j \leftarrow j + 1$
- 4: **end for**
- 5: **for**  $i := 1$  to  $J_{k-1}$  (*# of components existing at k*) **do**
- 6:    $w_{k|k-1}^j \leftarrow p_S w_{k-1}^i; \mathcal{N}_{k|k-1}^j \leftarrow \text{Pred}(\mathcal{N}_{k-1}^i); j \leftarrow j + 1$
- 7: **end for**
- 8:  $J_{k|k-1} \leftarrow j$  (*# of predicted components*)
- 9: **return**  $\{w_{k|k-1}^i, \mathcal{N}_{k|k-1}^i\}_{i=1}^{J_{k|k-1}}$

---

Assuming that the predicted intensity at time  $k$  is a GM of the form

$$D_{k|k-1}(X) = \sum_{i=1}^{J_{k+1|k}} w_{k|k-1}^i \mathcal{N}_{k|k-1}^i(X), \quad (3.12)$$

after employing (3.4), the corrected intensity  $D_k(X)$  is given as

$$D_k(X) = (1 - p_D) \sum_{i=1}^{J_{k|k-1}} w_{k|k-1}^i \mathcal{N}_{k|k-1}^i(X) + \sum_{i=1}^{J_{k|k-1}} \sum_{j=1}^{M_k} w_k^{i,j} \mathcal{N}_k^{i,j}(X). \quad (3.13)$$

where

$$w_k^{i,j} = \frac{p_D w_{k|k-1}^i q_k^{i,j}(Z)}{\lambda_Z c(Z) + p_D \sum_{l=1}^{J_{k|k-1}} w_{k|k-1}^l q_k^{l,j}(Z)}, \quad (3.14)$$

$$q_k^{i,j}(Z) = \mathcal{N}(Z_k^j; h(\mu_{k|k-1}^i), \mathcal{S}_k^{i,j}), \quad (3.15)$$

$$\mathcal{S}_k^{i,j} = \mathcal{H}_k^{i,j} \Sigma_{k|k-1}^{i,j} \mathcal{H}_k^{i,jT} + R_k, \quad (3.16)$$

while  $\mathcal{N}_k^{i,j} = \mathcal{N}(\mu_k^{i,j}, \Sigma_k^{i,j})$  denotes the result of EKF-like update of  $i$ -th predicted component with  $j$ -th measurement. Finally, the corrected number of objects can be calculated by taking the integral of (3.13) over the entire state space  $\mathcal{X}$

$$N_k = (1 - p_D) \sum_{i=1}^{J_{k|k-1}} w_{k|k-1}^i + \sum_{i=1}^{J_{k|k-1}} \sum_{j=1}^{M_k} w_k^{i,j}. \quad (3.17)$$

The key steps of the correction of EK-PHD filter are summarized in Alg. 2, where the function  $\text{INNOV}(\cdot)$  denotes the EKF innovation evaluation, function  $\text{CORRECT}(\cdot)$  represents the EKF correction of mean and covariance, and  $\text{REDUCTION}(\cdot)$  represents the execution of mixture reduction algorithm.

### 3.4 MIXTURE COMPONENT REDUCTION

During the recursion process of the PHD filter the number of components inevitably increases; first due to inclusion of newly birthed, or in some applications spawned, components



**Algorithm 2:** The correction step of the EK-PHD filter

---

**Require:**  $\{w_{k|k-1}^i, \mathcal{N}_{k|k-1}^i\}_{i=1}^{J_{k|k-1}}, \{Z_k^j \in \mathcal{Z}_k\}_{j=1}^{M_k}, p_D$

- 1: **for**  $i := 1$  to  $J_{k|k-1}$  (*non-detected components*) **do**
- 2:    $w_k^i \leftarrow (1 - p_D) w_{k|k-1}^i; \mathcal{N}_k^i \leftarrow \mathcal{N}_{k|k-1}^i$
- 3: **end for**
- 4:  $j \leftarrow 0$  (*measurement designator*)
- 5: **for all**  $Z_k \in \mathcal{Z}_k$  **do**
- 6:    $j \leftarrow j + 1, s^j \leftarrow 0$  (*per measurement intensity*)
- 7:   **for**  $i := 1$  to  $J_{k|k-1}$  (*detected components*) **do**
- 8:      $l \leftarrow i + j J_{k|k-1}$
- 9:      $[q_k^{i,j}(Z)] \leftarrow \text{INNOV}(\mathcal{N}_{k|k-1}^i, Z_k^j)$
- 10:      $w_k^l \leftarrow p_D w_{k|k-1}^i q_k^{i,j}(Z), s^j \leftarrow s^j + w_k^l$
- 11:      $\mathcal{N}_k^l \leftarrow \text{CORRECT}(\mathcal{N}_{k|k-1}^i, Z_k^j)$
- 12:   **end for**
- 13:   **for**  $i := 1$  to  $J_{k|k-1}$  (*re-weighting*) **do**
- 14:      $w_k^{i+j J_{k|k-1}} \leftarrow w_k^{i+j J_{k|k-1}} / (\lambda_{Z^j}(Z) + s^j)$
- 15:   **end for**
- 16: **end for**
- 17:  $J_k \leftarrow (j + 1) J_{k|k-1}$  (*# of components existing at k*)
- 18:  $\{w_k^{i,R}, \mathcal{N}_k^{i,R}\}_{i=1}^{J_k^R} \leftarrow \text{REDUCTION}(\{w_k^i, \mathcal{N}_k^i\}_{i=1}^{J_k})$
- 19: **return**  $\{w_k^{i,R}, \mathcal{N}_k^{i,R}\}_{i=1}^{J_k^R}$

---

and second due to the nature of the PHD correction step. Namely, correcting the predicted mixture by multiple measurements results in a geometrical increase in the component number, which can be seen from (3.13). Given that, component number reduction schemes are necessary [133]. Since this procedure is executed practically at each iteration, it should be computationally modest, but still keep a reasonable level of accuracy. Reduction procedures basically require three ingredients: (i) a component distance measure, (ii) a component picking algorithm and (iii) component merging equations.

#### 3.4.1 Component distance measure

The distance measure is a key ingredient in the reduction scheme and although numerous distance measures between distributions exist, motivated by to practical and theoretical aspects we concentrate on those appropriate for finite mixtures. Statistically and information theoretically motivated distance measure is the Kullback–Leibler (KL) distance, also known as the Kullback–Leibler divergence or the relative entropy [191], and defined as

$$D_{\text{KL}}(p, q) = \int_{\mathcal{X}} p(x) \log \left( \frac{p(x)}{q(x)} \right) dx.$$

It belongs to a wider class of distance measures called f-divergences or Ali-Silvey distances [192]. Another statistical and information theoretical class of generalized distances are Rényi

$\alpha$ -divergences [193] given by the following expression

$$D_R^{(\alpha)}(p, q) = \frac{1}{\alpha - 1} \log \int_{\mathcal{X}} p(x)^\alpha q(x)^{1-\alpha} dx$$

and parametrized by real parameter  $\alpha$ . In the limit  $\alpha \rightarrow 1$ , the Rényi  $\alpha$ -divergence yield the KL distance. Another well-established distance measure when  $\alpha = 1/2$  is called the Bhattacharyya distance [194]. However, given the discussion presented in [195], we rely our approaches on KL divergence and hence continue with further discussion on it.

#### 3.4.2 Symmetrized Kullback-Leibler divergence

Furthermore, since the mixtures of distributions appearing in PHD are weighted, in order to be used here, the measure needs to be customized for weighted (unnormalized) distributions, and additionally symmetrized. Since scaled symmetrized Rényi  $\alpha$ -divergences neglect the respective weights of components, for the purpose we consider the scaled symmetrized KL distance [195]. The distance measure between pdfs  $p$  and  $q$ , with their respective weights  $w_p$  and  $w_q$ , is then given as [192]

$$D_{sKL}(w_p p, w_q q) = \frac{1}{2} [w_p D_{KL}(p, q) + w_q D_{KL}(q, p)] + \frac{1}{2} (w_p - w_q) \log \frac{w_p}{w_q}. \quad (3.18)$$

▷ VON-MISES DISTRIBUTIONS. The equations for reducing the number of the components in a mixture of von Mises distributions is presented in [195]. For the completeness of the thesis we also provide the equations herein. Given two vMpdfs  $p(\mu_p, \kappa_p)$  and  $q(\mu_q, \kappa_q)$ , the KL distance is given as

$$D_{KL}(p, q) = \log \frac{I_0(\kappa_q)}{I_0(\kappa_p)} + A(\kappa_p)(\kappa_p - \kappa_q \cos(\mu_p - \mu_q)). \quad (3.19)$$

where  $A(x) = I_1(x)/I_0(x)$  with  $I_p(x)$  as the the modified Bessel function of the first kind and of order  $p$ .

▷ GAUSSIAN DISTRIBUTIONS. Given two Gaussian distribution pdfs,  $p(\mu_p, \Sigma_p)$  and  $q(\mu_q, \Sigma_q)$ , the KL distance is evaluated as

$$D_{KL}(p, q) = \frac{1}{2} \left\{ \text{tr}[(\Sigma_q)^{-1} \Sigma_p] - K + \log_{\mathbb{R}} \frac{|\Sigma_q|}{|\Sigma_p|} + (\mu_q - \mu_p)^T (\Sigma_q)^{-1} (\Sigma_q - \Sigma_p) \right\}, \quad (3.20)$$

where  $\text{tr}(\cdot)$  and  $|\cdot|$  designate matrix trace and determinant, respectively, while  $K$  is the mean vector dimension.

#### 3.4.3 Component picking strategy

With having defined the appropriate distance measure between the distributions we can now employ the component picking algorithm which will tell us how to screen the whole mixture and which components to pick for merging. Here we will consider two component picking strategies interesting from the practical viewpoint, i.e., (i) Exhaustive pairwise [196], and (ii)

West's [197] algorithms. The Exhaustive pairwise algorithm determines distances between all components and merges the closes two, while West's algorithm sorts the components according to their respective weights, then finds and merges the component most similar to the first one. The resulting component is then inserted back to the mixture with respect to its weight and the procedure is repeated until the desired number of components is reached.

#### 3.4.4 Component merging equations

▷ VON-MISES DISTRIBUTIONS. The merged vM component has the optimal parameters in the KL sense obtained by following

$$\begin{aligned}\mu^* &= \arctan \frac{w_p A(\kappa_p) \sin \mu_p + w_q A(\kappa_q) \sin \mu_q}{w_p A(\kappa_p) \cos \mu_p + w_q A(\kappa_q) \cos \mu_q} \\ w^* A^2(\kappa^*) &= w_p^2 A^2(\kappa_p) + 2w_p w_q A(\kappa_p) A(\kappa_q) \cos(\mu_p - \mu_q),\end{aligned}\tag{3.21}$$

where  $w^* = w_i + w_j$ , while  $w^*, \mu^*$  and  $\kappa^*$  designate the parameters resulting from the component merging procedure.

▷ GAUSSIAN DISTRIBUTIONS. Given several Gaussian distributions the component merging equations follow as [196]

$$\begin{aligned}w^* &= \sum_i w_i, & \mu^* &= \frac{1}{w^*} \sum_i w_i \mu_i \\ \Sigma^* &= \frac{1}{w^*} \sum_i w_i [\Sigma_i + \mu_i (\mu_i)^T] - \mu^* (\mu^*)^T\end{aligned}\tag{3.22}$$

where  $w^*, \mu^*$  and  $\Sigma^*$  designate the parameters resulting from the component merging. Although (3.22) works for an arbitrary number of components, in our case we will always merge just two components.

An example of the pseudocode of the merging algorithm using West's picking strategy and Gaussian distribution is given in Algorithm 3.

### 3.5 METRICS FOR EVALUATION

The metric for evaluating the MOT algorithm needs to account for various appearances in contrary to the single-object estimation where it is typically adequate to involve only a miss distances as the Euclidean or Mahalanobis distance. The MOT performance metric needs to involve measures of effectiveness (MoEs) such as missing tracks, false tracks, state estimation error (position, velocity, heading), track initiation delay, track overshoot, track label swaps, cardinality estimation, and is alongside strongly scenario and operation dependent. The problem of choosing MoEs is questionable from two viewpoints; (i) how to choose the relevant MoEs since it is fairly arbitrary and far from clear and (ii) which choice is adequate from the theoretical point of view, since MoEs can be correlated.

Since the performance evaluation approaches are strongly application dependent, it is hard to establish an adequate generic MOT evaluation framework that will embrace all the previously introduced MoEs. For this reason, here we focus our overview on popular

---

**Algorithm 3:** Mixture reduction using West's algorithm
 

---

**Require:**  $\mathcal{P} = \{w_i, \mathcal{N}_i\}_{i=1}^J$

- 1: *(Order set  $\mathcal{P}$  ascending by weights)*  
 $\mathcal{P} \leftarrow \{\mathcal{P} : w_i \leq w_j, i < j, i, j \in \{1, 2, \dots, |\mathcal{P}|\}\}$
- 2: **while**  $|\mathcal{P}| > N$  **do**
- 3:   **for**  $i = 2 : |\mathcal{P}|$  **do**
- 4:      $d(i) \leftarrow D_{\text{sKL}}(w_1 \mathcal{N}_1, w_i \mathcal{N}_i)$  calculate via (3.18)
- 5:   **end for**
- 6:    $j \leftarrow \arg \min_{i \in \{2, 3, \dots, |\mathcal{P}|\}} d(i)$
- 7:   *(Remove components 1 and j)*  
 $\mathcal{P} \leftarrow \mathcal{P} \setminus \{w_i, \mathcal{N}_i\}_{i=1, j}$
- 8:    $w^*, \mathcal{N}^* \leftarrow$  calculate via (3.22)
- 9:   *(Insert the merged component by weight)*  
 $\mathcal{P} \leftarrow \mathcal{P} \cup \{w^*, \mathcal{N}^*\}$
- 10: **end while**
- 11: **return**  $\{w_{i,R}, \mathcal{N}_{i,R}\}_{i=1}^{J_R}$

---

approaches that tempt to provide the generic physically intuitive and information-theoretic consistent metrics. These metrics are more suitable in cases where a ground truth data is available, which is most often the case for experiments provided on synthetic data. The alternative would include the algorithm-free metrics [198] that focus on different MoEs, but unfortunately merely one-at-the-time. The application dependent metrics have also been in the focus of recent research [199] (including CLEAR metrics [200], CLEAR MOT metrics [201], MOTA/MOTP [199]), but since we look for more general metrics, such are application dependent possibilities are not considered here.

One of the seminal works proposing the MOT performance metric is the Optimal Mass Transfer (OMAT) metric [202]. It is based on the Wasserstein distance and resolves some issues of the Hausdorff metric, such as the insensitivity to differences in the cardinality of the estimator as an important performance measure. However, several weaknesses of OMAT, such as its inability to operate with empty sets, have been addressed and resolved afterwards in [203]. This new metric is called OSPA and has comprehended both the spatial distance measure and the cardinality estimation. OSPA also provides a framework for penalizing the appearance of multiple estimates for a single object. The problem at hand, where two sets are collections of tracks and not collections of vectors is deeply addressed in [204], proposing a metric called the ‘OSPA metric for track’ (OSPAT). This metric further accounts for the distance violation related to the mislabelling, which is of vital significance in variety of MOT applications. A work presented in [205] has gone further solving a few more issues resulting in ‘OSPA for multiple tracks’ (OSPAMT). It aims at providing the framework such that the resulting metric, which is the sum of spatial distance and label distance, does not violate the triangle inequality. Furthermore, it discusses the redefinition of optimal assignment of pairs of tracks between two sets that more directly addresses the MOT problem.

### 3.5.1 Metric definition

Let us define a metric space  $(\mathcal{X}, \mathcal{D})$ , where function  $\mathcal{D} : \mathcal{X} \times \mathcal{X} \rightarrow \mathbb{R}_+ = [0, \infty)$  is a metric that satisfies the following three axioms for all  $X, Y, Z \in \mathcal{X}$

1. *Identity*:  $\mathcal{D}(X, Y) = 0$  if and only if  $X = Y$ .
2. *Symmetry*:  $\mathcal{D}(X, Y) = \mathcal{D}(Y, X)$ .
3. *Triangle inequality*:  $\mathcal{D}(X, Y) \leq \mathcal{D}(X, Z) + \mathcal{D}(Z, Y)$ .

Upon that, the metric should be incorporating physical meaning and employing relevant MoEs for MOT problem.

### 3.5.2 Optimal subpattern assignment

Let  $d^c(x, y) \triangleq \min(c, d(x, y))$  be the distance between  $x, y \in W$ ,  $W \in \mathbb{R}^N$ , cut off at  $c > 0$ . Let further  $\Pi_k$  be the set of permutations on  $\{1, 2, \dots, k\}$  for any  $k \in \mathbb{N} = \{1, 2, \dots\}$ . For  $1 \leq p < \infty$  and arbitrary subsets  $X = \{x_1, \dots, x_n\}$  and  $Y = \{y_1, \dots, y_m\}$  of  $W$ , where  $m \leq n$ ,  $m, n \in \mathbb{N}_0$ , define the following

$$\mathcal{D}_p^c(X, Y) \triangleq \left( \frac{1}{n} \left( \min_{\pi \in \Pi_n} \sum_{i=1}^m d^c(x_i, y_{\pi(i)})^p + c^p(n-m) \right) \right)^{\frac{1}{p}} \quad (3.23)$$

and if  $m > n$ ,  $\mathcal{D}_p^c(X, Y) \triangleq \mathcal{D}_p^c(Y, X)$ . Furthermore, for  $p \rightarrow \infty$

$$\mathcal{D}_\infty^c(X, Y) \triangleq \begin{cases} \min_{\pi \in \Pi_n} \max_{1 \leq i \leq n} d^c(x_i, y_{\pi(i)}) & \text{if } m = n \\ c & \text{if } m \neq n \end{cases}. \quad (3.24)$$

The function  $\mathcal{D}_p^c$  is called the OSPA metric of order  $p$  and cut off  $c$ . It is interesting to mention that OSPA satisfies the metric definition conditions, and a formal proof is given in [203]. OSPA is shown to eliminate some shortcomings of OMAT as follows:

- *Consistency*. The OSPA metric penalizes relative differences in cardinality by introducing an additive component on top of the average distance.
- *Intuitive construction*. The OSPA construction eliminates any element of arbitrariness by providing an objective and intuitively reasonable criterion for the assignment, while at the same time observing the metric axioms.
- *Geometry dependence*. For a given  $c$  and  $p$ ,  $\mathcal{D}_p^c$  distance does not substantially depend on the size of the ground truth pattern.
- *Cardinality zero*. The OSPA metric is defined between any two point patterns.
- *Compatibility with mathematical theory*. The OSPA generates the vague topology on the space of finite point patterns on  $W$ , which is the standard topology used in point process theory.

The OSPA metric can be computed efficiently by using the Hungarian or Munkres methods for optimal assignment, which is by theoretical complexity just as good as OMAT.

The combined localization and cardinality error represented by the OSPA metric conceals the reason for the large distance, whence the metric may be split up into a localization and cardinality error

$$\mathcal{D}_p^{c,\text{loc}}(X, Y) \triangleq \left( \frac{1}{n} \min_{\pi \in \Pi_n} \sum_{i=1}^m d^c(x_i, y_{\pi(i)})^p \right)^{\frac{1}{p}} \quad (3.25)$$

$$\mathcal{D}_p^{c,\text{card}}(X, Y) \triangleq \left( \frac{1}{n} c^p(n - m) \right)^{\frac{1}{p}}. \quad (3.26)$$

Although this is not a metric on the space of finite subsets any more, it can be interpreted as error measures due to localization only and cardinality only (penalized at maximal distance).

For object tracking, however, we often require a metric on the space of finite sets of tracks, where a track has been defined as a labeled temporal sequence. For such requirements the OSPA metric does not provide the full support, hence its extensions have come to the focus of consideration for the MOT research. This extensions need to be directed towards incorporation of information about track continuity or switching of track labels. However, since we do not consider the labeling problem specifically, we chose original OSPA as an adequate metric for our applications of interest.

## The main scientific contributions of the thesis

THE four original contributions of the thesis essentially revolve about probabilistic methods in estimation and multiple moving objects tracking relying on the models of uncertainty respecting the pertaining geometry of the system described using Lie groups. The first and the last contributions of the thesis deal with the problem of multiple moving objects tracking when the state arises on non-Euclidean manifold [Pub1, Pub7, Pub8]. The second and third contributions deal with the problem of estimation in the space of the special Euclidean group [Pub2, Pub3, Pub4, Pub5], the extended information filter tailored for the geometry of matrix Lie groups [Pub6]. The discussion on contributions follows in the sequel.

### *#1 Method for multiple moving objects tracking on the unit sphere based on the von Mises distribution and the random finite sets*

The state of the system can generally appear to be non-Euclidean which with all the usual issues makes the MOT problem even more complex. In particular, most of the MOT approaches somehow rely on the Bayesian recursion and although there is nothing intrinsic in this concept, it is a real challenge to develop a computationally tractable solution for the non-Euclidean geometries. Firstly, it is challenging to solve the Chapman–Kolmogorov equation (Bayesian prediction) in closed form, such that it results with the same type of distribution as the beginning one. Secondly, given a distribution associated to a predicted value and employing a measurement likelihood, it is challenging evaluate the Bayes rule (Bayesian update) hopefully again obtaining the same type of distribution.

The  $\nu\text{M}$  is an example of directional distribution defined on the unit circle and as such captures the geometry of the state space in a global manner. Given two  $\nu\text{M}$ s, the convolution integral of Bayesian prediction does have an exact solution, but the result is not a  $\nu\text{M}$  distribution. However, the resulting distribution can be well-approximated with another  $\nu\text{M}$  based on circular moment matching. The update step on the other hand exhibits a  $\nu\text{M}$  distribution without approximations.

The first contribution deals with the MOT task on the unit circle, based on the PHD filter which represents an approximation of the optimal multi-object Bayes filter developed upon the theory of RFS. We particularly derive a closed-form recursion of the PHD filter yielding a finite  $\nu\text{M}$  mixture approximation ( $\nu\text{M}$ -PHD) [Pub1]. The  $\nu\text{M}$ -PHD is compared to the GM-PHD on a synthetic dataset of 100 randomly generated multi-object scenarios and

on the real-world PETS<sub>2009</sub> dataset, and achieved respectively a decrease of 10.5% and 2.8% in the OSPA metric.

### *#2 Method for moving object tracking in the space of the special Euclidean group based on the extended Kalman filter on Lie groups*

Lie groups are natural ambient spaces for description of the dynamics of rigid body mechanical systems. A common state space representation of a rigid body object pose is the one using semi-direct product of the SO group for orientation and the Euclidean translation vector, yielding the 2D and 3D counterparts denoted SE(2) and SE(3). Although development of a convenient distribution defined directly on an SE group represents a significant research goal, so far there does not exist such solution suitable for employment in the standard Bayesian framework. Hence, the global approach used for development of the first contribution is not possible when the underlying state space is SE rather than the simple unit circle. The CGD is a distribution with parameters which partially combine both worlds, including a mean value defined on a Lie group and the uncertainty described with the Gaussian variance in the Euclidean world arising as a tangent space at the mean value.

The research respecting this contribution begins with the consideration of special orthogonal group SO(2) and emulation of the constant acceleration model used within LG-EKF, and was applied for the problem of speaker tracking with a microphone array [Pub2]. An important concluding remark of [Pub2] is that application of SO(2) group within LG-EKF yields the same result as heuristically wrapping the angular variable within the EKF framework which is due to commutativity of this group. Next, we continued with the research on pose estimation employing the SE(2) group and emulating the constant velocity model used within LG-EKF suitable for tracking of an omnidirectional motion [Pub3]. By using this modeling approach we inherently account for the nature of coupling between the rotation and translation parts of SE group. In accordance, association of uncertainty to an SE(2) group exhibits more flexibility, i.e., supports the banana shaped forms of uncertainty contours, rather than only elliptical contours. When compared to the classical constant velocity KF/EKF in a omnidirectional motion tracking application, the proposed filter outperforms the classical approach for a wide range of acceleration change intensities. Finally, we developed the constant acceleration model within LG-EKF framework for the full body human motion estimation employing SO(2), SO(3) and SE(3) groups, by relying on 3D marker position measurements in [Pub4] and inertial measurement units in [Pub5]. In both cases we provided derivation of the LG-EKF recursion for the articulated motion estimation. Detailed derivation of accelerometer based update is given in supplementary material [\*Pub5]. We compared the performance of the proposed approaches with the Euler angles-based EKF, and showed that these algorithms achieve better performance in both simulations and real-world experiments.

### *#3 Extended information Kalman filter for state estimation on matrix Lie groups*

The IF is the dual of the classical KF, and is the subject of the same assumptions underlying the KF. Whereas the KF is represented by mean and covariance, the IF relies on the parametrization consisting of an information matrix and an information vector. Probably the simplest



advantage of the IF is recognized in the update step when number of measurements is larger than state space size, while the opposite applies for the KF.

Although IFs have been successfully applied in a number of applications facing large number of measurements, features or demanding a decentralized filter form, a quite prominent example of an application where the need arises for computational benefits of the IF is SLAM. Additionally, in SLAM applications the need arises for the geometric accuracy of Lie groups as well. The earliest SLAM solutions were based on the EKF, which turned out being inadequate approach due to limitations in maps size, hence EIF soon became widely accepted for SLAM and reached its zenith with SEIF and ESDSF. However, the pose in SLAM usually conforms the variables arising on  $SE(3)$  groups, and therefore in some recent solutions it was determined that the approximation in state space geometry represents a significant cause of error, and the new approaches accounting for this geometry were developed. However, these SLAM solutions exclusively relied on graph optimization approaches since no filtering approaches in the form of IF on Lie groups were available.

As a third contribution, the extended information filter on matrix Lie groups (LG-EIF) is proposed [Pub6]. We provided the theoretical development of the LG-EIF recursion equations and the applicability of the proposed approach is demonstrated on a rigid body attitude tracking problem with multiple sensors. We particularly compared the proposed LG-EIF to an EIF based on Euler angles, and analyzed its computational complexity regarding the multisensor update with respect to the LG-EKF. The results showed that the proposed filter achieves higher performance consistency and smaller error by tracking the state directly on the Lie group and that it keeps smaller computational complexity of the information form with respect to large number of measurements.

#### *#4 Method for multiple moving objects tracking on Lie Groups based on the concentrated Gaussian distribution and the random finite sets*

While the first contribution deals with a global approach to MOT problem [Pub1] as a long-term goal for nearly any non-Euclidean probabilistic application, many MOT applications deal with objects and measurements whose state space is non-Euclidean and is often more complex than a simple unit circle. Furthermore, both (i) diverse traditional engineering disciplines (intelligence, surveillance, air traffic control, resident space objects tracking) and (ii) some modern engineering fields (autonomous systems and robotics) deal with the objects described with their pose including the orientation variables, which instantly defines their non-Euclidean nature. Many of those applications can successfully rely on Lie group representation of the tracked objects, particularly employing either SE group, and the filtering approach presented as part of the second contribution. Now, when put into MOT context several additional questions arises.

As the first part of this contribution we proposed to use a solution based on the JIPDA filter, which was shown to be derived within the RFS framework (as part of the family of JPDA-like approaches). Our MOT solution uses a modified JIPDA filter suitable for operation on matrix Lie groups [Pub7]. In particular, the probabilities of each event of the filter do not reason over the space of the variable itself, but rather in the tangent Lie algebra space associated to the predicted state of some considered object. Only after the innovation vector is determined,

we use the addition operator, which on the group appears as matrix multiplication, and hence update the considered object state. The proposed approach is tested using a real-world dataset collected in urban traffic scenarios with the multisensor setup consisting of a radar and a stereo camera mounted on top of a vehicle. The uncertainties of sensors were modeled in polar coordinates on Lie Groups, while the states were represented with  $SE(2)$  groups.

As the second part of this contribution we proposed a mixture approximation of the PHD filter tailored for matrix Lie groups, denoted LG-PHD. It is based on the mixture of CGDs, and as any PHD filter, it inherently faces the problem of an ever increasing number of mixture components. For this purpose, the growth of components must be controlled by approximating the original mixture with the mixture of a reduced size. As part of the thesis we propose a reduction approach for mixture of CGDs. This entails appropriate reparametrization of CGD parameters to compute the KL divergence, and pick and merge the CGD mixture components. Since reparametrization of two different components requires choosing the appropriate tangent space, we also provide an extensive analysis on the choice thereof. Detailed derivation of the LG-PHD is given in supplementary material [\*Pub8]. We compared the performance of LG-PHD filters relying on different choices of tangent space using the OSPA metric.

## Conclusions and future work

AUTONOMOUS navigation represents a highly disruptive technology that will certainly change the way people live and behave, and transform the work practices raising the efficiency and safety in different types of services. A problem of multiple moving objects tracking has been the focus of different research studies for several decades and represents an essential feature in the autonomous navigation task. Still, the ‘tracking research community’ in majority of applications approach this problem by neglecting the non-Euclidean state space geometry of typically tracked objects, and usually assume the underlying statistics follow a ‘classical’ Gaussian distribution.

### 5.1 THE MAIN CONCLUSIONS OF THE THESIS

This thesis considers the MOT task by emphasizing the problem of the geometry of the state space associated to tracked objects and employed measurements, especially from the viewpoint of uncertainty description. The problem of associating uncertainty to different non-Euclidean geometries is herein considered in the twofold manner; first by using the statistics which globally captures geometry, and second by using an uncertainty description which locally accounts for it. However, the estimation approaches capable of accounting for a global geometry of the non-Euclidean ambient space represent an ultimate goal.

One part of the thesis dealt with the MOT problem when the underlying state and measurement space was a direction/a unit circle. This approach was based on the  $\nu$ M distribution which is defined directly on the space of interest. Since given two  $\nu$ Ms, the convolution integral of Bayesian prediction can be approximated with another  $\nu$ M, and since Bayesian update given two  $\nu$ Ms results explicitly with another  $\nu$ M, we could proceed with development of the MOT solution. The main challenge when applying this distribution in a MOT application was to account for many additional statistical appearances that do not exist in an estimation-only task. The thesis started by developing a method for directional MOT application and derivation of a novel mixture approximation of the PHD filter tailored specifically for the system on the unit circle ( $\nu$ M-PHD). The resulting filter required some principled approximations to achieve closed-form and ensure numerical stability. The conclusion respecting the optimal subpattern assignment metric is that globally accounting for the circular geometry of the state space can significantly boost accuracy of MOT applications arising on this type of manifold.

Although the global uncertainty description seems to be attractive, its practical applica-

bility is often very limited. For this purpose, next part of the thesis dealt with the description of dynamics of a rigid body mechanical system representing its pose with the special Euclidean group (SE) and orientation with the special orthogonal group (SO). The uncertainty was associated to these Lie groups relying on the concept of CGD, parametrized with the mean value on the group and the Gaussian variance in the Euclidean space obtained as a tangent space at the mean value. As part of this research we studied several models on Lie groups employed in different applications, including alternatives to Euclidean space based constant velocity and constant acceleration models but this time arising on Lie groups.

Before proceeding with different motion models, as probably the simplest Lie group representative, we studied the  $SO(2)$  group by analyzing it in the context of the mathematically grounded framework of LG-EKF. We have shown that the similar result is obtained by heuristically wrapping the EKF. This result did not seem unexpected given that  $SO(2)$  is abelian, i.e., commutative, but gives an interesting theoretical perspective on estimation and tracking with the heuristically modified EKF. On the other hand, it was shown that employment of  $SE(2)$  group in the case when rotational dynamics exists can significantly boost the quality of estimation. In particular, when both dynamics in translation and rotation induce the system it is more appropriate to use a constant velocity model on  $SE(2)$  than the EKF based constant velocity and turn rate model or the linear KF based constant velocity model. As part of the thesis we further combined  $SE(3)$ ,  $SO(2)$  and  $SO(3)$  Lie group representatives in a novel algorithms for the full body human motion estimation based on (i) body worn marker position measurements and (ii) inertial measurement units. The human joints were described with  $SO(2)$  or  $SO(3)$  groups depending on the number of dofs, while the initial joint representing the connection of the body with the world reference frame was represented with an  $SE(3)$ . The motion was assumed to follow the constant acceleration model within the LG-EKF framework. We evaluated the performance of the proposed methods on both simulation and real-world motion capture data, comparing it with the Euler angles-based EKF, and additionally with the commercial software Vicon IK when dealing with marker measurements. It was shown that the LG-EKF-based solutions improve estimation for highly dynamic motions and are not affected by gimbal lock.

Next, the thesis deals with the problem of estimation on matrix Lie groups when it may be adequate to apply an information form. Given the advantages of the IF form and dealing with filtering on Lie groups, a natural question on casting the LG-EKF in the information form while keeping its additivity and computational advantages arises. We proposed a new state estimation method which embedded the LG-EKF with an EIF form for non-linear systems, thus endowing the filter with the information forms advantages, while keeping the accuracy of the LG-EKF for stochastic inference. The filter was tested on the problem of rigid body attitude tracking assuming a constant velocity model with multiple sensors. The results have shown that the filter can accurately track the attitude and exhibits lower RMSE with respect to the Euler angles based EIF, and keeps the computational advantages of the update step with respect to the LG-EKF.

Finally, two solutions to the MOT problem for the system arising on Lie groups were proposed in the thesis. The first one was based on the JIPDA filter, and modified such that it is able to operate on Lie groups, hence reasoning about probabilities and the combined innovation vector in the tangential Lie algebra space. The proposed MOT approach was

tested in an advanced driver assistance system application on a real-world dataset collected using a radar and a stereo camera mounted on top of a vehicle. The stereo camera estimated relative displacement of the vehicle, using stereo visual odometry, generating measurements as cluster centers of optical flow vectors not conforming to the estimated motion. The radar directly reported its measurements to the filter, thus complementing the stereo camera measurements. Both radar and stereo camera were modeled as polar sensors, while the vehicle state resided on  $SE(2)$  group, thus enabling more reliable model of uncertainties supporting the banana-shaped contours, in contrast to elliptical uncertainty contours given by the ‘classical’ Gaussian distribution.

We have also developed the PHD filter tailored for the topology of Lie groups (LG-PHD), and studied the problem of manipulating the size of the mixture of CGD components. For this purpose, the reduction scheme for mixture of CGD components, including evaluation of the KL divergence, as well as component picking and merging scheme are considered.

## 5.2 FURTHER RESEARCH DIRECTIONS

The thesis includes some theoretical results that could possibly be further applied in different applications. One such example is the LG-EIF which represents an estimation framework that could be applied for further development of filtering based SLAM approaches. In particular, the filtering based SLAM solutions reached its zenith with appearances of sparsification approaches applied over some original EIF implementations, resulting with sparse EIF and exactly sparse delayed-state filters. Soon after, optimization based SLAM solutions prevailed over the filtering based solutions since they dominated in performance over a wider range of applications. The herein presented LG-EIF could represent a basis for development of a new filter-based back-end for solving SLAM.

The thesis deals with the global estimation approach if it was possible to have a distribution closed under convolution and Bayes rule. Otherwise, it relies on the approximations developed upon the concept of concentrated Gaussian distribution. Unfortunately, subtle global distributions characterized with useful properties, such as an analytic solution to the Chapman-Kolmogorov convolution integral or closed form under application of the Bayes rule, are generally uncommon. For this purpose, further research direction in terms of theoretical aspects may point towards development of some better approximations of Lie group random variables rather than relying on the concept of CGD.

Considering the MOT applications, it is important to note that the question of an optimal solution to a complex MOT system is still open, while the key goal of the ongoing research is to develop near-optimal, scalable and numerically efficient algorithms. Furthermore, alongside the traditional fields where MOT was applied, some new large-scale real-world problems such as space objects tracking and giga-pixel video surveillance system, have come in the research focus. These problems usually include thousands of tracked objects and appearance of some additional issues that were neglected in this thesis, such as extended objects appearance, multiple source measurements, coalescence problem, etc. Additionally, although MOT field is experiencing a rapid development relying on a large scientific community working on new algorithms, an interesting contribution to the community would be providing an exhaustive comparison of different MOT approaches since the research in this area is limited.

## List of publications

- Pub1 I. Marković, J. Ćesić and I. Petrović. Von Mises Mixture PHD Filter. *IEEE Signal Processing Letters*, 22(12):2229–2233, 2015, IF: 1.661 (Q<sub>2</sub>).
- Pub2 I. Marković, J. Ćesić and I. Petrović. On wrapping the Kalman filter and estimating with the SO(2) group. *International Conference on Information Fusion (FUSION)*. Heidelberg, Germany, 2245–2250, 2016.
- Pub3 J. Ćesić, I. Marković and I. Petrović. Moving object tracking employing rigid body motion on matrix Lie groups. *International Conference on Information Fusion (FUSION)*. Heidelberg, Germany, 2109–2115, 2016.
- Pub4 J. Ćesić, V. Joukov, I. Petrović and D. Kulić. Full Body Human Motion Estimation on Lie Groups Using 3D Marker Position Measurements. *IEEE-RAS International Conference on Humanoid Robotics (Humanoids)*. Cancun, Mexico, 826–833, 2016.
- Pub5 V. Joukov, J. Ćesić, K. Westermann, I. Marković, D. Kulić and I. Petrović. Human motion estimation on Lie groups using IMU measurements. *IEEE/RSJ International Conference on Intelligent Robots and Systems (IROS)* Vancouver, Canada, 1965–1972, 2017.
- \*Pub5 Supplementary material to Pub5
- Pub6 J. Ćesić, I. Marković, M. Bukal and I. Petrović. Extended information filter on matrix Lie groups. *Automatica*, 53(9):226–234, 2017, IF: 5.451 (Q<sub>1</sub>).
- Pub7 J. Ćesić, I. Marković, I. Cvišić and I. Petrović. Radar and stereo vision fusion for multitarget tracking on the special Euclidean group. *Robotics and autonomous systems*, 83:338–348, 2016, IF: 1.950 (Q<sub>2</sub>).
- Pub8 J. Ćesić, I. Marković and I. Petrović. Mixture Reduction on Matrix Lie Groups. *IEEE Signal Processing Letters*, 24(11):1719–1723, 2017, IF: 2.528 (Q<sub>2</sub>).
- \*Pub8 Supplementary material to Pub8

## Author's contribution to publications

THE results presented in this thesis are based on the research carried out during the period of 2013 – 2017 in the Laboratory for autonomous systems and mobile robotics (LAMOR) headed by Professor Ivan Petrović, at the University of Zagreb, Faculty of Electrical Engineering and Computing, Croatia, as a part of three research projects: including:

- [2013 – 2015] *VISTA - Computer Vision Innovations for Safe Traffic* (IPA2007/HR/16IPO/001-040514) which was financially partially supported by the European Union from the European Regional Development Fund.
- [2015 – 2016] *FER-KIET - Advanced Technologies in Power Plants and Rail Vehicles* (RC.2.2.08-0015) which was as well financially supported by the European Union from the European Regional Development Fund.
- [2016 – 2017] *cloudSLAM - Cooperative cloud based simultaneous localization and mapping in dynamic environments* (25/15) which was funded by the Unity Through Knowledge Fund (UKF).

A part of the thesis also includes the research carried out at the Adaptive systems laboratory headed by Professor Dana Kulić, at the University of Waterloo, Canada, who was actively participating as partner in the cloudSLAM project.

The thesis includes eight publications written in collaboration with co-authors of the published papers. The author's contribution to each paper consists of the text writing, the software implementation, performing the required simulations and experiments, and results analysis and presentation.

Pub1 In the paper entitled *Von Mises Mixture PHD Filter* the author proposed a novel mixture approximation of the PHD filter tailored specifically for the topology of an MOT system on the unit circle relying on the vM distribution, which arises whenever the state and the sensor measurements are circular. The author has implemented the newly proposed algorithm in Matlab and analyzed the performance of the proposed filter comparing it with the GM-PHD on a synthetic dataset of 100 randomly generated multi-object scenarios with respect to the optimal subpattern assignment metric.

Pub2 In the paper entitled *On wrapping the Kalman filter and estimating with the SO(2) group* the author analyzes the LG-EKF for directional tracking of moving object in

2D assuming the constant angular acceleration model on the Lie groups including  $SO(2)$  (orientation) and Euclidean variables (velocity and acceleration). The author particularly shows that LG-EKF filter derivation based on the mathematically grounded framework of filtering on Lie groups (including  $SO(2)$  group) yields the same result as heuristically wrapping the angular variables within the EKF framework. The author has applied the proposed filter for a real-world speaker tracking with a microphone array using the implementation under the Robotic Operating System (ROS), while the accuracy was evaluated with ground truth data obtained by a motion capture system.

- Pub3 In the paper entitled *Moving object tracking employing rigid body motion on matrix Lie groups* the author proposed a novel method for estimating rigid body motion by modeling the object state using special Euclidean group  $SE(2)$  and employing the LG-EKF constant velocity model. The performance of the filter is then analyzed using Matlab implementation on a large number of synthetic trajectories and compared with (i) the EKF constant velocity and turn rate model and (ii) the linear KF constant velocity model.
- Pub4 In the paper entitled *Full Body Human Motion Estimation on Lie Groups Using 3D Marker Position Measurements*, in collaboration with co-authors, the author proposed a new algorithm for full body human motion estimation using 3D marker position measurements. For this purpose, the LG-EKF is used for stochastic inference on  $SO(2)$ ,  $SO(3)$  and  $SE(3)$  groups. The motion prediction follows the constant acceleration model, while the update and observation equations are derived for positional measurements, accounting for the kinematic chain. The performance of the filter was evaluated in both simulation and on real-world motion capture data, comparing it with the Euler angles based EKF.
- Pub5 In the paper entitled *Human motion estimation on Lie groups using IMU measurements*, in collaboration with co-authors, the author proposed a new algorithm for full body human motion estimation using inertial measurement units. The LG-EKF was employed for an arbitrary chain configuration consisting of  $SO(2)$  or  $SO(3)$  joints. The motion prediction follows the constant acceleration model, while the update was derived for gyro and accelerometer measurements, accounting for influence of the kinematic chain. The performance of the filter was evaluated in simulations and on real-world data, comparing it with the Euler angles based EKF.
- \*Pub5 This material provides a detailed derivation of accelerometer update within the LG-EKF framework employing an arbitrary kinematic chain, thus serving as a supplementary material to [Pub5].
- Pub6 In the paper entitled *Extended information filter on matrix Lie groups* the author proposed a new state estimation algorithm called the extended information filter on Lie groups (LG-EIF) The paper presents the theoretical development of the LG-EIF recursion equations and the applicability of the proposed approach is demonstrated on a rigid body attitude tracking problem with multiple sensors, comparing the



proposed LG-EIF to an EIF based on Euler angles, and analyzing its computational complexity with respect to the LG-EKF.

Pub7 In the paper entitled *Radar and stereo vision fusion for multitarget tracking on the special Euclidean group* the author uses a combination of a radar and a stereo vision system to perform the MOT task, by relying on the measurements and object states described using Lie groups. The paper also presents the adaptation of the JIPDA filter for MOT application on matrix Lie groups. The implementation in ROS was used for testing the algorithm on a real-world dataset collected with the described multi-sensor setup in urban traffic scenarios.

Pub8 In the paper entitled *Mixture Reduction on Matrix Lie Groups* the author proposes a mixture reduction approach for CGDs defined on matrix Lie groups. This entails appropriate reparametrization of CGD parameters to compute the KL divergence, pick and merge the mixture components. The author also describes an MOT filter, i.e., probability hypothesis density filter on matrix Lie groups (LG-PHD) with approximation based on a finite mixture of CGDs, and uses it as a study example for the proposed mixture reduction method.

\*Pub8 This material provides a more detailed overview of derivation of LG-PHD, thus serving as a supplementary material to [Pub8].

---

## BIBLIOGRAPHY

- [1] Sebastian Thrun, Wolfram Burgard, and Dieter Fox. *Probabilistic Robotics*. MIT Press, 2006.
- [2] Mahendra Mallick, Ba-Ngu Vo, Thia Kirubarajan, and Sanjeev Arulampalam. Introduction to the issue on multitarget tracking. *IEEE Journal of Selected Topics in Signal Processing*, 7(3):373–375, 2013.
- [3] Ronald P. S. Mahler. Multitarget bayes filtering via first-order multitarget moments. *IEEE Transactions on Aerospace and Electronic Systems*, 39(4):1152–1178, 2003.
- [4] I. R. Goodman, Ronald P. Mahler, and Hung T. Nguyen. *Mathematics of Data Fusion*. Kluwer Academic Publishers, Norwell, MA, USA, 1997.
- [5] R. E. Kalman. A New Approach to Linear Filtering and Prediction Problems. *Journal of Basic Engineering*, 82(1):35, 1960.
- [6] P.-A. Absil, R. Mahony, and R. Sepulchre. *Optimization Algorithms on Matrix Manifolds*. Princeton University Press, Princeton, 2008.
- [7] K.V. Mardia and P.E. Jupp. *Directional Statistics*. Wiley Series in Probability and Statistics. John Wiley & Sons, Inc., 1999.
- [8] Richard von Mises. Über die ‘Ganzzahligkeit’ der Atomgewicht und Verwandte Fragen. *Physikalische Zeitschrift*, 19:490–500, 1918.
- [9] Andrew W Long, Kevin C Wolfe, Michael J Mashner, and Gregory S Chirikjian. The Banana Distribution is Gaussian : A Localization Study with Exponential Coordinates. In *Robotics: Science and Systems (RSS)*, Sydney, Australia, 2012.
- [10] Timothy D. Barfoot and Paul T. Furgale. Associating Uncertainty With Three-Dimensional Poses for Use in Estimation Problems. *IEEE Transactions on Robotics*, 30(3):679–693, jun 2014.
- [11] Gregory S. Chirikjian. *Stochastic Models, Information Theory, and Lie Groups, Volume 1: Classical Results and Geometric Methods*. Springer, 2012.
- [12] Simo Srkk. *Bayesian Filtering and Smoothing*. Cambridge University Press, New York, NY, USA, 2013.

- [13] R. E. Kalman and R. S. Bucy. New results in linear filtering and prediction theory. *Journal of Basic Engineering*, 83(1):95–108, 1961.
- [14] Mohinder S. Grewal and Angus P. Andrews. *Kalman filtering: theory and practice*. John Wiley & Sons, Inc., second edition, 2001.
- [15] Brian D. O. Anderson and John B Moore. *Optimal Filtering*. Prantice Hall, Inc., Englewood Cliffs, New Jersey 07632, 1979.
- [16] A.H. Jazwinski. *Stochastic Processes and Filtering Theory*. Dover Books on Electrical Engineering Series. Dover Publications, 2007.
- [17] Simon Julier and Jeffrey Uhlmann. Unscented Filtering and Non Linear Estimation. *Proceedings of the IEEE*, 92(3):401–422, 2004.
- [18] Eric A. Wan and Rudolph Van Der Merwe. The Unscented Kalman Filter for Non-linear Estimation. In *Adaptive Systems for Signal Processing, Communications, and Control Symposium (AS-SPCC)*, pages 153–158, Lake Louise, Alta, 2000. IEEE.
- [19] Fredrik Gustafsson and Gustaf Hendeby. Some relations between extended and unscented Kalman filters. *IEEE Transactions on Signal Processing*, 60(2):545–555, 2012.
- [20] I. Arasaratnam and S. Haykin. Cubature Kalman Filters. *IEEE Transactions on Automatic Control*, 54(6):1254–1269, jun 2009.
- [21] Bin Jia, Ming Xin, and Yang Cheng. The high-degree cubature Kalman filter. In *Conference on Decision and Control (CDC)*, number 2, pages 4095–4100. IEEE, dec 2012.
- [22] K. Ito and K. Xiong. Gaussian filters for nonlinear filtering problems. *IEEE Transactions on Automatic Control*, 45(5):910–927, may 2000.
- [23] Ienkaran Arasaratnam, Simon Haykin, and Robert J Elliott. Discrete-Time Nonlinear Filtering Algorithms Using Gauss – Hermite Quadrature. *Proceedings of the IEEE*, 95(5):953–977, 2007.
- [24] S. Arulampalam, S. Maskell, N. Gordon, and T. Clapp. A tutorial on particle filters for online nonlinear/non-Gaussian Bayesian tracking. *IEEE Transactions on Signal Processing*, 50(2):174–188, 2002.
- [25] D. Alspach and H. Sorenson. Nonlinear bayesian estimation using gaussian sum approximations. *IEEE Transactions on Automatic Control*, 17(4):439–448, 1972.
- [26] Rong Chen and Jun S. Liu. Mixture Kalman filters. *Journal of the Royal Statistical Society: Series B (Statistical Methodology)*, 62(3):493–508, 2000.
- [27] P S Maybeck. *Stochastic models, estimation, and control*, volume Vol 1. Academic Press, Inc., 1979.

- [28] B. Grocholsky, A. Makarenko, and H. Durrant-Whyte. Information-theoretic coordinated control of multiple sensor platforms. In *International Conference on Robotics and Automation (ICRA)*, volume 1, pages 1521–1526. IEEE, 2003.
- [29] Tom Vercauteren and Xiaodong Wang. Decentralized sigma-point information filters for target tracking in collaborative sensor networks. *IEEE Transactions on Signal Processing*, 53(8):2997–3009, 2005.
- [30] Mark E. Campbell and William W. Whitacre. Cooperative tracking using vision measurements on SeaScan UAVs. *IEEE Transactions on Control Systems Technology*, 15(4):613–626, 2007.
- [31] Guoliang Liu, Florentin Wörgötter, and Irene Markelić. Square-Root Sigma-Point Information Filtering. *IEEE Transactions on Automatic Control*, 57(11):2945–2950, 2012.
- [32] Shiyuan Wang, Jiuchao Feng, and Chi K. Tse. A class of stable square-root nonlinear information filters. *IEEE Transactions on Automatic Control*, 59(7):1893–1898, 2014.
- [33] Deok-Jin Lee. Nonlinear Estimation and Multiple Sensor Fusion Using Unscented Information Filtering. *IEEE Signal Processing Letters*, 15(2):861–864, 2008.
- [34] Sebastian Thrun, Yufeng Liu, Daphne Koller, Andrew Y. Ng, Zoubin Ghahramani, and Hugh Durrant-Whyte. Simultaneous Localization and Mapping with Sparse Extended Information Filters. *The International Journal of Robotics Research*, 23(7-8):693–716, 2004.
- [35] Ryan M. Eustice, Hanumant Singh, and John J. Leonard. Exactly sparse delayed-state filters for View-Based SLAM. *IEEE Transactions on Robotics*, 22(6):1100–1114, 2006.
- [36] Volkan Cevher, Rajbabu Velmurugan, and James H. McClellan. Acoustic multitarget tracking using direction-of-arrival batches. *IEEE Transactions on Signal Processing*, 55(6):2810–2825, 2007.
- [37] Johannes Traa and Paris Smaragdis. A Wrapped Kalman Filter for Azimuthal Speaker Tracking. *IEEE Signal Processing Letters*, 20(12):1257–1260, 2013.
- [38] Hagit Shatkay and Leslie Pack Kaelbling. Learning geometrically-constrained hidden Markov models for robot navigation: bridging the topological-geometrical gap. *Journal of Artificial Intelligence Research*, 16(1):167–207, 2002.
- [39] Nicholas Roy, Geoffrey Gordon, and Sebastian Thrun. Finding approximate POMDP solutions through belief compression. *Journal of Artificial Intelligence Research*, 23:1–40, 2005.
- [40] Ivan Marković and Ivan Petrović. Speaker Localization and Tracking in Mobile Robot Environment Using a Microphone Array. *Robotics and Autonomous Systems*, 58(11):1185–1196, 2010.

- [41] Ivan Marković and Ivan Petrović. Applying von Mises Distribution to Microphone Array Probabilistic Sensor Modelling. In *Robotics (ISR), 2010 41st International Symposium on and 2010 6th German Conference on Robotics (ROBOTIK)*, pages 1 – 7, Munich, Germany, 2010. VDE.
- [42] Ivan Marković and Ivan Petrović. Bearing-Only Tracking with a Mixture of von Mises Distributions. In *International Conference on Intelligent Robots and Systems (IROS)*, pages 707 – 712, Vilamoura, Portugal, 2012. IEEE.
- [43] Ivan Markovic, Alban Portello, Patrick Danes, Ivan Petrovic, and Sylvain Argentieri. Active speaker localization with circular likelihoods and bootstrap filtering. In *International Conference on Intelligent Robots and Systems (IROS)*, pages 2914–2920. IEEE/RSJ, 2013.
- [44] Simone Calderara, Andrea Prati, and Rita Cucchiara. Mixtures of von Mises Distributions for People Trajectory Shape Analysis. *IEEE Transactions on Circuits and Systems for Video Technology*, 21(4):457–471, 2011.
- [45] David Crouse. Maximum Likelihood Postdetection Radar Ambiguity Resolution. *IEEE Transactions on Aerospace and Electronic Systems*, 50(3):1876–1883, 2014.
- [46] Yang Yi and Haohui Xu. Hierarchical data association framework with occlusion handling for multiple targets tracking. *IEEE Signal Processing Letters*, 21(3):288–291, 2014.
- [47] N. I. I. Fisher. *Statistical Analysis of Circular Data*. Cambridge University Press, 1993.
- [48] Ivan Marković, François Chaumette, and Ivan. Moving object detection , tracking and following using an omnidirectional camera on a mobile robot. In *International Conference on Robotics and Automation (ICRA)*, pages 5630 – 5635, Hong Kong, 2014. IEEE.
- [49] Ivan Marković, Mario Bukal, Josip Ćesić, and Ivan Petrović. Multitarget tracking with the von Mises-Fisher filter and probabilistic data association. *Journal of Advances in Information Fusion*, pages 1–12.
- [50] Jared Glover, G. Bradski, and Radu Bogdan Rusu. Monte Carlo pose estimation with quaternion kernels and the Bingham distribution. In *Proceedings of Robotics: Science and Systems*, Los Angeles, CA, USA, 2011.
- [51] G. Kurz, I. Gilitschenski, S. Julier, and U. D. Hanebeck. Recursive estimation of orientation based on the Bingham distribution. In *International Conference on Information Fusion (FUSION)*, 2013.
- [52] Gerhard Kurz, Igor Gilitschenski, and Uwe D. Hanebeck. The partially wrapped normal distribution for SE(2) estimation. In *International Conference on Multisensor Fusion and Information Integration for Intelligent Systems (MFI)*, 2014.

- [53] Jared Glover and Leslie Pack Kaelbling. Tracking the spin on a ping pong ball with the quaternion Bingham filter. In *International Conference on Robotics and Automation (ICRA)*, pages 4133–4140, Hong Kong, China, may 2014. IEEE.
- [54] Richard M Murray, Zexiang Li, and S Shankar Sastry. *A Mathematical Introduction to Robotic Manipulation*, volume 29. CRC Press, 1994.
- [55] J. M. Selig. Lie Groups and Lie Algebras in Robotics. In *Computational Noncommutative Algebra and Applications*, pages 101–125. 2005.
- [56] Shun-Feng Su and C. S. George Lee. Manipulation and propagation of uncertainty and verification of applicability of actions in assembly tasks. *IEEE Transactions on Systems, Man, and Cybernetics*, 22(6):1376–1389, 1992.
- [57] Kevin C Wolfe, Michael Mashner, and Gregory S Chirikjian. Bayesian Fusion on Lie Groups. *Journal of Algebraic Statistics*, 2(1):75–97, 2011.
- [58] Guillaume Bourmaud. *Parameter estimation on Lie groups: Application to mapping and localization from a monocular camera*. PhD thesis, University of Bordeaux, 2015.
- [59] Yunfeng Wang and G.S. Chirikjian. Error propagation on the Euclidean group with applications to manipulator kinematics. *IEEE Transactions on Robotics*, 22(4):591–602, aug 2006.
- [60] Guillaume Bourmaud, Rémi Mégret, Marc Arnaudon, and Audrey Giremus. Continuous-Discrete Extended Kalman Filter on Matrix Lie Groups Using Concentrated Gaussian Distributions. *Journal of Mathematical Imaging and Vision*, 51(1):209–228, 2015.
- [61] Guillaume Bourmaud, Rémi Mégret, Audrey Giremus, and Yannick Berthoumieu. Discrete Extended Kalman Filter on Lie Groups. In *European Signal Processing Conference (EUSIPCO)*, pages 1–5, 2013.
- [62] Christoph Hertzberg, René Wagner, Udo Frese, and Lutz Schröder. Integrating Generic Sensor Fusion Algorithms with Sound State Representations through Encapsulation of Manifolds. *Information Fusion*, 14(1):57–77, jul 2013.
- [63] Igor Gilitschenski, Gerhard Kurz, Simon J Julier, and Uwe D Hanebeck. A New Probability Distribution for Simultaneous Representation of Uncertain Position and Orientation. In *International Conference on Information Fusion (FUSION)*, 2014.
- [64] Muriel Lang, Oliver Dunkley, and Sandra Hirche. Gaussian process kernels for rotations and 6D rigid body motions. In *International Conference on Robotics and Automation (ICRA)*, pages 5165–5170, 2014.
- [65] Wendelin Feiten, Muriel Lang, and Sandra Hirche. Rigid Motion Estimation using Mixtures of Projected Gaussians. In *International Conference on Information Fusion (FUSION)*, pages 1465 – 1472, Istanbul, Turkey, 2013. IEEE.

- [66] Jakob Engel, Thomas Schops, and Daniel Cremers. LSD-SLAM: Large-Scale Direct Monocular SLAM. In *European Conference on Computer Vision (ECCV)*, pages 1–16, 2014.
- [67] Quentin Rentmeesters, P. A. Absil, Paul Van Dooren, Kyle Gallivan, and Anuj Srivastava. An efficient particle filtering technique on the grassmann manifold. In *International Conference on Acoustics, Speech and Signal Processing (ICASSP)*, pages 3838–3841. IEEE, 2010.
- [68] Zulfiqar Hasan Khan and Irene Yu-Hua Gu. Nonlinear dynamic model for visual object tracking on Grassmann manifolds with partial occlusion handling. *IEEE Transactions on Cybernetics*, 43(6):2005–19, 2013.
- [69] Søren Hauberg, François Lauze, and Kim Steenstrup Pedersen. Unscented kalman filtering on riemannian manifolds. *Journal of Mathematical Imaging and Vision*, 46(1):103–120, 2013.
- [70] Maxime Devanne, Hazem Wannous, Stefano Berretti, Pietro Pala, Mohamed Daoudi, and Alberto Del Bimbo. 3-D Human Action Recognition by Shape Analysis of Motion Trajectories on Riemannian Manifold. *IEEE Transactions on Cybernetics*, 45(7):1340–1352, 2015.
- [71] Yui Man Lui. Advances in matrix manifolds for computer vision. *Image and Vision Computing*, 30(6-7):380–388, jun 2012.
- [72] Jesus Martinez-Del-Rincon, Michal Lewandowski, Jean Christophe Nebel, and Dimitrios Makris. Generalized Laplacian eigenmaps for modeling and tracking human motions. *IEEE Transactions on Cybernetics*, 44(9):1646–1660, 2014.
- [73] Meng Ding and Guolian Fan. Multilayer Joint Gait-Pose Manifolds for Human Gait Motion Modeling. *IEEE Transactions on Cybernetics*, 45(11):2413–2424, 2015.
- [74] Motilal Agrawal. A lie algebraic approach for consistent pose registration for general euclidean motion. In *International Conference on Intelligent Robots and Systems (IROS)*, pages 1891–1897, Beijing, China, 2006. IEEE.
- [75] Joseph Knuth and Prabir Barooah. Error growth in position estimation from noisy relative pose measurements. *Robotics and Autonomous Systems*, 61(3):229–244, mar 2013.
- [76] M Bloesch, S Omari, P Fankhauser, H Sommer, C Gehring, J Hwangbo, M A Hoepflinger, M Hutter, and R Siegwart. Fusion of optical flow and inertial measurements for robust egomotion estimation. In *International Conference on Intelligent Robots and Systems (IROS)*, pages 3102–3107, 2014.
- [77] Michael Bloesch, Christian Gehring, Peter Fankhauser, Marco Hutter, Mark a. Hoepflinger, and Roland Siegwart. State estimation for legged robots on unstable and slippery terrain. In *International Conference on Intelligent Robots and Systems (IROS)*, pages 6058–6064, 2013.

- [78] Faraz M Mirzaei and Stergios I Roumeliotis. A Kalman Filter-Based Algorithm for IMU-Camera Calibration: Observability Analysis and Performance Evaluation. *IEEE Transactions on Robotics*, 24(5):1143–1156, 2008.
- [79] Mehdi Benallegue and Florent Lamiroux. Estimation and Stabilization of Humanoid Flexibility Deformation Using Only Inertial Measurement Units and Contact Information. *International Journal of Humanoid Robotics*, 12(3):1550025, 2015.
- [80] V. Joukov, R. D’Souza, and D. Kulić. Human pose estimation from imperfect sensor data via the extended kalman filter. In *International Symposium on Experimental Robotics (ISER 2016)*. IEEE, 2016.
- [81] Agnieszka Szczęsna and Przemysław Pruszowski. Model-based extended quaternion Kalman filter to inertial orientation tracking of arbitrary kinematic chains. *SpringerPlus*, 5(1965):34, 2016.
- [82] Sachit Butail and Derek A. Paley. Vision-based estimation of three-dimensional position and pose of multiple underwater vehicles. In *International Conference on Intelligent Robots and Systems (IROS)*, number 3, pages 2477–2482, St. Louis, MO, USA, oct 2009. Ieee.
- [83] Changhyun Choi and Henrik I. Christensen. Robust 3D visual tracking using particle filtering on the SE(3) group. In *International Conference on Robotics and Automation (ICRA)*, number 3, pages 4384–4390, 2011.
- [84] Edgar Kraft. A Quaternion-based Unscented Kalman Filter for Orientation Tracking. In *International Conference on Information Fusion (FUSION)*, number 01, pages 47–54, Cairns, Queensland, Australia, 2003.
- [85] Angelo M. Sabatini. Quaternion-based extended Kalman filter for determining orientation by inertial and magnetic sensing. *IEEE Transactions on Biomedical Engineering*, 53(7):1346–1356, 2006.
- [86] Brian J. Sipos. Application of the manifold-constrained unscented Kalman filter. In *Position, Location and Navigation Symposium*, pages 30–43, Monterey, CA, USA, 2008. IEEE.
- [87] Axel Barrau and Silvère Bonnabel. Intrinsic Filtering on Lie Groups With Applications to Attitude Estimation. *IEEE Transactions on Automatic Control*, 60(2):436–449, 2015.
- [88] Taeyoung Lee, Melvin Leok, and N. Harris McClamroch. Global symplectic uncertainty propagation on SO(3). In *Conference on Decision and Control (CDC)*, number 3, pages 61–66. IEEE, 2008.
- [89] Taeyoung Lee. Stochastic Optimal Motion Planning and Estimation for the Attitude Kinematics on SO(3). In *Conference on Decision and Control (CDC)*, pages 588–593, Florence, Italy, 2013. IEEE.



- [90] John L. Crassidis, F. Landis Markley, and Yang Cheng. Survey of Nonlinear Attitude Estimation Methods. *Journal of Guidance, Control, and Dynamics*, 30(1):12–28, 2007.
- [91] Isabelle Mazon and Rachid Alami. Representation and propagation of positioning uncertainties through manipulation robot programs. Integration into a Task-level Programming System. In *International Conference on Robotics and Automation (ICRA)*, pages 646–652. IEEE, 1989.
- [92] Yunfeng Wang and Gregory S. Chirikjian. Nonparametric Second-Order Theory of Error Propagation on Motion Groups. *The International Journal of Robotics Research*, 27(11):1258–1273, 2008.
- [93] Wooram Park, Yan Liu, Yu Zhou, Matthew Moses, and Gregory S. Chirikjian. Kinematic state estimation and motion planning for stochastic nonholonomic systems using the exponential map. *Robotica*, 26:419–434, 2008.
- [94] Wooram Park, Kyle B Reed, Allison M Okamura, and Gregory S Chirikjian. Estimation of Model Parameters for Steerable Needles. In *International Conference on Robotics and Automation (ICRA)*, number 3, pages 3703–3708, Anchorage, Alaska, USA, jan 2010. IEEE.
- [95] Rangaprasad Arun Srivatsan, Matthew Travers, and Howie Choset. Using Lie algebra for shape estimation of medical snake robots. In *International Conference on Intelligent Robots and Systems (IROS)*, Chicago, USA, 2014. IEEE/RSJ.
- [96] Stephan M Weiss. *Vision Based Navigation for Micro Helicopters (PhD Thesis - Weiss 2012)*. PhD thesis, 2012.
- [97] Stephan Weiss, Markus W. Achtelik, Margarita Chli, and Roland Siegwart. Versatile distributed pose estimation and sensor self-calibration for an autonomous MAV. In *International Conference on Robotics and Automation (ICRA)*, pages 31–38, 2012.
- [98] Jonathan Kelly and Gaurav S Sukhatme. Visual-Inertial Sensor Fusion: Localization, Mapping and Sensor-to-Sensor Self-calibration. *The International Journal of Robotics Research*, 30(1):56–79, 2011.
- [99] Simon Lynen, Markus W Achtelik, Stephan Weiss, Margarita Chli, and Roland Siegwart. A Robust and Modular Multi-Sensor Fusion Approach Applied to MAV Navigation. In *International Conference on Intelligent Robots and Systems (IROS)*, pages 3923–3929. IEEE/RSJ, 2013.
- [100] Jonathan Brookshire and Seth Teller. Extrinsic Calibration from Per-Sensor Egomotion. In *Robotics: Science and Systems (RSS)*, 2012.
- [101] R. Wagner, O. Birbach, and U. Frese. Rapid development of manifold-based graph optimization systems for multi-sensor calibration and SLAM. In *International Conference on Intelligent Robots and Systems (IROS)*, pages 3305–3312, San Francisco, CA, sep 2011. IEEE.

- [102] J.A. Castellanos, J.M.M. Montiel, J. Neira, and J.D. Tardos. The SPmap: a probabilistic framework for simultaneous localization and map building. *IEEE Transactions on Robotics and Automation*, 15(5):948–952, 1999.
- [103] Andrew J. Davison. Real-time simultaneous localisation and mapping with a single camera. In *International Conference on Computer Vision (ICCV)*, volume 2, pages 1403–1410, Nice, France, 2003. IEEE.
- [104] G. Silveira, E. Malis, and P. Rives. An Efficient Direct Approach to Visual SLAM. *IEEE Transactions on Robotics*, 24(5):969–979, 2008.
- [105] Christian Forster, Luca Carlone, Frank Dellaert, and Davide Scaramuzza. IMU preintegration on manifold for efficient visual-inertial maximum-a-posteriori estimation. In *Robotics: Science and Systems (RSS)*, 2015.
- [106] Tim Bailey, Ben Upcroft, and Hugh Durrant-Whyte. Validation gating for non-linear non-Gaussian target tracking. In *International Conference on Information Fusion (FUSION)*, Florence, Italy, 2006.
- [107] Hauke Strasdat, J M M Montiel, and Andrew J Davison. Scale Drift-Aware Large Scale Monocular SLAM. In *Robotics: Science and Systems (RSS)*, Zaragoza, Spain, 2010.
- [108] German Ros, Julio Guerrero, Angel D Sappa, Daniel Ponsa, and Antonio M Lopez. VSLAM pose initialization via Lie groups and Lie algebras optimization. In *International Conference on Robotics and Automation (ICRA)*, pages 5740 – 5747, Karlsruhe, 2013. IEEE.
- [109] Rainer Kummerle, Giorgio Grisetti, Hauke Strasdat, Kurt Konolige, and Wolfram Burgard.  $g^2o$ : A General Framework for Graph Optimization. In *International Conference on Robotics and Automation (ICRA)*, pages 3607–3613, 2011.
- [110] Chi Hay Tong, Sean Anderson, Hang Dong, and Timothy D. Barfoot. Pose Interpolation for Laser-based Visual Odometry. *Journal of Field Robotics*, 31(5):731–757, sep 2014.
- [111] Raul Mur-Artal, J. M. M. Montiel, and Juan D. Tardos. ORB-SLAM: A Versatile and Accurate Monocular SLAM System. *IEEE Transactions on Robotics*, 31(5):1147–1163, 2015.
- [112] Joel A. Hesch, Dimitrios G. Kottas, Sean L. Bowman, and Stergios I. Roumeliotis. Camera-IMU-based Localization: Observability Analysis and Consistency Improvement. *The International Journal of Robotics Research*, 33(1):182–201, 2013.
- [113] Giuseppe Loianno, Michael Watterson, and Vijay Kumar. Visual inertial odometry for quadrotors on  $SE(3)$ . In *International Conference on Robotics and Automation (ICRA)*, number 3, pages 1544–1551. IEEE, 2016.

- [114] Josip Ćesić, Ivan Marković, and Ivan Petrović. Moving objects tracking on the unit sphere using a multiple-camera system on a mobile robot. In *International Conference on Intelligent Autonomous Systems (IAS)*, Padua, Italy, 2014.
- [115] M. Roth and F. Gustafsson. An efficient implementation of the second order extended Kalman filter. In *International Conference on Information Fusion (FUSION)*, pages 1913–1918, 2011.
- [116] Ivan Marković, Mario Bukal, Josip Ćesić, and Ivan Petrović. Multitarget tracking with the von Mises-Fisher filter and probabilistic data association. *Journal of Advances in Information Fusion*, pages 1–12, 2017.
- [117] John Stillwell. *Naive Lie Theory*. Springer-Verlag New York, New York, 2008.
- [118] I. D. Ado. The representation of Lie algebras by matrices. *Uspekhi Mat. Nauk*, 2:159–173, 1947.
- [119] Wooram Park, Yunfeng Wang, and Gregory S. Chirikjian. The Path-of-Probability Algorithm for Steering and Feedback Control of Flexible Needles. *The International Journal of Robotics Research*, 29(7):813–830, 2010.
- [120] Guillaume Bourmaud, Rémi Mégret, Audrey Giremus, and Yannick Berthoumieu. From Intrinsic Optimization to Iterated Extended Kalman Filtering on Lie Groups. *Journal of Mathematical Imaging and Vision*, 55(3):284–303, 2016.
- [121] Josip Ćesić, Ivan Marković, Mario Bukal, and Ivan Petrović. Extended Information Filter on Matrix Lie Groups. *Automatica (accepted for publication)*, 53(9), 2017.
- [122] W. Miller. *Symmetry Groups and Their Applications*. Pure and Applied Mathematics. Elsevier Science, 1973.
- [123] Y. Bar-Shalom, X.R. Li, and T. Kirubarajan. *Estimation with Applications to Tracking and Navigation: Theory Algorithms and Software*. Wiley, 2001.
- [124] S. S. Blackman, R. J. Dempster, M. T. Busch, and R. F. Popoli. IMM/MHT solution to radar benchmark tracking problem. *IEEE Transactions on Aerospace and Electronic Systems*, 35(2):730–738, 1999.
- [125] Yaakov Bar-Shalom and Edison Tse. Tracking in a cluttered environment with probabilistic data association. *Automatica*, 11(5):451–460, 1975.
- [126] T. Fortmann, Y. Bar-Shalom, and M. Scheffe. Sonar tracking of multiple targets using joint probabilistic data association. *IEEE Journal of Oceanic Engineering*, 8(3):173–184, 1983.
- [127] Donald B. Reid. An algorithm for tracking multiple targets. *IEEE Transactions on Automatic Control*, 24(6):843–854, 1979.
- [128] Samuel S. Blackman. Multiple Hypothesis Tracking For Multiple Target Tracking. *IEEE Aerospace and Electronic Systems Magazine*, 19(1):5–18, 2004.

- [129] Ronald Mahler. "Statistics 101" for Multisource, Multitarget Data Fusion. *IEEE Aerospace and Electronic Systems Magazine*, 19(1):53–64, 2004.
- [130] Ronald P. S. Mahler. *Statistical Multisource-Multitarget Information Fusion*. 2007.
- [131] Jason L. Williams. Marginal multi-bernoulli filters: RFS derivation of MHT, JIPDA, and association-based member. *IEEE Transactions on Aerospace and Electronic Systems*, 51(3):1664–1687, 2015.
- [132] Sumeetpal S. Singh, Ba-Ngu Vo, Adrian Baddeley, and Sergei Zuyev. Filters for spatial point processes. *SIAM Journal on Control and Optimization*, 48(4):2275–2295, 2009.
- [133] Ba-Ngu Vo and W.-K. Ma. The Gaussian Mixture Probability Hypothesis Density Filter. *IEEE Transactions on Signal Processing*, 54(11):4091–4104, 2006.
- [134] Ronald Mahler. PHD Filters of Higher Order in Target Number. *IEEE Transactions on Aerospace and Electronic Systems*, 43(4):1523–1543, 2007.
- [135] Ba-Tuong Vo, Ba-Ngu Vo, and Antonio Cantoni. Analytic Implementations of the Cardinalized Probability Hypothesis Density Filter. *IEEE Transactions on Signal Processing*, 55(7):3553–3567, 2007.
- [136] Ba Tuong Vo, Ba N. Vo, and Antonio Cantoni. The cardinality balanced multi-target multi-Bernoulli filter and its implementations. *IEEE Transactions on Signal Processing*, 57(2):409–423, 2009.
- [137] Ronald Mahler. "Statistics 102" for Multisource-Multitarget Detection and Tracking. *IEEE Journal of Selected Topics in Signal Processing*, 7(3):376–389, 2013.
- [138] Ba-Ngu Vo, Mahendra Mallick, Yaakov Bar-Shalom, Stefano Coraluppi, III Richard Osborne, Ronald Mahler, and Ba-Tuong Vo. Multi-Target Tracking. In *Wiley Encyclopedia of Electrical and Electronics Engineering*. 2015.
- [139] Thuraiappah Sathyan, Tat-Jun Chin, Sanjeev Arulampalam, and David Suter. A Multiple Hypothesis Tracker for Multitarget Tracking With Multiple Simultaneous Measurements. *IEEE Journal of Selected Topics in Signal Processing*, 7(3):448–460, 2013.
- [140] T. Kurien. Issues in the design of practical multitarget tracking algorithms. In Y. Bar-Shalom, editor, *Multitarget-Multisensor Tracking: Advanced Applications*, chapter 3, pages 43–83. Artech House, 1990.
- [141] Nicolas Chenouard, Isabelle Bloch, and Jean Christophe Olivo-Marin. Multiple hypothesis tracking for cluttered biological image sequences. *IEEE Transactions on Pattern Analysis and Machine Intelligence*, 35(11):2736–2750, 2013.
- [142] T. Sathyan, A. Sinha, T. Kirubarajan, Michael McDonald, and Thomas Lang. MDA-based data association with prior track information for passive multitarget tracking. *IEEE Transactions on Aerospace and Electronic Systems*, 47(1):539–556, 2011.

- [143] Ingemar J. Cox and Sunita L. Hingorani. Efficient implementation of Reid's multiple hypothesis tracking algorithm and its evaluation for the purpose of visual tracking. *IEEE Transactions on Pattern Analysis and Machine Intelligence*, 18(2):138–150, 1996.
- [144] Roy L Streit and Tod E Luginbuhl. Probabilistic Multi-Hypothesis Tracking. Technical Report February, NUWC-NPT Technical Report 10,428, 1995.
- [145] Peter Willett, Yanhua Ruan, and Roy Streit. PMHT: Problems and some solutions. *IEEE Transactions on Aerospace and Electronic Systems*, 38(3):738–754, 2002.
- [146] Yanhua Ruan and Peter Willett. The Turbo PMHT. *IEEE Transactions on Aerospace and Electronic Systems*, 40(4):1388–1398, 2004.
- [147] David F. Crouse, Marco Guerriero, Peter Willett, Roy Streit, and Darin Dunham. A Look at the PMHT. In *International Conference on Information Fusion (FUSION)*, pages 332–339, 2009.
- [148] Yaakov Bar-Shalom, Fred Daum, and Jim Huang. The Probabilistic Data Association Filter. *IEEE Control Systems Magazine*, 29(6):82–100, 2009.
- [149] Henk A P Blom and Edwin A Bloem. Probabilistic Data Association Avoiding Track Coalescence. *IEEE Transactions on Automatic Control*, 45(2):247–259, 2000.
- [150] Paul Horridge and Simon Maskell. Real-time tracking of hundreds of targets with efficient exact JPDAF implementation. In *International Conference on Information Fusion (FUSION)*. IEEE, 2006.
- [151] D. Musicki, R. Evans, and S. Stankovic. Integrated Probabilistic Data Association. *IEEE Transactions on Automatic Control*, 39(6):1237–1241, 1994.
- [152] D. Musicki and R. Evans. Joint Integrated Probabilistic Data Association - JIPDA. *IEEE Transactions on Aerospace and Electronic Systems*, 40(3):1093 – 1099, 2004.
- [153] Taek Lyul Song, Hyoung Won Kim, and Darko Mušicki. Iterative Joint Integrated Probabilistic Data Association for Multitarget Tracking. *IEEE Transactions on Aerospace and Electronic Systems*, 51(1):642–653, 2015.
- [154] Seyed Hamid Rezatofighi, Anton Milan, Zhen Zhang, Qinfeng Shi, Anthony Dick, and Ian Reid. Joint probabilistic data association revisited. In *International Conference on Computer Vision (ICCV)*, pages 3047–3055. IEEE, 2016.
- [155] O. Erdinc, P. Willett, and Y. Bar-Shalom. The Bin-Occupancy Filter and Its Connection to the PHD Filters. *IEEE Transactions on Signal Processing*, 57(11):4232–4246, 2009.
- [156] B N Vo, Sumeetpal Singh, and Arnaud Doucet. Sequential Monte Carlo methods for Bayesian multi-target filtering with random finite sets. *IEEE Transactions on Aerospace and Electronic Systems*, 41(4):1224–1245, 2005.

- [157] Mirko Maehlich, Roland Schweiger, Werner Ritter, and Klaus Dietmayer. Multisensor Vehicle Tracking with the Probability Hypothesis Density Filter. In *International Conference on Information Fusion (FUSION)*, pages 1021 – 1026. IEEE, 2006.
- [158] Emilio Maggio, Murtaza Taj, and Andrea Cavallaro. Efficient multitarget visual tracking using random finite sets. *IEEE Transactions on Circuits and Systems for Video Technology*, 18(8):1016–1027, 2008.
- [159] Nick Whitley, Sumeetpal Singh, and Simon Godsill. Auxiliary Particle Implementation. In *International Symposium on Image and Signal Processing and Analysis (ISPA)*, pages 510–515, 2007.
- [160] Branko Ristic, Daniel Clark, Ba-Ngu Vo, and Ba-Tuong Vo. Adaptive Target Birth Intensity for PHD and CPHD Filters. *IEEE Transactions on Aerospace and Electronic Systems*, 48(2):1656–1668, 2012.
- [161] Daniel Clark and Ba-Ngu Vo. Convergence Analysis of the Gaussian Mixture PHD Filter. *IEEE Transactions on Signal Processing*, 55(4):1204–1212, 2007.
- [162] Kusha Panta, Daniel E. Clark, and Ba-Ngu Vo. Data Association and Track Management for the Gaussian Mixture Probability Hypothesis Density Filter. *IEEE Transactions on Aerospace and Electronic Systems*, 45(3):1003–1016, 2009.
- [163] Ba Tuong Vo, Ba Ngu Vo, and Antonio Cantoni. The cardinalized probability hypothesis density filter for linear Gaussian multi-target models. In *Annual Conference on Information Sciences and Systems (CISS)*, pages 681–686. IEEE, 2006.
- [164] M Ulmke, Fgan Fkie, and Peter Willett. Gaussian Mixture Cardinalized PHD Filter for Ground Moving Target Tracking. In *International Conference on Information Fusion (FUSION)*. IEEE, 2007.
- [165] Feng Lian, Chongzhao Han, and Weifeng Liu. Estimating unknown clutter intensity for PHD filter. *IEEE Transactions on Aerospace and Electronic Systems*, 46(4):2066–2078, 2010.
- [166] Taek Lyul Song and Darko Mušicki. Adaptive clutter measurement density estimation for improved target tracking. *IEEE Transactions on Aerospace and Electronic Systems*, 47:1457–1466, 2011.
- [167] R. P. S. Mahler. CPHD Filtering With Unknown Clutter Rate and Detection Profile. *IEEE Transactions on Signal Processing*, 59(8):3497–3513, aug 2011.
- [168] Michael Beard, Ba-Tuong Vo, and Ba-Ngu Vo. Multitarget Filtering With Unknown Clutter Density Using a Bootstrap GMCPHD Filter. *IEEE Signal Processing Letters*, 20(4):323–326, 2013.
- [169] Michael Beard, Ba Tuong Vo, Ba-Ngu Vo, and Sanjeev Arulampalam. A Partially Uniform Target Birth Model for Gaussian Mixture PHD/CPHD Filtering. *IEEE Transactions on Aerospace and Electronic Systems*, 49(4):2835–2844, 2013.

- [170] Syed Ahmed Pasha, Ba Ngu Vo, Hoang Duong Tuan, and Wing Kin Ma. A Gaussian mixture PHD filter for jump Markov system models. *IEEE Transactions on Aerospace and Electronic Systems*, 45(3):919–936, 2009.
- [171] R. Mahler. PHD filters for nonstandard targets, I: Extended targets. In *International Conference on Information Fusion (FUSION)*, pages 448–452, 2009.
- [172] Karl Granström and Umut Orguner. A PHD Filter for Tracking Multiple Extended Targets Using Random Matrices. *IEEE Transactions on Signal Processing*, 60(11):5657–5671, 2012.
- [173] Christoph Stiller, Fernando Puente Leon, and Marco Kruse. Information fusion for automotive applications - An overview. *Information Fusion*, 12(4):244–252, 2011.
- [174] Michael Beard and Sanjeev Arulampalam. Performance of PHD and CPHD Filtering Versus JIPDA for Bearings-only Multi-target Tracking. In *International Conference on Information Fusion (FUSION)*, pages 542–549. IEEE, 2012.
- [175] Ba-Tuong Vo, Ba-Ngu Vo, Reza Hoseinnezhad, and Ronald P. S. Mahler. Robust Multi-Bernoulli Filtering. *IEEE Journal of Selected Topics in Signal Processing*, 7(3):399–409, 2013.
- [176] Branko Ristic, Ba Tuong Vo, Ba Ngu Vo, and Alfonso Farina. A tutorial on Bernoulli filters: Theory, Implementation and Applications. *IEEE Transactions on Signal Processing*, 61(13):3406–3430, 2013.
- [177] Ba-tuong Vo and Ba-ngu Vo. Labeled Random Finite Sets and Multi-Object Conjugate Priors. *IEEE Transactions on Signal Processing*, 61(13):3460–3475, 2013.
- [178] Ba Ngu Vo, Ba Tuong Vo, and Dinh Phung. Labeled random finite sets and the bayes multi-target tracking filter. *IEEE Transactions on Signal Processing*, 62(24):6554–6567, 2014.
- [179] Stephan Reuter, Ba Tuong Vo, Ba Ngu Vo, and Klaus Dietmayer. The labeled multi-Bernoulli filter. *IEEE Transactions on Signal Processing*, 62(12):3246–3260, 2014.
- [180] Francesco Papi, Ba-Ngu Vo, Ba-Tuong Vo, Claudio Fantacci, and Michael Beard. Generalized labeled multi-Bernoulli approximation of multi-object densities. *IEEE Transactions on Signal Processing*, 63(20):5487–5497, 2015.
- [181] Ba Ngu Vo, Ba Tuong Vo, and Hung Gia Hoang. An Efficient Implementation of the Generalized Labeled Multi-Bernoulli Filter. *IEEE Transactions on Signal Processing*, 65(8):1975–1987, 2017.
- [182] Felix Kunz, Dominik Nuss, Jurgen Wiest, Hendrik Deusch, Stephan Reuter, Franz Gritschneider, Alexander Scheel, Manuel Stubler, Martin Bach, Patrick Hatzelmann, Cornelius Wild, and Klaus Dietmayer. Autonomous driving at Ulm University: A modular, robust, and sensor-independent fusion approach. In *Intelligent Vehicles Symposium*, pages 666–673. IEEE, 2015.

- [183] John Mullane, Ba Ngu Vo, and Martin D. Adams. Rao-Blackwellised PHD SLAM. In *International Conference on Robotics and Automation (ICRA)*, pages 5410–5416. IEEE, 2010.
- [184] John Mullane, Ba-Ngu Vo, Martin D. Adams, and Ba-Tuong Vo. A Random-Finite-Set Approach to Bayesian SLAM. *IEEE Transactions on Robotics*, 27(2):268–282, 2011.
- [185] D. Moratuwage, Ba-Ngu Vo, and Danwei Wang. A Hierarchical Approach to the Multi-Vehicle SLAM Problem. In *International Conference on Information Fusion (FUSION)*, pages 1119–1125, 2012.
- [186] Chee Sing Lee, Daniel E. Clark, and Joaquim Salvi. SLAM with single cluster PHD filters. In *International Conference on Robotics and Automation (ICRA)*, pages 2096–2101. IEEE, 2012.
- [187] Chee Sing Lee, Sharad Nagappa, Narcis Palomeras, Daniel E. Clark, and Joaquim Salvi. SLAM with SC-PHD filters: An underwater vehicle application. *IEEE Robotics and Automation Magazine*, 21(2):38–45, 2014.
- [188] Diluka Moratuwage, Danwei Wang, Akshay Rao, Namal Senarathne, and Han Wang. RFS collaborative multivehicle SLAM: SLAM in dynamic high-clutter environments. *IEEE Robotics and Automation Magazine*, 21(2):53–59, 2014.
- [189] Martin Adams, Ba Ngu Vo, Ronald Mahler, and John Mullane. SLAM gets a PHD: New concepts in map estimation. *IEEE Robotics and Automation Magazine*, 21(2):26–37, 2014.
- [190] Hendrik Deusch, Stephan Reuter, and Klaus Dietmayer. The Labeled Multi-Bernoulli SLAM Filter. *IEEE Signal Processing Letters*, 22(10):1561–1565, 2015.
- [191] S. Kullback. *Information Theory and Statistics*. Dover Publications, Inc., New York, NY, USA, 1968.
- [192] Shun Ichi Amari.  $\alpha$ -Divergence Is Unique, Belonging To Both  $f$ -Divergence and Bregman Divergence Classes. *IEEE Transactions on Information Theory*, 55(11):4925–4931, 2009.
- [193] Alfréd Rényi. On measures of entropy and information. In *Fourth Berkeley Symposium on Mathematical Statistics and Probability, Volume 1: Contributions to the Theory of Statistics*, pages 547–561, Berkeley, Calif., 1961. University of California Press.
- [194] Frank Nielsen and Sylvain Boltz. The Burbea-Rao and Bhattacharyya centroids. *IEEE Transactions on Information Theory*, 57(8):5455–5466, 2011.
- [195] Mario Bukal, Ivan Marković, and Ivan Petrović. Composite distance based approach to von Mises mixture reduction. *Information Fusion*, 20(1):136–145, 2014.



- [196] D. J. Salmond. Mixture reduction algorithms for point and extended object tracking in clutter. *IEEE Transactions on Aerospace and Electronic Systems*, 45(2):667–686, 2009.
- [197] Mike West. Approximating Posterior Distributions by Mixture. *Journal of the Royal Statistical Society. Series B (Methodological)*, 55(2):409–422, 1993.
- [198] A. A. Gorji, R. Tharmarasa, and T. Kirubarajan. Performance Measures for Multiple Target Tracking Problems. In *International Conference on Information Fusion (FUSION)*, pages 1560–1567, 2011.
- [199] Laura Leal-Taix, Anton Milan, Ian Reid, Stefan Roth, and Konrad Schindler. MOTChallenge 2015: Towards a Benchmark for Multi-Target Tracking. Technical report, 2015.
- [200] Rainer Stiefelhagen, Keni Bernardin, Rachel Bowers, R. Travis Rose, Martial Michel, and John Garofolo. The CLEAR 2007 evaluation. In *Lecture Notes in Computer Science*, volume 4625 LNCS, pages 3–34. 2008.
- [201] Keni Bernardin and Rainer Stiefelhagen. Evaluating multiple object tracking performance: The CLEAR MOT metrics. *Journal on Image and Video Processing*, 2008(246309):10, 2008.
- [202] J.R. Hoffman and R.P.S. Mahler. Multitarget miss distance via optimal assignment. *IEEE Transactions on Systems, Man, and Cybernetics - Part A: Systems and Humans*, 34(3):327–336, 2004.
- [203] Dominic Schuhmacher, Ba-Tuong Vo, and Ba-Ngu Vo. A Consistent Metric for Performance Evaluation of Multi-Object Filters. *IEEE Transactions on Signal Processing*, 56(8):3447–3457, 2008.
- [204] B. Ristic, Ba-Ngu Vo, D. Clark, and Ba-Tuong Vo. A Metric for Performance Evaluation of Multi-Target Tracking Algorithms. *IEEE Transactions on Signal Processing*, 59(7):3452–3457, 2011.
- [205] Tuyet Vu and Rob Evans. A New Performance metric for Multiple target tracking based on Optimal Subpattern Assignment. In *International Conference on Information Fusion (FUSION)*. IEEE, 2014.

---

## PUBLICATIONS

### PUBLICATION 1

I. Marković, J. Ćesić and I. Petrović. Von Mises Mixture PHD Filter. *IEEE Signal Processing Letters*, 22(12):2229–2233, 2015.

# Von Mises Mixture PHD Filter

Ivan Marković, *Member, IEEE*, Josip Česić, *Student Member, IEEE*, and Ivan Petrović, *Member, IEEE*

**Abstract**—This letter deals with the problem of tracking multiple targets on the unit circle, a problem that arises whenever the state and the sensor measurements are circular, i.e. angular-only, random variables. To tackle this problem, we propose a novel mixture approximation of the probability hypothesis density filter based on the von Mises distribution, thus constructing a method that globally captures the non-Euclidean nature of the state and the measurement space. We derive a closed-form recursion of the filter and apply principled approximations where necessary. We compared the performance of the proposed filter with the Gaussian mixture probability hypothesis density filter on a synthetic dataset of 100 randomly generated multitarget trajectory examples corrupted with noise and clutter, and on the PETS2009 dataset. We achieved respectively a decrease of 10.5% and 2.8% in the optimal subpattern assignment metric (notably 16.9% and 10.8% in the localization component).

**Index Terms**—Directional statistics, multitarget tracking, probability hypothesis density filter, von Mises distribution.

## I. INTRODUCTION

MULTITARGET TRACKING (MTT) is a complex problem in which, apart from single target tracking issues like process and sensor noise, false alarms and imperfect detection, we have to additionally contend with measurement origin uncertainty, data association and target births and deaths [1]. The data association-based seminal MTT algorithms such as multiple hypothesis tracker (MHT) [2] and joint probabilistic data association (JPDA) filter [3] approach the MTT problem by considering explicit measurement-to-target association. In contrast, the formulation based on random finite sets (RFSs) does not demand explicit associations between measurements and targets, but rather treats the collections of states and measurements as RFSs where both the set elements and its cardinality are random variables. This approach to MTT allows the casting of foundation for the optimal multitarget Bayes filter [4]. Within this concept various algorithms for multitarget and multisensor tracking were developed, such as the probability hypothesis density (PHD) [4]–[6], cardinalized PHD (CPHD) [7], [8], and multi-Bernoulli filters [9]–[12].

In this letter, we propose a novel mixture approximation of the PHD filter tailored specifically for the topology of a

MTT system on a non-Euclidean geometry, namely the unit circle. This problem arises whenever the state and the sensor measurements are circular, i.e. angular-only, variables and appear when tracking targets with omnidirectional cameras, microphone arrays and similar omnidirectional sensors [13]. The filter is based on the von Mises (vM) distribution defined on the unit circle itself, thus yielding a finite mixture approximation in the vein of [6] and can be theoretically applied to all the RFS algorithms involving finite mixture implementations. Previous works that performed estimation on the unit circle described the state either with a single component [14]–[19] or a finite mixture [20]–[23]. However, none of the previous works approach the MTT problem based on the theory of RFS directly on the unit circle.

## II. THE MULTITARGET BAYES FILTER

In an MTT scenario, at time  $k - 1$  the scene might consist of  $n_{k-1}$  targets,  $x_{k-1,1}, \dots, x_{k-1,n_{k-1}} \in \mathcal{X}$ , whose number is a subject to change due to births and deaths. In turn, the targets give rise to  $m_k$  measurements,  $z_{k,1}, \dots, z_{k,m_k} \in \mathcal{Z}$ , whose origin is unknown; some targets might not have been detected while some measurements are false alarms. The multitarget approach of [9] addresses this problem by modeling the states and measurements as RFSs, which consist of random variables where the set cardinality is also a random variable. More formally at time  $k$

$$\begin{aligned} X_k &= \{x_{k,1}, \dots, x_{k,n_k}\} \in \mathcal{F}(\mathcal{X}) \\ Z_k &= \{z_{k,1}, \dots, z_{k,m_k}\} \in \mathcal{F}(\mathcal{Z}), \end{aligned} \quad (1)$$

where  $\mathcal{F}(\mathcal{X})$  and  $\mathcal{F}(\mathcal{Z})$  denote spaces of all finite subsets  $\mathcal{X}$  and  $\mathcal{Z}$ , respectively. The final goal of the multitarget Bayes filtering [9] is to estimate the multitarget posterior probability distribution  $p(X_k|Z_k)$  via ‘classical’ Bayes filter form

$$\begin{aligned} p(X_k|Z^{k-1}) &= \int p(X_k|X_{k-1})p(X_{k-1}|Z^{k-1})\delta X_{k-1} \\ p(X_k|Z^k) &= \frac{p(Z_k|X_k)p(X_k|Z^{k-1})}{\int p(Z_k|X_k)p(X_k|Z^{k-1})\delta X_k}, \end{aligned} \quad (2)$$

where  $Z^k = \{Z_1, \dots, Z_k\}$  is the history of all the measurements,  $p(X_k|X_{k-1})$  is the multitarget Markov transition density,  $p(Z_k|X_k)$  is the multisource likelihood function and the integrals in (2) are *set integrals* as defined by the multitarget calculus in [9]. Analytic solution to (2) is derived in [24]–[26] with generalization to general multiobject densities presented in [27]. However, often utilized are principled approximations among which the PHD filter is an example.

### A. The Probability Hypothesis Density Filter

The idea of the PHD filter is to propagate the *intensity function*  $D_k$ , i.e. the first order statistical moment of the multitarget

Manuscript received July 16, 2015; accepted August 20, 2015. Date of publication August 25, 2015; date of current version September 01, 2015. This work was supported by European Community’s Seventh Framework Programme under Grant Agreement 285939 (ACROSS), and by research project VISTA (EuropeAid/131920/M/ACT/HR). The associate editor coordinating the review of this manuscript and approving it for publication was Prof. Ba-Tuong Vo.

The authors are with the University of Zagreb, Faculty of Electrical Engineering and Computing, Department of Control and Computer Engineering, Zagreb, Croatia (e-mail: ivan.markovic@fer.hr; josip.cesic@fer.hr; ivan.petrovic@fer.hr).

Color versions of one or more of the figures in this paper are available online at <http://ieeexplore.ieee.org>.

Digital Object Identifier 10.1109/LSP.2015.2472962

density, in lieu of the multitarget density  $p(X_k|Z_{1:k})$  itself. Although there is information loss due to this step, it is outweighed by the gain in alleviating the computational intractability of the multitarget Bayes filter. Function  $D_k$  is not a density function, but is uniquely characterized by the property that given a region  $S$  of single-target space  $\mathcal{X}$  the integral  $\int_S D_k(x)dx$  yields the expected number of targets in  $S$ . Hence, the PHD filter reasons first on the level of group behavior and then attempts to detect and track individual targets only as the quantity and quality of data permits [9].

Given that, the PHD filter operates by evaluating two successive steps—prediction and correction. The PHD prediction is governed by the following equation [9]

$$D_{k|k-1}(x_k) = b(x_k) + \int_{\mathcal{X}} p_{S,k}(x_{k-1})p(x_k|x_{k-1})D_{k-1}(x_{k-1})dx_{k-1}, \quad (3)$$

where  $p(x_k|x_{k-1})$  is single-target Markov transition density,  $p_{S,k}(x_{k-1})$  is the probability of survival of existing objects given their previous state and  $b(x_k)$  is the target birth intensity.

In the sequel we shall make assumptions that do not restrict the proposed method just to such scenarios, but serve only for the purposes of the clarity of presentation. For example, note that we have omitted spawning from existing targets, thus (3) does not represent a general form of the PHD filter prediction, and we shall also assume that  $p_{S,k}(x_{k-1}) = p_S$  is constant and independent of the previous target state. In conjunction, the PHD correction is governed by

$$D_k(x_k) = [1 - p_{D,k}(x_k)] D_{k|k-1}(x_k) + \sum_{z_k \in Z_k} \frac{p_{D,k}(x_k)p(z_k|x_k)D_{k|k-1}(x_k)}{\lambda_z c(z) + D_{k|k-1}[p_{D,k}(x_k)p(z_k|x_k)]}, \quad (4)$$

where  $D_{k|k-1}[f(x)] = \int_{\mathcal{X}} f(x)D_{k|k-1}(x)dx$ ,  $\lambda_z$  is clutter intensity with its spatial distribution  $c(z)$ ,  $p(z_k|x_k)$  is single-source likelihood function and  $p_{D,k}(x_k) = p_D$  is probability of object detection given its current state. In the sequel we shall assume that the spatial distribution of clutter  $c(z)$  is uniform over the whole measurement space  $\mathcal{Z}$  and that  $p_{D,k}(x_k) = p_D$  is constant and independent of the current object state.

Recursions (3) and (4) are derived under the assumptions that [6], [9]: (i) each object evolves and generates independent observations, (ii) clutter is Poisson distributed and independent of object-originated measurements and (iii) the predicted multitarget  $p(X_k|Z_{1:k-1})$  in (2) is distributed according to the multitarget Poisson distribution. The PHD recursion does not admit closed-form solutions in general [9], however sequential Monte Carlo (SMC) approximations [5] and the linear Gaussian multitarget model approach based on Gaussian mixtures (GM) render the aforementioned problem soluble. In this letter, in the vein of [6], we derive a closed-form solution for the vM -PHD filter.

### III. THE VON MISES PHD FILTER

#### A. Von Mises Distribution

The vM distribution is a continuous parametric probability distribution defined on the unit circle, or equivalently on interval  $[0, 2\pi)$ , with pdf given by [28]

$$\mathcal{M}_{\kappa}(x - \mu) = \frac{1}{2\pi I_0(\kappa)} \exp \{ \kappa \cos(x - \mu) \}, \quad (5)$$

where  $0 \leq x < 2\pi$ ,  $\mu \in [0, 2\pi)$  denotes the mean angle,  $\kappa \geq 0$  is the concentration parameter and  $I_0$  is the modified Bessel function of the first kind and of order zero [29]. The vM distribution is often referred as the circular analogue of the normal distribution on the real line: it is unimodal, symmetric around mean angle  $\mu$ , and the concentration parameter  $\kappa$  is analogous to the inverse of the variance.

#### B. Mathematical Preliminaries

As stated in Section II we are working with angular-only measurement and are interested in estimating target directions in one dimension, thus our state space  $\mathcal{X} = [0, 2\pi)$  and our measurement space  $\mathcal{Z} = [0, 2\pi)$ .

*Proposition 1:* Given two vM densities,  $\mathcal{M}_{\kappa_i}(x - \mu_i)$  and  $\mathcal{M}_{\kappa_j}(x - \mu_j)$ , the following relations hold:

(a) *convolution formula* [29]

$$\int_0^{2\pi} \mathcal{M}_{\kappa_i}(x - \xi - \mu_i) \mathcal{M}_{\kappa_j}(\xi - \mu_j) d\xi \approx \mathcal{M}_{\tilde{\kappa}}(x - \tilde{\mu}), \quad (6)$$

where  $\tilde{\mu} = \mu_i + \mu_j$ ,  $\tilde{\kappa} = A^{-1}(A(\kappa_i)A(\kappa_j))$  and  $A(x) = I_1(x)/I_0(x)$  with  $I_p(x)$  as the modified Bessel function of the first kind and of order  $p$ . The integral in (6) does have an exact solution, but the result is not a vM distribution and would prevent obtaining a closed-form filter. Therefore, the approximation (6) based on circular moment matching is used, which has been shown to be quite satisfactory [14], [15], [29].

(b) *product formula*

$$\begin{aligned} & \mathcal{M}_{\kappa_i}(x - \mu_i) \mathcal{M}_{\kappa_j}(x - \mu_j) \\ &= \frac{I_0(\kappa_{i,j})}{2\pi I_0(\kappa_i)I_0(\kappa_j)} \mathcal{M}_{\kappa_{i,j}}(x - \mu_{i,j}), \end{aligned} \quad (7)$$

where

$$\mu_{i,j} = \mu_i + \arctan \left( \frac{-\sin(\mu_i - \mu_j)}{\frac{\kappa_i}{\kappa_j} + \cos(\mu_i - \mu_j)} \right) \quad (8)$$

$$\kappa_{i,j} = \sqrt{\kappa_i^2 + \kappa_j^2 + 2\kappa_i\kappa_j \cos(\mu_i - \mu_j)}. \quad (9)$$

The scaling factor that multiplies the vM density in (7) can be seen as the result of integrating the left-hand side in  $x$ , thus similarly to (6) can be approximated as [13]

$$\frac{I_0(\kappa_{i,j})}{2\pi I_0(\kappa_i)I_0(\kappa_j)} \approx \mathcal{M}_{\tilde{\kappa}}(\mu_i - \mu_j). \quad (10)$$

The result can be seen as a vM ‘innovation’—similar behavior is also exhibited by the Gaussian distribution [6], [30]. The approximation is only necessary for numerical stability due to large concentration parameters and unlike (6), it is not a prerequisite for analytical tractability. We now turn to stating explicitly the required PHD filter models.

*Assumption 1:* The single-target Markov transition density and the single-source sensor likelihood functions are both defined by vM densities

$$p(x_k|x_{k-1}) = \mathcal{M}_{\kappa_Q}(x_k - x_{k-1}) \quad (11)$$

$$p(z_k|x_k) = \mathcal{M}_{\kappa_R}(z_k - x_k), \quad (12)$$

where  $\kappa_Q$  and  $\kappa_R$  are concentration parameters modeling process and measurement noise. The given transition density essentially models a Brownian-type motion on the circle.

*Assumption 2:* The birth intensity function is a von Mises mixture of the form

$$b(x_k) = \sum_{i=1}^{J_{b,k}} w_{b,i}^i \mathcal{M}_{\kappa_b^i}(x_k - \mu_b^i). \quad (13)$$

The number of the newly birthed targets is governed by a Poisson distribution with the corresponding intensity  $\lambda_b$ .

*Assumption 3:* The false alarm rate is governed by a Poisson distribution with the corresponding intensity  $\lambda_z$ , while the spatial distribution of false alarms is considered to be uniform over the whole measurement space  $\mathcal{Z}$ , thus  $c(z) = 1/2\pi$ .

### C. The Von Mises Mixture PHD Filter Recursion

At this point we finally have all the necessary ingredients to derive the proposed vM -PHD filter.

*Proposition 2:* Given the Assumptions 1–2 and that the posterior intensity at time  $k-1$  is a vM mixture

$$D_{k-1}(x_{k-1}) = \sum_{i=1}^{J_{k-1}} w_{k-1}^i \mathcal{M}_{\kappa_{k-1}^i}(x_{k-1} - \mu_{k-1}^i) \quad (14)$$

the predicted intensity  $D_{k|k-1}(x_k)$  is also a vM mixture

$$D_{k|k-1}(x_k) = b(x_k) + p_S \sum_{i=1}^{J_{k-1}} w_{k|k-1}^i \mathcal{M}_{\kappa_{k-1}^i}(x_k - \mu_{k-1}^i), \quad (15)$$

where  $\tilde{\kappa}_{k-1}^i = A^{-1}(A(\kappa_Q)A(\kappa_{k-1}^i))$ . What basically happens at the prediction stage is that the birth intensity function is added to the  $k-1$  posterior vM mixture, which is in the second summation predicted to time  $k$ .

The predicted number of objects can be calculated by taking the integral of (15) over the whole state space  $\mathcal{X}$

$$N_{k|k-1} = \sum_{i=1}^{J_{b,k}} w_{b,i}^i + p_S \sum_{i=1}^{J_{k-1}} w_{k|k-1}^i. \quad (16)$$

*Proposition 3:* Given the Assumptions 1–3 and that the predicted intensity at time  $k$  is a vM mixture

$$D_{k|k-1}(x_k) = \sum_{i=1}^{J_{k|k-1}} w_{k|k-1}^i \mathcal{M}_{\kappa_{k|k-1}^i}(x_k - \mu_{k|k-1}^i), \quad (17)$$

where  $J_{k|k-1} = J_{b,k} + J_{k-1}$ , the posterior intensity at time  $k$  is also a vM mixture of the following form

$$D_k(x_k) = (1 - p_D)D_{k|k-1}(x_k) + \sum_{i=1}^{J_{k|k-1}} \sum_{j=1}^{J_{z,k}} w_k^{i,j} \mathcal{M}_{\kappa_k^{i,j}}(x_k - \mu_k^{i,j}), \quad (18)$$

where  $J_{z,k}$  is the number of measurements and

$$w_k^{i,j} = p_D \frac{w_{k|k-1}^i w_z^j I_0(\kappa_k^{i,j})}{2\pi I_0(\kappa_{k|k-1}^i) I_0(\kappa_z^j)}$$

$$w_z^j = \left( \lambda_z c(z) + p_D D_{k|k-1}[p(z_k^j|x_k)] \right)^{-1}$$

$$D_{k|k-1}[p(z_k^j|x_k)] = \sum_{i=1}^{J_{k|k-1}} \frac{w_{k|k-1}^i I_0(\kappa_k^{i,j})}{2\pi I_0(\kappa_z) I_0(\kappa_{k|k-1}^i)} \quad (19)$$

and  $\mu_k^{i,j}$  and  $\kappa_k^{i,j}$  are given by (8) and (9) with  $\{\mu_{k|k-1}^i, z_k^j\}$  and  $\{\kappa_{k|k-1}^i, \kappa_z^j\}$  in lieu of  $\{\mu_i, \mu_j\}$  and  $\{\kappa_i, \kappa_j\}$ . The first summa-

tion accounts for the undetected components, while the double summation term accounts for the crossproduct of all the predicted components and the obtained measurements.

By taking the integral of (18) over the whole state space  $\mathcal{X}$  we can calculate the posterior number of targets in the scene

$$N_k = (1 - p_D)N_{k|k-1} + p_D \sum_{z_k \in \mathcal{Z}_k} \frac{D_{k|k-1}[p(z_k|x_k)]}{\lambda_z c(z) + p_D D_{k|k-1}[p(z_k|x_k)]}. \quad (20)$$

At this stage, as in the case of the GM-PHD filter [6], at the end of each iteration we will have a vM mixture representing the intensity function of the posterior multitarget distribution. What remains is (i) to extract the estimated states of the tracked targets and (ii) to handle the geometrically growing number of components after each correction step (18) in order to keep the computational tractability.

### D. PHD Mixture Component Reduction and State Estimation

The component reduction needs to be computationally cheap since it will be executed after each iteration step. In [31] we have analyzed and compared reduction algorithms for the exponential family of distributions by using the vM distribution as a study example. Although there were several more accurate reduction techniques, the reduction based on West's algorithm [32] was computationally the least intensive.

For the distance measure in the present letter we use the symmetrized scaled Kullback-Leibler (KL) distance [33], which for two vM weighted components,  $w_i \mathcal{M}_i = w_i \mathcal{M}_{\kappa_i}(x - \mu_i)$  and  $w_j \mathcal{M}_j = w_j \mathcal{M}_{\kappa_j}(x - \mu_j)$ , is given by

$$d_{sKL}(w_i \mathcal{M}_i, w_j \mathcal{M}_j) = \frac{1}{2} [w_i d_{KL}(\mathcal{M}_i, \mathcal{M}_j) + w_j d_{KL}(\mathcal{M}_j, \mathcal{M}_i)] + \frac{1}{2} (w_i - w_j) \log \frac{w_i}{w_j}, \quad (21)$$

where  $d_{KL}(\mathcal{M}_i, \mathcal{M}_j)$  is the 'standard' KL distance [34] between two vM densities [31]

$$d_{KL}(\mathcal{M}_i, \mathcal{M}_j) = \log \frac{I_0(\kappa_j)}{I_0(\kappa_i)} + A(\kappa_i)(\kappa_i - \kappa_j \cos(\mu_i - \mu_j)). \quad (22)$$

The West's algorithm works on the principle of ordering the mixture components according to their weights and then finds the closest component to the first one according to the chosen distance measure. Then, the closest pair of components is merged and the resulting one is inserted back into the mixture per its respective weight. The merged component  $\mathcal{M}_{\kappa^*}(x - \mu^*)$  has the following parameters optimal in the KL sense

$$\tan \mu^* = \frac{w_i A(\kappa_i) \sin \mu_i + w_j A(\kappa_j) \sin \mu_j}{w_i A(\kappa_i) \cos \mu_i + w_j A(\kappa_j) \cos \mu_j}$$

$$w^* A^2(\kappa^*) = w_i^2 A^2(\kappa_i) + 2w_i w_j A(\kappa_i) A(\kappa_j) \cos(\mu_i - \mu_j), \quad (23)$$

where  $w^* = w_i + w_j$ . The procedure is repeated until the desired, application dependent, number of components  $J_k'$  is reached. For more details regarding the reduction algorithm and component merging method please confer [31].

In [6] for the GM-PHD filter it was proposed to estimate the states of the tracked targets by picking  $N_k$  components with largest weights. We follow the same train of thought except that

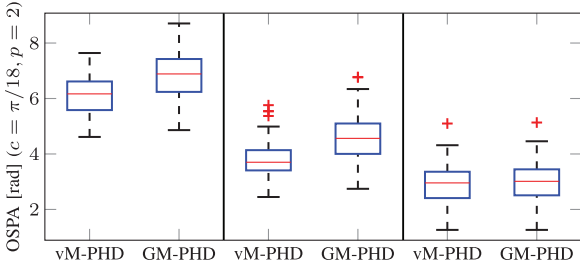


Fig. 1. Matlab's boxplot of cumulative OSPA over 100 multitarget trajectories. On average the vM-PHD outperforms the GM-PHD by 10.5% in total OSPA (left), out of which 16.9% in the localization component (middle), and 2.6% in the cardinality component (right).

before the picking we reduce the PHD mixture with the West's algorithm to  $\alpha N_k$ , where  $\alpha > 1$  is a scaling factor. Empirically we have noticed that this lowers the chance of losing peaks belonging to tracked targets. Note that the mixture with  $\alpha N_k$  components is used only for target state estimation, while the mixture with  $J_k' > \alpha N_k$  components is utilized in the future filtering steps. Furthermore, special attention was given to numerical issues, since the function  $I_0(\kappa)$  for  $\kappa > 700$  quickly reaches the maximum value that can be stored in double precision floating point representation. Hence, we have implemented numerically stable evaluations of the  $\log(I_0(\kappa))$  [35] and the Bessel function ratio  $A(\kappa)$  [36], while the inverse  $A^{-1}(\kappa)$  was numerically calculated [37].

#### IV. EXPERIMENTS

In order to validate and test the performance of the vM-PHD filter, we have devised a multitarget simulation scenario with angle-only measurements. The targets moved on the unit circle with constant angular velocity of 1 deg/s to which zero-mean Gaussian noise with standard deviation of 0.25 deg/s was sequentially added. Initial number of objects in the scene was set to three, the probability of survival was 0.99, while the Poisson rate of births was 0.05. Each object had 0.95 probability of being detected by the sensor corrupted with zero-mean vM noise and a concentration parameter corresponding to a standard deviation of 1.5 deg [15]. False alarms were uniformly distributed with a Poisson rate of 1.6 false alarms per scan. We generated 100 examples of such a multitarget scenario and compared the performance of the vM-PHD with the GM-PHD filter (taking into account the state cardinality). The filters were also compared on the PETS2009 dataset [38], [39] by tracking the azimuth of the backprojected world coordinates. As a performance metric we used the optimal subpattern assignment (OSPA) metric [40], which was developed with the goal of being a consistent metric for performance evaluation of multitarget filters.

In Fig. 1 we present performance comparison of the vM-PHD and GM-PHD filter, where for each of the 100 trajectories a cumulative OSPA was calculated and its statistics is depicted. The vM-PHD noticeably outperforms the GM-PHD filter in the localization component of the OSPA (even with small measurement noise), while in cardinality the difference is less pronounced. In Fig. 2 localization and cardinality estimation are depicted for an example of the vM-PHD where in total 7 targets were successfully tracked. A time instant from this example with correctly estimated targets even when the number of false alarms (5) is larger than the number of objects (4) is depicted in Fig. 3(a). A

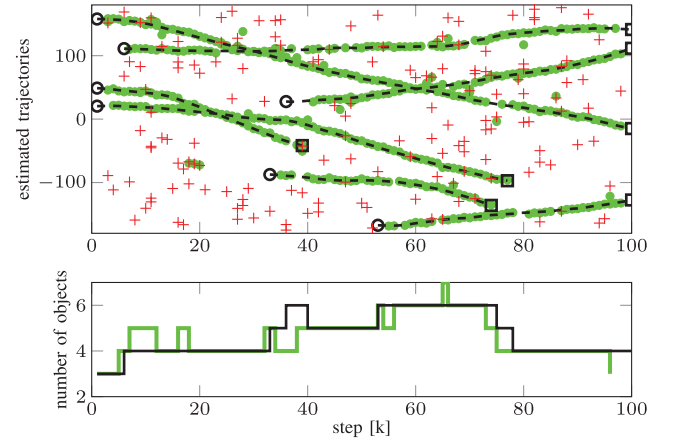


Fig. 2. Results for a scenario with 7 targets. In the upper figure black dashed lines are true trajectories with black circles and squares as trajectory starting and terminating points. Green circles are estimated states, while red pluses are false alarms. In the lower figure the black and green lines represent the true and the estimated number of objects. The Matlab source code and a supplementary MP4 format movie clip are available at <http://ieeexplore.ieee.org>.

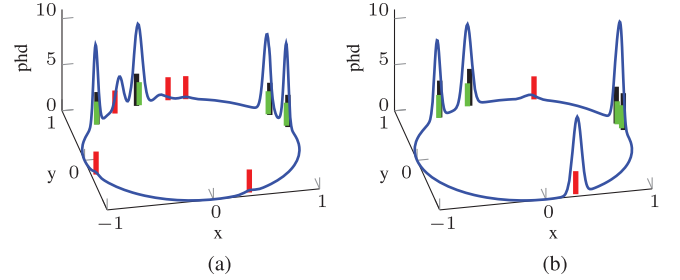


Fig. 3. The vM mixture corrected PHDs (blue solid line) after reduction to 5 components for state extraction along with false alarms (red vertical lines), four targets (black vertical lines) and four measurements (green vertical lines): (a)  $k = 16$ ,  $N_{k|k} = 4$  (b)  $k = 20$ ,  $N_{k|k} = 4$ .

more rare example where false alarms were erroneously chosen as target estimates due to closely spaced targets and several consecutive false alarms (around  $k = 20$ ) is shown in Fig. 3(b). On the PETS2009 dataset the total OSPA was reduced 2.8%, out of which 10.8% in the localization, while cardinality component was equal.

#### V. CONCLUSION

In this letter we have proposed a novel mixture approximation of the PHD filter tailored specifically for multitarget tracking system on the unit circle. We have achieved this by modeling the state and measurements as circular random variables whose uncertainty was described by the von Mises distribution. The resulting filter required some principled approximations to achieve closed-form and ensure numerical stability. Using the OSPA metric we compared the performance of the vM-PHD to the GM-PHD on 100 multitarget trajectories and the PETS2009 dataset, achieving respectively on average a decrease in the OSPA metric by 10.5% and 2.8% (notably 16.9% and 10.8% in the localization component). The vM-PHD has potential applications in all the multitarget tracking scenarios working with circular state and measurement representations.

#### ACKNOWLEDGMENT

The authors would like to thank M. Bukal of the University of Zagreb for his helpful comments and suggestions.

## REFERENCES

- [1] M. Mallick, B.-N. Vo, T. Kirubarajan, and S. Arulampalam, "Introduction to the on multitarget tracking," *IEEE J. Sell. Topics Signal Process.*, vol. 7, no. 3, pp. 373–375, Jun. 2013.
- [2] D. Reid, "An algorithm for tracking multiple targets," *IEEE Trans. Automat. Contr.*, vol. 24, no. 6, pp. 843–854, 1979.
- [3] Y. Bar-Shalom and E. Tse, "Sonar tracking of multiple targets using joint probabilistic data association filter," *Automatica*, vol. 11, pp. 451–460, 1975.
- [4] R. P. S. Mahler, "Multitarget Bayes filtering via first-order multitarget moments," *IEEE Trans. Aerosp. Electron. Syst.*, vol. 39, no. 4, pp. 1152–1178, Oct. 2003.
- [5] B.-N. Vo, S. Singh, and A. Doucet, "Sequential Monte Carlo methods for multi-target filtering with random finite sets," *IEEE Trans. Aerosp. Electron. Syst.*, vol. 41, no. 4, pp. 1224–1245, Oct. 2005.
- [6] B.-N. Vo and W.-K. Ma, "The Gaussian mixture probability hypothesis density filter," *IEEE Trans. Signal Processing*, vol. 54, no. 11, pp. 4091–4104, Nov. 2006.
- [7] R. Mahler, "PHD filters of higher order in target number," *IEEE Trans. Aerosp. Electron. Syst.*, vol. 43, no. 4, pp. 1523–1543, 2007.
- [8] B.-T. Vo, B.-N. Vo, and A. Cantoni, "Analytic implementations of the cardinalized probability hypothesis density filter," *IEEE Trans. Signal Process.*, vol. 55, no. 7, pp. 3553–3567, Jul. 2007.
- [9] R. Mahler, *Statistical Multisource-Multitarget Information Fusion*. Norwood, MA, USA: Artech House, 2007.
- [10] B. T. Vo, B. N. Vo, and A. Cantoni, "The cardinality balanced multi-target multi-Bernoulli filter and its implementations," *IEEE Trans. Signal Process.*, vol. 57, no. 2, pp. 409–423, 2009.
- [11] S. Reuter, B. T. Vo, B. N. Vo, and K. Dietmayer, "The labeled multi-Bernoulli filter," *IEEE Trans. Signal Process.*, vol. 62, no. 12, pp. 3246–3260, 2014.
- [12] H. Deusch, S. Reuter, and K. Dietmayer, "The labeled multi-Bernoulli SLAM filter," *IEEE Signal Process. Lett.*, vol. 22, no. 10, pp. 1561–1565, 2015.
- [13] I. Marković, "Moving objects detection and tracking by omnidirectional sensors of a mobile robot," Ph.D. dissertation, Univ. Zagreb, Fac. Elect. Eng. Comput., Zagreb, Croatia, 2014.
- [14] M. Azmani, S. Reboul, J.-B. Choquel, and M. Benjelloun, "A recursive fusion filter for angular data," in *IEEE Int. Conf. Robotics and Biomimetics (ROBIO)*, Dec. 2009, pp. 882–887.
- [15] G. Kurz, I. Gilitschenski, and U. D. Hanebeck, "Recursive nonlinear filtering for angular data based on circular distributions," in *American Control Conf. (ACC)*, 2013, pp. 5439–5445.
- [16] J. Traa and P. Smaragdis, "A wrapped Kalman filter for azimuthal speaker tracking," *IEEE Signal Process. Lett.*, vol. 20, no. 12, pp. 1257–1260, 2013.
- [17] D. F. Crouse, "Maximum-likelihood post-detection radar ambiguity resolution," *IEEE Trans. Aerosp. Electron. Syst.*, vol. 50, no. 3, pp. 1876–1883, 2014.
- [18] Y. Yi and H. Xu, "Hierarchical data association framework with occlusion handling for multiple targets tracking," *IEEE Signal Process. Lett.*, vol. 21, no. 3, pp. 288–291, Mar. 2014.
- [19] G. Kurz, I. Gilitschenski, S. Julier, and U. D. Hanebeck, "Recursive bingham filter for directional estimation involving 180 degree symmetry," *J. Adv. Inf. Fusion*, vol. 9, no. 2, pp. 90–105, 2014.
- [20] V. Cevher, R. Velmurugan, and J. H. McClellan, "Acoustic multitarget tracking using direction-of-arrival batches," *IEEE Trans. Signal Process.*, vol. 55, no. 6, pp. 2810–2825, 2007.
- [21] S. Calderara, A. Prati, and R. Cucchiara, "Mixtures of von Mises distributions for people trajectory shape analysis," *IEEE Trans. Circuits Syst. Video Technol.*, vol. 21, no. 4, pp. 457–471, 2011.
- [22] I. Marković and I. Petrović, "Bearing-only tracking with a mixture of von Mises distributions," in *IEEE/RSJ Int. Conf. Intelligent Robots and Systems (IROS)*, 2012, pp. 707–712.
- [23] I. Marković, A. Portello, P. Danès, and I. Petrović, "Active speaker localization with circular likelihoods and bootstrap filtering," in *IEEE/RSJ Int. Conf. Intelligent Robots and Systems (IROS)*, 2013, pp. 2914–2920.
- [24] B. T. Vo and B. N. Vo, "Labeled random finite sets and multi-object conjugate priors," *IEEE Trans. Signal Process.*, vol. 61, no. 13, pp. 3460–3475, 2013.
- [25] B. N. Vo, B. T. Vo, and D. Phung, "Labeled random finite sets and the Bayes multi-target tracking filter," *IEEE Trans. Signal Process.*, vol. 62, no. 24, pp. 6554–6567, 2014.
- [26] H. G. Hoang, B.-T. Vo, and B.-N. Vo, "A generalized labeled multi-Bernoulli filter implementation using Gibbs sampling," *arXiv:1506.00821*, 2015.
- [27] F. Papi, B.-N. Vo, B.-T. Vo, C. Fantacci, and M. Beard, "Generalized labeled multi-Bernoulli approximation of multi-object densities," *arXiv:1412.5294*, 2014.
- [28] R. von Mises, "Über die 'Ganzzahligkeit' der Atomgewichte und Verwandte Fragen," *Phys. Zeitschrift*, vol. 19, pp. 490–500, 1918.
- [29] K. V. Mardia and P. E. Jupp, *Directional Statistics*. New York, NY, USA: Wiley, 1999.
- [30] H. W. Sorenson and D. L. Alspach, "Recursive Bayesian estimation using Gaussian sums," *Automatica*, vol. 7, no. 1, pp. 465–479, 1971.
- [31] M. Bukal, I. Marković, and I. Petrović, "Composite distance based approach to von Mises mixture reduction," *Inf. Fusion*, vol. 20, pp. 136–145, 2014.
- [32] M. West, "Approximating posterior distributions by mixtures," *J. Roy. Statist. Soc. B*, vol. 55, no. 2, pp. 409–442, 1993.
- [33] S. Amari, "Alpha-divergence is unique, belonging to both f-divergence and Bregman divergence classes," *IEEE Trans. Inf. Theory*, vol. 55, no. 11, pp. 4925–4931, 2009.
- [34] S. Kullback, *Information Theory and Statistics*. New York, NY, USA: Dover, 1997.
- [35] A. Tanabe, K. Fukumizu, S. Oba, T. Takenouchi, and S. Ishii, "Parameter estimation for von Mises–Fisher distributions," *Computati. Statist.*, vol. 22, no. 1, pp. 145–157, 2007.
- [36] W. Gautschi and J. Slavik, "On the computation of modified Bessel function ratios," *Math. Computat.*, vol. 32, no. 143, pp. 865–875, 1978.
- [37] J. P. Marques de Sá, *Applied Statistics using SPSS, Statistica, Matlab and R*. Berlin, Germany: Springer-Verlag, 2007.
- [38] J. Ferryman and A. Shahrokni, "PETS2009: Dataset and challenge," in *IEEE Int. Workshop on Performance Evaluation of Tracking Surveillance*, 2009.
- [39] L. Leal-Taixé, A. Milan, I. Reid, S. Roth, and K. Schindler, "MOTChallenge 2015: Towards a benchmark for multi-target tracking," *arXiv:1504.01942 [cs]*, 2015.
- [40] D. Schuhmacher, B. T. Vo, and B. N. Vo, "A consistent metric for performance evaluation of multi-object filters," *IEEE Trans. Signal Process.*, vol. 56, pp. 3447–3457, 2008.

## PUBLICATION 2

I. Marković, J. Ćesić and I. Petrović. On wrapping the Kalman filter and estimating with the  $SO(2)$  group. *International Conference on Information Fusion (FUSION)*. Heidelberg, Germany, 2245–2250, 2016.



# On wrapping the Kalman filter and estimating with the $SO(2)$ group

Ivan Marković, Josip Ćesić, Ivan Petrović

University of Zagreb, Faculty of Electrical Engineering and Computing, Unska 3, 10000 Zagreb, Croatia

Email: ivan.markovic@fer.hr, josip.cesic@fer.hr, ivan.petrovic@fer.hr

**Abstract**—This paper analyzes directional tracking in 2D with the extended Kalman filter on Lie groups (LG-EKF). The study stems from the problem of tracking objects moving in 2D Euclidean space, with the observer measuring direction only, thus rendering the measurement space and object position on the circle—a non-Euclidean geometry. The problem is further inconvenienced if we need to include higher-order dynamics in the state space, like angular velocity which is a Euclidean variables. The LG-EKF offers a solution to this issue by modeling the state space as a Lie group or combination thereof, e.g.,  $SO(2)$  or its combinations with  $\mathbb{R}^n$ . In the present paper, we first derive the LG-EKF on  $SO(2)$  and subsequently show that this derivation, based on the mathematically grounded framework of filtering on Lie groups, yields the same result as heuristically wrapping the angular variable within the EKF framework. This result applies only to the  $SO(2)$  and  $SO(2) \times \mathbb{R}^n$  LG-EKFs and is not intended to be extended to other Lie groups or combinations thereof. In the end, we showcase the  $SO(2) \times \mathbb{R}^2$  LG-EKF, as an example of a constant angular acceleration model, on the problem of speaker tracking with a microphone array for which real-world experiments are conducted and accuracy is evaluated with ground truth data obtained by a motion capture system.

## I. INTRODUCTION

In moving object tracking, it is not uncommon to work with sensors that can provide only direction to the object in question. The measurement and estimation state space have a specific geometry of their own, which is different from the geometry of the true trajectory space. The problem is challenging, because, although the motion of the object resides either in 3D or 2D Euclidean space, corresponding measurements reside either on the sphere or the circle, respectively. Namely, if we are measuring and estimating only the direction to the object in 2D, i.e., the azimuth, the state and measurements will bear the non-Euclidean properties of angles. However, if we are to extend the state space so that it includes both the angular velocity and acceleration (which are Euclidean variables), so that we can apply a higher-order dynamic motion model, we are faced with constructing a ‘hybrid’ state space consisting of both the non-Euclidean and Euclidean variables.

There exist Bayesian methods based on the principle of assumed density filtering with directional distributions on the circle, namely the von Mises distribution, the wrapped Gaussian distribution and the Bingham distribution (which actually models variables with  $180^\circ$  symmetry), that capture intrinsically the non-Euclidean nature of angular random variables [1]–[6]. The benefit of these approaches is that they take globally into account the geometry of the state space.

For example, in the case of the von Mises distribution it has been shown that the filter outperforms the naive Kalman filter, which treats angles like regular Euclidean variables, and the modified Kalman filter, which takes into account the nature of angles by wrapping them on the circle [4], [7]. However, extending the state space with additional variables of different geometry, e.g., to analytically model the azimuth with the von Mises distribution and the range or the angular velocity with the Gaussian distribution and capture correctly the cross-correlations, remains a challenge.

The  $SO(2)$  group is a set of orthogonal matrices with determinant one, whose elements geometrically represent rotations. This makes it an interesting candidate for estimation with angular variables. Furthermore, a filter could be derived not just for  $SO(2)$ , but also for combinations of  $SO(2)$  with  $\mathbb{R}$ . This would enable us to create the aforementioned ‘hybrid’ state vector that would join both non-Euclidean and Euclidean variables within the same filter and enable a seamless utilization of higher-order system models with constant angular velocity or acceleration. An extended Kalman filter on matrix Lie groups was recently proposed in [8]. It provides us with a mathematical framework for solving the ‘hybrid’ state space problem. Indeed, the filter can be applied directly for any state that is a combination of Lie groups, since a Cartesian product of Lie groups is a Lie group [8]. However, it should be noted that the LG-EKF is a local approach, in the sense that it does not take globally the geometry of the state space into account, but locally captures the geometry of state space via exponential mapping. Another approach would be to model the whole state space as a Euclidean vector within the ‘classical’ Kalman filter framework, and wrap the operations involving angular variables. Indeed, this was performed in [4] to modify the unscented Kalman filter for angular state estimation, in [9] to take idiosyncrasies of directional statistics when using polar or spherical coordinates in the cubature Kalman filter, and in [7] to modify the Gaussian mixture probabilistic hypothesis density filter for multitarget tracking on a circle.

In this paper we propose to analyze the LG-EKF for directional tracking of moving objects in 2D. First, we look into deriving the LG-EKF on the  $SO(2)$ , which also serves as a gentle introduction to the subject matter since the LG-EKF introduces non-trivial notation. Second, we model the directional moving object tracking in 2D as an estimation problem on the Lie group composed of the direct product  $SO(2) \times \mathbb{R}^2$ , i.e., a group that represents the moving object

azimuth, angular velocity and angular acceleration. For the motion model, we use the constant angular acceleration model. In the end, we show that the  $\text{SO}(2)$  LG-EKF filter derivation based on the mathematically grounded framework of filtering on Lie groups yields the same result as heuristically wrapping the angular variables within the extended Kalman filter (EKF) framework. Since for the case of  $\mathbb{R}^n$  the LG-EKF evaluates to EKF [8], this results also extends to  $\text{SO}(2) \times \mathbb{R}^2$  LG-EKF and an  $\mathbb{R}^3$  EKF when wrapping the angular component. Please note that this result *applies only* to the  $\text{SO}(2)$  filter and is not intended to be extended to other Lie groups or combinations thereof. Indeed, given that  $\text{SO}(2)$  is abelian, i.e., commutative, the result does not seem unexpected, but we assert that it gives interesting theoretical perspective on estimation and tracking with the heuristically modified EKF. Before we proceed with the filter derivation, we introduce some necessary formal definitions and operators for working with matrix Lie groups.

## II. MATHEMATICAL BACKGROUND

### A. Wrapping the Kalman filter

In this section we shall assume that wrapping operation amounts to enforcing the angular variable to be in the  $[-\pi, \pi]$  interval, and we designate this operation as follows

$$w^\pi(x) = \text{mod}(x + \pi, 2\pi) - \pi. \quad (1)$$

Note that when computing the difference between two angular variables, the wrapping effect of the circle should be taken into account, e.g., the difference between  $178^\circ$  and  $-178^\circ$  should evaluate to  $4^\circ$ . This is also achieved by (1) when the difference is given as the argument, i.e., difference between two angles  $x$  and  $y$  is computed as  $w^\pi(x - y)$ .

Let us assume the following system model

$$x_{k+1|k} = f_k(x_k, u_k) + n_k, \quad n_k \sim \mathcal{N}(0, Q) \quad (2)$$

where  $x_k$  is the system state,  $u_k$  is the control input,  $n_k$  is process noise, and  $f_k(\cdot)$  is the non-linear system state equation. In the EKF the idiosyncrasies of angular data appear most prominently in the correction step when calculating the innovation, which should be computed as

$$x_{k+1} = x_{k+1|k} + K_k w^\pi(z_k - h_k(x_{k+1|k})), \quad (3)$$

where  $K_k$  is the Kalman gain,  $z_k$  is the measurement, and  $h_k(\cdot)$  is the non-linear measurement equation.

To demonstrate this, let us take a simple example of having an identity measurement equation,  $x_{k+1|k} = 358^\circ$ ,  $z_k = 2^\circ$  and  $K_k = 0.5$ . If we would not wrap the innovation, the updated state would yield a clearly incorrect result of  $x_{k+1} = 180^\circ$  in lieu of  $x_{k+1} = 360^\circ$ . For practical purposes, after correction and prediction the system state can be checked to the required interval by computing  $x_{k+1} \leftarrow w^\pi(x_{k+1})$ . In the sequel when we refer to the modified Kalman filter, it entails treating angular variables with the previously introduced operation. Furthermore, we assume that the reader is familiar with EKF equations, which we will not present or derive explicitly in order to keep the brevity of the paper.

### B. Lie Groups

A Lie group  $G$  is a group which is also a smooth manifold and the group composition and inverse are smooth functions on the manifold  $G$ . A manifold is an object that looks locally like a piece of  $\mathbb{R}^n$  and  $G$  is ‘smooth’ in the sense that it has a tangent space, of the appropriate dimension, at each point. Take for example the circle, a curve in  $\mathbb{R}^2$  which looks locally (but not globally) like  $\mathbb{R}^1$ . For a matrix Lie group the composition and inverse are simply matrix multiplication and inversion, with the identity element  $\mathbf{I}^{n \times n}$  [10].

A Lie Algebra  $\mathfrak{g}$  is an open neighborhood of  $\mathbf{0}^{n \times n}$  in the tangent space of  $G$  at the identity  $\mathbf{I}^{n \times n}$ . The matrix exponential  $\exp_G$  and matrix logarithm  $\log_G$  establish a local diffeomorphism between Lie groups and Lie algebras [8]

$$\exp_G : \mathfrak{g} \rightarrow G, \quad \log_G : G \rightarrow \mathfrak{g}. \quad (4)$$

The Lie Algebra  $\mathfrak{g}$  associated to a  $p$ -dimensional matrix Lie group  $G \subset \mathbb{R}^{n \times n}$  is a  $p$ -dimensional vector space [10]. A linear isomorphism between  $\mathfrak{g}$  and  $\mathbb{R}^p$  is given by

$$[\cdot]_G^\vee : \mathfrak{g} \rightarrow \mathbb{R}^p, \quad [\cdot]_G^\wedge : \mathbb{R}^p \rightarrow \mathfrak{g}. \quad (5)$$

Lie Groups are not necessarily commutative. The following two operators capture this property

- the adjoint representation of  $G$  on  $\mathbb{R}^p$

$$\text{Ad}_G : \text{Ad}_G(X)x = [X[x]_G^\wedge X^{-1}]_G^\vee \quad (6)$$

- the adjoint representation of  $\mathbb{R}^p$  on  $\mathbb{R}^p$

$$\text{ad}_G : \text{ad}_G(x)y = [[x]_G^\wedge [y]_G^\wedge - [y]_G^\wedge [x]_G^\wedge]_G^\vee \quad (7)$$

where  $x, y \in \mathbb{R}^p$ . In the sequel, these operators, the exponential and logarithmic mapping are given concrete form for the pertinent Lie groups.

### C. The $\text{SO}(2)$ group

In this example our system state (azimuth of the tracked object) is modeled as the group  $G = \text{SO}(2)$ , i.e., as the rotation matrix  $X_k = R_{\theta_k}$

$$R_{\theta_k} = \begin{bmatrix} \cos \theta_k & -\sin \theta_k \\ \sin \theta_k & \cos \theta_k \end{bmatrix}. \quad (8)$$

The composition and inverse in  $\text{SO}(2)$  are simply evaluated as  $X_1 X_2 = R_1 R_2$ ,  $X^{-1} = R^T$ . For this case the associated Lie algebra which bridges  $X_k \in G$  and  $x_k = \theta_k \in \mathbb{R}^1$  is  $\mathfrak{g} = \mathfrak{so}(2)$ , and the following holds

$$[\theta_k]_G^\wedge = \begin{bmatrix} 0 & -\theta_k \\ \theta_k & 0 \end{bmatrix}. \quad (9)$$

The link between  $\text{SO}(2)$  and  $\mathfrak{so}(2)$  is given by the exponential and logarithmic mapping

$$\exp_G([\theta_k]_G^\wedge) = R_{\theta_k} : \mathfrak{so}(2) \rightarrow \text{SO}(2), \quad (10)$$

$$\log_G(R_{\theta_k}) = [\theta_k]_G^\wedge : \text{SO}(2) \rightarrow \mathfrak{so}(2). \quad (11)$$

Due to the commutativity of  $\text{SO}(2)$ , the adjoint operators are

$$\text{ad}_G(\theta_k) = 0, \quad \text{Ad}_G(\exp_G([\theta_k]_G^\wedge)) = 1. \quad (12)$$

These properties greatly simplify the LG-EKF formulae for the  $\text{SO}(2)$  group which will become evident in the sequel.

#### D. The $SO(2) \times \mathbb{R}^2$ group

In this section we propose to model the system state as the Cartesian product of groups  $G = SO(2) \times \mathbb{R}^2$ . This is a slight abuse of notation intended for clarity, since when talking about  $\mathbb{R}$  within the group or algebra, we are actually referring to the group of algebra representation of  $\mathbb{R}$ , for which the explicit representation is given further in the paper. The moving object state  $X_k$  will represent the azimuth of the target as a rotation matrix  $R_{\theta_k} \in SO(2)$ , angular velocity as a real number  $\omega_k \in \mathbb{R}$ , and angular acceleration also as a real number  $\alpha_k \in \mathbb{R}$ . The system state  $X_k$  can be symbolically represented as

$$X_k = \begin{bmatrix} R_k & & \\ & \begin{bmatrix} 1 & \omega_k \\ 0 & 1 \end{bmatrix} & \\ & & \begin{bmatrix} 1 & \alpha_k \\ 0 & 1 \end{bmatrix} \end{bmatrix} = \begin{pmatrix} R_k \\ \omega_k \\ \alpha_k \end{pmatrix}_G. \quad (13)$$

Note that composition and inverse on such a group is evaluated as follows

$$X_1 X_2 = \begin{pmatrix} R_1 R_2 \\ \omega_1 + \omega_2 \\ \alpha_1 + \alpha_2 \end{pmatrix}_G, \quad X^{-1} = \begin{pmatrix} R^T \\ -\omega \\ -\alpha \end{pmatrix}_G. \quad (14)$$

The associated Lie algebra is  $\mathfrak{g} = \mathfrak{so}(2) \times \mathbb{R}^2$  which bridges the state on the Lie group  $X_k \in G$  with the vector  $x_k = [\theta_k \ \omega_k \ \alpha_k]^T \in \mathbb{R}^3$ , and the following holds

$$[x_k]_G^\wedge = \begin{bmatrix} [\theta_k]_{\mathfrak{so}(2)}^\wedge & & \\ & [\omega_k]_{\mathbb{R}}^\wedge & \\ & & [\alpha_k]_{\mathbb{R}}^\wedge \end{bmatrix} = \begin{pmatrix} [\theta_k]_{\mathfrak{so}(2)}^\wedge \\ \omega_k \\ \alpha_k \end{pmatrix}_{\mathfrak{g}}, \quad (15)$$

where  $[\theta_k]_{\mathfrak{so}(2)}^\wedge$  is given by (9), while

$$[\omega_k]_{\mathbb{R}}^\wedge = \begin{bmatrix} 0 & \omega_k \\ 0 & 0 \end{bmatrix} \quad \text{and} \quad [\alpha_k]_{\mathbb{R}}^\wedge = \begin{bmatrix} 0 & \alpha_k \\ 0 & 0 \end{bmatrix}. \quad (16)$$

The link between the group  $G$  and the associated algebra  $\mathfrak{g}$  is defined by the exponential mapping

$$\exp_G([x_k]_G^\wedge) = \begin{pmatrix} \exp_{\mathfrak{so}(2)}([ \theta_k ]_{\mathfrak{so}(2)}^\wedge) & & \\ & \omega_k & \\ & & \alpha_k \end{pmatrix}_G = \begin{pmatrix} R_k \\ \omega_k \\ \alpha_k \end{pmatrix}_G, \quad (17)$$

and logarithmic mapping

$$\log_G(X_k) = \begin{pmatrix} \log_{\mathfrak{so}(2)}(R_k) \\ \omega_k \\ \alpha_k \end{pmatrix}_{\mathfrak{g}} = \begin{pmatrix} [\theta_k]_{\mathfrak{so}(2)}^\wedge \\ \omega_k \\ \alpha_k \end{pmatrix}_{\mathfrak{g}}. \quad (18)$$

Furthermore, since  $SO(2)$  and  $\mathbb{R}$  are abelian and the Cartesian product of abelian groups is abelian, the adjoint operators are again trivial

$$\text{ad}_G(x_k) = \mathbf{0}^{3 \times 3}, \quad \text{Ad}_G(\exp_G([x_k]_G^\wedge)) = \mathbf{I}^{3 \times 3}. \quad (19)$$

### III. THE EKF ON MATRIX LIE GROUPS

As in the case of classical Kalman filtering, we need to begin by defining a motion model by which we will calculate the prediction. For general filtering on matrix Lie groups, the system model is defined by the following equation [8]

$$X_{k+1} = f(X_k, u_k, n_k) = X_k \exp_G([\hat{\Omega}_k + n_k]_G^\wedge), \quad (20)$$

where  $X_k \in G$  is the system state at time  $k$ ,  $G$  is a  $p$ -dimensional Lie Group,  $n_k \sim \mathcal{N}_{\mathbb{R}^p}(\mathbf{0}^{p \times 1}, Q_k)$  is white Gaussian noise and  $\hat{\Omega}_k = \Omega(X_k, u_k) : G \times \mathbb{R}^w \rightarrow \mathbb{R}^p$  is the system state equation which describes how the model acts on the state and control input in order to calculate the displacement.

Note that the function of  $\hat{\Omega}_k$  is to take the system state which resides on  $G$  and the control input which resides on  $\mathbb{R}^w$ , calculate the displacement by applying the system model, and then transfer the displacement to the vector space  $\mathbb{R}^p$  where additive noise is added. This displacement is then transferred to the associated Lie algebra by the  $[\cdot]_G^\wedge$  operator and then exponentially mapped back to the Lie group to be added by way of composition to the system state  $X_k$ . Given that, a question arises how to implement a specific system model, since in LG-EKF it operates through a displacement? That is, how to construct  $\hat{\Omega}_k$  from  $f_k(x_k, u_k)$ ? The first step would be to write the system equation as  $f_k(x_k, u_k) = x_k + \hat{f}_k(x_k, u_k)$  which can then be practically ‘translated’ to appropriate  $\hat{\Omega}_k$ . Note that generality is not lost here since  $-x_k$  can be included within  $\hat{f}_k(x_k, u_k)$ .

The prediction step of the LG-EKF is governed by the following formulae [8]

$$\mu_{k+1|k} = \mu_k \exp_G([\hat{\Omega}_k]_G^\wedge) \quad (21)$$

$$P_{k+1|k} = \mathcal{F}_k P_k \mathcal{F}_k^T + \Phi_G(\hat{\Omega}_k) Q_k \Phi_G(\hat{\Omega}_k)^T, \quad (22)$$

where  $\mu_k \in G$  is the estimated mean value of the system state  $X_k$ ,  $P_k \in \mathbb{R}^{p \times p}$  is the estimated covariance matrix, while other terms are non-trivially calculated matrices

$$\mathcal{F}_k = \text{Ad}_G(\exp_G([\hat{\Omega}_k]_G^\wedge)) + \Phi_G(\hat{\Omega}_k) \mathcal{C}_k, \quad (23)$$

$$\Phi_G(\nu) = \sum_{m=0}^{\infty} \frac{(-1)^m}{(m+1)!} \text{ad}_G(\nu)^m, \quad \nu \in \mathbb{R}^p, \quad (24)$$

$$\mathcal{C}_k = \frac{\partial}{\partial \epsilon} \Omega(\mu_k \exp_G([\epsilon]_G^\wedge), u_{k-1})|_{\epsilon=0}. \quad (25)$$

The parameter  $\epsilon \in \mathbb{R}^p$  can be seen as a *Lie algebraic error* which is approximated as being distributed according to a classical Euclidean Gaussian distribution  $\epsilon \sim \mathcal{N}_{\mathbb{R}^p}(\mathbf{0}^{p \times 1}, P_k)$ . It is interesting to note that the mean value  $\mu_k$  resides on the Lie group  $G$ , while the covariance matrix  $P_k$  describes uncertainty in  $\mathbb{R}^p$ . Although at first this appears peculiar, it is a consequence of modeling the uncertainty of states on Lie groups by the assumption of the concentrated Gaussian distribution  $X_k \sim \mathcal{G}(\mu_k, P_k)$ . In essence, the state resides on the group, but its uncertainty resides on the tangential vector space. For a more formal introduction of this concept, please confer [8].

The discrete measurement model on the matrix Lie Group is given as follows

$$z_{k+1} = h(X_{k+1}) \exp_{G'}([m_{k+1}]_{G'}^\wedge), \quad (26)$$

where  $z_{k+1} \in G'$ ,  $h: G \rightarrow G'$ , and  $m_{k+1} \sim \mathcal{N}_{\mathbb{R}^q}(\mathbf{0}^{q \times 1}, R_k)$  is white Gaussian noise. Note that here a different group  $G'$  is used since the system state and measurements might belong to different groups. Having the measurement model defined, we can proceed now to the update step which will first constitute the calculation of the Kalman gain

$$K_{k+1} = P_{k+1|k} \mathcal{H}_{k+1}^T (\mathcal{H}_{k+1} P_{k+1|k} \mathcal{H}_{k+1}^T + R_{k+1})^{-1}, \quad (27)$$

where the measurement matrix  $\mathcal{H}_{k+1}$  is calculated via

$$\mathcal{H}_{k+1} = \frac{\partial}{\partial \epsilon} [\log_{G'}(h(\mu_{k+1|k})^{-1} h(\mu_{k+1|k} \exp_G([\epsilon]_G^\wedge)))]_{G'}^\vee \Big|_{\epsilon=0}. \quad (28)$$

Furthermore, the innovation vector multiplied by Kalman gain is computed as

$$\nu_{k+1} = K_{k+1} [\log_{G'}(h(\mu_{k+1|k})^{-1} z_{k+1})]_{G'}^\vee. \quad (29)$$

Finally, the update of the system state and covariance matrix can be evaluated as [8]

$$\mu_{k+1} = \mu_{k+1|k} \exp_G([\nu_{k+1}]_G^\wedge) \quad (30)$$

$$P_{k+1} = \Phi_G(\nu_{k+1}) (\mathbf{I}^{p \times p} - K_{k+1} \mathcal{H}_{k+1}) P_{k+1|k} \Phi_G(\nu_{k+1})^T. \quad (31)$$

We can notice similarities between the LG-EKF and EKF equations and, indeed, when  $G$  and  $G'$  are Euclidean spaces the LG-EKF reduces to EKF [8]. Furthermore, due to the results (12) and (19), matrices  $\mathcal{F}_k$  and  $\Phi_G(\nu)$  for both  $\text{SO}(2)$  and  $\text{SO}(2) \times \mathbb{R}^2$  evaluate to

$$\Phi_G(\nu) = \mathbf{I}, \quad \mathcal{F}_k = \mathbf{I} + \mathcal{C}_k. \quad (32)$$

In the sequel we derive the LG-EKF for the groups which we propose to utilize for tracking of moving objects with angular measurements and show that in this special case the LG-EKF reduces to the heuristically modified EKF.

#### A. LG-EKF on $\text{SO}(2)$

In this section we derive the LG-EKF filter for state estimation on  $G = \text{SO}(2)$ . For this group, mathematically dense LG-EKF equations are simplified and serve well to intuitively grasp the mechanics of the filter.

1) *Prediction:* Let us take two examples of system models. In the first we assume a stationary process, i.e., in the prediction the mean value will remain unchanged except for the uncertainty that is added through the process noise (this is similar to the von Mises filter [1])

$$x_{k+1|k} = x_k + n_k, \quad n_k \sim \mathcal{N}_{\mathbb{R}^1}(0, \sigma_Q^2). \quad (33)$$

This yields the LG-EKF system model  $\Omega(X_k) = 0$  with the same process noise  $n_k$ , which when inserted in (21) will

evaluate through the exponential as an identity matrix, thus leaving the mean value unperturbed.

In order to compute the prediction of the covariance matrix via (22), given the result in (32), we only need to determine  $\mathcal{C}_k$ . In this case the Lie algebraic error is  $\epsilon \in \mathbb{R}^1$  and due to the system model the matrix  $\mathcal{C}_k$  evaluates to zero, thus leaving  $\mathcal{F}_k = 1$ , and the prediction equations are

$$\mu_{k+1|k} = \mu_k, \quad P_{k+1|k} = P_k + Q_k. \quad (34)$$

As we can see, these are the same formulae that an EKF prediction would yield with (33) as the system model.

As the second example, we take the non-linear system [4] where the robot rotary joint angle was estimated

$$x_{k+1|k} = x_k + c_1 \sin(x_k) + c_2 + n_k, \quad (35)$$

where second and third term account for gravity and velocity, while the final term is again one-dimensional white Gaussian noise. This yields the following LG-EKF system model

$$\Omega(X_k) = c_1 \sin([\log(X_k)]_G^\vee) + c_2. \quad (36)$$

Note that  $[\log(X_k)]_G^\vee$  is necessary to bring the rotation matrix with parameter  $\mu_k$  to a scalar angle in  $\mathbb{R}^1$ . The Lie algebraic error is again  $\epsilon \in \mathbb{R}^1$  and given the system model (36) matrix  $\mathcal{C}_k$  evaluates to

$$\begin{aligned} \mathcal{C}_k &= \frac{\partial}{\partial \epsilon} \Omega \left( \begin{bmatrix} \cos \mu_k & -\sin \mu_k \\ \sin \mu_k & \cos \mu_k \end{bmatrix} \begin{bmatrix} \cos \epsilon & -\sin \epsilon \\ \sin \epsilon & \cos \epsilon \end{bmatrix} \right)_{|\epsilon=0} \\ &= \frac{\partial}{\partial \epsilon} \Omega \left( \begin{bmatrix} \cos(\mu_k + \epsilon) & -\sin(\mu_k + \epsilon) \\ \sin(\mu_k + \epsilon) & \cos(\mu_k + \epsilon) \end{bmatrix} \right)_{|\epsilon=0} \\ &= \frac{\partial}{\partial \epsilon} (c_1 \sin(\mu_k + \epsilon) + c_2)_{|\epsilon=0} = c_1 \cos \mu_k \end{aligned} \quad (37)$$

This means that  $\mathcal{F}_k = 1 + c_1 \cos \mu_k$ , and that the LG-EKF prediction equations are

$$\begin{aligned} \mu_{k+1|k} &= \mu_k \exp_G([c_1 \sin([\log(X_k)]_G^\vee) + c_2]_G^\wedge) \\ P_{k+1|k} &= P_k (1 + c_1 \cos \mu_k)^2 + Q_k. \end{aligned} \quad (38)$$

We can see that the covariance prediction formula is identical to the EKF covariance prediction.

More generally, to demonstrate the equivalence of the modified EKF and  $\text{SO}(2)$  LG-EKF prediction steps we need to show that  $\mathcal{F}_k = 1 + \mathcal{C}_k$  is equal to

$$F_k = \frac{\partial f_k(x_k, u_k)}{\partial x_k} \Big|_{x_k = \mu_k}, \quad (39)$$

where  $F_k$  is the state transition matrix, i.e., the EKF system state Jacobian of (2). By inspecting (37) we can notice that for  $\text{SO}(2)$  the argument within  $\Omega$  will always be the sum of the mean value and the Lie algebraic error  $\mu_k + \epsilon$ . This gives

$$\begin{aligned} \mathcal{F}_k &= 1 + \frac{\partial}{\partial \epsilon} \Omega(\exp_G([\mu_k + \epsilon]_G^\wedge), u_k)_{|\epsilon=0} \\ &= 1 + \frac{\partial}{\partial \epsilon} \hat{f}_k(\mu_k + \epsilon, u_k)_{|\epsilon=0} \\ &= 1 + \frac{\partial}{\partial \epsilon} (f_k(\mu_k + \epsilon, u_k) - (\mu_k + \epsilon \theta))_{|\epsilon=0} \\ &= \frac{\partial f_k(\mu_k + \epsilon, u_k)}{\partial \epsilon} \Big|_{\epsilon=0} = \frac{\partial f_k(\xi_k, u_k)}{\partial \xi_k} \Big|_{\xi_k = \mu_k}, \end{aligned} \quad (40)$$

where variable substitution was performed in the last step:  $\xi_k \leftarrow \mu_k + \epsilon$ ,  $\partial \xi_k \leftarrow \partial \epsilon$ . In the end  $\mathcal{F}_k$  evaluates to the EKF Jacobian  $F_k$  when the underlying group is  $\text{SO}(2)$ .

2) *Correction*: Since we are measuring angles, we define the measurement Lie group as  $G' = \text{SO}(2)$  and the measurement function  $h : \text{SO}(2) \rightarrow \text{SO}(2)$

$$h(X_{k+1}) = R_{k+1}, \quad m_{k+1} \sim \mathcal{N}_{\mathbb{R}^1}(0, \sigma_R^2), \quad (41)$$

which is trivial since the measurement and state group are the same, while the measurement noise is a one-dimensional white Gaussian noise. As in the prediction step, the associated Lie algebra is  $\mathfrak{g}' = \mathfrak{so}(2)$ .

To compute the correction step, we need to evaluate (28) for the LG-EKF on  $\text{SO}(2)$ . The composition of the predicted mean  $\mu_{k+1|k}$  and the Lie algebraic error yields

$$h(\mu_{k+1|k} \exp_{\text{SO}(2)}([\epsilon]_{\text{SO}(2)}^\wedge)) = \begin{bmatrix} \cos(\mu_{k+1|k} + \epsilon) & -\sin(\mu_{k+1|k} + \epsilon) \\ \sin(\mu_{k+1|k} + \epsilon) & \cos(\mu_{k+1|k} + \epsilon) \end{bmatrix}. \quad (42)$$

Since  $h(\mu_{k+1|k})^{-1}$  is the transpose of the corresponding rotation matrix, by inserting these results in (28) we can calculate the measurement matrix

$$\mathcal{H}_{k+1} = \frac{\partial}{\partial \epsilon} \left( \left[ \log_G \left( \begin{bmatrix} \cos \epsilon & -\sin \epsilon \\ \sin \epsilon & \cos \epsilon \end{bmatrix} \right) \right]_G^\vee \right)_{|\epsilon=0} = 1 \quad (43)$$

Given this results it is straightforward to see that Kalman gain and covariance update equation of  $\text{SO}(2)$  LG-EKF are equal to the EKF equations. The state correction equations yield the same result, except that the LG-EKF takes wrapping into account by composition of rotation matrices, while the modified EKF computes everything in  $\mathbb{R}^1$  and would need to wrap the corrected state with  $w^\pi(\cdot)$ .

### B. LG-EKF on $\text{SO}(2) \times \mathbb{R}^2$

In this section we derive the LG-EKF filter for state estimation on  $G = \text{SO}(2) \times \mathbb{R}^2$ . Given the demonstrated equality of the  $\text{SO}(2)$  LG-EKF and the modified EKF and that LG-EKF reduces to EKF for Euclidean spaces, it is intuitive to expect that this result would extend to groups derived by composing  $\text{SO}(2)$  with Euclidean spaces. In the sequel we illustrate this property by deriving a constant angular acceleration model for tracking with angle-only measurements.

1) *Prediction*: Given the state representation, we can now define the system model. For this purpose, we use the constant angular acceleration model  $\hat{\Omega}_k = \Omega(X_k) : G \rightarrow \mathbb{R}^3$

$$\Omega(X_k) = \begin{bmatrix} T\omega_k + \frac{1}{2}T^2\alpha_k \\ T\alpha_k \\ 0 \end{bmatrix}, \quad n_k \sim \mathcal{N}_{\mathbb{R}^3}(0, Q). \quad (44)$$

Note that the displacement due to motion is calculated first in  $\mathbb{R}^3$  and then according to (21) transferred to Lie algebra  $\mathfrak{g}$ , exponentially mapped to the group  $G$  and then by way of composition added to the system state  $X_k$ .

In this case, the Lie algebraic error is  $\epsilon = [\epsilon_\theta \ \epsilon_\omega \ \epsilon_\alpha]^\top \in \mathbb{R}^3$ , hence the composition of the mean value  $\mu_k$  and  $\epsilon$  yields

$$\mu_k \exp_G([\epsilon]_G^\wedge) = \begin{pmatrix} R_k R_\epsilon \\ \omega_k + \epsilon_\omega \\ \alpha_k + \epsilon_\alpha \end{pmatrix}_G, \quad (45)$$

with  $R_k R_\epsilon$  has the same for as the matrix product in (42). By applying the motion model (44) on this results we get

$$\Omega(\mu_k \exp_G([\epsilon]_G^\wedge)) = \begin{bmatrix} T(\omega + \epsilon_\omega) + \frac{1}{2}T^2(\alpha + \epsilon_\alpha) \\ T(\alpha + \epsilon_\alpha) \\ 0 \end{bmatrix}. \quad (46)$$

To compute the prediction step for the covariance matrix, we need to calculate matrix  $\mathcal{F}_k$ . Since adjoint operators are trivial, using (46) we calculate

$$F_k = \mathbf{I} + \mathcal{F}_k = \begin{bmatrix} 1 & T & \frac{1}{2}T^2 \\ 0 & 1 & T \\ 0 & 0 & 1 \end{bmatrix}. \quad (47)$$

We can see that the matrix  $\mathcal{F}_k$  evaluates to the well known transition matrix of the classical EKF constant acceleration motion model.

2) *Correction*: Since here we track moving objects by measuring angles, we define the measurement Lie group  $G' = \text{SO}(2)$  and the measurement function  $h : \text{SO}(2) \times \mathbb{R}^2 \rightarrow \text{SO}(2)$

$$h(X_{k+1}) = R_{k+1}, \quad m_{k+1} \sim \mathcal{N}_{\mathbb{R}^1}(0, \sigma_R^2) \quad (48)$$

which in this case simply extracts the rotation matrix  $R_{k+1}$  from  $X_{k+1}$ . Calculation of the matrix  $\mathcal{H}_{k+1}$  is the same as in (28), except that  $\epsilon$  is now a vector

$$\mathcal{H}_{k+1} = \frac{\partial}{\partial \epsilon} (\epsilon_\theta)_{|\epsilon=0} = [1 \ 0 \ 0]. \quad (49)$$

Again, the same result as we would expect for the EKF measurement matrix.

## IV. EXPERIMENTS

As a practical example of an application of the studied filter we apply this on the problem of speaker tracking with a microphone array and in the present paper we test the  $\text{SO}(2) \times \mathbb{R}^2$  LG-EKF on real-world data. For the sound acquisition we used the ManyEars framework consisting of an 8-channel USB sound card [11], while for obtaining measurements we used the beamforming algorithm for speaker localization [12] implemented under the Robot Operating Systems [13] within the same framework. The maximum of the beamforming energy was picked as the speaker measurement.

The experiments were conducted in a 120m<sup>2</sup> room with parquet wooden flooring and one side covered with windows. The speaker was simulated by a loudspeaker playing an excerpt from Nature's podcast *Audiophile* in English. The area in which the loudspeaker moved was covered by a motion capture system, which was used to generate ground truth data. In order to handle outliers, we used validation gating; namely, the innovation matrix  $S_{k+1} = \mathcal{H}_{k+1} P_{k+1|k} \mathcal{H}_{k+1}^\top + R_{k+1}$  was calculated and we applied the standard  $\chi^2$ -test

$$\nu_{k+1} S_{k+1}^{-1} \nu_{k+1}^\top < \gamma, \quad (50)$$

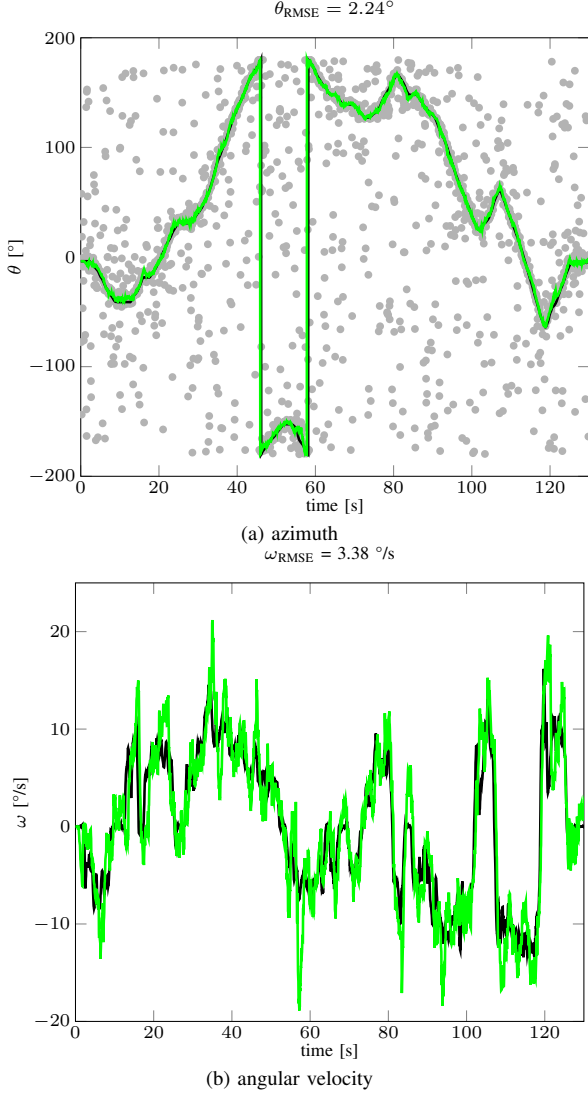


Fig. 1: Performance of the LG-EKF on  $\text{SO}(2) \times \mathbb{R}^2$  when tracking a moving speaker. The solid black line is the ground truth as given by the motion capture system, the green solid line is the estimated state of the speaker, while the gray circles represent measurements, i.e. outputs of the beamformer. State RMSE is given in the title of each of the subfigures.

where the threshold  $\gamma$  was determined from the inverse  $\chi_p^2$  cumulative distribution at a significance level  $\alpha = 0.95$  and  $p$  degrees-of-freedom. Figure 1 shows the experiment results and corroborates that the filter successfully manages to track the moving speaker in spite of the number of outliers. Note that the modified EKF would yield the same results, except that in the case of the LG-EKF the system state was defined on  $\text{SO}(2) \times \mathbb{R}^2$  and the idiosyncrasies of angular data were intrinsically taken care of.

## V. CONCLUSION

In this paper we have studied directional moving object tracking in 2D based on the extended Kalman filter on matrix Lie groups. First, we have proposed to analyze this estimation

problem by modeling the state to reside on the  $\text{SO}(2)$  group. Subsequently, we have shown that the  $\text{SO}(2)$  filter derivation based on the mathematically grounded framework of filtering on Lie groups yields evaluates to heuristically wrapping the extended Kalman filter. We emphasize that this result *applies only* to the  $\text{SO}(2)$  filter and is not intended to be extended to other Lie groups or combinations thereof. Second, we have derived the constant angular velocity  $\text{SO}(2) \times \mathbb{R}^2$  filter, where the system state consisted of azimuth, angular velocity and angular acceleration. For this filter we showcased a real-world experiment of a speaker tracking problem with a microphone array by assessing the accuracy using the ground truth obtained by a motion capture system.

## ACKNOWLEDGMENTS

This work has been supported from the European Union's Horizon 2020 research and innovation programme under grant agreement No 688117 (SafeLog) and the Unity Through Knowledge Fund under the project Cooperative Cloud based Simultaneous Localization and Mapping in Dynamic Environments.

## REFERENCES

- [1] M. Azmani, S. Reboul, J.-B. Choquel, and M. Benjelloun, "A recursive fusion filter for angular data," in *IEEE International Conference on Robotics and Biomimetics (ROBIO)*, dec 2009, pp. 882–887.
- [2] I. Marković and I. Petrović, "Speaker localization and tracking with a microphone array on a mobile robot using von Mises distribution and particle filtering," *Robotics and Autonomous Systems*, vol. 58, no. 11, pp. 1185–1196, 2010.
- [3] —, "Bearing-only tracking with a mixture of von Mises distributions," in *IEEE/RSJ International Conference on Intelligent Robots and Systems (IROS)*, 2012, pp. 707–712.
- [4] G. Kurz, I. Gilitschenski, and U. D. Hanebeck, "Recursive nonlinear filtering for angular data based on circular distributions," in *American Control Conference (ACC)*, 2013, pp. 5439–5445.
- [5] G. Kurz, I. Gilitschenski, S. Julier, and U. D. Hanebeck, "Recursive estimation of orientation based on the Bingham distribution," in *International Conference on Information Fusion (FUSION)*, 2013, pp. 1–16.
- [6] G. Stienne, S. Reboul, M. Azmani, J. Choquel, and M. Benjelloun, "A multi-temporal multi-sensor circular fusion filter," *Information Fusion*, vol. 18, pp. 86–100, jul 2014.
- [7] I. Marković, J. Česić, and I. Petrović, "Von Mises mixture PHD filter," *IEEE Signal Processing Letters*, vol. 22, no. 12, pp. 2229–2233, 2015.
- [8] G. Bourmaud, R. Mégard, M. Arnaudon, and A. Giremus, "Continuous-discrete extended Kalman filter on matrix Lie groups using concentrated Gaussian distributions," *Journal of Mathematical Imaging and Vision*, vol. 51, no. 1, pp. 209–228, 2015.
- [9] D. F. Crouse, "Cubature / Unscented / Sigma Point Kalman Filtering with Angular Measurement Models," in *International Conference on Information Fusion*, 2015, pp. 1550–1557.
- [10] G. S. Chirikjian, *Stochastic Models, Information Theory, and Lie Groups, Volume 2: Analytic Methods and Modern Applications*. Springer, 2012.
- [11] F. Grondin, D. Létourneau, F. Ferland, V. Rousseau, and F. Michaud, "The ManyEars open framework," *Autonomous Robots*, vol. 34, no. 3, pp. 217–232, 2013.
- [12] J.-M. Valin, F. Michaud, and J. Rouat, "Robust localization and tracking of simultaneous moving sound sources using beamforming and particle filtering," *Robotics and Autonomous Systems*, vol. 55, no. 3, pp. 216–228, 2007.
- [13] M. Quigley, B. Gerkey, K. Conley, J. Faust, T. Foote, J. Leibs, E. Berger, R. Wheeler, and A. Ng, "ROS : an open-source Robot Operating System," *IEEE International Conference on Robotics and Automation (ICRA), Workshop on Open Source Software*, 2009.

## PUBLICATION 3

J. Ćesić, I. Marković and I. Petrović. Moving object tracking employing rigid body motion on matrix Lie groups. *International Conference on Information Fusion (FUSION)*. Heidelberg, Germany, 2109–2115, 2016.

# Moving object tracking employing rigid body motion on matrix Lie groups

Josip Ćesić, Ivan Marković, Ivan Petrović

University of Zagreb, Faculty of Electrical Engineering and Computing, Unska 3, 10000 Zagreb, Croatia

Email: josip.cesic@fer.hr, ivan.markovic@fer.hr, ivan.petrovic@fer.hr

**Abstract**—In this paper we propose a novel method for estimating rigid body motion by modeling the object state directly in the space of the rigid body motion group  $SE(2)$ . It has been recently observed that a noisy manoeuvring object in  $SE(2)$  exhibits *banana-shaped* probability density contours in its pose. For this reason, we propose and investigate two state space models for moving object tracking: (i) a direct product  $SE(2) \times \mathbb{R}^3$  and (ii) a direct product of the two rigid body motion groups  $SE(2) \times SE(2)$ . The first term within these two state space constructions describes the current pose of the rigid body, while the second one employs its second order dynamics, i.e., the velocities. By this, we gain the flexibility of tracking omnidirectional motion in the vein of a constant velocity model, but also accounting for the dynamics in the rotation component. Since the  $SE(2)$  group is a matrix Lie group, we solve this problem by using the extended Kalman filter on matrix Lie groups and provide a detailed derivation of the proposed filters. We analyze the performance of the filters on a large number of synthetic trajectories and compare them with (i) the extended Kalman filter based constant velocity and turn rate model and (ii) the linear Kalman filter based constant velocity model. The results show that the proposed filters outperform the other two filters on a wide spectrum of types of motion.

## I. INTRODUCTION

A wide area of robotics research has extensively focused on the practical approaches of using different types of manifolds. Besides performance, filters operating on manifolds can provide other advantages as they avoid singularities when representing state spaces with either redundant degrees of freedom or constraint issues [1], [2]. Among the manifolds, the homogeneous transformation matrices, also referred to as the rigid body motion group  $SE(n)$ , hold a special repute. They have been used in a variety of applications, and have risen to popularity firstly through manipulator robotics [3], [4] and later through vision applications [5], [6]. Even though the state description using the rigid body motion group, for both the 2D and 3D case, has been a well known representation, techniques for associating the uncertainty came into focus later [7]. So far, the rigid body motion group with associated uncertainty has been used in several robotics applications such as SLAM [8], motion control [9], shape estimation [10], pose estimation [11] and pose registration [12].

Among them, pose estimation represents one of the central problems in robotics. Recently in [11] the authors discussed the advantages of employing uncertainties on  $SE(2)$  (therein called the exponential coordinates) with respect to Euclidean spaces and have provided the means for working in the exponential coordinates rather than representing the robot's

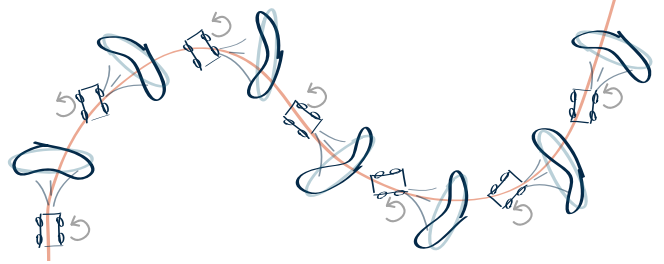


Fig. 1: An illustration of an omnidirectional mobile robot manoeuvring in both translational and rotational components. The banana shaped uncertainty contours, representing the positional uncertainty in the next step, are formed by modeling the uncertainty on the  $SE(2)$  group (blue), while the elliptical shaped contours appear modeling the uncertainty in  $\mathbb{R}^2$  (gray).

position with Gaussians in Cartesian coordinates. This stems from the fact that the uncertain robot motion, and consequently its pose, usually exhibit *banana-shaped* probability density contours rather than the elliptical ones [13], as illustrated in Fig. 1. The classical Kalman filter is designed to operate in the Cartesian space and as such does not provide a framework for filtering directly on the  $SE(2)$  group. Recently, some works have addressed the uncertainty on the  $SE(2)$  group proposing new distributions [14], [15]. However, these interesting approaches do not yet provide a closed-form Bayesian recursion framework (involving both the prediction and update) that can include higher order motion and non-linear models.

An extended Kalman filter on matrix Lie groups (LG-EKF) has been recently proposed in [16]. It provides an estimation framework for filtering directly on matrix Lie groups, of which the  $SE(2)$  group is a member. In accordance with the needs of moving object state estimation problems, higher order motion often needs to be exploited, as in the vein of the constant velocity (CV) or acceleration motion models [17], but in the space such as the rigid body motion group  $SE(2)$ . In the present paper we propose a method for moving object tracking employing its second order motion directly on the  $SE(2)$  group based on the discrete LG-EKF. For this purpose, we model the state space either as a direct product of (i) a rigid body motion group and a Euclidean vector or (ii) two rigid body motion groups, i.e.,

$$(i) SE(2) \times \mathbb{R}^3 \text{ or } (ii) SE(2) \times SE(2) = SE(2)^2. \quad (1)$$

In both cases the first term tracks the pose of the object, while



the second one handles the velocities. In the end, we conduct experimental validation of the proposed filters on synthetic data and compare their performance with the CV and constant turn rate and velocity (CTRV) motion models [18] used within the classical extended Kalman filter (EKF) framework.

The rest of the paper is organized as follows. Section II gives an insight into the motivation behind the present paper. Section III provides the preliminaries including the basic definitions and operators for working with matrix Lie groups, with emphasis on the special euclidean group SE(2). The method for exploiting higher order motion is presented in Section IV and the proposed estimation strategies are investigated on a synthetic dataset and compared with two Kalman filter based methods. Finally, concluding remarks are drawn in Section V.

## II. MOTIVATION

The choice of the state space and the approach to the motion modelling present a significant focus of this paper. The physical interpretation behind associating the uncertainty with the SE(2) group has been analyzed in [11]. Therein, the authors particularly study the shape of the uncertainty by considering differential drive mobile robot motion. The authors conclude that the SE(2) approach provides significant flexibility in describing the position uncertainty, enabling one to analytically work with banana-shaped uncertainty contours. In this work, given the previous moving object tracking discussion, we aim to track omnidirectional motion in order to achieve high flexibility in motion modeling. This is motivated by considering tracking in unknown dynamic environments comprising of multiple unknown moving objects. For example, a mobile robot building a map of an unknown environment consisting of humans and other robots with various kinematics, or a busy intersection with mixed traffic involving cars, trams, motorcycles, bicycles and pedestrians.

By searching for the flexibility to control the velocities in both  $x$  and  $y$  direction, as well as the rotational velocity, one comes to formulation of the state space as  $SE(2) \times \mathbb{R}^3$ . In this case, the SE(2) term tracks the pose of a rigid body object supporting the forming of banana-shaped uncertainty contours, while the  $\mathbb{R}^3$  term describes velocities along the three axis in a classical manner forming elliptical-only contours. Examples of omnidirectional mechanical robot platforms implementations which can be described by this state space construction are the *Palm Pilot Robot*, *Uranus*, and *Killough* [19], which are based on the Swedish 45°/90° wheels.

However, if we consider a robot construction that has additional flexibility of controlling the steering angle of one or more wheels, it turns out that by sampling such kinematic models the uncertainty in the space of velocities also has banana-shaped contours. Given that, we further propose to model the state space as  $SE(2)^2$  group where now the second term exploits the second order motion (velocities), and supports the flexibility of forming the banana-shaped uncertainty contours in the velocity space. Examples of mechanical omnidirectional robot platforms capable of such motion are the *Nomad XR4000* and *Hyperion* [19]. Detailed

physical and kinematic interpretations of these models are, however, out of the scope of this paper and are a subject for future work.

## III. PRELIMINARIES

### A. Lie groups and Lie algebra

In this section, we provide notations and properties for matrix Lie groups and the associated Lie algebras which will be used for the filter including the SE(2) group in the state space. For a more formal introduction of the used concepts, the interested reader is directed to [20], where the author provides a rigorous treatment of representing and propagating uncertainty on matrix Lie groups.

The SE(2), specifically, is a matrix Lie group. A Lie group is a group which has the structure of a smooth manifold, i.e., it is sufficiently often differentiable [2], such that group composition and inversion are smooth operations. Furthermore, for a matrix Lie group  $G$  these operations are simply matrix multiplication and inversion, with the identity matrix  $I^{n \times n}$  being the identity element [20]. An interesting property of Lie groups, basically curved objects, is that they can be almost completely captured by a flat object, such as the tangential space; and this leads us to another important concept—the Lie algebra  $\mathfrak{g}$  associated to a Lie group  $G$ .

Lie algebra  $\mathfrak{g}$  is an open neighborhood of  $\mathbf{0}^{n \times n}$  in the tangent space of  $G$  at the identity  $I^{n \times n}$ . The matrix exponential  $\exp_G$  and matrix logarithm  $\log_G$  establish a local diffeomorphism between these two worlds, i.e., Lie groups and Lie algebras

$$\exp_G : \mathfrak{g} \rightarrow G \quad \text{and} \quad \log_G : G \rightarrow \mathfrak{g}. \quad (2)$$

The Lie algebra  $\mathfrak{g}$  associated to a  $p$ -dimensional matrix Lie group  $G \subset \mathbb{R}^{n \times n}$  is a  $p$ -dimensional vector space defined by a basis consisting of  $p$  real matrices  $E_i$ ,  $i = 1, \dots, p$  [9]. A linear isomorphism between  $\mathfrak{g}$  and  $\mathbb{R}^p$  is given by

$$[\cdot]_G^\vee : \mathfrak{g} \rightarrow \mathbb{R}^p \quad \text{and} \quad [\cdot]_G^\wedge : \mathbb{R}^p \rightarrow \mathfrak{g}. \quad (3)$$

Lie groups are not necessarily commutative and require the use two operators to capture this property and thus, enable the *adjoint representation* of (i)  $G$  on  $\mathbb{R}^p$  denoted as  $\text{Ad}_G$  and (ii)  $\mathbb{R}^p$  on  $\mathbb{R}^p$  denoted as  $\text{ad}_G$  [20]. All the discussed operators in the present section are presented later in the paper for the proposed state space constructions.

### B. Concentrated Gaussian Distribution

Another important concept in the LG-EKF framework is that of the concentrated Gaussian distribution (CGD). In order to define the CGD on matrix Lie groups, the considered group needs to be a connected unimodular matrix Lie group [21], which is the case for the majority of matrix Lie groups used in robotics.

Let the probability density function (pdf) of  $X$ , a state on a  $p$ -dimensional matrix Lie group  $G$ , be defined as [22]

$$p(X) = \beta \exp \left( -\frac{1}{2} [\log_G(X)]_G^\vee P^{-1} [\log_G(X)]_G^\vee \right), \quad (4)$$

where  $\beta$  is a normalizing constant chosen such that (4) integrates to unity. In general  $\beta \neq (2\pi)^{-p/2}|P|^{-1/2}$  with  $|\cdot|$  being the matrix determinant and  $P$  a positive definite matrix.

Furthermore, let  $\epsilon$  be defined as  $\epsilon \triangleq [\log_G(X)]_G^\vee$ . If we now assume that the entire mass of probability is contained inside  $G$ , then  $\epsilon$  can be described by  $\epsilon \sim \mathcal{N}_{\mathbb{R}^p}(\mathbf{0}^{p \times 1}, P)$ . This represents the CGD on  $G$  around the identity [16]. Furthermore, it is a unique parametrization space where the bijection between  $\exp_G$  and  $\log_G$  exists. Now, the pdf of  $X$  can be ‘translated’ over the  $G$  by using the left action of the matrix Lie group

$$X = \mu \exp_G([\epsilon]_G^\wedge), \text{ with } X \sim \mathcal{G}(\mu, P), \quad (5)$$

where  $\mathcal{G}$  denotes the concentrated Gaussian distribution [16], [22] with the mean  $\mu$  and the covariance matrix  $P$ . In other words, the mean  $\mu$  of the state  $X$  resides on the  $p$ -dimensional matrix Lie group  $G$ , while the associated uncertainty is defined in the space of the Lie algebra  $\mathfrak{g}$ , i.e., by the linear isomorphism the Euclidean vector space  $\mathbb{R}^p$ . By this, we have introduced the distribution forming the base for the LG-EKF.

### C. The SE(2) group

The motion group SE(2) describes the rigid body motion in 2D and is formed as a semi-direct product of the plane  $\mathbb{R}^2$  and the special orthogonal group SO(2) corresponding to translational and rotational parts, respectively. It is defined as

$$\text{SE}(2) = \left\{ \begin{pmatrix} R & \mathbf{t} \\ \mathbf{0}^{1 \times 2} & 1 \end{pmatrix} \in \mathbb{R}^{3 \times 3} \mid \{R, \mathbf{t}\} \in \text{SO}(2) \times \mathbb{R}^2 \right\}. \quad (6)$$

Now, we continue with providing the basic ingredients for handling SE(2), giving the relations for operators from III-A, needed for manipulation between the triplet (Lie group  $G$ , Lie algebra  $\mathfrak{g}$ , Euclidean space  $\mathbb{R}^p$ ).

For the Euclidean spaced vector  $\mathbf{x} = [x \ y \ \theta]^T$ , the most often associated element of the Lie algebra  $\mathfrak{se}(2)$  is given as

$$[\mathbf{x}]_{\text{SE}(2)}^\wedge = \begin{bmatrix} 0 & -\theta & x \\ \theta & 0 & y \\ 0 & 0 & 0 \end{bmatrix} \in \mathfrak{se}(2). \quad (7)$$

Correspondingly, its inverse  $[\cdot]_{\text{SE}(2)}^\vee$  is trivial.

The exponential map for the SE(2) group is given as

$$\exp_{\text{SE}(2)}([\mathbf{x}]_G^\wedge) = \begin{bmatrix} \cos \theta & -\sin \theta & t_x \\ \sin \theta & \cos \theta & t_y \\ 0 & 0 & 1 \end{bmatrix} \in \text{SE}(2) \quad (8)$$

$$t_x = \frac{1}{\theta} [x \sin \theta + y(-1 + \cos \theta)] \quad (9)$$

$$t_y = \frac{1}{\theta} [x(1 - \cos \theta) + y \sin \theta]. \quad (10)$$

For  $T = \{R, \mathbf{t}\} \in \text{SE}(2)$ , the logarithmic map is

$$\log_{\text{SE}(2)}(T) = \begin{bmatrix} \mathbf{v} \\ \theta \end{bmatrix}_{\text{SE}(2)}^\wedge \in \mathfrak{se}(2) \quad (11)$$

$$\theta = \log_{\text{SO}(2)}(R) = \text{atan2}(R_{21}, R_{11}) \quad (12)$$

$$\mathbf{v} = \frac{\theta}{2(1 - \cos \theta)} \begin{bmatrix} \sin \theta & 1 - \cos \theta \\ \cos \theta - 1 & \sin \theta \end{bmatrix} \mathbf{t}. \quad (13)$$

The Adjoint operator  $\text{Ad}_G$  used for representing  $T \in \text{SE}(2)$  on  $\mathbb{R}^3$  is given as

$$\text{Ad}_{\text{SE}(2)}(T) = \begin{bmatrix} R & J\mathbf{t} \\ \mathbf{0}^{1 \times 2} & 1 \end{bmatrix} \text{ with } J = \begin{bmatrix} 0 & 1 \\ -1 & 0 \end{bmatrix}. \quad (14)$$

The adjoint operator  $\text{ad}_G$  for representing  $\mathbf{x} \in \mathbb{R}^3$  on  $\mathbb{R}^3$  is given by

$$\text{ad}_{\text{SE}(2)}(\mathbf{x}) = \begin{bmatrix} -\theta J & J\mathbf{v} \\ \mathbf{0}^{1 \times 2} & 1 \end{bmatrix}, \quad (15)$$

where  $\mathbf{v} = [x \ y]^T \in \mathbb{R}^2$ .

## IV. RIGID BODY MOTION TRACKING

### A. EKF on matrix Lie groups

For the general filtering approach on matrix Lie groups, the system is assumed to be modeled as satisfying the following equation [23]

$$X_{k+1} = f(X_k, n_k) = X_k \exp_G([\hat{\Omega}_k + n_k]_G^\wedge), \quad (16)$$

where  $X_k \in G$  is the state of the system at time  $k$ ,  $G$  is a  $p$ -dimensional Lie group,  $n_k \sim \mathcal{N}_{\mathbb{R}^p}(\mathbf{0}^{p \times 1}, Q_k)$  is white Gaussian noise and  $\hat{\Omega}_k = \Omega(X_k) : G \rightarrow \mathbb{R}^p$  is a non-linear  $\mathcal{C}^2$  function.

The prediction step of the LG-EKF, based on the motion model (16), is governed by the following formulae

$$\mu_{k+1|k} = \mu_k \exp_G([\hat{\Omega}_k]_G^\wedge) \quad (17)$$

$$P_{k+1|k} = \mathcal{F}_k P_k \mathcal{F}_k^T + \Phi_G(\hat{\Omega}_k) Q_k \Phi_G(\hat{\Omega}_k)^T, \quad (18)$$

where  $\mu_{k+1|k} \in G$  and  $P_{k+1|k} \in \mathbb{R}^{p \times p}$  are predicted mean value and the covariance matrix, respectively, hence the state remains  $\mathcal{G}$ -distributed  $X_{k+1|k} \sim \mathcal{G}(\mu_{k+1|k}, P_{k+1|k})$ . The operator  $\mathcal{F}_k$ , a matrix Lie group equivalent to the Jacobian of  $f(X_k, n_k)$ , and  $\Phi_G$  are given as follows

$$\mathcal{F}_k = \text{Ad}_G \left( \exp_G([\hat{\Omega}_k]_G^\wedge) \right) + \Phi_G(\hat{\Omega}_k) \mathcal{C}_k \quad (19)$$

$$\Phi_G(\mathbf{v}) = \sum_{m=0}^{\infty} \frac{(-1)^m}{(m+1)!} \text{ad}_G(\mathbf{v})^m, \quad \mathbf{v} \in \mathbb{R}^p \quad (20)$$

$$\mathcal{C}_k = \frac{\partial}{\partial \epsilon} \Omega(\mu_k \exp_G([\epsilon]_G^\wedge))|_{\epsilon=0}. \quad (21)$$

The discrete measurement model on the matrix Lie group is modelled as

$$Z_{k+1} = h(X_{k+1}) \exp_{G'}([m_{k+1}]_{G'}^\wedge), \quad (22)$$

where  $Z_{k+1} \in G'$ ,  $h : G \rightarrow G'$  is a  $\mathcal{C}^1$  function and  $m_{k+1} \sim \mathcal{N}_{\mathbb{R}^q}(\mathbf{0}^{q \times 1}, R_{k+1})$  is white Gaussian noise.

The update step of the filter, based on the measurement model (22), strongly resembles the standard EKF update procedure, relying on the Kalman gain  $K_{k+1}$  and innovation vector  $\nu_{k+1}$  calculated as follows

$$K_{k+1} = P_{k+1|k} \mathcal{H}_{k+1}^T (\mathcal{H}_{k+1} P_{k+1|k} \mathcal{H}_{k+1}^T + R_{k+1})^{-1} \quad (23)$$

$$\nu_{k+1} = K_{k+1} \left( [\log_{G'}(h(\mu_{k+1|k})^{-1} Z_{k+1})]_{G'}^\vee \right).$$

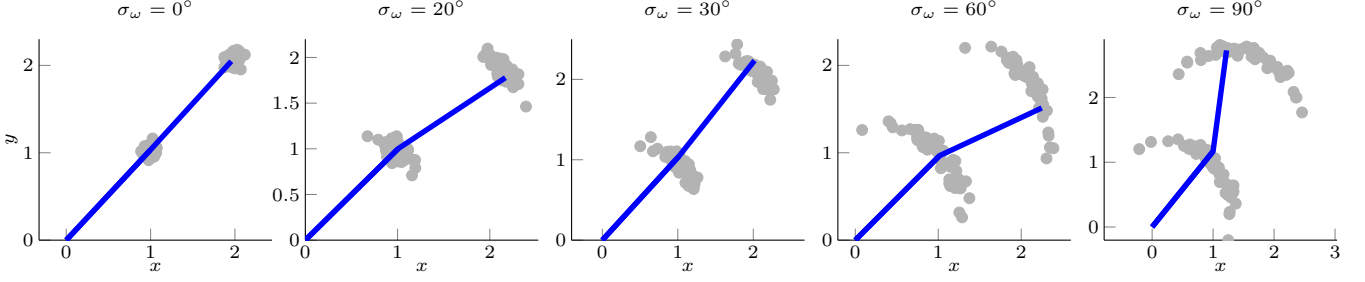


Fig. 2: Each of the subfigures represents an example of two compounding transformations for different levels of rotational uncertainty (given in blue). The grey circles represent 50 sampled uncertain transformations by employing both translational and rotational uncertainties. This particular situation appears when a robot moves from the current position to the next position associated with the next discrete moment in time, with standard deviation of the rotation  $\sigma_\omega$ .

The matrix  $\mathcal{H}_k$  can be seen as the measurement matrix of the system, i.e., a matrix Lie group equivalent to the Jacobian of  $h(X_k)$ , and is given as

$$\mathcal{H}_{k+1} = \frac{\partial}{\partial \epsilon} \left[ \log_{G'} (h(\mu_{k+1|k})^{-1} h(\mu_{k+1|k} \exp_G([\epsilon]^\wedge))) \right]_{G|_{\epsilon=0}}^\vee \quad (24)$$

Finally, having defined all the constituent elements, the update step is calculated via

$$\begin{aligned} \mu_{k+1} &= \mu_{k+1|k} \exp_G([\nu_{k+1}]^\wedge_G) \\ P_{k+1} &= \Phi_G(\nu_{k+1}) (I^{p \times p} - K_{k+1} \mathcal{H}_{k+1}) P_{k+1|k} \Phi_G(\nu_{k+1})^T. \end{aligned} \quad (25) \quad (26)$$

As in the case of the prediction step, the state  $X_{k+1} \sim \mathcal{G}(\mu_{k+1}, P_{k+1})$  remains  $\mathcal{G}$ -distributed after the correction as well. For a more formal derivation of the LG-EKF, the interested reader is referred to [16].

Since the employment of the  $SE(2) \times \mathbb{R}^3$  follows the similar, but slightly simpler derivation, in the sequel we derive the LG-EKF filter for estimation on the state space modelled as  $SE(2)^2$ . This approach is in our case applied, but not limited, to the problem of moving object tracking.

### B. LG-EKF on $SE(2)^2$

As mentioned previously, we model the state  $X$  to evolve on the matrix Lie group  $G = SE(2)^2$  which is symbolically represented by

$$X = \begin{bmatrix} \begin{bmatrix} R_\theta & \mathbf{t} \\ \mathbf{0}^{1 \times 2} & 1 \end{bmatrix} & \begin{bmatrix} R_\omega & \mathbf{t}_v \\ \mathbf{0}^{1 \times 2} & 1 \end{bmatrix} \end{bmatrix} = \begin{pmatrix} T_s \\ T_d \end{pmatrix}_G, \quad (27)$$

where  $T_s$  is the stationary component and  $T_d$  brings the second order dynamics. Note that the matrix Lie group composition and inversion are simple matrix multiplication and inversion, hence the previous symbolic representation can be used for all the calculations dealing with operations on  $G$ .

The Lie algebra associated to the Lie group  $G$  is denoted as  $\mathfrak{g} = \mathfrak{se}(2)^2$ , thereby for  $\mathbf{x} = [\mathbf{x}_p \ \mathbf{x}_d]^T \in \mathbb{R}^6$ , where  $\mathbf{x}_p = [x \ y \ \theta]^T$  and  $\mathbf{x}_d = [v_x \ v_y \ \omega]^T$ , the following holds

$$[\mathbf{x}]^\wedge_G = \begin{bmatrix} [\mathbf{x}_p]^\wedge_{SE(2)} \\ [\mathbf{x}_d]^\wedge_{SE(2)} \end{bmatrix} = \begin{pmatrix} [\mathbf{x}_p]^\wedge_{SE(2)} \\ [\mathbf{x}_d]^\wedge_{SE(2)} \end{pmatrix}_\mathfrak{g}. \quad (28)$$

The exponential map for such defined  $G$  is

$$\exp_G([\mathbf{x}]^\wedge_G) = \begin{pmatrix} \exp_{SE(2)}([\mathbf{x}_p]^\wedge_{SE(2)}) \\ \exp_{SE(2)}([\mathbf{x}_d]^\wedge_{SE(2)}) \end{pmatrix}_G. \quad (29)$$

Now, we have all the necessary ingredients for deriving the terms to be used within the LG-EKF. Several examples of the uncertain transformations following the  $SE(2)^2$  motion model are shown in Fig. 2 (the  $SE(2) \times \mathbb{R}^3$  model would exhibit similar behaviour).

1) *Prediction:* We propose to model the motion (16) of the system by

$$\begin{aligned} \Omega(X_k) &= [Tv_{x_k} \ Tv_{y_k} \ T\omega_k \ 0 \ 0 \ 0]^T \in \mathbb{R}^6, \\ n_k &= \left[ \frac{T^2}{2} n_{x_k} \ \frac{T^2}{2} n_{y_k} \ \frac{T^2}{2} n_{\omega_k} \ Tn_{x_k} \ Tn_{y_k} \ Tn_{\omega_k} \right]^T \in \mathbb{R}^6. \end{aligned} \quad (30)$$

With such a defined motion model, the system is corrupted with white noise over three separated components, i.e.,  $n_x$  the noise in the local  $x$  direction,  $n_y$  the noise in the local  $y$  direction and  $n_w$  as the noise in the rotational component. Given that, the intensity of the noise components acts as acceleration over the associated axes in the system. If the system state at the discrete time step  $k$  is described with  $X_k \sim \mathcal{G}(\mu_k, P_k)$ , the mean value and the covariance can be propagated using (17) and (18).

The covariance propagation is more challenging, since it requires the calculation of (21). For the Lie algebraic error  $\epsilon \triangleq [\epsilon_x \ \epsilon_y \ \epsilon_\theta \ \epsilon_{v_x} \ \epsilon_{v_y} \ \epsilon_\omega]$ , we need to set the following

$$\begin{aligned} \Omega(\mu_k \exp_G([\epsilon]^\wedge)) &= \begin{bmatrix} \Delta T v_{x_k} + \Delta T \cos \omega_k v_1 - \Delta T \sin \omega_k v_2 \\ \Delta T v_{y_k} + \Delta T \sin \omega_k v_1 + \Delta T \cos \omega_k v_2 \\ \Delta T \omega_k + \Delta T \epsilon_\omega \\ \mathbf{0}^{3 \times 1} \end{bmatrix}. \end{aligned} \quad (31)$$

where

$$\begin{aligned} v_1 &= [\epsilon_{v_x} \sin \epsilon_\omega + \epsilon_{v_y} (\cos \epsilon_\omega - 1)] \epsilon_\omega^{-1} \\ v_2 &= [\epsilon_{v_x} (1 - \cos \epsilon_\omega) + \epsilon_{v_y} \sin \epsilon_\omega] \epsilon_\omega^{-1}. \end{aligned} \quad (32)$$

Let  $\Omega_{1,k}$ ,  $\Omega_{2,k}$  and  $\Omega_{3,k}$  denote the first three rows of the vector (31), respectively (whereas the last three rows are trivial  $\Omega_{4,k} = \Omega_{5,k} = \Omega_{6,k} = 0$ ). Even though the multivariate limits  $\frac{\partial \Omega_{1,k}}{\partial \epsilon_\omega}|_{\epsilon=0}$  and  $\frac{\partial \Omega_{2,k}}{\partial \epsilon_\omega}|_{\epsilon=0}$  appear involved, their derivation

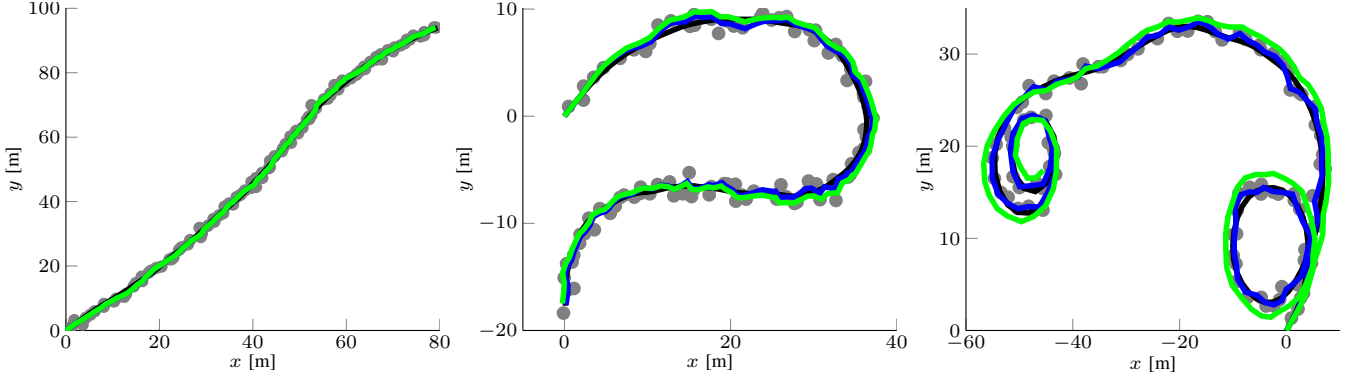


Fig. 3: Examples of three different simulated trajectories, generated with the  $SE(2)^2$  motion model, with different intensities of process noise over rotational components, i.e., standard deviation in rotational component was  $\sigma_\omega = [0.01 \ 0.1 \ 1]^\circ$ . The blue line corresponds to  $SE(2)^2$  filter, while the green line represents the CV model ( $SE(2) \times \mathbb{R}^3$  and CTRV are omitted for clarity).

$$\begin{aligned}
\frac{\partial \Omega_{1,k}}{\partial \epsilon_{v_x}}|_{\epsilon=0} &= \Delta T \cos \omega_k \frac{\sin \epsilon_\omega}{\epsilon_\omega} - \Delta T \sin \omega_k \frac{\cos \epsilon_\omega - 1}{\epsilon_\omega}|_{\epsilon=0} = \Delta T \cos \omega_k \\
\frac{\partial \Omega_{1,k}}{\partial \epsilon_{v_y}}|_{\epsilon=0} &= \Delta T \cos \omega_k \frac{\cos \epsilon_\omega - 1}{\epsilon_\omega} - \Delta T \sin \omega_k \frac{\sin \epsilon_\omega}{\epsilon_\omega}|_{\epsilon=0} = -\Delta T \sin \omega_k \\
\frac{\partial \Omega_{1,k}}{\partial \epsilon_\omega}|_{\epsilon=0} &= \Delta T \cos \omega \frac{(\epsilon_{v_x} \cos \epsilon_\omega - \epsilon_{v_y} \sin \epsilon_\omega) \epsilon_\omega - [\epsilon_{v_x} \sin \epsilon_\omega + \epsilon_{v_y} (\cos \epsilon_\omega - 1)]}{\epsilon_\omega^2} \\
&\quad - \Delta T \sin \omega \frac{(\epsilon_{v_x} \sin \epsilon_\omega + \epsilon_{v_y} \cos \epsilon_\omega) \epsilon_\omega - [\epsilon_{v_x} (\cos \epsilon_\omega - 1) + \epsilon_{v_y} \sin \epsilon_\omega]}{\epsilon_\omega^2}|_{\epsilon=0} = 0 \\
\frac{\partial \Omega_{2,k}}{\partial \epsilon_{v_x}}|_{\epsilon=0} &= \Delta T \sin \omega_k, \quad \frac{\partial \Omega_{2,k}}{\partial \epsilon_{v_y}}|_{\epsilon=0} = \Delta T \cos \omega_k, \quad \frac{\partial \Omega_{2,k}}{\partial \epsilon_\omega}|_{\epsilon=0} = 0 \\
\frac{\partial \Omega_{3,k}}{\partial \epsilon_{v_x}}|_{\epsilon=0} &= 0, \quad \frac{\partial \Omega_{3,k}}{\partial \epsilon_{v_y}}|_{\epsilon=0} = 0, \quad \frac{\partial \Omega_{3,k}}{\partial \epsilon_\omega}|_{\epsilon=0} = \Delta T
\end{aligned} \tag{33}$$

follow from patient algebraic manipulations. The resulting terms are shown in (33). The matrix  $\mathcal{C}_k$  is finally then given as

$$\mathcal{C}_k = \begin{bmatrix} \mathbf{0}^{3 \times 3} & \Delta T \cos \omega_k & -\Delta T \sin \omega_k & 0 \\ \Delta T \sin \omega_k & \Delta T \cos \omega_k & 0 & 0 \\ 0 & 0 & \Delta T & 0 \\ \mathbf{0}^{3 \times 3} & \mathbf{0}^{3 \times 3} & \mathbf{0}^{3 \times 3} & \mathbf{0}^{3 \times 3} \end{bmatrix}. \tag{34}$$

The adjoint operators  $Ad_G$  and  $ad_G$  are formed block diagonally as

$$\begin{aligned}
Ad_G(X) &= \text{diag} (Ad_{SE(2)}(T_s), Ad_{SE(2)}(T_d)), \\
ad_G(x) &= \text{diag} (ad_{SE(2)}(x_s), ad_{SE(2)}(x_d)).
\end{aligned} \tag{35}$$

The last needed ingredient is the process noise covariance matrix  $Q_k$ . Assuming the constant acceleration over the sampling period  $\Delta T$ , we model the process noise as a discrete white noise acceleration over the three components:  $n_{x_k}$ ,  $n_{y_k}$  and  $n_{\omega_k}$ . At this point, we can use the equation (18) for predicting the covariance of the system.

2) *Update*: The predicted system state is described with  $X_{k+1|k} \sim \mathcal{G}(\mu_{k+1|k}, P_{k+1|k})$  and now we proceed to updating the state by incorporating the newly arrived measurement  $Z_{k+1} \in G'$ . In this case, we choose the measurements to arise in the Euclidean space  $\mathbb{R}^2$ , measuring the current position of

the tracked object in 2D. This choice is application related and is more discussed in the next section. For this reason and since the Euclidean space is a trivial example of a matrix Lie group, we introduce the representation of  $z = [x_z \ y_z]^T \in \mathbb{R}^2$  in the form of a matrix Lie group  $Z \in G' \subset \mathbb{R}^{3 \times 3}$  and Lie algebra  $[z]_{\mathbb{R}^2}^\wedge \in \mathfrak{g}' \subset \mathbb{R}^{3 \times 3}$

$$Z = \begin{bmatrix} \mathbf{I}^{2 \times 2} & z \\ \mathbf{0}^{1 \times 2} & 1 \end{bmatrix} \quad \text{and} \quad [z]_{\mathbb{R}^2}^\wedge = \begin{bmatrix} \mathbf{0}^{2 \times 2} & z \\ \mathbf{0}^{1 \times 2} & 0 \end{bmatrix}. \tag{36}$$

Please note there exists a trivial mapping between the members of the triplet  $\mathbb{R}^2$ ,  $\mathfrak{g}'$  and  $G'$ , hence the formal inverses of the terms from (36) are omitted here.

The measurement function is the map  $h : SE(2)^2 \rightarrow \mathbb{R}^2$ . The element that specifically needs to be derived is the measurement matrix  $\mathcal{H}_{k+1}$ , which in the vein of (33), requires using partial derivatives and multivariate limits. Again, we start with definition of the Lie algebraic error  $\epsilon = [\epsilon_x \ \epsilon_y \ \epsilon_\theta \ \epsilon_{v_x} \ \epsilon_{v_y} \ \epsilon_\omega]$ . The function to be partially derived is given as

$$\begin{aligned}
&[\log_{G'} (h(\mu_{k+1|k})^{-1} h(\mu_{k+1|k} \exp_G([\epsilon]_G^\wedge)))]_G^\vee = \\
&\begin{bmatrix} \cos \theta_{k+1|k} p_1 - \sin \theta_{k+1|k} p_2 \\ \sin \theta_{k+1|k} p_1 + \cos \theta_{k+1|k} p_2 \end{bmatrix},
\end{aligned} \tag{37}$$

$$\begin{aligned}
\frac{\partial \mathcal{H}_{1,k+1}}{\partial \epsilon_x} \Big|_{\epsilon=0} &= \cos \theta_{k+1|k} \frac{\sin \epsilon_\theta}{\epsilon_\theta} - \sin \theta_{k+1|k} \frac{\cos \epsilon_\theta - 1}{\epsilon_\theta} \Big|_{\epsilon=0} = \cos \theta_{k+1|k} \\
\frac{\partial \mathcal{H}_{1,k+1}}{\partial \epsilon_y} \Big|_{\epsilon=0} &= \cos \theta_{k+1|k} \frac{\cos \epsilon_\theta - 1}{\epsilon_\theta} - \sin \theta_{k+1|k} \frac{\sin \epsilon_\theta}{\epsilon_\theta} \Big|_{\epsilon=0} = -\sin \theta_{k+1|k} \\
\frac{\partial \mathcal{H}_{1,k+1}}{\partial \epsilon_\theta} \Big|_{\epsilon=0} &= \cos \theta_{k+1|k} \frac{(\epsilon_x \cos \epsilon_\theta - \epsilon_y \sin \epsilon_\theta) \epsilon_\theta - [\epsilon_x \sin \epsilon_\theta + \epsilon_y (\cos \epsilon_\theta - 1)]}{\epsilon_\theta^2} \\
&\quad - \sin \theta_{k+1|k} \frac{(\epsilon_x \sin \epsilon_\theta + \epsilon_y \cos \epsilon_\theta) \epsilon_\theta - [\epsilon_x (\cos \epsilon_\theta - 1) + \epsilon_y \sin \epsilon_\theta]}{\epsilon_\theta^2} \Big|_{\epsilon=0} = 0 \\
\frac{\partial \mathcal{H}_{2,k+1}}{\partial \epsilon_x} \Big|_{\epsilon=0} &= \sin \theta_{k+1|k}, \quad \frac{\partial \mathcal{H}_{2,k+1}}{\partial \epsilon_y} \Big|_{\epsilon=0} = \cos \theta_{k+1|k}, \quad \frac{\partial \mathcal{H}_{2,k+1}}{\partial \epsilon_\theta} \Big|_{\epsilon=0} = 0
\end{aligned} \tag{39}$$

where

$$\begin{aligned}
p_1 &= [\epsilon_x \sin \epsilon_\theta + \epsilon_y (\cos \epsilon_\theta - 1)] \epsilon_\theta^{-1} \\
p_1 &= [\epsilon_x (1 - \cos \epsilon_\theta) + \epsilon_y \sin \epsilon_\theta] \epsilon_\theta^{-1}.
\end{aligned} \tag{38}$$

Let  $\mathcal{H}_{1,k+1}$  and  $\mathcal{H}_{2,k+1}$  denote the two rows of expression (37). In order to derive (24), we need to determine partial derivatives and multivariate limits over all directions of the Lie algebraic error vector, and the result is given in (39). The final measurement matrix  $\mathcal{H}_{k+1}$  amounts to

$$\mathcal{H}_{k+1} = \begin{bmatrix} \cos \theta_{k+1|k} & -\sin \theta_{k+1|k} & 0 & 0 & 0 & 0 \\ \sin \theta_{k+1|k} & \cos \theta_{k+1|k} & 0 & 0 & 0 & 0 \end{bmatrix}. \tag{40}$$

Again, the interested reader is directed to perform algebraic manipulations when calculating the multivariate limits for proving (40). Here we deal with rather simple and most common measurement space, but as well as in some recent works [24], the filter from Section IV-A enables us to incorporate nonlinear measurements if needed.

Now we have all the means for updating the filter by calculating the Kalman gain  $K_{k+1}$  and the innovation vector  $\nu_{k+1}$  (23), and finally correcting the mean  $\mu_{k+1}$  (25) and the covariance matrix  $P_{k+1}$  (26).

### C. Simulation

In order to test the performance of the proposed filters, we have simulated trajectories of a maneuvering object in 2D, where the motion of the system was described by the  $\text{SE}(2) \times \mathbb{R}^3$  and  $\text{SE}(2)^2$  models. Three examples of generated trajectories with the  $\text{SE}(2)^2$  model, with different levels of rotational process noise, are given in Fig. 3. In order to test performance of the proposed filters, we conducted statistical comparison of  $\text{SE}(2) \times \mathbb{R}^3$  and  $\text{SE}(2)^2$ , with two conventional approaches, i.e., (i) the EKF based constant turn rate and velocity and (ii) the KF based CV models.

The noise parameters that generated the trajectories were set as follows:  $n_{v_x} \sim \mathcal{N}(0, 0.1^2)$ ,  $n_{v_y} \sim \mathcal{N}(0, 0.1^2)$ ,  $n_\omega \sim \mathcal{N}(0, \sigma_\omega^2)$ , where  $\sigma_\omega$  took 30 equidistant values in the interval  $[0, 3]$ . For each of these values of  $\sigma_\omega$  we have generated 100 trajectories and compared the performance of the four filters. The measurement noise was set to  $m_x \sim \mathcal{N}(0, 0.5^2)$  and  $m_y \sim \mathcal{N}(0, 0.5^2)$ . Special attention was given to parametrization of process noise covariance matrices in order to make the comparison as fair as possible. Statistical

evaluation of the root-mean-square-error (RMSE) in object's position is depicted in Fig. 4. It can be seen that the  $\text{SE}(2)^2$  and  $\text{SE}(2) \times \mathbb{R}^3$  filters significantly outperform the other filters. Specifically, when the rotation is not very dynamic, the KF based CV filter follows the trajectories well, while with the increase in  $\sigma_\omega$  its performance drops significantly. On the contrary, when the rotation is not very dynamic, the EKF based CTRV filter struggles to follow the trajectories correctly, while with the increase in  $\sigma_\omega$  its performance gets closer to the one of the proposed filters.

Considering the varying dynamism in the rotation, we assert that the  $\text{SE}(2) \times \mathbb{R}^3$  and  $\text{SE}(2)^2$  show very similar behaviour, while significantly outperforming the other two filters. Particularly, they present the best of the two worlds: the CV and the CTRV behaviour. Here we present statistical evaluation conducted on the trajectories generated by the  $\text{SE}(2)^2$  model, Results on the trajectories generated by the  $\text{SE}(2) \times \mathbb{R}^3$  model showed similar inter-performance, they are omitted from the present paper. Furthermore, in simulations we only measured the position, i.e., the measurement space was in  $\mathbb{R}^2$ , while measuring additionally the orientation, i.e., making the measurement space  $\text{SE}(2)$ , would only further highlight the potential of the  $\text{SE}(2)^2$  filter. Both of the presented omnidirectional motion models are proven to be very flexible and capable of capturing various types of motion that can be encountered in, e.g., busy intersection consisting of cars, trams, bicycles, motorcycles, and pedestrians or an unknown environment that a robot enters for the first time consisting of different robot platforms and humans.

## V. CONCLUSION

In this paper we have proposed novel models for tracking a moving object exploiting its motion on the rigid body motion group  $\text{SE}(2)$ . The proposed filtering approach relied on the extended Kalman filter for matrix Lie groups, since the rigid body motion group itself is a matrix Lie group. Therefore, we have modeled the state space as either a direct product of the of the  $\text{SE}(2)$  group and the  $\mathbb{R}^3$  vector, i.e.,  $\text{SE}(2) \times \mathbb{R}^3$ , or two  $\text{SE}(2)$  groups, i.e.  $\text{SE}(2) \times \text{SE}(2)$ , where the first term described the current pose, while the second term handled second order dynamics. We have analyzed the performance of the proposed filters on a large number of

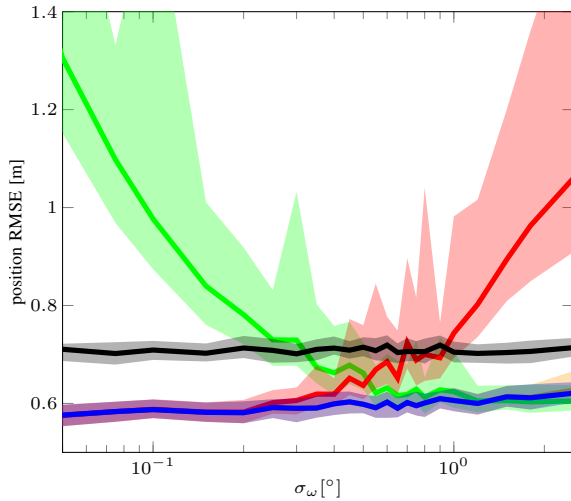


Fig. 4: Performance statistics obtained over 100 generated trajectories for 30 different values of  $\sigma_\omega$ . We have compared the proposed filter  $SE(2)^2$  (blue) and  $SE(2) \times \mathbb{R}^3$  (orange) with the EKF based CTRV (green), KF based CV (red), and measurements (black), where the solid lines corresponds to mean values, while transparent areas correspond to one standard deviation (in both  $+/ -$  directions) of each of the associated RMSEs. We can notice that the  $SE(2) \times \mathbb{R}^3$  and  $SE(2)^2$  filters, whose difference is barely noticeable, exhibit similar behaviour, outperforming the other two filters.

synthetic trajectories and compared them to (i) the EKF based constant velocity and turn rate and (ii) the KF based constant velocity models. The  $SE(2) \times \mathbb{R}^3$  and  $SE(2)^2$  filters showed similar performance on the synthetic dataset, and have significantly outperformed other well-established approaches for a wide range of intensities in the rotation component.

Even though the presented work was applied on a tracking problem, we believe it can serve as a starting point for further exploitation of estimation on matrix Lie groups and its applications on different problems. The use of higher order dynamics may be of special interest for the domain of robotics, as well as for multi-target tracking applications. Furthermore, these techniques could also find application in other rigid body motion estimation problems requiring precise pose estimation and higher-order motion.

#### ACKNOWLEDGMENTS

This work has been supported from the Unity Through Knowledge Fund under the project Cooperative Cloud based Simultaneous Localization and Mapping in Dynamic Environments (cloudSLAM) and the European Union's Horizon 2020 research and innovation programme under grant agreement No 688117 (SafeLog).

#### REFERENCES

[1] T. D. Barfoot and P. T. Furgale, "Associating Uncertainty With Three-Dimensional Poses for Use in Estimation Problems," *IEEE Transactions on Robotics*, vol. 30, no. 3, pp. 679–693, Jun. 2014.

[2] C. Hertzberg, R. Wagner, U. Frese, and L. Schröder, "Integrating Generic Sensor Fusion Algorithms with Sound State Representations through Encapsulation of Manifolds," *Information Fusion*, vol. 14, no. 1, pp. 57–77, Jul. 2013.

[3] R. M. Murray, Z. Li, and S. S. Sastry, *A Mathematical Introduction to Robotic Manipulation*. CRC Press, 1994, vol. 29.

[4] F. C. Park, J. E. Bobrow, and S. R. Ploen, "A Lie Group Formulation of Robot Dynamics," *The International Journal of Robotics Research*, vol. 14, no. 6, pp. 609–618, 1995.

[5] A. J. Davison, "Real-time simultaneous localisation and mapping with a single camera," in *International Conference on Computer Vision (ICCV)*, vol. 2. IEEE, 2003, pp. 1403–1410.

[6] Y. M. Lui, "Advances in matrix manifolds for computer vision," *Image and Vision Computing*, vol. 30, no. 6-7, pp. 380–388, Jun. 2012.

[7] S.-F. Su and C. S. G. Lee, "Manipulation and propagation of uncertainty and verification of applicability of actions in assembly tasks," *IEEE Transactions on Systems, Man, and Cybernetics*, vol. 22, no. 6, pp. 1376–1389, 1992.

[8] G. Silveira, E. Malis, and P. Rives, "An Efficient Direct Approach to Visual SLAM," *IEEE Transactions on Robotics*, vol. 24, no. 5, pp. 969–979, 2008.

[9] W. Park, Y. Wang, and G. S. Chirikjian, "The Path-of-Probability Algorithm for Steering and Feedback Control of Flexible Needles," *The International Journal of Robotics Research*, vol. 29, no. 7, pp. 813–830, 2010.

[10] R. A. Srivatsan, M. Travers, and H. Choset, "Using Lie algebra for shape estimation of medical snake robots," in *International Conference on Intelligent Robots and Systems (IROS)*, Chicago, USA, 2014.

[11] A. W. Long, K. C. Wolfe, M. J. Mashner, and G. S. Chirikjian, "The Banana Distribution is Gaussian : A Localization Study with Exponential Coordinates," in *Proceedings of Robotics: Science and Systems (RSS)*, 2012.

[12] M. Agrawal, "A lie algebraic approach for consistent pose registration for general euclidean motion," in *International Conference on Intelligent Robots and Systems (IROS)*. IEEE, 2006, pp. 1891–1897.

[13] S. Thrun, W. Burgard, and D. Fox, *Probabilistic Robotics*. MIT Press, 2006.

[14] G. Kurz, I. Gilitschenski, and U. D. Hanebeck, "The partially wrapped normal distribution for  $SE(2)$  estimation," in *International Conference on Multisensor Fusion and Information Integration for Intelligent Systems (MFI)*, 2014.

[15] I. Gilitschenski, G. Kurz, S. J. Julier, and U. D. Hanebeck, "A New Probability Distribution for Simultaneous Representation of Uncertain Position and Orientation," in *International Conference on Information Fusion (FUSION)*, 2014.

[16] G. Bourmaud, R. Mégret, M. Arnaudon, and A. Giremus, "Continuous-Discrete Extended Kalman Filter on Matrix Lie Groups Using Concentrated Gaussian Distributions," *Journal of Mathematical Imaging and Vision*, vol. 51, no. 1, pp. 209–228, 2015.

[17] Y. Bar-Shalom, T. Kirubarajan, and X.-R. Li, *Estimation with Applications to Tracking and Navigation*. John Wiley & Sons, Inc., 2002.

[18] R. Schubert, "Evaluating the utility of driving: Toward automated decision making under uncertainty," *IEEE Transactions on Intelligent Transportation Systems*, vol. 13, no. 1, pp. 354–364, 2012.

[19] R. Siegwart and I. R. Nourbakhsh, *Introduction to Autonomous Mobile Robots*. Scituate, MA, USA: Bradford Company, 2004.

[20] G. S. Chirikjian, *Stochastic Models, Information Theory, and Lie Groups, Volume 2: Analytic Methods and Modern Applications*. Springer, 2012.

[21] Y. Wang and G. S. Chirikjian, "Nonparametric Second-Order Theory of Error Propagation on Motion Groups," *International Journal of Robotic Research*, vol. 27, no. 11, pp. 1258–1273, 2008.

[22] K. C. Wolfe, M. Mashner, and G. S. Chirikjian, "Bayesian Fusion on Lie Groups," *Journal of Algebraic Statistics*, vol. 2, no. 1, pp. 75–97, 2011.

[23] G. Bourmaud, R. Mégret, A. Giremus, and Y. Berthoumieu, "Discrete Extended Kalman Filter on Lie Groups," in *European Signal Processing Conference (EUSIPCO)*, 2013, pp. 1–5.

[24] G. Chirikjian and M. Kobilarov, "Gaussian Approximation of Non-linear Measurement Models on Lie Groups," in *Conference on Decision and Control (CDC)*. IEEE, 2014, pp. 6401–6406.

## PUBLICATION 4

J. Ćesić, V. Joukov, I. Petrović and D. Kulić. Full Body Human Motion Estimation on Lie Groups Using 3D Marker Position Measurements. *IEEE-RAS International Conference on Humanoid Robotics (Humanoids)*. Cancun, Mexico, 826–833, 2016.



# Full Body Human Motion Estimation on Lie Groups Using 3D Marker Position Measurements

Josip Česić\*, Vladimir Joukov†, Ivan Petrović\* and Dana Kulić‡

**Abstract**—This paper proposes a new algorithm for full body human motion estimation using 3D marker position measurements. The joints are represented with Lie group members, including special orthogonal groups  $SO(2)$  and  $SO(3)$ , and a special euclidean group  $SE(3)$ . We employ the Lie Group Extended Kalman Filter (LG-EKF) for stochastic inference on groups, thus explicitly accounting for the non-euclidean geometry of the state space, and provide the derivation of the LG-EKF recursion for articulated motion estimation. We evaluate the performance of the proposed algorithm in both simulation and on real-world motion capture data, comparing it with the Euler angles based EKF. The results show that the proposed filter significantly outperforms the Euler angles based EKF, since it estimates human motion more accurately and is not affected by gimbal lock.

## I. INTRODUCTION

Human bodies have evolved to perform complex manipulation and locomotion tasks. We are able to accomplish very intricate movements, carry light and heavy loads, achieve energy efficient locomotion at various speeds, reject disturbances, and adapt to environment constraints. Inspired by the human body, robotics researchers aim to develop systems with similar capabilities. To design a humanoid that can perform as well as a person, researchers must first capture and analyze human motion. Accurate pose estimation allows the design of controllers to simulate human like movements on a robot through motion re-targeting and imitation learning. In human-robot interaction the participant's pose must be known to guarantee safety and to allow collaborative tasks. Finally, to improve the performance of assistive devices in rehabilitation or to enhance user's capabilities with an exoskeleton, the system must be able to reproduce human like movements [1].

Optical motion capture is a method to record the movements from body worn markers observed by multiple cameras. The 3D positions of the markers are extracted from the images using the relative positions of the cameras to each other and are analyzed to compute the pose.

Typically, a kinematic model of the participant is defined based on anthropomorphic tables or by measurement

and markers are assumed rigidly attached to the skeleton links. Unfortunately, for a full body skeletal model, there is no closed form solution for the inverse kinematics (IK). Differentiating the positions of the attached markers with respect to the joint angles and forming a Jacobian matrix allows to iteratively solve for joint angles using the pseudoinverse of the Jacobian. In singular configurations the Jacobian is not invertible. It is possible to include a non-zero damping constant in the least squares minimization to maintain full rank; various damping factors have been proposed [2].

The Jacobian inverse based methods do not account for stochastic error in marker position measurements, are greatly affected by outlier measurements, and are not capable of predicting future poses. By treating the skeleton pose as a state and 3D marker positions as measurements, recursive stochastic estimators can be used to help reduce the effect of stochastic marker position errors. Including the joint positions, velocities, and accelerations in the motion model of the filter helps to maintain correct pose estimate during short term occlusions. Various stochastic filters have been proposed for IK, such as the Smart Sampling Kalman Filter [3] and the Unscented Kalman Filter [4]. The filtering approach can even be used to perform estimation from unlabeled markers [5]. Bonnet *et al.* modelled not only kinematics but also the dynamics of a human body within an EKF to estimate the pose and dynamic parameters [6].

In the aforementioned methods the kinematic models are rigid links connected with joints that may be rotational, translational, or spherical. All of these formulations are representations of transformations in the euclidean space. However, human motion and many other types of motion of interest in robotics do not occur in Euclidean space, but rather arise on curved geometries often called manifolds. By using the manifold representations, the overall performance of wide variety of applications can be significantly improved [7]–[9]. In particular, the attitude of an object can be modelled as a special orthogonal group  $SO(n)$ ,  $n = 2, 3$ , while the pose can be modelled as a special euclidean group  $SE(n)$ ,  $n = 2, 3$  [7]. Notably, both  $SO(n)$  and  $SE(n)$  belong to a family of matrix Lie groups. Recently, several theoretically rigorous approaches for filtering on manifolds have been proposed. In [10] the authors proposed an EKF able to perform estimation respecting the geometry of matrix Lie groups. Alongside, the unscented transform-based [11] and the particle-based [12] approaches have also attracted significant attention.

The benefit of manifolds for human action recognition has already been explored in the literature. In [13] the

This work has been supported from the Unity Through Knowledge Fund under the project *Cooperative Cloud based Simultaneous Localization and Mapping in Dynamic Environments* (cloudSLAM) and by the Ministry of Science, Education and Sports of the Republic of Croatia under the grant *Center of Research Excellence for Data Science and Cooperative Systems* (CoE ACROSS).

\* Josip Česić and Ivan Petrović are with the University of Zagreb, Faculty of Electrical Engineering and Computing, Laboratory for Autonomous Systems and Mobile Robotics, Croatia. {josip.cesic@fer.hr, ivan.petrovic@fer.hr}

† Vladimir Joukov and Dana Kulić are with the University of Waterloo, Department of Electrical and Computer Engineering, Adaptive Systems Laboratory, Canada. {vjoukov@uwaterloo.ca, dkulic@uwaterloo.ca}



authors exploited the manifold structure by relying on the particle filter for learning purposes, while in [14] the authors use different manifolds as priors for manifold learning. Devanne *et al.* have used a spatio-temporal modeling of trajectories in a Riemannian manifold for action recognition purposes [15]. Recently, Brossette *et al.* have proposed the posture generation problem that encompasses non-Euclidean manifolds as well [16].

In this paper, we propose an algorithm for human motion estimation on Lie groups, which uses 3D marker position measurements. We explicitly account for the geometry of the state space and apply Lie group EKF (LG-EKF) for stochastic inference on Lie groups. We employ a constant acceleration model [17] in the motion prediction step and derive the update and observation equations for positional measurements. We compare the performance of the proposed approach with the Euler angles-based EKF, and show that the proposed algorithm achieves significantly better performance in both simulations and real-world experiments.

The paper is organized as follows. In Sec. II we present the theoretical preliminaries addressing the association of uncertainties to Lie groups, and provide the basic relations needed for forward kinematics of articulated bodies with groups. In Sec. III we derive the proposed estimation approach. In Sec. IV we describe the Euler angle-based approach, while in Sec. V we present the validation results.

## II. MATHEMATICAL BACKGROUND

In this section we provide the mathematical background for performing human motion estimation on matrix Lie groups. We first discuss a human body modeling approach and the corresponding state space construction, and after provide the relations for manipulating the required Lie group members.

### A. Construction of the state space

Before proceeding to filtering, we first construct the state space for representing a human that models body flexibility to a satisfactory level. Therefore we determine the appropriate Lie Group representation for each joint based on its mobility. For example, 1 DoF revolute joints are represented with a special orthogonal group  $SO(2)$ , while 3 DoF spherical joints are modelled with a special orthogonal group  $SO(3)$ . To localize the human in 6 DoF space, we use a special euclidean group member  $SE(3)$  for connecting the origin of the space with the base of the body, modeling both translational and rotational motion. Finally, the state of the system modelling a human is constructed by concatenating Lie group members via a Cartesian product, starting with  $SE(3)$ , and extending with either  $SO(2)$  or  $SO(3)$  groups.

For example, a human leg can be constructed as

$$SE(3) \times SO(3) \times SO(2) \times SO(2) \times SO(2). \quad (1)$$

Here, the first term represents the 3D position and orientation of the waist with respect to the reference frame, the second term represents the hip as a spherical joint, the third describes the knee, while the last two represent the two dimensional ankle as shown in Fig. 1 (left).

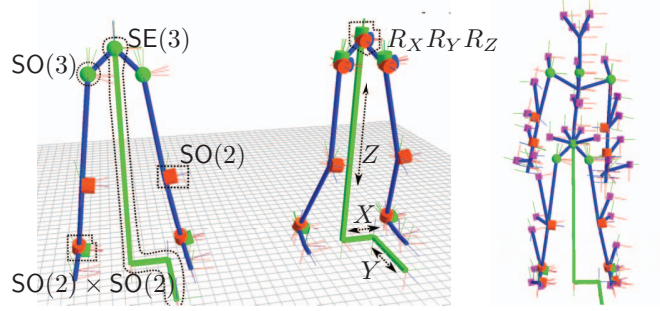


Fig. 1: Left: Lower body kinematic model joints represented by their respective group members. Middle: Same lower body in prismatic and revolute (Euler angle) joint representation. Right: Full body Lie Group model with attached markers.

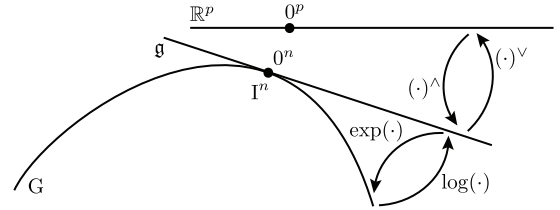


Fig. 2: An illustration of mappings within the triplet of Lie group  $G$ , Lie algebra  $\mathfrak{g}$  and the Euclidean space  $\mathbb{R}^P$ .

### B. Lie groups and Lie algebra

We now introduce the concept of Lie groups and Lie algebra as prerequisites for estimation on Lie groups [18].

Generally, a Lie group  $G$  is a group which has the structure of a smooth manifold. Group operators, composition and inversion, are smooth operations, given simply as matrix multiplication and inversion. Lie algebra  $\mathfrak{g}$  elements represent a tangent space of a group at the identity element [19]. In particular, a Lie algebra is an open neighborhood around  $0^P$  in the tangent space of  $G$  at the identity  $I^n$ . The matrix exponential  $\exp_G$  and matrix logarithm  $\log_G$  establish a local diffeomorphism between  $G$  and  $\mathfrak{g}$  as

$$\exp_G : \mathfrak{g} \rightarrow G \quad \text{and} \quad \log_G : G \rightarrow \mathfrak{g}. \quad (2)$$

The Lie algebra  $\mathfrak{g}$  associated to a  $p$ -dimensional matrix Lie group  $G \subset \mathbb{R}^{n \times n}$  is a  $p$ -dimensional vector space defined by a basis consisting of  $p$  real matrices  $E_r$ ,  $r = 1, \dots, p$ , often referred to as generators [20]. A linear isomorphism between  $\mathfrak{g}$  and  $\mathbb{R}^p$  is given by

$$[\cdot]_G^v : \mathfrak{g} \rightarrow \mathbb{R}^p \quad \text{and} \quad [\cdot]_G^\wedge : \mathbb{R}^p \rightarrow \mathfrak{g}. \quad (3)$$

An illustration of the above mappings is given in Fig. 2.

In addition, in Lie group based calculus we need two more operators – adjoint representation of a Lie group, denoted as  $\text{Ad}_G$  and Lie algebra  $\text{ad}_G$ . More detailed discussion on adjoints and the used notation can be found in [18] and [10], respectively.

### C. Concentrated Gaussian distribution

To make use of EKF on Lie groups, the Gaussian error distribution covariance must be established. Distribution on the group tightly focused around the identity element  $X^I$

can be expressed on the Lie algebra [21] with probability density function given as

$$p(X^I) = \beta \exp \left( -\frac{1}{2} [\log_G(X^I)]_G^{\vee T} P^{-1} [\log_G(X^I)]_G^{\vee} \right),$$

where  $\beta$  is a normalizing constant and  $P$  is a positive definite matrix. If  $\epsilon \triangleq [\log_G(X^I)]_G^{\vee}$  is tightly focused, it can be described with a classical Gaussian  $\epsilon \sim \mathcal{N}_{\mathbb{R}^p}(\mathbf{0}^{p \times 1}, P)$ . The distribution of random variable  $X^I$  can be translated over  $G$  by using the left action of the Lie group, and finally a random variable  $X$  can be seen as

$$X = \mu \exp_G(\epsilon_G^{\wedge}), \text{ with } X \sim \mathcal{G}(\mu, P), \quad (4)$$

where  $\mathcal{G}$  denotes the so called concentrated Gaussian distribution (CGD) [21]. For a more formal introduction, the interested reader is referred to [18].

#### D. Special orthogonal group $SO(2)$

The  $SO(2)$  group represents a rotation around a single axis:

$$SO(2) = \{X \in \mathbb{R}^{2 \times 2} \mid X^T X = I, \det(X) = 1\}. \quad (5)$$

For a euclidean space vector consisting of an angle  $x = \phi$ , the Lie algebra  $\mathfrak{so}(2)$ , is given as

$$x_{SO(2)}^{\wedge} = \begin{bmatrix} 0 & -\phi \\ \phi & 0 \end{bmatrix} \in \mathfrak{so}(2). \quad (6)$$

where  $(\cdot)_{SO(2)}^{\wedge} : \mathbb{R}^1 \rightarrow \mathfrak{so}(2)$ . Its inverse,  $(\cdot)_{SO(2)}^{\vee} : \mathfrak{so}(2) \rightarrow \mathbb{R}^1$ , follows trivially from relation (6). The exponential for  $SO(2)$ , performing mapping  $\exp_{SO(2)} : \mathfrak{so}(2) \rightarrow SO(2)$ , is given as

$$\exp_{SO(2)}(x_{SO(2)}^{\wedge}) = \begin{bmatrix} \cos \phi & -\sin \phi \\ \sin \phi & \cos \phi \end{bmatrix}, \quad (7)$$

while the inverse operator,  $\log_{SO(2)} : SO(2) \rightarrow \mathfrak{so}(2)$ , can be evaluated from (7). Due to the commutativity of  $SO(2)$ , the adjoint operators are given as

$$\text{Ad}_{SO(2)}(X) = 1 \text{ and } \text{ad}_{SO(2)}(x) = 0. \quad (8)$$

These properties will greatly simplify the LG-EKF formulae.

#### E. Special orthogonal group $SO(3)$

The  $SO(3)$  group represents an orientation of a rigid body in 3D space, and is defined as

$$SO(3) = \{X \in \mathbb{R}^{3 \times 3} \mid X^T X = I, \det(X) = 1\}. \quad (9)$$

For a euclidean joint space vector  $x = [\phi_1 \ \phi_2 \ \phi_3]^T$ , the Lie algebra  $\mathfrak{so}(3)$  is given as a skew symmetric matrix

$$x_{SO(3)}^{\wedge} = \begin{bmatrix} 0 & -\phi_3 & \phi_2 \\ \phi_3 & 0 & -\phi_1 \\ -\phi_2 & \phi_1 & 0 \end{bmatrix} \in \mathfrak{so}(3). \quad (10)$$

where  $(\cdot)_{SO(3)}^{\wedge} : \mathbb{R}^3 \rightarrow \mathfrak{so}(3)$ . Its inverse,  $(\cdot)_{SO(3)}^{\vee} : \mathfrak{so}(3) \rightarrow \mathbb{R}^3$ , follows trivially from (10). The exponential for  $SO(3)$ , performing mapping  $\exp_{SO(3)} : \mathfrak{so}(3) \rightarrow SO(3)$ , is given as

$$\exp_{SO(3)}(x_{SO(3)}^{\wedge}) = \cos(|x|)I^3 + (1 - \cos(|x|))\frac{xx^T}{|x|^2} + \sin(|x|)\frac{x_{SO(3)}^{\wedge}}{|x|}. \quad (11)$$

The logarithm, performing mapping  $\log_{SO(3)} : SO(3) \rightarrow \mathfrak{so}(3)$ , is given as

$$\begin{aligned} \log_{SO(3)}(X) &= \frac{\theta}{2 \sin(\theta)}(X - X^T) \\ \text{s.t. } 1 + 2 \cos(\theta) &= \text{Tr}(X) \\ \begin{cases} \theta \neq 0 & -\pi < \theta < \pi \\ \theta = 0 & \log(X) = 0 \end{cases} \end{aligned} \quad (12)$$

The adjoints  $\text{Ad}_{SO(3)}$  and  $\text{ad}_{SO(3)}$  are respectively given as

$$\text{Ad}_{SO(3)}(X) = X \text{ and } \text{ad}_{SO(3)}(x) = x_{SO(3)}^{\wedge}. \quad (13)$$

#### F. Special euclidean group $SE(3)$

The group  $SE(3)$  describes 6 DoF rigid body pose and is formed as a semi-direct product of the euclidean space vector  $\mathbb{R}^3$  and the special orthogonal group  $SO(3)$ <sup>1</sup>, corresponding to translational and rotational parts, respectively. This group is defined as

$$SE(3) = \left\{ \begin{pmatrix} R & t \\ \mathbf{0} & 1 \end{pmatrix} \in \mathbb{R}^{4 \times 4} \mid \{R, t\} \in SO(3) \times \mathbb{R}^3 \right\}.$$

For a euclidean space vector representing the pose of a rigid body consisting of a 3DoF position vector  $t$  and a 3DoF orientation vector  $\phi$ , where  $x = [t \ \phi]^T$ , the Lie algebra  $\mathfrak{se}(3)$  is

$$x_{SE(3)}^{\wedge} = \begin{bmatrix} \phi_{SO(3)}^{\wedge} & t \\ \mathbf{0} & 0 \end{bmatrix} \in \mathfrak{se}(3). \quad (14)$$

where  $(\cdot)_{SE(3)}^{\wedge} : \mathbb{R}^6 \rightarrow \mathfrak{se}(3)$ . Its inverse,  $(\cdot)_{SE(3)}^{\vee} : \mathfrak{se}(3) \rightarrow \mathbb{R}^6$ , follows trivially from (14). The exponential for  $SE(3)$ , performing mapping  $\exp_{SE(3)} : \mathfrak{se}(3) \rightarrow SE(3)$ , is given as

$$\exp_{SE(3)}(x_{SE(3)}^{\wedge}) = \begin{bmatrix} C & Lt \\ \mathbf{0} & 1 \end{bmatrix} \quad (15)$$

$$C = \exp_{SO(3)}(\phi_{SO(3)}^{\wedge})$$

$$L = \frac{\sin(|\phi|)}{|\phi|}I^3 + (1 - \frac{\sin(|\phi|)}{|\phi|})\frac{\phi\phi^T}{|\phi|^2} + \frac{1 - \cos(|\phi|)}{|\phi|^2}\phi_{SO(3)}^{\wedge}.$$

The logarithm, performing mapping  $\log_{SE(3)} : SE(3) \rightarrow \mathfrak{se}(3)$ , is calculated by deconstructing  $X$ , and determining  $\phi$  by using (12). Then, from (15) we can determine  $t$ .

In order to determine the adjoints for  $SE(3)$ , we need to deconstruct the state  $X \in SE(3)$  and vector  $x \in \mathbb{R}^6$ . Firstly, we extract the rotation part  $C$  and translation part  $t$  from  $X$ , and secondly, we split the translation part  $t$  and orientation part  $\phi$  from  $x$ . Then, the adjoints  $\text{Ad}_{SE(3)}$  and  $\text{ad}_{SE(3)}$  are

$$\text{Ad}_{SE(3)}(X) = \begin{bmatrix} C & tC \\ \mathbf{0} & C \end{bmatrix}, \text{ad}_{SE(3)}(x) = \begin{bmatrix} \phi_{SO(3)}^{\wedge} & t_{SO(3)}^{\wedge} \\ \mathbf{0} & \phi_{SO(3)}^{\wedge} \end{bmatrix}.$$

We next present the new human motion estimation method based on the LG-EKF.

<sup>1</sup>The euclidean space can be formed only by employing direct product, while other ways to concatenate Lie groups also exist, i.e., semi-direct product, twisted product, etc.

### III. HUMAN MOTION ESTIMATION ON LIE GROUPS

The LG-EKF performs motion prediction and measurement update steps recursively, assuming a constant acceleration model (CA) [17] for each joint.

#### A. Motion prediction step

The LG-EKF approach assumes the motion model of the system can be described with the following equation

$$X_{k+1} = f(X_k, n_k) = X_k \exp_G([\hat{\Omega}_k + n_k]_G^\wedge), \quad (16)$$

where  $X_k \in G$  is the state of the system at time  $k$ ,  $G$  is a  $p$ -dimensional Lie group,  $n_k \sim \mathcal{N}_{\mathbb{R}^p}(\mathbf{0}^{p \times 1}, Q_k)$  is zero mean white Gaussian noise with covariance  $Q_k$  and  $\hat{\Omega}_k = \Omega(X_k) : G \rightarrow \mathbb{R}^p$  is a non-linear  $\mathcal{C}^2$  function.

For example, assuming a CA motion model and considering a single  $SO(2)$  joint with associated angular velocity and angular acceleration, the state would be given by  $X \in G = SO(2) \times \mathbb{R}^1 \times \mathbb{R}^1$ , and

$$\hat{\Omega}_k = \begin{bmatrix} T\dot{q}_k + \frac{T^2}{2}\ddot{q}_k \\ T\ddot{q}_k \\ 0 \end{bmatrix} \in \mathbb{R}^3, \quad n_k = \begin{bmatrix} \frac{T^2}{2}n_k^a \\ Tn_k^a \\ n_k^a \end{bmatrix} \in \mathbb{R}^3, \quad (17)$$

where  $q_k$ ,  $\dot{q}_k$  and  $\ddot{q}_k$  are the angle, angular velocity and angular acceleration represented in tangential space, respectively<sup>2</sup>. The term  $n_k^a$  represents the acceleration increment during the  $k$ -th sampling period [17].

In general, the state of the system  $X$  is formed by using direct (Cartesian) product between the group members, i.e., by placing them block-diagonally. Then, after applying  $\exp_G$  or  $\log_G$ , the element will stay in the block diagonal arrangement. The motion model  $\hat{\Omega}_k$  can be seen as representing an addition to the current state, and for  $N$  joints it is given as  $\hat{\Omega}_k = [\hat{\Omega}_k^1 \ \hat{\Omega}_k^2 \ \dots \ \hat{\Omega}_k^N]^T$ . The motion model and the process noise associated with the  $i$ -th joint, i.e.,  $\hat{\Omega}_k^i$  and  $n_k^i$ , are elements of euclidean space  $\mathbb{R}^r$ , where  $r = 3 \times (\# \text{ DoF})$  since position, velocity and acceleration are included. Hence, for the associated group member  $SO(2)$ ,  $SO(3)$  and  $SE(3)$ , the coefficient is  $r = 3$ ,  $r = 9$  and  $r = 18$ .

We assume the posterior distribution at step  $k - 1$  follows the concentrated Gaussian distribution assumption  $\mathcal{G}(\mu_{k-1}, P_{k-1})$ . The mean propagation of the LG-EKF is then governed by

$$\mu_{k+1|k} = \mu_k \exp_G([\hat{\Omega}_k]_G^\wedge), \quad (18)$$

while the covariance prediction is governed by

$$P_{k+1|k} = \mathcal{F}_k P_k \mathcal{F}_k^T + \Phi_G(\hat{\Omega}_k) Q_k \Phi_G(\hat{\Omega}_k)^T. \quad (19)$$

The operator  $\mathcal{F}_k$  represents a matrix Lie group equivalent to the Jacobian of  $f(X_k, n_k)$ , and is calculated by

$$\begin{aligned} \mathcal{F}_k &= \text{Ad}_G \left( \exp_G([\hat{\Omega}_k]_G^\wedge) \right) + \Phi_G(\hat{\Omega}_k) \mathcal{C}_k \\ \mathcal{C}_k &= \frac{\partial}{\partial \epsilon} \Omega(\mu_k \exp_G(\epsilon_G^\wedge))|_{\epsilon=0}. \end{aligned} \quad (20)$$

<sup>2</sup>Euclidean space  $\mathbb{R}^p$  belongs to a family of Lie groups, while for constructing  $G$  we employ its matrix representation obtained by matrix embedding. It is also a subgroup of  $SE(n)$  where a pure translation is employed [18].

$\mathcal{C}_k$  represents the linearisation term where the argument of the motion model is the current state  $X_k$  with an incremental perturbation additively added in each of the  $p$  directions. Contrary to the conventional EKF, a linear additive process noise injects the system as a function of the current state of the system over the transformation  $\Phi_G(\hat{\Omega}_k) Q_k \Phi_G(\hat{\Omega}_k)^T$ , where  $\Phi_G$  appears due to the displacement of the tangential space during the prediction step, and is given as

$$\Phi_G(v) = \sum_{i=0}^{\infty} \frac{(-1)^i}{(i+1)!} \text{ad}_G(v)^i, \quad v \in \mathbb{R}^p. \quad (21)$$

#### B. Measurement update step

We next derive the update step by employing position measurements of markers attached to a human body obtained by a motion capture system. The markers are assumed to be rigidly attached to a predetermined skeletal model. The discrete measurement model on the matrix Lie group is modelled as

$$Z_{k+1} = h(X_{k+1}) \exp_{G'}([m_{k+1}]_{G'}^\wedge), \quad (22)$$

where  $Z_{k+1} \in G'$ ,  $h : G \rightarrow G'$  is a  $\mathcal{C}^1$  function and  $m_{k+1} \sim \mathcal{N}_{\mathbb{R}^q}(\mathbf{0}^{q \times 1}, R_{k+1})$  is zero-mean white Gaussian noise with covariance  $R_{k+1}$ . The measurement function, in our marker based approach, is given as  $h(X_{k+1}) = \text{diag}\{h(X_{k+1})^1, h(X_{k+1})^2, \dots, h(X_{k+1})^M\}$ , where  $M$  block-diagonally placed measurement components correspond to  $M$  marker position measurements, and hence the measurement space is given as  $G' = \mathbb{R}^{3M}$ .

The update step of the filter strongly resembles the standard EKF update procedure, relying on the Kalman gain  $K_{k+1}$  and innovation vector  $\nu_{k+1}$  calculated as

$$\begin{aligned} K_{k+1} &= P_{k+1|k} \mathcal{H}_{k+1}^T (\mathcal{H}_{k+1} P_{k+1|k} \mathcal{H}_{k+1}^T + R_{k+1})^{-1} \\ \nu_{k+1} &= K_{k+1} \left( [\log_{G'}(h(\mu_{k+1|k})^{-1} Z_{k+1})]_{G'}^\vee \right). \end{aligned} \quad (23)$$

The matrix  $\mathcal{H}_{k+1}$  can be seen as a matrix Lie group equivalent to the Jacobian of  $h(X_{k+1})$ , and is given as

$$\mathcal{H}_{k+1} = \frac{\partial}{\partial \epsilon} \left[ \log_{G'} \left( h(\mu_{k+1|k})^{-1} h(\mu_{k+1|k}^\epsilon) \right) \right]_{G'}^\vee|_{\epsilon=0},$$

where  $h(\mu_{k+1|k}^\epsilon) = h(\mu_{k+1|k} \exp_G(\epsilon_G^\wedge))$ , describes the variation of markers' positions for an infinitesimal motion  $\epsilon$ . We now evaluate the part of  $\mathcal{H}_{k+1}$  corresponding to the  $i$ -th marker's measurement  $Z_{k+1}^i$ . This relation is given as

$$\begin{aligned} \mathcal{H}_{k+1}^i &= \frac{\partial}{\partial \epsilon} \left( \log_{G'} \left( h(\mathcal{K}_{s_i}^0(X_{k+1|k}))^{-1} \right. \right. \\ &\quad \left. \left. h(\mathcal{K}_{s_i}^0(X_{k+1|k}^\epsilon)) \right) \right)_{G'}^\vee|_{\epsilon=0} \\ &= \frac{\partial}{\partial \epsilon} \left( \log_{G'} \left( \begin{bmatrix} I & \mathcal{K}_{s_i}^0(X_{k+1|k}^\epsilon) \end{bmatrix} \begin{bmatrix} 0 \\ 0 \\ 0 \\ 1 \end{bmatrix} \right) \right)_{G'}^\vee|_{\epsilon=0}, \end{aligned} \quad (24)$$

where  $\mathcal{K}_{s_i}^0(X_{k+1|k})$  stands for the forward kinematics of the  $i$ -th marker for a given predicted state  $X_{k+1|k}$ , while  $\mathcal{K}_{s_i}^0(X_{k+1|k}^\epsilon) = \mathcal{K}_{s_i}^0(X_{k+1|k} \exp_G(\epsilon_G^\wedge))$  corresponds to the

forward kinematics for the infinitesimally perturbed state  $X_{k+1|k}$ . Note that the term  $\mathcal{K}_{s_i}^0(X_{k+1|k})^{-1}$  vanishes after applying the partial derivatives over  $\epsilon$ . We now decompose the kinematics term  $\mathcal{K}_{s_i}^0(X_{k+1|k})$  into several parts as

$$\mathcal{K}_{s_i}^0(X_{k+1|k}) = \mathcal{K}_j^0(X_{k+1|k}) \mathcal{K}_{k+1|k}^j \mathcal{K}_{s_i}^{j+1}(X_{k+1|k}), \quad (25)$$

where  $\mathcal{K}_j^0(X_{k+1|k})$  represents the transformation from the base frame to joint  $j$  and  $\mathcal{K}_{s_i}^{j+1}(X_{k+1|k})$  represents the transformation from joint  $j+1$  towards sensor  $i$ .

Let us now consider a part of the  $\mathcal{H}_{k+1}^{i,j}$  term relating the  $i$ -th measurement with the  $j$ -th joint, denoted as  $\mathcal{H}_{k+1}^{i,j}$ . Furthermore, let us assume the  $j$ -th joint is represented with an SE(3) term, hence covering the most general case, since SO(2) and SO(3) are simplifications of SE(3). Then, by exploiting results from [19],  $\mathcal{H}_{k+1}^{i,j}$  can be expressed as

$$\begin{bmatrix} \mathcal{H}_{k+1}^{i,j,r} \\ 1 \end{bmatrix} = \mathcal{K}_j^0(X_{k+1|k}) \mathcal{K}_{k+1|k}^j E^r \mathcal{K}_{s_i}^{j+1}(X_{k+1|k}) \begin{bmatrix} 0 \\ 0 \\ 0 \\ 1 \end{bmatrix},$$

where  $E^r$  represents the  $r$ -th generator of SE(3) group, i.e.,  $r = 1, \dots, 6$  [21]. Each of the 6 generators represents an infinitesimal motion in one of the directions of SE(3) space, and  $\mathcal{H}_{k+1}^{i,j} = [\mathcal{H}_{k+1}^{i,j,1} \dots \mathcal{H}_{k+1}^{i,j,6}]$ . Since marker position measurements are only a function of the joint positions, the part of the  $\mathcal{H}_{k+1}$  matrix relating measurements with velocity and acceleration components is filled with zero values.

Finally, the measurement update step is calculated as

$$\begin{aligned} \mu_{k+1} &= \mu_{k+1|k} \exp_G([\nu_{k+1}]_G^\wedge) \\ P_{k+1} &= \Phi_G(\nu_{k+1}) (I^p - K_{k+1} \mathcal{H}_{k+1}) P_{k+1|k} \Phi_G(\nu_{k+1})^T. \end{aligned} \quad (26)$$

For a more formal derivation of the LG-EKF update, the interested reader is referred to [10].

#### IV. EULER ANGLE BASED APPROACH

The proposed approach is compared to conventional EKF applied to a standard kinematic model defined with revolute and prismatic joints [22]. Three perpendicular revolute joints (Euler angles) can be used to model human spherical joints such as the shoulder and the hip. The transformation between the world frame and the base of the body can be modelled with three prismatic and three perpendicular revolute joints, as shown in Fig. 1 (right). The state of the EKF is defined as the position  $q$ , velocity  $\dot{q}$ , and acceleration  $\ddot{q}$  of the joints. Assuming constant acceleration the linear motion model is

$$\begin{aligned} q_{k+1} &= q_k + T\dot{q}_k + \frac{T^2}{2}\ddot{q}_k \\ \dot{q}_{k+1} &= \dot{q}_k + T\ddot{q}_k \\ \ddot{q}_{k+1} &= \ddot{q}_k. \end{aligned} \quad (27)$$

Treating the attached markers as end effectors, the measurement Jacobian for the  $i$ -th marker,  $H_i$ , is the

velocity Jacobian in the base frame.

$$H^i = [Jv^{i1} Jv^{i2} \dots Jv^{in}] \quad (28)$$

$$Jv^{ij} = \begin{cases} z^j \times (o^i - o^j) & \text{for revolute joint } j \\ z^j & \text{for prismatic joint } j \end{cases} \quad (29)$$

where joint  $j$  is centered at  $o^j$  and actuates about  $z^j$  axis and  $o^i$  is the end effector position. With the Jacobians defined EKF can be set up to estimate the positions, velocities, and accelerations of all the joints in the kinematic model based on motion capture marker measurements.

#### V. VALIDATION RESULTS

We validate the proposed approach with three datasets. First, in simulation, we demonstrate the benefits of LG-EKF over EKF during highly dynamical movements whose motion is better described on the group and show that unlike EKF, LG-EKF is not affected by gimbal lock. Next, to show the benefits of SO(3) representation, we evaluate the performance of LG-EKF and EKF on real motion capture data of arm boxing movement. Finally, we perform full body estimation of a highly dynamic martial arts movement sequence to verify the effectiveness of the SE(3) joint connecting between world origin and the body base frame and demonstrate the overall benefits of LG-EKF over EKF.

##### A. Simulation Validation

1) *Dynamic Motion*: To test the convergence and estimation properties of LG-EKF, we simulate a human arm composed of the shoulder, elbow, and wrist joints, the state is an element of  $SO(3) \times SO(2) \times SO(3)$  group respectively. Two simulated motion capture markers are placed at the shoulder and elbow and 4 about the wrist. The kinematic chain is visualized in Fig. 3 (middle). We generate angular velocity on the group using a Fourier series with 5 harmonics and coefficients from a uni-variate distribution, the angular velocity is then propagated at 100Hz according to the motion model defined in equation 16 with no additive noise. The simulated marker positions are computed with forward kinematics and Gaussian noise with standard deviation  $\sigma_{\text{dev}} = 1$  mm is added to simulate errors in 3D marker measurement. This creates a highly dynamic motion as can be seen from the positions of the four wrist markers in Fig. 4. The measurement noise was set to 0.01 for both LG-EKF and EKF. No further tuning was performed to improve estimation of either filter, the initial covariances were set to identity and process noise for all states was 0.01.

To compare the estimate with the ground truth, we use the deviation from the identity matrix as the distance metric [23]

$$\mathcal{D}_F = \|I - R_e^T R_{gt}\|_F \quad (30)$$

where  $R_e$  and  $R_{gt}$  are the estimated and ground truth rotation matrices of each joint and  $\|\cdot\|_F$  denotes the Frobenius norm, which is functionally equivalent to the geodesic on SO(3) [23]. Figure 5 shows the comparison in estimation of rotation matrices for each of the three joints



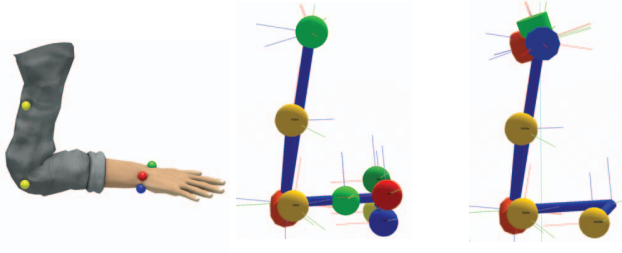


Fig. 3: Left: 3D Arm model showing simulation marker placement. Middle: Lie group-based arm model with attached markers for dynamic motion simulation. Right: Euler angle-based arm model for the CMU dataset (no wrist) with CMU markers attached.

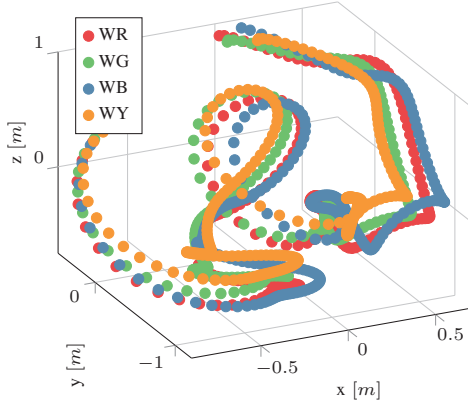


Fig. 4: Trajectories of wrist markers attached to the simulated arm model undergoing the generated highly dynamic motion over 2.5 s.

between LG-EKF and EKF using this distance metric. On average LG-EKF improves estimation over EKF by 20.9%. The observed improvement is composed of gimbal lock avoidance, described in the next section, and a better error covariance representation on the manifold.

2) *Gimbal Lock*: Any set of Euler angles will lose a degree of freedom when two of the rotation axes align [24], implying that in that configuration the rotation about the locked axis cannot be correctly estimated by EKF. Typically the order of the joint axes is carefully selected to try and avoid the lock, however in human motion estimation gimbal lock often takes place at the shoulder joint due to its high manoeuvrability. Unlike the Euler angle formulation, an  $SO(3)$  representation of the spherical joint does not suffer from gimbal lock and thus LG-EKF will accurately estimate any 3D rotation.

To demonstrate the benefits of LG-EKF over EKF during gimbal lock we simulate a single spherical joint at the origin with three motion capture markers attached at offsets of  $[0.3, 0.1, 0]^T$ ,  $[0.3, -0.1, 0]^T$ , and  $[0.3, 0, 0.1]^T$  for full observability. To ensure continuation in position, velocity, and acceleration we use a quintic polynomial to generate a smooth trajectory, sampling at 200 Hz. First, the model experiences a 1 second rotation about the world  $y$  axis with initial position 0 rads and final positions  $\frac{\pi}{2}$  rads and zero initial and final velocity and acceleration. Since the second joint of the Euler model is aligned with the  $y$  axis this

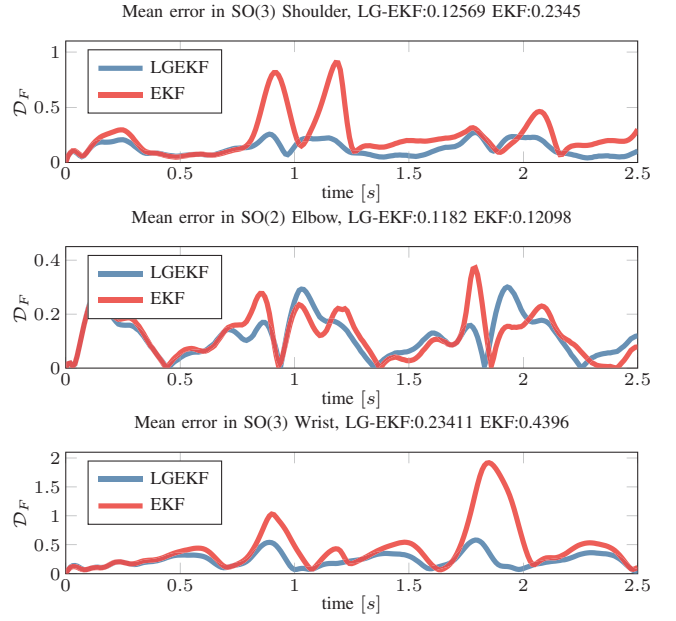


Fig. 5: Rotation matrices error for each of the three joints in the simulated lower body.

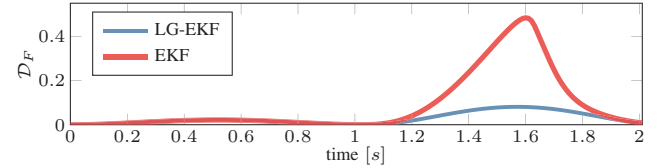


Fig. 6: LG-EKF and EKF estimation during gimbal lock. Both filters accurately estimate the rotation about the  $y$  axis until 1 second. After the rotation about  $y$  the Euler angle model is in gimbal lock and thus EKF cannot accurately track the orientation until the lock is escaped at 1.5 seconds. LG-EKF estimation is unaffected by gimbal lock.

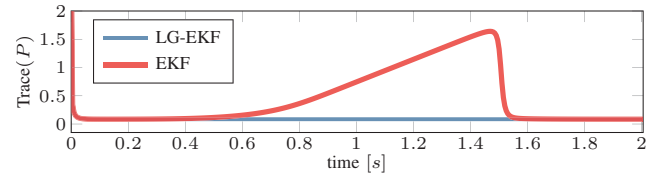


Fig. 7: Trace of the LG-EKF and EKF position error covariance. Both filters start with the same error covariance that quickly converges to a low value. As the Euler angles approach the gimbal lock the EKF position error covariance increases and continues to grow until EKF escapes the lock. LG-EKF position error covariance is unaffected.

effectively puts the Euler angle model into gimbal lock. Next, the model experiences the same 1 s rotation in the now locked world  $z$  axis. In order to focus only on the gimbal lock problem, no noise was added to the marker measurements. Measurement noise, process noise, and initial covariances were set as described in Sec. V-A.1.

Figures 6 and 7 show respectively the distance metric described in (30) and the trace of the position error covariance of both filters.

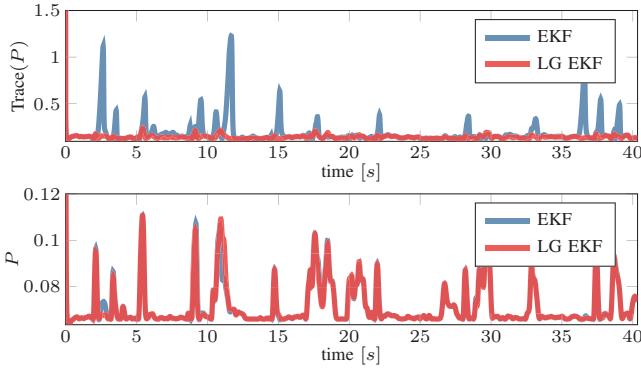


Fig. 8: Position error covariance of LG-EKF and EKF for the spherical shoulder joint (top) and hinge elbow joint (bottom) during boxing motion estimation.

### B. Real-world experiment - boxing arm

To evaluate the benefits of estimating real human motion with the proposed method we compare the filters on a highly dynamic boxing motion from the CMU Graphics Lab Motion Capture Database [25]. The movement is captured at 120 Hz with a Vicon motion capture system using 12 cameras. Skeletal model of each participant is created with the Vicon BodyBuilder software and markers are attached at predetermined bony landmarks. We simplify the model by ignoring finger joints and extra joints in the spine Vicon software generates in post processing. In order to focus on the performance of the  $SO(3)$  joint, only the motion of the right arm is estimated. The kinematic chain consists of a spherical joint at the shoulder and a hinge joint at the elbow. Three motion capture markers are used, placed on the upper arm, elbow, and forearm. Figure 3 shows the Euler angle and Lie group models side by side.

To conduct a fair comparison the filters are initialized with the same noise parameters; the initial error covariances, process noise for all states, and observation noise are set to identity, 0.01, and 0.01 respectively. Furthermore, both filters are initialized with a good initial guess obtained from Vicon inverse kinematics available as part of the CMU dataset. We evaluate the performance of each filter by looking at the error covariance as well as using the estimated state to compute the forward kinematics and compare the actual and predicted marker positions. Figure 8 shows the position error covariances of the filters for the spherical shoulder and revolute elbow joints. The shoulder movement is better estimated on the  $SO(3)$  group and thus the error covariance is significantly more uniform than its Euler angles counterpart. Generally, the  $SO(2)$  is expected to behave identically as wrapped  $\mathbb{R}^1$  [26]. Table I shows the RMSE between the actual and estimated marker positions. LG-EKF has a better representation of error covariance and avoids gimbal lock at the  $SO(3)$  shoulder joint leading to a lower RMSE in the upper arm and elbow markers. The better estimation at the shoulder is propagated through the kinematic chain leading to a lower RMSE in the forearm marker even though the  $SO(2)$  joint behaves identically to a single Euler angle.

TABLE I: Root mean squared error in cm between actual and predicted marker positions for boxing arm motion. Where UPA, ELB, and FRA are the upper arm, elbow, and forearm markers respectively. On average LG-EKF improves estimation by 14%.

	UPA	ELB	FRA
EKF	2.61	3.04	2.79
LG-EKF	<b>2.30</b>	<b>2.69</b>	<b>2.27</b>

TABLE II: Root mean squared error in cm between actual and predicted marker positions for markers attached to the waist of the full body model. Where RF, LF, RB, and LB are the right and left, front and back markers respectively. On average estimation on SE3 improves RMSE by 8.2%.

	RF	LF	RB	LB
EKF	1.76	1.91	1.57	1.61
LG-EKF	<b>1.66</b>	<b>1.70</b>	<b>1.42</b>	<b>1.46</b>

### C. Real-world experiment - full body

To enable localization of the actor in the world frame we add  $SE(3)$  as the first element of LG-EKF's state vector and express the entire full body as a collection of  $SO(3)$  and  $SO(2)$  elements presented in Fig. 1 (right).  $SE(3)$  element connects the world frame to the base of the kinematic model. Shoulders, hips, and neck joints are modelled as  $SO(3)$  elements. Elbows, knees, and wrists are described using a single  $SO(2)$  element and the ankles with two perpendicular  $SO(2)$  elements. A total of 37 markers are attached to the body following the Vicon motion capture manual [25]. To demonstrate the benefits of the  $SE(3)$  representation of localization over a sequence of prismatic and revolute joints and the overall improvement of LG-EKF we use a dynamic full body martial arts movement sequence from the CMU database. Both filters are initialized identically with the same noise parameters as described in Sec. V-B and with a good initial state from the Vicon IK.

Figure 9 compares the position error covariance of the LG-EKF's  $SE(3)$  element state and the EKF's prismatic and revolute joint states. As seen from the uniform covariance, the fast full body rotations and translations are better represented on the  $SE(3)$  group. This can also be observed in the RMSE of the predicted and actual marker positions of the 4 pelvis markers shown in Table II. As an extra comparison we use the Vicon CMU IK results and their more complex full-body model to run forward kinematics and compare the RMSE of predicted and actual marker positions. Table III provides RMSE for the rest of the markers on the body including that of Vicon IK. Even without tuning the noise parameters and initial covariances, the stochastic filtering approaches significantly outperform the Vicon IK method. Furthermore, the LG-EKF achieves a much lower RMSE in almost all the markers over the EKF. The lower error covariance and avoidance of gimbal lock at the  $SE(3)$  joint provides a better estimation of the entire skeleton position and orientation. The improvement in the estimation at the base and each  $SO(3)$  joint is propagated down the kinematic tree reducing the RMSE of the markers.

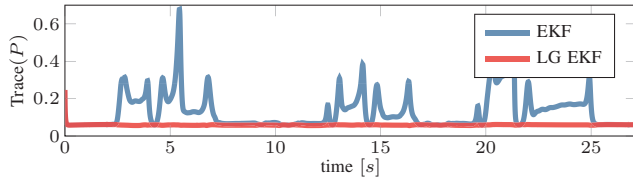


Fig. 9: LG-EKF and EKF position error covariance of the transformation of an  $SE(3)$  from world to base of the kinematic model. Since the transformation is an  $SE(3)$  element LG-EKF is able to accurately estimate it and its evolution over time. Prismatic joints and Euler angles do not correctly represent  $SE(3)$  thus EKF covariance increases during highly dynamic motion.

TABLE III: Root mean square error between predicted and actual marker positions for full body motion capture. LG-EKF outperforms both EKF and VICON IK for most of the markers. Refer to [25] for marker placement and naming details. Note, VICON IK prioritizes ankle markers to avoid unrealistic sliding at the feet.

R Arm	RSHO	RELB	RUPA	RFRM	RWRA	RWRB	
VICON	6.33	4.57	5.17	4.64	7.01	6.91	
EKF	2.89	3.04	<b>2.82</b>	2.87	2.43	2.39	
LG-EKF	<b>2.6</b>	<b>2.67</b>	2.91	<b>2.58</b>	<b>2.29</b>	<b>2.23</b>	
L Arm	LSHO	LELB	LUPA	LFRM	LWRA	LWRB	
VICON	7.82	5.96	6.32	8.19	11.11	10.74	
EKF	2.98	4.51	3.95	2.77	4.22	2.32	
LG-EKF	<b>2.82</b>	<b>4.15</b>	<b>3.86</b>	<b>2.59</b>	<b>4.1</b>	<b>2.02</b>	
Torso and Head	CLAV	T10	STRN	RFHD	LFHD	RBHD	LBHD
VICON	6.09	2.98	2.22	12.85	13.07	10.65	10.59
EKF	1.74	1.55	1.72	1.3	1.18	1.5	1.49
LG-EKF	<b>1.64</b>	<b>1.45</b>	<b>1.59</b>	<b>1.26</b>	<b>1.13</b>	<b>1.45</b>	<b>1.43</b>
R Leg	RTHI	RKNE	RSHN	RANK	RHEE	RTOE	RMT5
VICON	3.99	4.78	4.27	<b>0.4</b>	1.47	2.54	1.81
EKF	2.06	2.42	2.34	1.15	1.18	0.94	1.06
LG-EKF	<b>1.93</b>	<b>2.4</b>	<b>2.33</b>	1.14	<b>1.16</b>	<b>0.93</b>	<b>1.04</b>
L Leg	LTHI	LKNE	LSHN	LANK	LHEE	LTOE	LMT5
VICON	4.36	4.45	2.48	<b>0.53</b>	1.4	2.29	2.4
EKF	2.09	2.01	1.35	1.06	1.22	1	1.18
LG-EKF	<b>2.07</b>	<b>1.98</b>	<b>1.34</b>	1.04	<b>1.21</b>	1	<b>1.16</b>

## VI. CONCLUSION

We proposed a novel algorithm for human motion estimation based on body worn marker position measurements. The human joints were described as Lie group members, including special orthogonal groups  $SO(2)$  and  $SO(3)$ , and a special euclidean group  $SE(3)$ . For stochastic inference on Lie groups the LG-EKF was employed, thus explicitly accounting for the non-euclidean geometry of the state space. A constant acceleration motion model for human motion estimation on the group was developed and the Jacobian of the marker position measurements was derived. The performance of the proposed method was evaluated on both simulation and real-world motion capture data, comparing it with the Euler angles-based EKF as well as Vicon IK for full body estimation. We showed that LG-EKF improves estimation for highly dynamic motions and is not affected by gimbal lock.

## REFERENCES

- [1] D. Kulić, G. Venture, K. Yamane, E. Demircan, I. Mizuuchi, and K. Mombaur, "Anthropomorphic Movement Analysis and Synthesis : A Survey of Methods and Applications," *IEEE Transactions on Robotics*, vol. 32, no. 4, pp. 776–795, 2016.
- [2] T. Sugihara, "Solvability-unconcerned inverse kinematics by the levenberg-marquardt method," *IEEE Transactions on Robotics*, vol. 27, no. 5, pp. 984–991, 2011.
- [3] J. Steinbring, C. Mandery, N. Vahrenkamp, T. Asfour, and U. D. Hanebeck, "High-accuracy real-time whole-body human motion tracking based on constrained nonlinear kalman filtering," *arXiv preprint arXiv:1511.04278*, 2015.
- [4] A. Aristidou and J. Lasenby, "Real-time marker prediction and cor estimation in optical motion capture," *The Visual Computer*, vol. 29, no. 1, pp. 7–26, 2013.
- [5] J. Steinbring, C. Mandery, F. Pfaff, F. Faion, T. Asfour, and U. D. Hanebeck, "Real-Time Whole-Body Human Motion Tracking Based on Unlabeled Markers," in *IEEE Int. Conf. on Multisensor Fusion and Integration for Intell. Systems (MFI)*. IEEE, 2016, pp. 607–614.
- [6] V. Bonnet, G. Daune, V. Joukov, R. Dumas, P. Fraisse, D. Kulić, A. Seilles, S. Andary, and G. Venture, "A constrained extended kalman filter for dynamically consistent inverse kinematics and inertial parameters identification," in *International Conference on Biomedical Robotics and Biomechanics (BioRob)*. IEEE, 2016, pp. 952–957.
- [7] T. D. Barfoot and P. T. Furgale, "Associating Uncertainty With Three-Dimensional Poses for Use in Estimation Problems," *IEEE Transactions on Robotics*, vol. 30, no. 3, pp. 679–693, jun 2014.
- [8] M. Benallegue and F. Lamiraud, "Estimation and Stabilization of Humanoid Flexibility Deformation Using Only Inertial Measurement Units and Contact Information," *International Journal of Humanoid Robotics*, vol. 12, no. 3, p. 1550025, 2015.
- [9] J. Česić, I. Marković, I. Cvišić, and I. Petrović, "Radar and stereo vision fusion for multitarget tracking on the special euclidean group," *Robotics and Autonomous Systems*, vol. 83, pp. 338 – 348, 2016.
- [10] G. Bourmaud, R. Mégret, M. Arnaudon, and A. Giremus, "Continuous-Discrete Extended Kalman Filter on Matrix Lie Groups Using Concentrated Gaussian Distributions," *Journal of Mathematical Imaging and Vision*, vol. 51, no. 1, pp. 209–228, 2015.
- [11] C. Hertzberg, R. Wagner, U. Frese, and L. Schröder, "Integrating Generic Sensor Fusion Algorithms with Sound State Representations through Encapsulation of Manifolds," *Information Fusion*, vol. 14, no. 1, pp. 57–77, jul 2013.
- [12] Q. Rentmeesters, P. A. Absil, P. Van Dooren, K. Gallivan, and A. Srivastava, "An efficient particle filtering technique on the grassmann manifold," in *IEEE International Conference on Acoustics, Speech and Signal Processing (ICASSP)*, 2010, pp. 3838–3841.
- [13] J. Martinez-Del-Rincon, M. Lewandowski, J. C. Nebel, and D. Makris, "Generalized Laplacian eigenmaps for modeling and tracking human motions," *IEEE Trans. on Cyb.*, vol. 44, no. 9, pp. 1646–1660, 2014.
- [14] M. Ding and G. Fan, "Multilayer Joint Gait-Pose Manifolds for Human Gait Motion Modeling," *IEEE Transactions on Cybernetics*, vol. 45, no. 11, pp. 2413–2424, 2015.
- [15] M. Devanne, H. Wannous, S. Berretti, P. Pala, M. Daoudi, and A. Del Bimbo, "3-D Human Action Recognition by Shape Analysis of Motion Trajectories on Riemannian Manifold," *IEEE Transactions on Cybernetics*, vol. 45, no. 7, pp. 1340–1352, 2015.
- [16] S. Brossette, A. Escande, G. Duchemin, B. Chrétien, and A. Kheddar, "Humanoid posture generation on non-Euclidean manifolds," *IEEE-RAS Int. Conf. on Humanoid Robots*, pp. 352–358, 2015.
- [17] Y. Bar-Shalom, T. Kirubarajan, and X.-R. Li, *Estimation with Applications to Tracking and Navigation*. John Wiley & Sons, 2002.
- [18] G. S. Chirikjian, *Stochastic Models, Inform. Theory, and Lie Groups, Vol. 2: Analytic Methods and Modern Applications*. Springer, 2012.
- [19] J. M. Selig, "Lie Groups and Lie Algebras in Robotics," in *Comput. Noncommutative Algebra and Applications*, 2005, pp. 101–125.
- [20] W. Park, Y. Wang, and G. S. Chirikjian, "The Path-of-Probability Algorithm for Steering and Feedback Control of Flexible Needles," *Int. Journal of Robotics Research*, vol. 29, no. 7, pp. 813–830, 2010.
- [21] Y. Wang and G. S. Chirikjian, "Nonparametric Second-Order Theory of Error Propagation on Motion Groups," *The International Journal of Robotics Research*, vol. 27, no. 11, pp. 1258–1273, 2008.
- [22] V. Joukov, R. D'Souza, and D. Kulić, "Human pose estimation from imperfect sensor data via the extended kalman filter," in *International Symposium on Experimental Robotics (ISER 2016)*. IEEE, 2016.
- [23] D. Q. Huynh, "Metrics for 3d rotations: Comparison and analysis," *J. of Math. Imaging and Vision*, vol. 35, no. 2, pp. 155–164, 2009.
- [24] F. S. Grassia, "Practical parameterization of rotations using the exponential map," *J. of graphics tools*, vol. 3, no. 3, pp. 29–48, 1998.
- [25] F. De la Torre, J. Hodgins, A. Bargteil, X. Martin, J. Macey, A. Collado, and P. Beltran, "Guide to the carnegie mellon university multimodal activity (cmu-mmact) database," *Rob. Inst.*, p. 135, 2008.
- [26] I. Marković, J. Česić, and I. Petrović, "On wrapping the Kalman filter and estimating with the  $SO(2)$  group," *International Conference on Information Fusion (FUSION)*, pp. 1–6, 2016.

## PUBLICATION 5

V. Joukov, J. Ćesić, K. Westermann, I. Marković, D. Kulić and I. Petrović. Human motion estimation on Lie groups using IMU measurements. *IEEE/RSJ International Conference on Intelligent Robots and Systems (IROS)*. Vancouver, Canada, 1965–1972, 2017.



# Human motion estimation on Lie groups using IMU measurements

Vladimir Joukov\*, Josip Česić<sup>‡</sup>, Kevin Westermann\*, Ivan Marković<sup>‡</sup>, Dana Kulić\* and Ivan Petrović<sup>‡</sup>

**Abstract**—This paper proposes a new algorithm for human motion estimation using inertial measurement unit (IMU) measurements. We model the joints by matrix Lie groups, namely the special orthogonal groups  $SO(2)$  and  $SO(3)$ , representing rotations in 2D and 3D space, respectively. The state space is defined by the Cartesian product of the rotation groups and their velocities and accelerations, given a kinematic model of the articulated body. In order to estimate the state, we propose the Lie Group Extended Kalman Filter (LG-EKF), thus explicitly accounting for the non-Euclidean geometry of the state space, and we derive the LG-EKF recursion for articulated motion estimation based on IMU measurements. The performance of the proposed algorithm is compared to the EKF based on Euler angle parametrization in both simulation and real-world experiments. The results show that for motion near gimbal lock regions, which is common for shoulder movement, the proposed filter is a significant improvement over the Euler angles EKF.

## I. INTRODUCTION

Human motion measurement is a key enabling technology in many applications, including human motion analysis, rehabilitation, imitation learning and human-robot interaction [1]. A number of different sensing modalities have been proposed for human motion measurement, including camera, magnetic and wearable systems [1]. When line of sight between the sensor and the human cannot be ensured, and when motion is to be captured in large or outdoor spaces, wearable sensing, based on inertial measurement units (IMUs) is preferred.

Many previous works focus on human pose estimation using wearable IMUs. A simple approach is to integrate the gyroscope to estimate the orientation of each limb, however, due to gyroscope drift error accumulates over time [2]. Stochastic filter methods are often used to combine gyroscope and accelerometer signals to reduce drift and allow for estimation of highly dynamic motions. Without taking into account the kinematic model of the human body, the orientation of each limb can be estimated separately [3], [4] with the Kalman filter. In post processing kinematic constraints can be incorporated and the joint angle estimated via optimization [5].

This work has been supported from the Unity Through Knowledge Fund under the project *Cooperative Cloud based Simultaneous Localization and Mapping in Dynamic Environments* (cloudSLAM) and by the Ministry of Science, Education and Sports of the Republic of Croatia under the grant *Center of Research Excellence for Data Science and Cooperative Systems* (CoE ACROSS).

\* Vladimir Joukov, Kevin Westermann and Dana Kulić are with the University of Waterloo, Department of Electrical and Computer Engineering, Adaptive Systems Laboratory, Canada. {vjoukov@uwaterloo.ca, kgwester@uwaterloo.ca, dkulic@uwaterloo.ca}

<sup>‡</sup> Josip Česić, Ivan Marković and Ivan Petrović are with the University of Zagreb, Faculty of Electrical Engineering and Computing, Laboratory for Autonomous Systems and Mobile Robotics, Croatia. {josip.cesic@fer.hr, ivan.markovic@fer.hr, ivan.petrovic@fer.hr}

To retrieve the joint angles directly, human kinematic constraints must be incorporated into the estimation. If the kinematic model is available a priori, stochastic filter methods can be used to directly estimate human pose from IMU measurements. Modeling the human body as a set of rigid links connected with hinge joints Lin and Kulić [6] and El-Gohary and McNames [7] used the Extended and the Unscented Kalman filters to estimate arbitrary 3D leg and arm motion respectively. Model based extended quaternion Kalman filter was used by Szczesna to track a 3-segment inverted pendulum motion [8]. Finally, having a model of the motion in addition to the kinematic constraints can further improve human pose estimation [2], [9].

In most of the aforementioned works the joints of the kinematic model are described using Euler angles. While [8] uses a quaternion joint representation, the approach cannot represent different constraints for human joints with different degrees of freedom (dof): 3 at the hip and shoulder, 2 in the elbow and wrist, and a single dof at the knee. In our previous work [10] we showed that Lie group based kinematic modeling can correctly represent the degrees of freedom of the human body and that Lie group based extended Kalman filter can significantly improve marker based pose estimation. A number of other studies have also investigated uncertainty modeling and representation on Lie groups. In [11] representation and propagation of uncertainty on Lie groups was studied in the context of manipulator kinematics and camera trajectory estimation, and later in [12] the authors studied the stochastic kinematic model of a differential drive mobile robot on  $SE(2)$ . Uncertainty association, propagation and fusion on  $SE(3)$  was investigated in [13]. In [14] the authors preintegrated a number of IMU measurements for visual-inertial navigation by properly addressing the geometry of the rotation group and defining the uncertainty in the pertaining tangent space. Finally, an extended Kalman filter on Lie groups (LG-EKF) was proposed in [15], [16] and has been further developed to an iterative version [17].

In this paper we propose a novel approach for human motion estimation based solely on IMU measurements. To the best of our knowledge, this work is the first to propose the LG-EKF formulation for kinematic chain state estimation using IMU measurements and derive the necessary measurement Jacobians. The proposed filtering approach performs stochastic inference of human motion by defining the state space to reside on a Lie group, with each state element corresponding to the kinematic model of the analysed human body part. Then, the LG-EKF is derived, where the prediction step is based on the constant acceleration model [18], while the update step depends on the gyro and accelerometer mea-

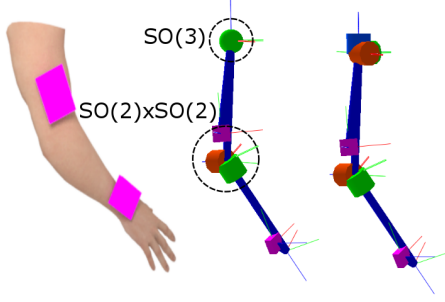


Fig. 1. Left: 3D Arm model showing simulation IMU placement. Middle: Lie group-based arm model with attached IMU units for dynamic motion simulation. Right: Euler angle-based arm model.

measurements of the IMU units. We compare the performance of the proposed algorithm with an EKF based on the Euler angles parametrization both in simulation and real-world experiments. The results show that the proposed approach significantly improves performance and is not affected by gimbal lock.

The rest of the paper is organised as follows. In Section II we present the mathematical fundamentals addressing Lie groups and associated uncertainties. In Section III we present the novel LG-EKF, while in Section IV we briefly describe the EKF based on Euler angles. Section V presents the validation results and Section VI concludes the paper.

## II. MATHEMATICAL BACKGROUND

In this section we provide the mathematical background for human motion estimation on matrix Lie groups, based on the human body modeling approach and the corresponding state space construction first proposed in [19].

### A. Construction of the state space

We construct the state space by using Lie group representatives for each joint of interest. As an example we consider the model of a human arm illustrated in Fig. 1. An example of group  $G$  representing the state space for this model is

$$G = \overbrace{\text{SO}(3)}^{\text{shoulder}} \times \overbrace{\text{SO}(2) \times \text{SO}(2)}^{\text{elbow}}. \quad (1)$$

The first element in (1) describes the shoulder employing a special orthogonal group  $\text{SO}(3)$  and providing 3 DoF mobility, while the second and third elements jointly model the 2 DoF motion of the flexion/extension and internal rotation of the elbow joint, where each element of a special orthogonal group  $\text{SO}(2)$  contributes a single DoF. Note that the choice of the state space only incorporates system variables and not the kinematic model geometry.

### B. Lie groups and Lie algebra

A Lie group  $G$  is a group which also has the structure of a smooth manifold. The group operators, composition and inversion, are smooth operations. Each point  $X \in G$  has an associated tangent space  $T_X(G)$  [20]. This linear tangent space is usually placed at the group identity, and is called the Lie algebra of  $G$ , which we denote by  $\mathfrak{g}$  [21]. The Lie algebra

$\mathfrak{g}$ , which is of the same dimension as  $G$ , admits a binary operation  $[\cdot, \cdot]$  called the Lie bracket, which reflects the non-commutative content of the group operation. Furthermore, if the group  $G$  is a matrix Lie group, then  $G \subset \mathbb{R}^{n \times n}$  and group operations are simply matrix multiplication and inversion.

The Lie algebra  $\mathfrak{g} \subset \mathbb{R}^{n \times n}$  associated to a  $p$ -dimensional matrix Lie group  $G \subset \mathbb{R}^{n \times n}$  is a  $p$ -dimensional vector space defined by a basis consisting of  $p$  real matrices  $E_r$ ,  $r = 1, \dots, p$ , often referred to as generators [22]. In particular, a Lie algebra is an open neighbourhood around  $\mathbf{0}^p$  in the tangent space of  $G$  at the identity  $\mathbf{I}^n$ . The matrix exponential  $\exp_G$  and matrix logarithm  $\log_G$  establish a local diffeomorphism between  $G$  and  $\mathfrak{g}$  as

$$\exp_G : \mathfrak{g} \rightarrow G \quad \text{and} \quad \log_G : G \rightarrow \mathfrak{g}. \quad (2)$$

Furthermore, a natural relation exists between the  $p$ -dimensional Lie algebra  $\mathfrak{g}$  and the Euclidean space  $\mathbb{R}^p$ , and is given through a linear isomorphism

$$[\cdot]_G^\vee : \mathfrak{g} \rightarrow \mathbb{R}^p \quad \text{and} \quad [\cdot]_G^\wedge : \mathbb{R}^p \rightarrow \mathfrak{g}. \quad (3)$$

For brevity, we will use the following notation [17]

$$\exp_G^\wedge(x) = \exp_G([x]_G^\wedge) \quad \text{and} \quad \log_G^\vee(X) = [\log_G(X)]_G^\vee, \quad (4)$$

where  $x \in \mathbb{R}^p$  and  $X \in G$ .

Since Lie groups are generally non-commutative, i.e.,  $XY \neq YX$ , we also need to employ the adjoint representations. The adjoint representation of  $G$  on  $\mathfrak{g}$ ,  $\text{Ad}_G$ , can be seen as a way of representing the elements of the group as a linear transformation of the group's algebra, and in general, it measures the failure of  $X \in G$  to commute with elements of  $G$  near the identity [23]. The adjoint representation of  $\mathfrak{g}$ ,  $\text{ad}_G$ , is in fact the differential of  $\text{Ad}_G$  at the identity element. For a commutative group, the map  $\text{ad}$  evaluates to zero.

### C. Concentrated Gaussian distribution

To make use of EKF on Lie groups, we need to establish first a notion of a Gaussian distribution on Lie groups. A distribution on a Lie group that is tightly focused, meaning that almost all the mass of the distribution is concentrated in a small neighborhood around the mean, can be expressed in the Lie algebra [13], [24], and this concept is called a concentrated Gaussian distribution.

Let  $X \in G$  be a random variable following a concentrated Gaussian distribution with mean  $\mu$  and covariance  $P$  as

$$X = \mu \exp_G^\wedge(\epsilon), \quad X \sim \mathcal{G}(\mu, P), \quad (5)$$

where  $\epsilon \sim \mathcal{N}_{\mathbb{R}^p}(\mathbf{0}^p, P)$  is a zero-mean Gaussian distribution with covariance  $P \subset \mathbb{R}^{p \times p}$  defined in the Lie algebra, i.e., the Euclidean space  $\mathbb{R}^p$ . We can see from (5) that the mean value  $\mu$  is defined on  $G$ , while the associated uncertainty resides in  $\mathbb{R}^p$ . Roughly, this concept allows us to work with the covariance directly in  $\mathbb{R}^p$  and use Euclidean tools, almost as we would with a 'classical' Gaussian distribution [16].

#### D. Special orthogonal groups $SO(2)$ and $SO(3)$

The special orthogonal group  $SO(n)$  is the matrix group

$$SO(n) = \{X \in \mathbb{R}^{n \times n} \mid X^T X = I, \det(X) = 1\}. \quad (6)$$

For  $n = 2, 3$  this group defines rotations in 2D and 3D, respectively. The algebra  $\mathfrak{so}(n)$  comprises of  $n \times n$  skew-symmetric matrices. For Euclidean vectors  $x = \phi$  and  $x = [\phi_1 \ \phi_2 \ \phi_3]^T$ , the algebras  $\mathfrak{so}(2)$  and  $\mathfrak{so}(3)$  amount to

$$x_{SO(2)}^\wedge = \begin{bmatrix} 0 & -\phi \\ \phi & 0 \end{bmatrix}, \quad x_{SO(3)}^\wedge = \begin{bmatrix} 0 & -\phi_3 & \phi_2 \\ \phi_3 & 0 & -\phi_1 \\ -\phi_2 & \phi_1 & 0 \end{bmatrix}, \quad (7)$$

where  $(\cdot)_{SO(n)}^\wedge : \mathbb{R}^n \rightarrow \mathfrak{so}(n)$ , while its inverse,  $(\cdot)_{SO(n)}^\vee : \mathfrak{so}(n) \rightarrow \mathbb{R}^n$ , follows trivially from (7).

For  $SO(2)$ , the exponential map yields the classical 2D rotation matrix, while the logarithm evaluates to simple extraction of  $\phi$  into a skew-symmetric matrix form in (7). Since  $SO(2)$  is commutative, its adjoint representations are trivial:  $\text{Ad}_{SO(2)}$  is a unit map and  $\text{ad}_{SO(2)}$  is zero. The exponential for  $SO(3)$ , performing mapping  $\exp_{SO(3)} : \mathfrak{so}(3) \rightarrow SO(3)$ , is given as

$$\exp_{SO(3)}^\wedge(x) = \cos(|x|)I^3 + (1 - \cos(|x|))\frac{xx^T}{|x|^2} + \sin(|x|)\frac{x_{SO(3)}^\wedge}{|x|}. \quad (8)$$

The logarithm, performing mapping  $\log_{SO(3)} : SO(3) \rightarrow \mathfrak{so}(3)$ , is given as

$$\begin{aligned} \log_{SO(3)}(X) &= \frac{\theta}{2\sin(\theta)}(X - X^T) \\ \text{s.t. } 1 + 2\cos(\theta) &= \text{Tr}(X) \\ \begin{cases} \theta \neq 0 & -\pi < \theta < \pi \\ \theta = 0 & \log(X) = 0 \end{cases} \end{aligned} \quad (9)$$

The adjoints  $\text{Ad}_{SO(3)}$  and  $\text{ad}_{SO(3)}$  are respectively given as

$$\text{Ad}_{SO(3)}(X) = X \text{ and } \text{ad}_{SO(3)}(x) = x_{SO(3)}^\wedge. \quad (10)$$

In the sequel we present the new human motion estimation method based on the LG-EKF using IMU measurements.

### III. HUMAN MOTION ESTIMATION ON LIE GROUPS

Our goal is to estimate the pose of a kinematic chain represented via Lie groups (as described in section II-A), as well as its velocity and acceleration, using measurements from rigidly attached inertial measurement units at each link. To utilize LG-EKF for such state estimation, assuming a constant acceleration model (CA) [25] for each joint, we derive the necessary gyroscope and accelerometer measurement models and their Jacobians.

#### A. Motion prediction step

We assume that the motion model of the system can be described with the following equation [16]

$$X_{k+1} = f(X_k, n_k) = X_k \exp_G^\wedge(\hat{\Omega}_k + n_k), \quad (11)$$

where  $X_k \in G$  is the state of the system at time  $k$ ,  $G$  is a  $p$ -dimensional Lie group,  $n_k \sim \mathcal{N}_{\mathbb{R}^p}(\mathbf{0}^{p \times 1}, Q_k)$  is zero mean white Gaussian noise with covariance  $Q_k$ , and  $\hat{\Omega}_k = \Omega(X_k) : G \rightarrow \mathbb{R}^p$  is a non-linear  $\mathcal{C}^2$  function.

In our approach, similar to our previous work [19], we assume the human motion to follow a constant acceleration model and our state space  $G$  is then constructed to include the positional, velocity and acceleration components block-diagonally. Hence exponentials and logarithms will keep the state in the block diagonal arrangement as well. The motion model of a single joint  $i$  is given as

$$\hat{\Omega}_k^i = \begin{bmatrix} T\omega_k^i + \frac{T^2}{2}\alpha_k^i \\ T\alpha_k^i \\ 0 \end{bmatrix} \in \mathbb{R}^{3d_i}, \quad n_k = \begin{bmatrix} \frac{T^2}{2}n_k^i \\ Tn_k^i \\ n_k^i \end{bmatrix} \in \mathbb{R}^{3d_i} \quad (12)$$

where  $\omega_k^i$  and  $\alpha_k^i$  are the angular velocity and angular acceleration represented in the Lie algebra<sup>1</sup>. The term  $n_k^i$  represents the acceleration increment during the  $k$ -th sampling period [25],  $d_i$  represents the number of DoFs of the  $i$ -th joint, and  $T$  is the sampling period.

Assuming that the posterior distribution at step  $k$  follows the concentrated Gaussian distribution  $\mathcal{G}(\mu_k, P_k)$ , and following the LG-EKF prediction step [19], the resulting prediction can be approximated with a concentrated Gaussian distribution  $\mathcal{G}(\mu_{k+1|k}, P_{k+1|k})$ . The mean propagation of the LG-EKF is:

$$\mu_{k+1|k} = \mu_k \exp_G^\wedge(\hat{\Omega}_k), \quad (13)$$

while the covariance prediction is computed as

$$P_{k+1|k} = \mathcal{F}_k P_k \mathcal{F}_k^T + \Phi_G(\hat{\Omega}_k) Q_k \Phi_G(\hat{\Omega}_k)^T. \quad (14)$$

The operator  $\mathcal{F}_k$  can be seen as a matrix Lie group equivalent to the Jacobian of  $f(X_k, n_k)$ , and is calculated by

$$\begin{aligned} \mathcal{F}_k &= \text{Ad}_G \left( \exp_G^\wedge(-\hat{\Omega}_k) \right) + \Phi_G(\hat{\Omega}_k) \mathcal{L}_k \\ \mathcal{L}_k &= \frac{\partial}{\partial \epsilon} \Omega(\mu_k \exp_G^\wedge(\epsilon))|_{\epsilon=0}. \end{aligned} \quad (15)$$

The term  $\mathcal{L}_k$  represents the linearisation term where the argument of the motion model is the mean of the current state  $X_k$  with an incremental perturbation additively added in each of the  $p$  directions. Contrary to the conventional EKF, a linear additive process noise affects the system as a function of the current state of the system over the transformation  $\Phi_G(\hat{\Omega}_k) Q_k \Phi_G(\hat{\Omega}_k)^T$ , where  $\Phi_G$  appears due to the displacement of the tangential space during the prediction step, and is given by:

$$\Phi_G(v) = \sum_{i=0}^{\infty} \frac{(-1)^i}{(i+1)!} \text{ad}_G(v)^i, \quad v \in \mathbb{R}^p. \quad (16)$$

<sup>1</sup>Euclidean space  $\mathbb{R}^p, p \in \mathbb{N}$  is a matrix Lie group and in order to construct  $G$  we employ its matrix representation obtained by simple matrix embedding. The matrix representation of the Euclidean space is also a subgroup of  $SE(n)$  where a pure translation is employed [26].

### B. Measurement update step

We next derive the update step by employing gyro and accelerometer measurements of IMUs attached to a human body. The discrete measurement model on the matrix Lie group is modelled as:

$$Z_{k+1} = h(X_{k+1}) \exp_{G'}^{\wedge}(m_{k+1}), \quad (17)$$

where  $Z_{k+1} \in G'$ ,  $h : G \rightarrow G'$  is a  $\mathcal{C}^1$  function,  $G'$  is a  $p'$ -dimensional Lie group and  $m_{k+1} \sim \mathcal{N}_{\mathbb{R}^q}(\mathbf{0}^{q \times 1}, R_{k+1})$  is zero-mean white Gaussian noise with covariance  $R_{k+1}$ . The update step of the filter strongly resembles the standard EKF update procedure, relying on the Kalman gain  $K_{k+1}$  and innovation vector  $\nu_{k+1}$  calculated as:

$$\begin{aligned} K_{k+1} &= P_{k+1|k} \mathcal{H}_{k+1}^T (\mathcal{H}_{k+1} P_{k+1|k} \mathcal{H}_{k+1}^T + R_{k+1})^{-1} \\ \nu_{k+1} &= K_{k+1} \log_{G'}^{\vee} (h(\mu_{k+1|k})^{-1} Z_{k+1}). \end{aligned} \quad (18)$$

The matrix  $\mathcal{H}_{k+1}$  can be seen as the matrix Lie group equivalent of the Jacobian of  $h(X_{k+1})$ , and is given as:

$$\mathcal{H}_{k+1} = \frac{\partial}{\partial \epsilon} \log_{G'}^{\vee} (h(\mu_{k+1|k})^{-1} h(\mu_{k+1|k}^{\epsilon})) \Big|_{\epsilon=0},$$

where  $h(\mu_{k+1|k}^{\epsilon}) = h(\mu_{k+1|k} \exp_G^{\wedge}(\epsilon))$ , describes the variation of measurements for an infinitesimal motion  $\epsilon$ . We now evaluate the matrix  $\mathcal{H}_{k+1}$  based on gyro and accelerometer measurements.

### C. Gyro update

The measurement function of the gyro measurement is:

$$h(X_{k+1|k}) = \sum_{i=1}^n \mathcal{K}_i^{s,R} \omega_{k+1|k}^i, \quad (19)$$

where  $n$  is the number of joints preceding the gyro sensor  $s$ . The term  $\mathcal{K}_i^{s,R} = \mathcal{K}_i^{s,R}(X_{k+1|k})$  is the rotational component of the forward kinematics between the  $i$ -th joint and the gyro sensor  $s$ , thus affecting its measurement [27]. The gyro measurements are affected by position (through kinematics) and velocity, hence the corresponding parts of  $\mathcal{H}_{k+1}$  matrix need to be evaluated.

By applying partial derivatives and evaluating the multivariate limits similarly to [28], the part of  $\mathcal{H}_{k+1}$  relating the gyro measurement to the orientation of the  $l$ -th joint  $\mathcal{H}_{k+1}^{\theta,l}$  is:

$$\mathcal{H}_{k+1}^{\theta,l,r} = \sum_{i=1}^{l-1} \mathcal{K}_i^{s,R} E^{l,r} \theta_{k+1|k}^{l-1} \mathcal{K}_i^{l,R} \omega_{k+1|k}^i, \quad (20)$$

where  $\mathcal{K}_i^{i,R}$  represents the rotation between the  $i$ -th and  $l$ -th joint,  $\theta_{k+1|k}^l$  is the position of the  $l$ -th joint, while  $E^{l,r}$  represents the  $r$ -th generator of a Lie group representing the  $l$ -th joint [24]. Each of the generators represents an infinitesimal motion in one of the directions of a Lie group.

The part of  $\mathcal{H}_{k+1}$  relating the gyro measurement to the velocity of the  $l$ -th joint  $\mathcal{H}_{k+1}^{\omega,l}$  is given as:

$$\mathcal{H}_{k+1}^{\omega,l} = \mathcal{K}_l^{s,R}. \quad (21)$$

Since gyro measurement (19) is not a function of the joint accelerations, the part of the  $\mathcal{H}_{k+1}$  matrix relating gyro

measurements to  $l$ -th joint acceleration components is filled with zero values;  $\mathcal{H}_{k+1}^{\alpha,l} = 0$ .

### D. Accelerometer update

The measurement function corresponding to the accelerometer measurement is:

$$h(X_{k+1|k}) = \overbrace{\mathcal{K}_0^{s,R} \ddot{p}_{k+1|k}}^{\text{point acceleration}} + \overbrace{\mathcal{K}_0^{s,R} g}^{\text{gravity component}}, \quad (22)$$

where the first term emerges due to dynamics of a body, while the second term arises due to gravity. The superscript  $R$  denotes that only the rotation part is embedded into an SE(3) member, while the translation part is set to 0. The term  $\ddot{p}_{k+1|k}$  represents an acceleration of the sensor  $s$  represented in the base frame and given in homogeneous coordinates, while  $g$  is the gravity vector in homogeneous coordinates. In order to evaluate  $\ddot{p}_{k+1|k}$ , we start from defining the IMU position as:

$$p_{k+1|k} = \mathcal{K}_s^0 \mathcal{O} \quad (23)$$

where  $\mathcal{O} = [0 \ 0 \ 0 \ 1]^T$  is the origin represented in homogeneous coordinates. The forward kinematics are:

$$\mathcal{K}_s^0 = T_1^0 \theta_{k+1|k}^1 T_2^1 \theta_{k+1|k}^2 \cdots T_n^{n-1} \theta_{k+1|k}^n \quad (24)$$

Each part of the forward kinematics  $\mathcal{K}_i^{i-1} = T_i^{i-1} \theta_{k+1|k}^i$  consists of the constant transformation  $T_i^{i-1}$  and the position of the  $i$ -th joint  $\theta_{k+1|k}^i$ . In order to sequentially apply a matrix multiplication inducing each joint state, we describe joints as  $4 \times 4$  transformation matrices (in terms of Lie groups denoted as special euclidean group SE(3)). We now evaluate the first two derivatives of sensor position  $p_{k+1|k}$ . The velocity of the point  $p_{k+1|k}$  evaluates to:

$$\dot{p}_{k+1|k} = \sum_{i=1}^n \left( \mathcal{K}_i^0 S_{k+1|k}^{i,\omega} \mathcal{K}_s^i \right) \mathcal{O}, \quad (25)$$

where the summation iterates over  $n$  joints affecting sensor  $s$ , while the term  $S_{k+1|k}^{i,\omega}$  is given as:

$$S_{k+1|k}^{i,\omega} = \sum_{r=1}^{d_i} \left( \omega_{k+1|k}^{i,r} E^{i,r} \right), \quad (26)$$

which is a function of the number of degrees of freedom  $d_i$  of the  $i$ -th joint, and the superscript  $\omega$  denotes that the velocity components are summed up. The acceleration of the point  $p_{k+1|k}$  evaluates to:

$$\begin{aligned} \ddot{p}_{k+1|k} &= \overbrace{\sum_{i=1}^n \left( \sum_{j=1}^i \left( \mathcal{K}_j^0 S_{k+1|k}^{j,\omega} \mathcal{K}_i^j \right) S_{k+1|k}^{i,\omega} \mathcal{K}_s^i \right) \mathcal{O}}^{\text{centripetal force component I}} + \\ &\quad \overbrace{\sum_{i=1}^n \left( \mathcal{K}_i^0 S_{k+1|k}^{i,\omega} \sum_{j=i+1}^n \left( \mathcal{K}_j^i S_{k+1|k}^{j,\omega} \mathcal{K}_s^j \right) \right) \mathcal{O}}^{\text{centripetal force component II}} + \\ &\quad \underbrace{\sum_{i=1}^n \left( \mathcal{K}_i^0 S_{k+1|k}^{i,\alpha} \mathcal{K}_s^i \right) \mathcal{O}}_{\text{joint acceleration component}}. \end{aligned} \quad (27)$$

The acceleration  $\ddot{p}_{k+1|k}$  consists of two components – the centripetal force component and joint acceleration component, which we emphasize in (27).

We now proceed to linearize and evaluate the part of  $\mathcal{H}_{k+1}$  corresponding to the accelerometer measurement and joint  $l$ :

$$\begin{bmatrix} \mathcal{H}_{k+1}^l \\ 1 \end{bmatrix} = \frac{\partial \mathcal{K}_0^{s,R}}{\partial X_{k+1|k}^l} (\ddot{p}_{k+1|k} + g) + \mathcal{K}_0^{s,R} \frac{\partial \ddot{p}_{k+1|k}}{\partial X_{k+1|k}^l}. \quad (28)$$

In order to evaluate (28) we compute partial derivatives of  $\mathcal{K}_0^{s,R}$  and  $\ddot{p}_{k+1|k}$  with respect to position, velocity, and acceleration of  $X_{k+1|k}^l$ . The detailed derivation is provided in the supplementary material [29].

Finally, having evaluated  $\mathcal{H}_{k+1}$ , the measurement update step is calculated as [16]:

$$\begin{aligned} \mu_{k+1} &= \mu_{k+1|k} \exp_{\mathcal{G}}^{\wedge}(\nu_{k+1}) \\ P_{k+1} &= \Phi_{\mathcal{G}}(\nu_{k+1}) (I - K_{k+1} \mathcal{H}_{k+1}) P_{k+1|k} \Phi_{\mathcal{G}}(\nu_{k+1})^T. \end{aligned} \quad (29)$$

#### IV. EULER ANGLE BASED APPROACH

The proposed approach is compared to a conventional EKF applied to a standard kinematic model defined with revolute and prismatic joints [30]. Three perpendicular revolute joints (Euler angles) can be used to model human spherical joints such as the shoulder and the hip. The state of the EKF is defined as the position  $q$ , velocity  $\dot{q}$ , and acceleration  $\ddot{q}$  of the joints. Just as in the LG-EKF formulation we assume constant acceleration of each joint.

It is also possible to model the kinematics using quaternions to represent the joint state. Since rotations are represented by unit quaternions, one approach when using EKF is to normalize the state estimate after each iteration [8]. This normalization, while correctly propagating the error covariance, no longer optimally performs the state update step [31]. Similar to rotation matrices quaternions have a tangent space and thus, it is possible to apply LG-EKF to a quaternion based state representation using the SU(2) group, in this case we expect similar results to our formulation.

#### V. VALIDATION RESULTS

We validate the proposed approach both in simulation and with real human motion. First, in simulation, we demonstrate the benefits of LG-EKF over EKF when using IMU measurements during highly dynamical movements whose motion is better described on the group and show that unlike EKF, LG-EKF is not affected by gimbal lock. Next, we evaluate the performance of LG-EKF and EKF on real IMU data of a dynamic figure eight arm movement sequence.

##### A. Simulation Validation

1) *Dynamic Motion*: To test the properties of LG-EKF, we simulate a human shown in Fig. 1, modeled with (1). Two IMUs are attached to the humerus and radius at offsets of  $[0.1 \ 0.1 \ 0.3]^T$ , and  $[0.1 \ 0.1 \ 0.4]^T$  respectively.

It is possible to generate Brownian motion either on the group or on Euler angles to exactly match the constant acceleration with zero mean Gaussian noise assumption of LG-EKF or EKF. Since large constant acceleration in one

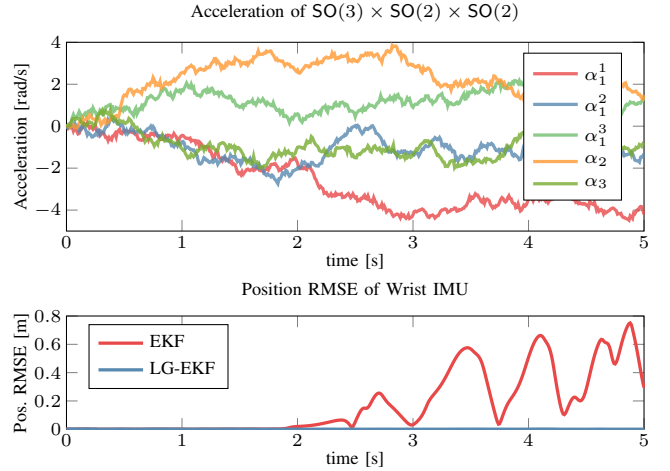


Fig. 2. Performance of EKF and LG-EKF based on Brownian motion on Lie Algebra. Since LG-EKF has an accurate motion model it correctly tracks the arm movement. Once the angular accelerations on the Lie Algebra become large, the constant Euler angle acceleration model of EKF does not provide a good state prediction and EKF cannot maintain an accurate estimate.  $\alpha_1$  denotes SO(3) with 3 dofs, while  $\alpha_2$  and  $\alpha_3$  correspond to SO(2) joints with a single dof.

representation implies a quickly changing acceleration in the other, we can expect the filter with the correct motion model to significantly outperform the other in high acceleration regions. Figure 2 shows the Brownian motion generated on the group representation of the arm and the root mean squared error (RMSE) in position estimation of the wrist IMU for EKF and LG-EKF. It is clear that during high constant accelerations on the group, Euler angle based EKF cannot accurately track the motion.

However, it is unlikely that human motion will satisfy the constant acceleration assumption. Thus, in order to compare EKF and LG-EKF without being biased to a specific motion representation we generate a dynamic trajectory in task space and utilize inverse kinematics to recover joint angles of the Euler angle model. Next we numerically differentiate the trajectory to retrieve joint velocities and accelerations and generate the IMU measurements using forward kinematics. The task space trajectory is created by cubic splining of points in the reachable workspace generated from a univariate distribution. This setup creates a highly dynamic motion as can be seen from the positions of the two IMUs shown in Fig. 3. Simulated IMUs are sampled at 100 Hz and zero mean Gaussian noise with standard deviations of  $0.01 \frac{\text{rad}}{\text{s}}$  and  $0.1 \frac{\text{m}}{\text{s}^2}$  is added to the gyroscope and accelerometer measurements respectively. For both filters the initial covariances were set to a diagonal matrix of a  $10^{-3}$  denoting accurate knowledge of the initial state. For the process noise, for each triplet  $[\phi \ \omega \ \alpha]$  or  $[q \ \dot{q} \ \ddot{q}]$ , noise of standard deviation  $\eta$  is injected into  $\alpha$  and is propagated to  $\omega$  and  $\phi$  by integration. Thus, for each triplet the process noise covariance is  $GG^T$  where  $G = [\frac{T^2}{2} \ T \ 1]\eta$ . For the dynamic motion simulation  $\eta$  was set to  $10 \frac{\text{rad}}{\text{s}^2}$  per iteration. The observation noise was set to the true sensor noise values.

To compare the estimate with the ground truth, we use

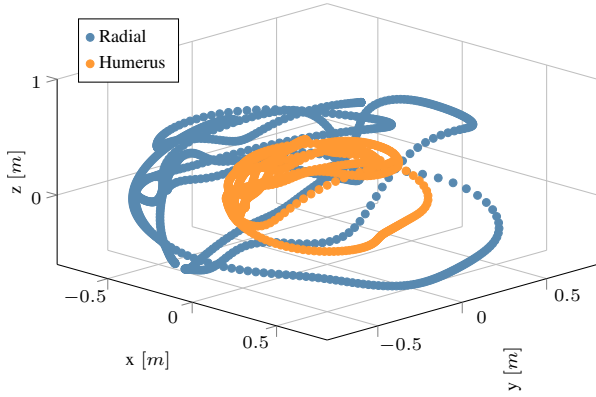


Fig. 3. 10 Second simulation trajectory of the IMUs attached to the humerus and radial undergoing the generated highly dynamic motion.

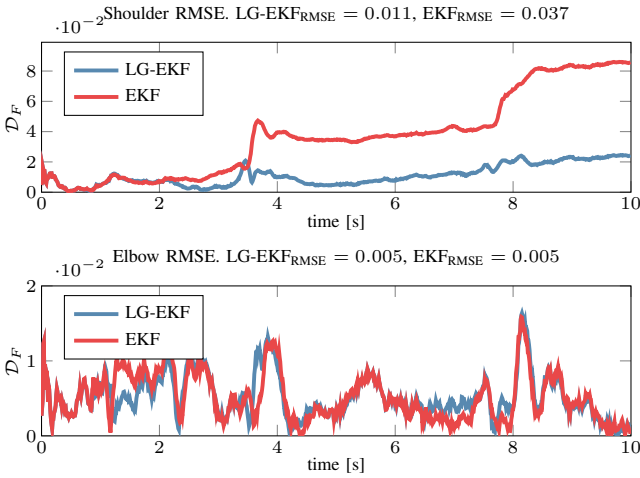


Fig. 4. Error between the actual and estimated rotations at the shoulder and elbow joint for LG-EKF and EKF during task space generated dynamic motion. Estimation of shoulder rotation is significantly improved using the SO(3) model.

the deviation from the identity matrix as the distance metric [32]:

$$\mathcal{D}_F = \|I - R_e^T R_{gt}\|_F \quad (30)$$

where  $R_e$  and  $R_{gt}$  are the estimated and ground truth rotation matrices of each joint and  $\|\cdot\|_F$  denotes the Frobenius norm.

Figure 4 shows the comparison between the LG-EKF and EKF using this distance metric for the shoulder and elbow joints. The LG-EKF significantly outperforms the EKF filter, which is due to LG-EKF's ability to handle gimbal lock as explained in the next section.

2) *Gimbal Lock*: Next we investigate the impact of gimbal lock on the proposed approach. Any set of Euler angles will lose a degree of freedom when two of the rotation axes align [33], implying that in that configuration the rotation about the locked axis cannot be correctly estimated by EKF. Typically the order of the joint axes is carefully selected to try and avoid the lock, however in human motion estimation, gimbal lock often takes place at the shoulder joint due to its high manoeuvrability. Unlike the Euler angle formulation, an

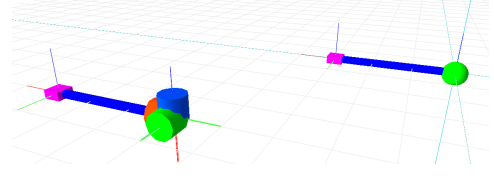


Fig. 5. Simulation model used for gimbal lock validation.

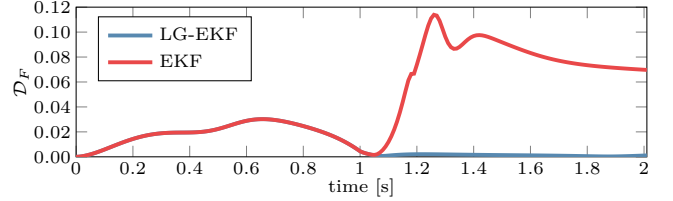


Fig. 6. LG-EKF and EKF estimation during gimbal lock. Both filters accurately estimate the rotation about the  $y$  axis until the system gets close to the gimbal lock, which happens at 1 second. After the rotation about  $y$  the Euler angle model is in gimbal lock and thus EKF cannot accurately track the orientation until the lock is escaped at 1.5 seconds. Once Euler angles escape the gimbal lock, EKF can regain an accurate estimate of the roll and pitch orientation using the accelerometer's gravity measurement. However, any error in yaw during gimbal lock accumulates. LG-EKF estimation is unaffected by gimbal lock.

SO(3) representation of the spherical joint does not suffer from gimbal lock and thus LG-EKF will accurately estimate any rotation.

To demonstrate the benefits of LG-EKF over EKF during gimbal lock we simulate a single spherical joint at the origin with a single IMU attached at an offset of 0.1 meters in  $x$ . The simulated model is shown in Fig. 5. A quintic polynomial is used to generate a smooth trajectory, sampling at 100 Hz. First, the model experiences a 1 second rotation about the world  $y$  axis with initial position 0 rad and final positions  $\frac{\pi}{2}$  rad and zero initial and final velocity and acceleration. In the Euler angle model this motion aligns the first and third revolute joint axes putting it into a singularity and removing a degree of freedom (gimbal lock). Next, the model experiences the same 1 s rotation in the now locked world  $z$  axis. In order to focus only on the gimbal lock problem, no noise was added to the IMU measurements. Measurement noise, process noise, and initial covariances were set as described in Sec. V-A.1. Figure 6 shows the distance metric described in (30).

When Euler angles enter gimbal lock, the Euler angle based Jacobian is singular and thus the linearized system is no longer observable. In this case EKF cannot accurately estimate the states. By plotting the condition number of the observability matrix  $\mathcal{O}_b = [\mathcal{H}_k \mathcal{H}_k \mathcal{F}_k \dots]^T$  of the linearized system we can visualize the ability of the filters to handle gimbal lock (Fig. 7).

Furthermore we show that the Lie group motion model is superior for process noise representation over the Euler angle motion model. Consider a single SO(3) joint with an IMU attached at some offset. Independent of the initial SO(3) state, addition of zero mean, Gaussian process noise to the state results in a consistent distribution of the end effector



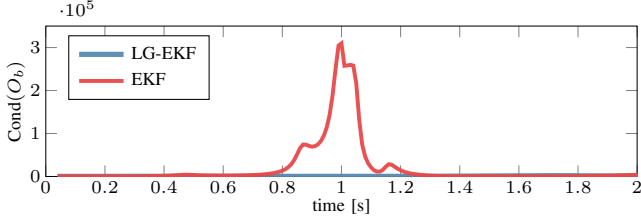


Fig. 7. Condition number of the observability matrix of the linearized system at each iteration during gimbal lock. The condition number of EKF increases rapidly from 0.75 seconds when the Euler angles are still  $12^\circ$  away from gimbal lock. In this region EKF may incorrectly estimate large state increments. LG-EKF retains observability during gimbal lock.

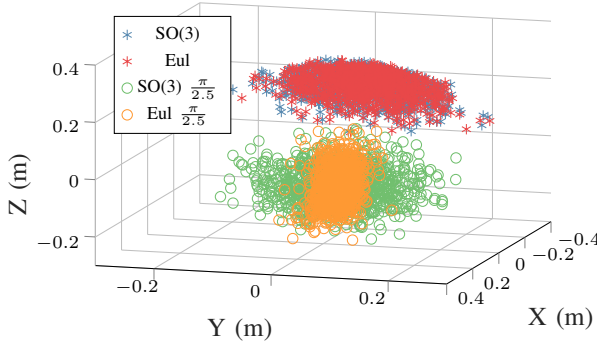


Fig. 8. An IMU is attached to an SO(3) joint with an offset of (0.1,0.1,0.3) in (x,y,z) axes. Zero mean Gaussian noise with standard deviation of 0.2 is added to the identity state and when the configuration is rotated by  $\frac{\pi}{2.5}$  radians. The Lie group representation (red and green) retains the distribution properties through the rotation about the y axis. In the Euler angle representation the distribution is significantly altered when the axes are no longer perpendicular.

position. With the Euler Angle model, adding the same process noise results in end effector position distribution that is state dependent, as illustrated in Fig. 8. Thus near gimbal lock Euler EKF requires higher process noise to capture the variability in a highly maneuverable 3D joint such as the shoulder while LG-EKF process noise will remain constant and lower for the entire state space. Thus it should be easier to tune LG-EKF for better performance over the entire state space.

### B. Real-world experiment

We validate the proposed approach by comparing the distance between actual and estimated wrist and elbow positions during a dynamic figure eight human arm motion collected in a motion capture studio. The motion capture studio utilizes 8 Motion Analysis cameras capturing at 200Hz. Our IMUs are based on the MPU9250 sensor and were set to sample at 100Hz, they were calibrated [34] prior to data collection. The kinematic model of the participant was generated based on motion capture markers placed on the shoulder and medial and lateral sides of the elbow and wrist. Three motion capture markers were placed on each IMU to compute their offset and rotation from the humerus and radius.

For the best performance of both filters it is imperative to tune the initial covariance, observation noise, and process noise parameters. In our experiment the initial pose of the

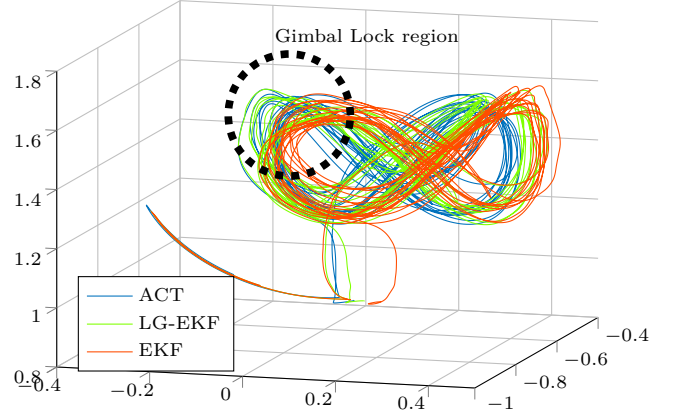


Fig. 9. Actual and estimated 3d wrist position.

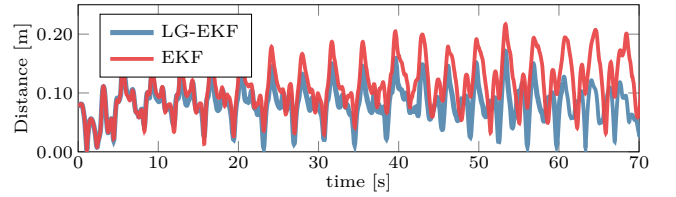


Fig. 10. Distance between the actual and estimated wrist positions. With each pass near gimbal lock, the Euler angle model EKF accumulates error about world Z axis.

participant is known and thus we set the initial covariance to  $10^{-3}$  along the diagonal. The observation noise parameters are set to match those of the IMUs based on 30 seconds of static data. We assumed discrete constant acceleration process noise [25] of magnitude  $\eta$  as described in section V-A.1 and used the Matlab optimization toolbox to find the optimal process noise parameters for EKF and LG-EKF such that the distance between the estimated and actual elbow and wrist positions is minimized over 3 repetitions of the figure eight motion. The optimal process noise parameters were found to be  $\eta_{\text{EKF}} = 389.1$  and  $\eta_{\text{LG-EKF}} = 264.8$  for EKF and LG-EKF respectively. The significantly lower optimal process noise for the Lie group motion model shows that human motion is better estimated on the group.

Figure 9 shows the estimated and actual wrist positions for both EKF and LG-EKF. Figure 10 plots the distance between actual and estimated wrist positions. Both filters begin with equally accurate estimation. With each pass through the corner of the figure 9 near gimbal lock, EKF accumulates error about the world Z axis. Since LG-EKF is not affected by gimbal lock its performance stays consistent throughout the entire motion. Table I shows the RMSE and standard deviation for elbow and wrist position estimation.

## VI. CONCLUSION

We proposed a novel algorithm for human motion estimation based on body worn IMU sensors. Based on the kinematics of the human body, we formed the state as a Cartesian product of Lie groups. In order to stochastically infer the state of such a Lie group, we employed the LG-EKF, thus

TABLE I

ROOT MEAN SQUARED ERROR OF ESTIMATED AND ACTUAL ELBOW AND WRIST POSITIONS FOR THE TWO FILTERS. THE PROPOSED LG-EKF IMPROVES THE POSITION ESTIMATE BY 30% OVER EKF.

	Elbow RMSE [cm]	Wrist RMSE [cm]
LG-EKF	<b>5.2 ± 2.6</b>	<b>6.9 ± 2.7</b>
EKF	7.4 ± 3.6	9.9 ± 3.8

explicitly accounting for the non-Euclidean geometry of the state space. A constant acceleration motion model on the group was developed for the LG-EKF prediction step and the Jacobian of the IMU (gyroscope and accelerometer measurements), was derived for the update step. The performance of the proposed method was evaluated in both simulation and real-world data, comparing it with the EKF based on Euler angles. The proposed algorithm can estimate human motion with lower end effector position RMSE than the EKF and is not affected by gimbal lock. Future work will include full body pose estimation based on wearable IMU sensors and investigating using SE(3) joint types that can represent transformation matrices to accommodate for translations in 3D space and handle the free flyer problem.

## REFERENCES

- [1] D. Kulić, G. Venture, K. Yamane, E. Demircan, I. Mizuuchi, and K. Mombaur, "Anthropomorphic movement analysis and synthesis: A survey of methods and applications," *IEEE Transactions on Robotics*, vol. 32, no. 4, pp. 776–795, 2016.
- [2] V. Bonnet, C. Mazzà, J. McCamley, and A. Cappozzo, "Use of weighted fourier linear combiner filters to estimate lower trunk 3d orientation from gyroscope sensors data," *Journal of neuroengineering and rehabilitation*, vol. 10, no. 1, p. 29, 2013.
- [3] X. Yun and E. R. Bachmann, "Design, implementation, and experimental results of a quaternion-based kalman filter for human body motion tracking," *IEEE transactions on Robotics*, vol. 22, no. 6, pp. 1216–1227, 2006.
- [4] G. Ligorio and A. M. Sabatini, "A novel kalman filter for human motion tracking with an inertial-based dynamic inclinometer," *IEEE Transactions on Biomedical Engineering*, vol. 62, no. 8, pp. 2033–2043, 2015.
- [5] H. Zhou, T. Stone, H. Hu, and N. Harris, "Use of multiple wearable inertial sensors in upper limb motion tracking," *Medical engineering & physics*, vol. 30, no. 1, pp. 123–133, 2008.
- [6] J. F. Lin and D. Kulić, "Human pose recovery using wireless inertial measurement units," *Physiological measurement*, no. 12, p. 2099, 2012.
- [7] M. El-Gohary and J. McNames, "Shoulder and elbow joint angle tracking with inertial sensors," *Biomedical Engineering, IEEE Transactions on*, vol. 59, no. 9, pp. 2635–2641, 2012.
- [8] A. Szczesna and P. Prusowski, "Model-based extended quaternion kalman filter to inertial orientation tracking of arbitrary kinematic chains," *SpringerPlus*, vol. 5, no. 1, p. 1965, 2016.
- [9] V. Joukov, B. Vincent, M. Karg, V. Gentiane, and D. Kulic, "Rhythmic ekf for pose estimation during gait," in *Humanoid Robots, 2016 IEEE-RAS*. IEEE, 2015.
- [10] J. Česić, V. Joukov, I. Petrović, and D. Kulić, "Full body human motion estimation on lie groups using 3d marker position measurements," in *Humanoid Robots, 2016 IEEE-RAS*. IEEE, 2016, pp. 826–833.
- [11] Y. Wang and G. S. Chirikjian, "Error propagation on the Euclidean group with applications to manipulator kinematics," *IEEE Transactions on Robotics*, vol. 22, no. 4, pp. 591–602, 2006.
- [12] A. Long, K. Wolfe, M. Mashner, and G. S. Chirikjian, "The Banana Distribution is Gaussian: A Localization Study with Exponential Coordinates," in *Robotics, Science and Systems*, 2012, p. 8.
- [13] T. D. Barfoot and P. T. Furgale, "Associating uncertainty with three-dimensional poses for use in estimation problems," *IEEE Transactions on Robotics*, vol. 30, no. 3, pp. 679–693, 2014.
- [14] C. Forster, L. Carlone, F. Dellaert, and D. Scaramuzza, "IMU Preintegration on Manifold for Efficient Visual-Inertial Maximum-a-Posteriori Estimation," in *Robotics: Science and Systems*, 2015, p. 9.
- [15] G. Bourmaud, R. Mégret, A. Giremus, and Y. Berthoumieu, "Discrete Extended Kalman Filter on Lie Groups," in *European Signal Processing Conference (EUSIPCO)*, 2013, pp. 1–5.
- [16] G. Bourmaud, R. Mégret, M. Arnaudon, and A. Giremus, "Continuous-Discrete Extended Kalman Filter on Matrix Lie Groups Using Concentrated Gaussian Distributions," *Journal of Mathematical Imaging and Vision*, vol. 51, no. 1, pp. 209–228, 2015.
- [17] G. Bourmaud, R. Mégret, A. Giremus, and Y. Berthoumieu, "From Intrinsic Optimization to Iterated Extended Kalman Filtering on Lie Groups," *Journal of Mathematical Imaging and Vision*, vol. 55, no. 3, pp. 284–303, 2016.
- [18] Y. Bar-Shalom, X. R. Li, and T. Kirubarajan, *Estimation with Applications To Tracking and Navigation*. John Wiley & Sons, Inc., 2001, vol. 9.
- [19] J. Česić, I. Marković, and I. Petrović, "Moving object tracking employing rigid body motion on matrix Lie groups," in *19th International Conference on Information Fusion (FUSION), Special Session on Directional Estimation*, 2016, p. 7.
- [20] J. Stillwell, *Naive Lie Theory*. Springer, 2008.
- [21] J. M. Selig, "Lie Groups and Lie Algebras in Robotics," in *Computational Noncommutative Algebra and Applications*, 2005, pp. 101–125.
- [22] W. Park, Y. Wang, and G. S. Chirikjian, "The Path-of-Probability Algorithm for Steering and Feedback Control of Flexible Needles," *The International Journal of Robotics Research*, vol. 29, no. 7, pp. 813–830, 2010.
- [23] K. Tapp, *Matrix Groups for Undergraduates*. American Mathematical Society, 2005.
- [24] Y. Wang and G. S. Chirikjian, "Nonparametric Second-Order Theory of Error Propagation on Motion Groups," *The International Journal of Robotics Research*, vol. 27, no. 11, pp. 1258–1273, 2008.
- [25] Y. Bar-Shalom, T. Kirubarajan, and X.-R. Li, *Estimation with Applications to Tracking and Navigation*. John Wiley & Sons, Inc., 2002.
- [26] G. S. Chirikjian, *Stochastic Models, Information Theory, and Lie Groups, Volume 2: Analytic Methods and Modern Applications*. Springer, 2012.
- [27] M. W. Spong, S. Hutchinson, and M. Vidyasagar, *Robot Modeling and Control*. John Wiley & Sons, Inc., 2006.
- [28] J. Česić, I. Marković, I. Cvišić, and I. Petrović, "Radar and stereo vision fusion for multitarget tracking on the special Euclidean group," *Robotics and Autonomous Systems*, 2016.
- [29] V. Joukov, J. Česić, K. Westermann, I. Marković, D. Kulić, and I. Petrović, "Supplementary material to Human motion estimation on Lie groups using IMU measurements," 2017. [Online]. Available: <http://cloudslam.fer.hr/images/50018512/mainSupplementary.pdf>
- [30] V. Joukov, M. Karg, and D. Kulić, "Online tracking of the lower body joint angles using imus for gait rehabilitation," in *IEEE Engineering in Medicine and Biology Conference*, Aug 2014, pp. 2310–2313.
- [31] I. Bar-Itzhack and Y. Oshman, "Attitude determination from vector observations: Quaternion estimation," *IEEE Transactions on Aerospace and Electronic Systems*, no. 1, pp. 128–136, 1985.
- [32] D. Q. Huynh, "Metrics for 3d rotations: Comparison and analysis," *Journal of Mathematical Imaging and Vision*, vol. 35, no. 2, pp. 155–164, 2009.
- [33] F. S. Grassia, "Practical parameterization of rotations using the exponential map," *Journal of graphics tools*, vol. 3, no. 3, pp. 29–48, 1998.
- [34] D. Tedaldi, A. Pretto, and E. Menegatti, "A robust and easy to implement method for imu calibration without external equipments," in *ICRA*. IEEE, 2014, pp. 3042–3049.



## PUBLICATION 5 - SUPPLEMENTARY MATERIAL

V. Joukov, J. Ćesić, K. Westermann, I. Marković, D. Kulić and I. Petrović. Supplementary material to Human motion estimation on Lie groups using IMU measurements. *IEEE/RSJ International Conference on Intelligent Robots and Systems (IROS)*. Vancouver, Canada, 1965–1972, 2017.

# Supplementary material to

## Human motion estimation on Lie groups using IMU measurements

Vladimir Joukov\*, Josip Ćesić<sup>‡</sup>, Kevin Westermann\*, Ivan Marković<sup>‡</sup>, Dana Kulić\* and Ivan Petrović<sup>‡</sup>

### DERIVATION OF $\mathcal{H}_{k+1}$ GIVEN ACCELEROMETER MEASUREMENTS

The full state of the system  $X_k$  is of the form

$$\begin{aligned} X_k &= \text{blkdiag}\{\theta_k, \omega_k, \alpha_k\}, \\ \theta_k &= \text{blkdiag}\{\theta_k^1, \dots, \theta_k^m\}, \\ \omega_k &= \text{blkdiag}\{\omega_k^1, \dots, \omega_k^m\}, \\ \alpha_k &= \text{blkdiag}\{\alpha_k^1, \dots, \alpha_k^m\}, \end{aligned}$$

where subscript  $k$  denotes time instant,  $\theta_k^i$  is position of the  $i$ -th joint,  $\omega_k^i$  is velocity of the  $i$ -th joint,  $\alpha_k^i$  is acceleration of the  $i$ -th joint, and  $m$  is the number of joints of a body. Measurement Jacobian  $\mathcal{H}_{k+1}$  relating the accelerometer measurement and joint  $l$  is given as

$$\begin{bmatrix} \mathcal{H}_{k+1}^l \\ 1 \end{bmatrix} = \frac{\partial \mathcal{K}_0^{s,R}}{\partial X_{k+1|k}^l} (\ddot{p}_{k+1|k} + g) + \mathcal{K}_0^{s,R} \frac{\partial \ddot{p}_{k+1|k}}{\partial X_{k+1|k}^l}, \quad (1)$$

where  $\mathcal{K}_j^{i,R}$  stands for the rotational component of the forward kinematics between the  $i$ -th and  $j$ -th joints (alternatively 0 represents origin, and  $s$  denotes sensor),  $\ddot{p}_{k+1|k}$  represents an acceleration of the sensor  $s$  represented in the base frame and given in homogeneous coordinates, while  $g$  is the gravity vector in homogeneous coordinates. The subscript  $k+1|k$  denotes prediction at time instant  $k+1$  given the measurement up to and including time instant  $k$ . In order to evaluate (1) we need to compute partial derivatives of  $\mathcal{K}_0^{s,R}$  and  $\ddot{p}_{k+1|k}$  with respect to position, velocity, and acceleration of the full system state for joint  $l$ , i.e.,  $X_{k+1|k}^l$ .

#### A. Positional part

Here we consider the evaluation of  $\mathcal{H}_{k+1}^l$  with respect to position  $\theta_{k+1|k}^l$ . We start by evaluating the partial derivative of forward kinematics  $\mathcal{K}_0^{s,R}$  with respect to the positional variable  $\theta_{k+1|k}^{l,r}$ , where  $r$  relates to the  $r$ -th generator,  $r = 1, \dots, d_l$ , with  $d_l$  being the number of degrees of freedom of joint  $l$ . This evaluates to

$$\frac{\partial \mathcal{K}_0^{s,R}}{\partial \theta_{k+1|k}^{l,r}} = \mathcal{K}_0^{l,R} \theta_{k+1|k}^{l,r} E^r \mathcal{K}_l^{s,R}, \quad (2)$$

where  $E^{l,r}$  represents the  $r$ -th generator of a Lie group representing the  $l$ -th joint. The evaluation of the partial derivative of acceleration  $\ddot{p}_{k+1|k}$  with respect to the positional variable  $\theta_{k+1|k}^{l,r}$  evaluates to

$$\begin{aligned} \frac{\partial \ddot{p}_{k+1|k}}{\partial \theta_{k+1|k}^{l,r}} &= \sum_{i=1}^n \left( \sum_{j=1}^i \left\{ \begin{aligned} &\mathcal{K}_l^0 E^{l,r} \mathcal{K}_j^l S_{k+1|k}^{j,\omega} \mathcal{K}_i^j S_{k+1|k}^{i,\omega} \mathcal{K}_s^i, & l \leq j \\ &\mathcal{K}_j^0 S_{k+1|k}^{j,\omega} \mathcal{K}_l^j E^{l,r} \mathcal{K}_i^l S_{k+1|k}^{i,\omega} \mathcal{K}_s^i, & j < l \leq i \\ &\mathcal{K}_j^0 S_{k+1|k}^{j,\omega} \mathcal{K}_i^j S_{k+1|k}^{i,\omega} \mathcal{K}_l^l E^{l,r} \mathcal{K}_s^l, & i < l \end{aligned} \right\} \right) \mathcal{O}_+ \\ &\quad \sum_{i=1}^n \left( \sum_{j=i+1}^n \left\{ \begin{aligned} &\mathcal{K}_l^0 E^{l,r} \mathcal{K}_i^l S_{k+1|k}^{i,\omega} \mathcal{K}_j^j S_{k+1|k}^{j,\omega} \mathcal{K}_s^j, & l \leq i \\ &\mathcal{K}_i^0 S_{k+1|k}^{i,\omega} \mathcal{K}_l^l E^{l,r} \mathcal{K}_j^j S_{k+1|k}^{j,\omega} \mathcal{K}_s^j, & i < l \leq j \\ &\mathcal{K}_i^0 S_{k+1|k}^{i,\omega} \mathcal{K}_j^j S_{k+1|k}^{j,\omega} \mathcal{K}_l^l E^{l,r} \mathcal{K}_s^l, & j < l \end{aligned} \right\} \right) \mathcal{O}_+ \\ &\quad \sum_{i=1}^n \left\{ \begin{aligned} &\mathcal{K}_l^0 E^{l,r} \mathcal{K}_i^l S_{k+1|k}^{i,\alpha} \mathcal{K}_s^i, & l \leq i \\ &\mathcal{K}_i^0 S_{k+1|k}^{i,\alpha} \mathcal{K}_l^l E^{l,r} \mathcal{K}_s^l, & i < l \end{aligned} \right\} \mathcal{O}, \end{aligned} \quad (3)$$

This work has been supported from the Unity Through Knowledge Fund under the project *Cooperative Cloud based Simultaneous Localization and Mapping in Dynamic Environments* (cloudSLAM) and by the Ministry of Science, Education and Sports of the Republic of Croatia under the grant *Center of Research Excellence for Data Science and Cooperative Systems* (CoE ACROSS).

\* Vladimir Joukov, Kevin Westermann and Dana Kulić are with the University of Waterloo, Department of Electrical and Computer Engineering, Adaptive Systems Laboratory, Canada. {vjoukov@uwaterloo.ca, kgwester@uwaterloo.ca, dkulic@uwaterloo.ca}

<sup>‡</sup> Josip Ćesić, Ivan Marković and Ivan Petrović are with the University of Zagreb, Faculty of Electrical Engineering and Computing, Laboratory for Autonomous Systems and Mobile Robotics, Croatia. {josip.cesic@fer.hr, ivan.markovic@fer.hr, ivan.petrovic@fer.hr}

where

$$S_{k+1|k}^{i,\omega} = \sum_{r=1}^{d_i} \left( \omega_{k+1|k}^{i,r} E^{i,r} \right), \quad (4)$$

which is a function of the number of degrees of freedom  $d_i$  of the  $i$ -th joint, and the superscript  $\omega$  denotes that the velocity components are summed up. The three parts in (3) arise from evaluating partial derivatives of the three components existing in equation (27) of the original manuscript, i.e., the two centripetal components and the joint acceleration component. Depending on the location within kinematic chain of the considered joint  $l$ , different terms need to be applied. However, this is still a direct result of evaluating partial derivatives of (27) of the original manuscript. The complete positional component can now be calculated as

$$\begin{bmatrix} \mathcal{H}_{k+1}^{\theta,l,r} \\ 1 \end{bmatrix} = \frac{\partial \mathcal{K}_0^{s,R}}{\partial \theta_{k+1|k}^{l,r}} (\ddot{p}_{k+1|k} + g) + \mathcal{K}_0^{s,R} \frac{\partial \ddot{p}_{k+1|k}}{\partial \theta_{k+1|k}^{l,r}}. \quad (5)$$

### B. Velocity part

Since  $\mathcal{K}_0^{s,R}$  is only a function of the joint position  $\theta_{k+1|k}^l$ , the partial derivative of forward kinematics with respect to the velocity component is

$$\frac{\partial \mathcal{K}_0^{s,R}}{\partial \omega_{k+1|k}^{l,r}} = 0. \quad (6)$$

We now evaluate the partial derivative of acceleration  $\ddot{p}_{k+1|k}$ , with respect to the velocity variable  $\omega_{k+1|k}^{l,r}$ , which evaluates to the following expression

$$\begin{aligned} \frac{\partial \ddot{p}_{k+1|k}}{\partial \omega_{k+1|k}^{l,r}} &= \mathcal{K}_l^0 E^{l,r} \sum_{i=l}^n \left( \mathcal{K}_i^l S_{k+1|k}^{i,\omega} \mathcal{K}_s^i \right) \mathcal{O} + \sum_{j=1}^l \left( \mathcal{K}_j^0 S_{k+1|k}^{j,\omega} \mathcal{K}_l^j \right) E^{l,r} \mathcal{K}_s^l \mathcal{O} + \\ &\quad \mathcal{K}_l^0 E^{l,r} \sum_{j=l+1}^n \left( \mathcal{K}_j^l S_{k+1|k}^{j,\omega} \mathcal{K}_s^j \right) \mathcal{O} + \sum_{i=1}^{l-1} \left( \mathcal{K}_i^0 S_{k+1|k}^{i,\omega} \mathcal{K}_l^i \right) E^{l,r} \mathcal{K}_s^l \mathcal{O}. \end{aligned} \quad (7)$$

The four parts of this derivative arise from the two centripetal force components (two per each) given in equation (27) of the original manuscript. The complete velocity component can now be calculated as

$$\begin{bmatrix} \mathcal{H}_{k+1}^{\omega,l,r} \\ 1 \end{bmatrix} = \frac{\partial \mathcal{K}_0^{s,R}}{\partial \omega_{k+1|k}^{l,r}} (\ddot{p}_{k+1|k} + g) + \mathcal{K}_0^{s,R} \frac{\partial \ddot{p}_{k+1|k}}{\partial \omega_{k+1|k}^{l,r}}. \quad (8)$$

### C. Acceleration part

Here, we evaluate the acceleration term. Since  $\mathcal{K}_0^{s,R}$  is only function of the joint position  $\theta_{k+1|k}^l$ , the partial derivative of forward kinematics with respect to the acceleration component is

$$\frac{\partial \mathcal{K}_0^{s,R}}{\partial \alpha_{k+1|k}^{l,r}} = 0. \quad (9)$$

The partial derivative of acceleration  $\ddot{p}_{k+1|k}$  with respect to the  $r$ -th component of the acceleration of the  $l$ -th joint,  $\alpha_{k+1|k}^{l,r}$ , evaluates as

$$\frac{\partial \ddot{p}_{k+1|k}}{\partial \alpha_{k+1|k}^{l,r}} = \mathcal{K}_l^0 E^{l,r} \mathcal{K}_s^l \mathcal{O}. \quad (10)$$

This derivative arise from the joint acceleration component given in equation (27) of the original manuscript. The complete acceleration component can now be calculated as

$$\begin{bmatrix} \mathcal{H}_{k+1}^{\alpha,l,r} \\ 1 \end{bmatrix} = \frac{\partial \mathcal{K}_0^{s,R}}{\partial \alpha_{k+1|k}^{l,r}} (\ddot{p}_{k+1|k} + g) + \mathcal{K}_0^{s,R} \frac{\partial \ddot{p}_{k+1|k}}{\partial \alpha_{k+1|k}^{l,r}}. \quad (11)$$

Finally, the full  $\mathcal{H}_{k+1}$  relating sensor measurement and the system variables associated to  $m$  joints is constructed as

$$\mathcal{H}_{k+1}^l = \begin{bmatrix} \mathcal{H}_{k+1}^{\theta,l} & \mathcal{H}_{k+1}^{\omega,l} & \mathcal{H}_{k+1}^{\alpha,l} \end{bmatrix}. \quad (12)$$

## PUBLICATION 6

J. Ćesić, I. Marković, M. Bukal and I. Petrović. Extended information filter on matrix Lie groups. *Automatica*, 53(9):226–234, 2017.



# Extended information filter on matrix Lie groups<sup>☆</sup>



Josip Česić, Ivan Marković<sup>1</sup>, Mario Bukal, Ivan Petrović

University of Zagreb Faculty of Electrical Engineering and Computing, Unska 3, HR-10000, Zagreb, Croatia

## ARTICLE INFO

### Article history:

Received 6 June 2016

Received in revised form

8 March 2017

Accepted 12 April 2017

### Keywords:

Extended Kalman filters

Information filter

Lie groups

## ABSTRACT

In this paper we propose a new state estimation algorithm called the extended information filter on Lie groups. The proposed filter is inspired by the extended Kalman filter on Lie groups and exhibits the advantages of the information filter with regard to multisensor update and decentralization, while keeping the accuracy of stochastic inference on Lie groups. We present the theoretical development and demonstrate its performance on multisensor rigid body attitude tracking by forming the state space on the  $SO(3) \times \mathbb{R}^3$  group, where the first and second component represent the orientation and angular rates, respectively. The performance of the filter is compared with respect to the accuracy of attitude tracking with parametrization based on Euler angles and with respect to execution time of the extended Kalman filter formulation on Lie groups. The results show that the filter achieves higher performance consistency and smaller error by tracking the state directly on the Lie group and that it keeps smaller computational complexity of the information form with respect to high number of measurements.

© 2017 Elsevier Ltd. All rights reserved.

## 1. Introduction

The information filter (IF) is the dual of the Kalman filter (KF) relying on the state representation by a Gaussian distribution (Maybeck, 1979), and hence is the subject of the same assumptions underlying the KF. Whereas the KF family of algorithms is represented by the first two moments involving the mean and covariance, the IF relies on the canonical parametrization consisting of an information matrix and information vector (Grocholsky, Makarenko, & Durrant-Whyte, 2003). Both the KF and IF operate cyclically in two steps: the prediction and update step. The advantages of the IF lie in the update step, especially when the number of measurements is significantly larger than the size of the state space, since this step is additive for the IF. For the KF, the opposite applies; it is the prediction step which is additive and computationally less complex. What is computationally complex in one parametrization turns out to be simple in the other (and vice-versa) (Thrun, Burgard, & Fox, 2006). Given this duality, the IF has proven its mettle in a number of applications facing large number of measurements, features or demanding a decentralized

filter form. For example, if the system is linear and the state is modeled as Gaussian, then multisensor fusion can be performed with the decentralized KF proposed in Rao, Durrant-Whyte, and Sheen (1993), which enables fusion of not only the measurements, but also of the local independent KFs. Therein, the inverse covariance form is utilized, thus resulting in additive fusion equations, which can further be elegantly translated to the IF form as shown in Nettleton, Durrant-Whyte, and Sukkarieh (2003). In Zhang, Chai Soh, and Chen (2005) an IF is presented for robust decentralized estimation based on the robustness property of the  $H_\infty$  filter with respect to noise statistics, whereas in Battistelli and Chisci (2016) stability of consensus extended Kalman filter for distributed state estimation was investigated. In Onel, Ersoy, and Delic (2009) collaborative target tracking is developed for wireless sensor networks and a mutual-information-based sensor selection is adopted for participation in the IF form fusion process. In Fu, Ling, and Tian (2012) the IF form is used in multitarget tracking sensor allocation based on solving a constrained optimization problem. In Vercauteren and Wang (2005) a sigma-point IF was used for decentralized target tracking, in Campbell and Whitacre (2007) a square root form of the same filter was used for cooperative tracking with unmanned aerial vehicles, and in Liu, Wörgötter, and Markelić (2012); Wang, Feng, and Tse (2014) square-root information filtering was further explored with respect to numerical stability. The unscented IF was presented in Lee (2008) for tracking of a re-entry vehicle entering into an atmosphere from space, and in Pakki, Chandra, and Postlethwaite (2013) the square root cubature IF was proposed and

<sup>☆</sup> The material in this paper was not presented at any conference. This paper was recommended for publication in revised form by Associate Editor Brett Ninness under the direction of Editor Torsten Söderström.

E-mail addresses: [josip.cesic@fer.hr](mailto:josip.cesic@fer.hr) (J. Česić), [ivan.markovic@fer.hr](mailto:ivan.markovic@fer.hr) (I. Marković), [mario.bukal@fer.hr](mailto:mario.bukal@fer.hr) (M. Bukal), [ivan.petrovic@fer.hr](mailto:ivan.petrovic@fer.hr) (I. Petrović).

<sup>1</sup> Fax: +3851 6129 795

demonstrated on the example of speed and rotor position estimation of a two phase permanent magnet synchronous motor.

Another important aspect of estimation is the state space geometry, hence many works have been dedicated to dealing with uncertainty and estimation techniques accounting for it. For example, Lie groups are natural ambient (state) spaces for description of the dynamics of rigid body mechanical systems (Murray, Li, & Sastry, 1994; Selig, 1996). Furthermore, error propagation on the SE(3) group with applications to manipulator kinematics was presented in Wang and Chirikjian (2006a) by developing closed-form solutions for the convolution of the concentrated Gaussian distributions on SE(3). Furthermore, in Wolfe, Mashner, and Chirikjian (2011) the authors propose a solution to Bayesian fusion on Lie groups by assuming conditional independence of observations on the group, thus setting the fusion result as a product of concentrated Gaussian distributions, and finding the single concentrated Gaussian distribution parameters which are closest to the starting product. Uncertainty association, propagation and fusion on SE(3) was investigated in Barfoot and Furgale (2014) along with sigma point method for uncertainty propagation through a non-linear camera model. In Forster, Carlone, Dellaert, and Scaramuzza (2015) the authors preintegrated a large number of inertial measurement unit measurements for visual-inertial navigation into a single relative motion constraint by respecting the structure of the SO(3) group and defining the uncertainty thereof in the pertaining tangent space. A state estimation method based on an observer and a predictor cascade for invariant systems on Lie groups with delayed measurements was proposed in Khosravian, Trumpf, Mahony, and Hamel (2015). Recently, some works have also addressed the uncertainty on the SE(2) group proposing new distributions (Gilitschenski, Kurz, Julier, & Hanebeck, 2014; Kurz, Gilitschenski, & Hanebeck, 2014); however, these approaches do not yet provide a closed-form Bayesian recursion framework (involving both the prediction and update) that can include higher order motion and non-linear models. A least squares optimization and nonlinear KF on manifolds in the vein of the unscented KF was proposed in Hertzberg, Wagner, Frese, and Schröder (2013) along with an accompanying software library. Therein the authors demonstrate the filter on a synthetic dataset addressing the problem of trajectory estimation by posing the system state to reside on the manifold  $\mathbb{R}^3 \times \text{SO}(3) \times \mathbb{R}^3$ , i.e., the position, orientation and velocity. In the end, the authors also demonstrate the approach on real-world simultaneous localization and mapping (SLAM) data and perform pose relation graph optimization. In the vein of the extended Kalman filter (EKF) a nonlinear continuous–discrete extended Kalman filter on Lie groups (LG-EKF) was proposed in Bourmaud, Mégret, Arnaudon, and Giremus (2015). Therein, the prediction step is presented in the continuous domain, while the update step is discrete. The authors have demonstrated the efficiency of the filter on a synthetic camera pose filtering problem by forming the system state to reside on the  $\text{SO}(3) \times \mathbb{R}^9$  group, i.e. the camera orientation, position, angular and radial velocities. In an earlier publication (Bourmaud, Mégret, Giremus, & Berthoumieu, 2013), the authors have presented a discrete version of the LG-EKF, which serves as the inspiration for the filter proposed in the present paper. In Česić, Marković, Cvišić, and Petrović (2016) we have explored modeling of the pose of tracked objects on the SE(2) group within the LG-EKF framework, and applied it on the problem of multitarget tracking by fusing a radar sensor and stereo vision. Given the advantages of the IF and filtering on Lie groups, a natural question arises; Can LG-EKF be cast in the information form and will the corresponding information filter on Lie groups keep the additivity and computational advantages of the update step?

A quite prominent example of an application where the need arises for computational benefits of the IF and the geometric accuracy of Lie groups is SLAM. SLAM is of great practical

importance in many robotic and autonomous system applications and the earliest solutions were based on the EKF. However, EKF in practice can handle maps that contain a few hundred features, while in many applications maps are orders of magnitude larger (Thrun et al., 2004). Therefore, the extended information filter (EIF) is often employed and widely accepted for SLAM (Bailey, Upcroft, & Durrant-Whyte, 2006), and has reached its zenith with sparsification approaches resulting with sparse EIF (SEIF) (Thrun et al., 2004) and exactly sparse delayed-state filter (ESDF) (Eustice, Singh, & Leonard, 2006). However, the localization component of SLAM conforms the pose estimation problem as arising on Lie groups, i.e., describing the pose in the special euclidean group SE(3) (Barfoot & Furgale, 2014). Furthermore, the mapping part of SLAM consists of landmarks whose position, as well, arises on SE(3). Therefore, some recent SLAM solutions approached the problem by respecting the geometry of the state space (Kümmerle et al., 2011; Ros, Guerrero, Sappa, Ponsa, & Lopez, 2013), since significant cause of error in such application was determined to stem from the state space geometry approximations. However, these SLAM solutions, although able to account for the geometry of the state space, exclusively rely on graph optimization (Engel, Sch, & Cremers, 2014; Mur-Artal, Montiel, & Tardos, 2015), but not on filtering approaches. By using the herein proposed algorithm, one can extend the SLAM filtering approaches, such as SEIF or ESDF, and at the same time respect the geometry of the state space via formulation on Lie groups.

The main contribution of this paper is a new state estimation algorithm called the extended information filter on Lie groups (LG-EIF), which exhibits the advantages of the IF with regard to multisensor update and decentralization, while keeping the accuracy of the LG-EKF for stochastic inference on Lie groups. We present the theoretical development of the LG-EIF recursion equations and the applicability of the proposed approach is demonstrated on a rigid body attitude tracking problem with multiple sensors. In the experiments we define the state space to reside on the Cartesian product of the special orthogonal group SO(3) and  $\mathbb{R}^3$ , with the first component representing the attitude of the rigid body and the second component representing the pertaining angular rates. Given that, the model of the system is then set as a constant angular rate model acting on the state space  $\text{SO}(3) \times \mathbb{R}^3$ . Note that, just like the LG-EKF, the proposed filter can be applied on any matrix Lie group or combination thereof. In the end, we compare the proposed LG-EIF to an EIF based on Euler angles, and we analyze the computational complexity of the LG-EIF multisensor update with respect to the LG-EKF. The results show that the proposed filter achieves higher performance consistency and smaller error by tracking the state directly on the Lie group and that it keeps smaller computational complexity of the information form with respect to large number of measurements.

The rest of the paper is organized as follows. In Section 2 we present the theoretical preliminaries addressing Lie groups and uncertainty definition in the form of the concentrated Gaussian distribution. In Section 3 we derive the proposed LG-EIF, while in Section 4 we present the experimental results. In the end, Section 5 concludes the paper.

## 2. Preliminaries

### 2.1. Lie groups and Lie algebras

Generally, a Lie group is a group which has also the structure of a differentiable manifold and the group operations (product and inversion) are differentiable. In this paper we restrict our attention to a special class of Lie groups, the matrix groups over the field of reals, where the group operations are matrix multiplication and inversion, with the identity matrix  $I^d$  being the identity element

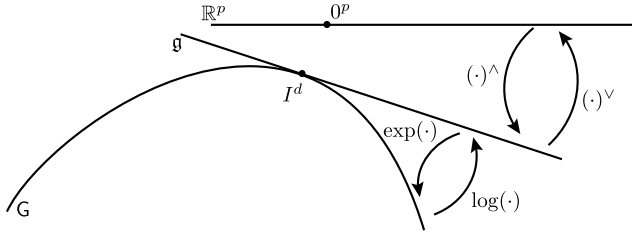


**Fig. 1.** An illustration of mappings within the triplet of Lie group  $G$  – Lie algebra  $\mathfrak{g}$  – Euclidean space  $\mathbb{R}^p$ .

of the group. These groups are frequently called, especially in the engineering literature, matrix Lie groups. The name emphasizes the fact that every matrix group is a Lie group, as well as the differential geometric viewpoint that is regularly employed. A matrix Lie group  $G$  can be characterized as a closed subgroup of a general linear group  $GL(d; \mathbb{R})$ , in the sense that: if  $(A_n)$  is a sequence of matrices in  $G$  and  $A_n$  converges to a matrix  $A$ , with respect to a norm on  $\mathbb{R}^{d \times d}$ , then  $A \in G$  or  $A \notin GL(d; \mathbb{R})$ , i.e.,  $A$  is not invertible (Hall, 2003). Ubiquitous examples of real matrix Lie groups are the general linear group  $GL(d; \mathbb{R})$ , special linear group  $SL(d; \mathbb{R})$ , orthogonal  $O(d)$  and special orthogonal  $SO(d)$  groups, etc. For an introductory, but rigorous mathematical treatment of matrix Lie groups, the interested reader is advised to confer (Hall, 2003).

To every Lie group  $G$ , there is an associated Lie algebra  $\mathfrak{g}$  – a linear space (of the same dimension as  $G$ ) endowed with a binary operation  $[\cdot, \cdot]$  called the Lie bracket. From the differential geometric point of view, it is an open neighborhood of the origin in the tangent space of  $G$  at the identity element. A local diffeomorphism between a Lie group (manifold) and associated Lie algebra (tangent space) is established through the exponential mapping  $\exp : \mathfrak{g} \rightarrow G$  and its inverse  $\log : G \rightarrow \mathfrak{g}$  called the logarithm. This is a crucial mechanism for transfer of information between the group and its algebra. In case of matrix Lie groups, the exponential mapping is simply the matrix exponential

$$\exp(X) = \sum_{n=0}^{\infty} \frac{1}{n!} X^n,$$

and its inverse is of course the matrix logarithm defined for all  $d \times d$  matrices  $A$  satisfying  $\|A - I^d\| < 1$ . Moreover, the matrix exponential can even be used to characterize the matrix Lie algebra – if  $G$  is a matrix Lie group, then its Lie algebra, denoted by  $\mathfrak{g}$ , is the set of all matrices  $X$  such that  $\exp(tX) \in G$  for all  $t \in \mathbb{R}$  (Hall, 2003). Being a linear space, a (real)  $p$ -dimensional matrix Lie algebra  $\mathfrak{g}$  is naturally related to the Euclidean space  $\mathbb{R}^p$  through a linear isomorphism  $(\cdot)^\vee : \mathfrak{g} \rightarrow \mathbb{R}^p$  and its inverse denoted by  $(\cdot)^\wedge : \mathbb{R}^p \rightarrow \mathfrak{g}$ . An illustration of these concepts is given in Fig. 1 (Bourmaud et al., 2015).

The adjoint representation of a matrix Lie group  $G$  is the map  $\text{Ad} : G \rightarrow GL(\mathfrak{g})$  defined by  $A \mapsto \text{Ad} A$ , where  $\text{Ad} A$  is a linear invertible operator  $\text{Ad} A : \mathfrak{g} \rightarrow \mathfrak{g}$  given by

$$\text{Ad} A(X) = AXA^{-1}, \quad X \in \mathfrak{g}.$$

Due to the natural isomorphism between  $\mathfrak{g}$  and  $\mathbb{R}^p$ , essentially  $GL(\mathfrak{g}) = GL(p; \mathbb{R})$  and  $\text{Ad}$  is to be understood as a group homomorphism. Therefore, there exists a unique linear map  $\text{ad} : \mathfrak{g} \rightarrow GL(\mathfrak{g})$ , called the adjoint representation of the Lie algebra  $\mathfrak{g}$ , defined by  $X \mapsto \text{ad} X$ , where  $\text{ad} X$  is a linear operator on  $\mathfrak{g}$  given by  $\text{ad} X(Y) = [X, Y] = XY - YX$ ,  $Y \in \mathfrak{g}$ .

In fact, from the differential geometric point of view,  $\text{ad}$  is the differential of  $\text{Ad}$  at the identity of  $G$ , and they are related through the following Hall (2003)

$$\text{Ad} \exp(X) = \exp(\text{ad} X), \quad \text{for all } X \in \mathfrak{g}. \quad (1)$$

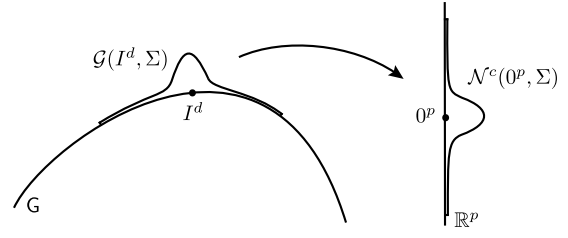


**Fig. 2.** An illustration of the concentrated Gaussian distribution  $\mathcal{G}(I^d, \Sigma)$ . The mean value  $I^d$  resides on the group  $G \subset GL(d; \mathbb{R})$  while the covariance matrix  $\Sigma$  belongs to  $GL(p; \mathbb{R})$ . On the right we depict the truncated or compactly supported corresponding  $\mathcal{N}^c$  Gaussian in  $\mathbb{R}^p$  with mean value  $0^p$  and covariance matrix  $\Sigma$ .

The action of both adjoints can be further transferred from  $\mathfrak{g}$  to  $\mathbb{R}^p$  by the above isomorphism, and we denote them by  $\text{Ad}^\vee$  and  $\text{ad}^\vee$ , respectively.

## 2.2. Concentrated Gaussian distribution

Let  $G$  be a connected unimodular real matrix group. Unimodular means that its integration (Haar) measure  $\zeta$  is both left and right translation invariant, i.e.,  $\zeta(A\mathcal{E}) = \zeta(\mathcal{E}A) = \zeta(\mathcal{E})$  for all  $A \in G$  and all Borel subsets  $\mathcal{E}$  of  $G$ . Prominent examples like  $SO(3)$  and  $SE(3)$  are unimodular matrix groups (Chirikjian & Kyatkin, 2000). Let us assume that a random variable  $X$  taking values in  $G$  has the probability distribution with the probability density function (pdf) of the following form (Wang & Chirikjian, 2006b)

$$p(X; \Sigma) = \beta \exp \left( -\frac{1}{2} (\log(X)^\vee)^\top \Sigma^{-1} \log(X)^\vee \right), \quad (2)$$

where  $\beta$  is a normalizing constant such that (2) integrates to unity (over  $G$  with respect to  $\zeta$ ), and  $\Sigma$  is a positive definite  $p \times p$  matrix. Seemingly, in notation  $\varepsilon = \log(X)^\vee \in \mathbb{R}^p$ , density (2) has the structure of a zero mean Gaussian with covariance matrix  $\Sigma$ . However, observe that the normalizing constant  $\beta$  differs from  $(2\pi)^{-p/2} (\det \Sigma)^{-1/2}$  and, in the sense of  $\mathbb{R}^p$ , it is only defined on an open neighborhood of the origin, which is the image of the  $\log^\vee$  map. Random variables on  $G$  having the probability distribution given by density (2) are therefore called *normally (or Gauss) distributed* with mean  $I^d$  and covariance  $\Sigma$ . Additionally, we will assume that all eigenvalues of  $\Sigma$  are small, thus, almost all the mass of the distribution is concentrated in a small neighborhood around the mean value, and such a distribution is called a *concentrated Gaussian distribution* (Wang & Chirikjian, 2006b). Furthermore, we say that a random variable  $X$  has a concentrated Gaussian distribution of mean  $M \in G$  and covariance matrix  $\Sigma$ , written  $X \sim \mathcal{G}(M, \Sigma)$ , if  $M^{-1}X$  has the concentrated Gaussian distribution of mean  $I^d$  and covariance  $\Sigma$  (Wang & Chirikjian, 2006b), i.e., the density of  $\mathcal{G}(M, \Sigma)$  is given by

$$p(X; M, \Sigma) = \beta \exp \left( -\frac{1}{2} (\log(M^{-1}X)^\vee)^\top \Sigma^{-1} \log(M^{-1}X)^\vee \right). \quad (3)$$

An illustration of the concentrated Gaussian distribution is provided in Fig. 2.

It is well known that in the Euclidean setting multivariate Gaussian distributions  $\mathcal{G}(m, \Sigma)$  form an exponential family (Nielsen & Garcia, 2009) and in the canonical representation source parameters  $(m, \Sigma)$  are replaced by the corresponding natural parameters  $(y, Y) = (\Sigma^{-1}m, \frac{1}{2}\Sigma^{-1})$ , which also uniquely determine the Gaussian distribution. Canonical representation has many advantages, in particular, it is very useful for implementation of the standard IF. In the present paper we pursue the same idea for concentrated Gaussian distribution  $\mathcal{G}(M, \Sigma)$  defined on matrix Lie groups. Using the BCH expansion (A.2) we have

$$\log(M^{-1}X) = -\log M + \log X - \frac{1}{2}[\log X, \log M] + \dots, \quad (4)$$



thus, according to (3),  $\mathcal{G}(M, \Sigma)$  is also completely determined by the so called information vector–matrix pair  $(y, Y)$  given by

$$y = \Sigma^{-1}(\log M)^\vee \quad \text{and} \quad Y = \Sigma^{-1}. \quad (5)$$

Given that, we have formed the basis for the derivation of the LG-EIF.

### 3. The extended information filter on matrix Lie groups

Just as the standard KF, the LG-EIF recursion is divided in two steps: prediction and update and in the sequel we derive the equations of the proposed information form of the LG-EKF. First, we start with the prediction step where the same logic applies as in the case of the standard IF; namely, the computational burden is increased since, in order to apply the motion model, we need to convert the information vector to the mean. Second, the update step of the filter is derived where the advantages of the information form are kept, thus facilitating updates with multiple sensors or opening the way for decentralization approaches.

#### 3.1. Motion and measurement models

Let  $G$  be a matrix Lie group and  $X_k \in G$  denote a system state at time step  $k \geq 0$ . We assume that the motion model of the system (the state equation) is described by a non-linear twice continuously differentiable function<sup>2</sup>  $\Omega : \mathcal{U} \supset G \rightarrow \mathbb{R}^p$  and the left action of the current state as follows Bourmaud et al. (2015)

$$X_{k+1} = X_k \exp(\Omega(X_k)^\wedge + n_k^\wedge), \quad k \geq 0, \quad (6)$$

where  $n_k \sim \mathcal{N}_{\mathbb{R}^p}(0_{p \times 1}, Q_k)$  is Gaussian noise in  $\mathbb{R}^p$ . For example, such models have appeared in Bourmaud et al. (2015), Česić, Joukov, Petrović, and Kulić (2016) and Česić, Marković et al. (2016) modeling motion as constant velocity on SE(2) and constant acceleration on SO(2), SO(3) and SE(3), respectively.

The discrete measurement model on the matrix Lie group is modeled by a continuously differentiable function  $h : \mathcal{U} \supset G \rightarrow G'$  and the group perturbation as Bourmaud et al. (2015)

$$Z_{k+1} = h(X_{k+1}) \exp(r_{k+1}^\wedge), \quad (7)$$

where  $r_{k+1} \sim \mathcal{N}_{\mathbb{R}^q}(0^{q \times 1}, R_{k+1})$  is a Gaussian noise in  $\mathbb{R}^q$  and  $\exp$  denotes the exponential mapping on a  $q$ -dimensional matrix Lie group  $G'$ .

#### 3.2. LG-EIF prediction

We assume that the posterior distribution at time step  $k$  is given by the concentrated Gaussian distribution  $\mathcal{G}(M_k, \Sigma_k)$ , shortly  $\mathcal{G}_k$ . In fact, we assume that  $\mathcal{G}_k$  is known through the canonical parameters  $(y_k, Y_k)$ , for which we aim to derive the filter recursions. Note that, according to relation (5),  $\Sigma_k = Y_k^{-1}$  and  $M_k = \exp((Y_k^{-1}y_k)^\wedge)$ .

Following the idea proposed in Bourmaud et al. (2015), we first consider the covariance propagation under the motion model. For that purpose the Lie algebraic error, defined by  $\varepsilon_k^\wedge = \log(M_k^{-1}X_k)$ , is propagated under the motion model according to

$$\exp(\varepsilon_{k+1|k}^\wedge) = M_{k+1|k}^{-1}X_{k+1},$$

where  $M_{k+1|k} = M_k \exp(\Omega(M_k)^\wedge)$ . Therefore, the predicted state error on  $G$  can be expressed as

$$\exp(\varepsilon_{k+1|k}^\wedge) = \exp(-\Omega_k^\wedge) \exp(\varepsilon_k^\wedge) \exp(\Omega(X_k)^\wedge + n_k^\wedge),$$

where  $\Omega_k^\wedge = \Omega(M_k)^\wedge$ . Linearizing  $\Omega$  in  $M_k$  and using the BCH expansion (A.2), defined in Appendix A, one obtains the following propagated Lie algebraic error

$$\varepsilon_{k+1|k} = \mathcal{F}_k \varepsilon_k + \Psi(\Omega_k) n_k + \mathcal{O}(|\varepsilon_k, n_k|^2), \quad (8)$$

where  $\mathcal{O}(|\varepsilon_k, n_k|^2)$  is short for  $\mathcal{O}(|\varepsilon_k|^2) + \mathcal{O}(|n_k|^2) + \mathcal{O}(|\varepsilon_k n_k|)$ . Operators  $\mathcal{F}_k$ , the matrix Lie group equivalent to the Jacobian of the nonlinearity of the motion model, and  $\Psi$  are given by the following formulae:

$$\mathcal{F}_k = \text{Ad}^\vee(\exp(-\Omega_k^\wedge)) + \Psi(\Omega_k) \mathcal{C}_k, \quad (9)$$

$$\Psi(v) = \sum_{m=0}^{\infty} \frac{(-1)^m}{(m+1)!} \text{ad}^\vee(v)^m, \quad v \in \mathbb{R}^p, \quad (10)$$

$$\mathcal{C}_k = \frac{\partial}{\partial \varepsilon} \Omega(M_k \exp(\varepsilon^\wedge))|_{\varepsilon=0}. \quad (11)$$

Operator  $\Psi$  is called the right Jacobian of  $G$  (Barfoot & Furgale, 2014), while  $\mathcal{C}_k$  denotes the linearization of the motion model (6) at  $M_k$ . The above formulae can be found in Bourmaud et al. (2015, 2013); however, without a detailed derivation, which we provide for the reader's convenience in Appendix A. Neglecting the second-order terms in (8) and using the fact that  $\mathbb{E}(\varepsilon_k) = 0$ , which is satisfied by the construction of the concentrated Gaussian distribution (see (3)), the expectation of  $\varepsilon_{k+1|k}$  becomes

$$\mathbb{E}(\varepsilon_{k+1|k}) = \mathcal{F}_k \mathbb{E}(\varepsilon_k) = 0.$$

The predicted covariance matrix  $\Sigma_{k+1|k}$  is the covariance matrix of the predicted Lie algebraic error  $\varepsilon_{k+1|k}$  and due to the linear equation (8) it evaluates to

$$\begin{aligned} \Sigma_{k+1|k} &= \mathbb{E}[\varepsilon_{k+1|k} \varepsilon_{k+1|k}^\top] \\ &= \mathcal{F}_k \Sigma_k \mathcal{F}_k^\top + \Psi(\Omega_k) Q_k \Psi(\Omega_k)^\top. \end{aligned}$$

Applying the Woodbury's matrix identity (Woodbury, 1950),  $Y_{k+1|k} = \Sigma_{k+1|k}^{-1}$  evaluates to

$$Y_{k+1|k} = \tilde{Q}_k^{-1} - \tilde{Q}_k^{-1} \mathcal{F}_k (Y_k + \mathcal{F}_k^\top \tilde{Q}_k^{-1} \mathcal{F}_k)^{-1} \mathcal{F}_k^\top \tilde{Q}_k^{-1},$$

where  $\tilde{Q} = \Psi_k Q_k \Psi_k^\top$ ,  $\Psi_k = \Psi(\Omega_k)$ , and all inverse matrices are assumed to exist. Finally, the predicted information vector  $y_{k+1|k} = Y_{k+1|k}(\log M_{k+1|k})^\vee$  amounts to

$$y_{k+1|k} = Y_{k+1|k} \log(\exp((Y_k^{-1}y_k)^\wedge) \exp(\Omega_k^\wedge))^\vee. \quad (12)$$

**Remark 1.** Assuming that  $M_k$  and  $\exp(\Omega_k^\wedge)$  are such that according to the BCH expansion (A.2)

$$\log(\exp((Y_k^{-1}y_k)^\wedge) \exp(\Omega_k^\wedge))^\vee \approx Y_k^{-1}y_k + \Omega_k + \frac{1}{2}[Y_k^{-1}y_k, \Omega_k]^\vee,$$

then the prediction formula (12) simplifies to

$$y_{k+1|k} = Y_{k+1|k} \left( Y_k^{-1}y_k + \Omega_k + \frac{1}{2}[Y_k^{-1}y_k, \Omega_k]^\vee \right). \quad (13)$$

#### 3.3. LG-EIF update

Let us define the innovation term as

$$z_{k+1} = \log(h(M_{k+1|k})^{-1} Z_{k+1})^\vee.$$

Again, applying the BCH formula (A.2) and linearizing the nonlinear terms at  $M_{k+1|k}$ , we obtain (Bourmaud et al., 2015)

$$z_{k+1} = \mathcal{H}_{k+1} \varepsilon_{k+1|k} + r_{k+1} + \mathcal{O}(|\varepsilon_{k+1|k} r_{k+1}|), \quad (14)$$

<sup>2</sup> For the ease of differentiability requirement, we assume that  $\Omega$  is defined on  $\mathcal{U}$ , which is an open subset of  $\mathbb{R}^{d \times d}$  containing the group  $G$ .



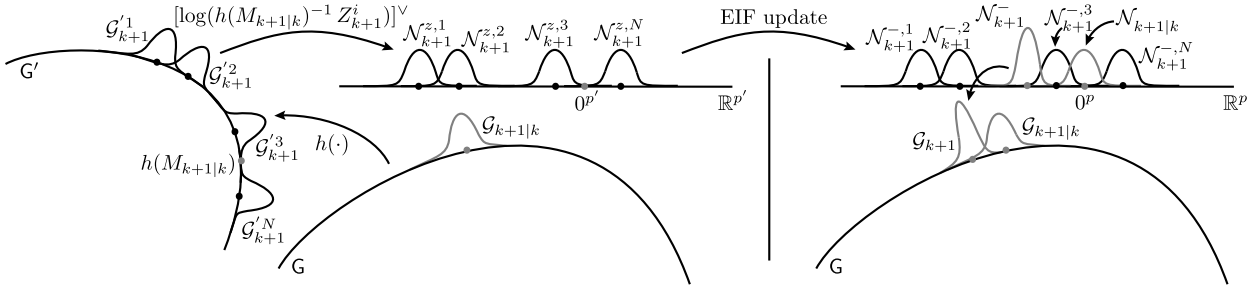


**Fig. 3.** An illustration of the LG-EIF update step. The predicted  $\mathcal{G}_{k+1|k}$  on the group  $G$  is updated with  $N$  measurements  $\mathcal{G}_{k+1}^{i,i}$  on group  $G'$ . First, the predicted mean value  $M_{k+1|k}$  is mapped to  $G'$  via measurement function  $h(\cdot)$  and innovations  $\mathcal{N}_{k+1}^{z,i}$  are calculated in the tangent space  $\mathbb{R}^{p'}$  of  $h(M_{k+1|k})$ . Then, the innovations are mapped to the tangent space  $\mathbb{R}^p$  of  $M_{k+1|k}$ , where the  $\mathcal{N}_{k+1|k}$  corresponding to  $\mathcal{G}_{k+1|k}$  is at the origin. The predicted distribution  $\mathcal{N}_{k+1|k}$  is updated with the mapped measurements  $\mathcal{N}_{k+1}^{-,i}$  resulting with a distribution displaced from the origin  $\mathcal{N}_{k+1}^{-,i}$  which needs to be reparametrized and mapped back to  $G$  as the finally updated  $\mathcal{G}_{k+1}$ .

with

$$\mathcal{H}_{k+1} = \frac{\partial}{\partial \varepsilon} \left[ \log \left( h(M_{k+1|k})^{-1} h \left( M_{k+1|k} \exp(\varepsilon^\wedge) \right) \right) \right]_{\varepsilon=0}^\vee. \quad (15)$$

Since (14) is linear in the Lie algebraic error  $\varepsilon_{k+1|k}$ , we assert that the standard update equations of the IF (Thrun et al., 2006) can be applied. From the previous section we know that  $\varepsilon_{k+1|k}$  is distributed according to the truncated zero mean Gaussian with covariance matrix  $\Sigma_{k+1|k}$ , which is assumed to be well approximated by the Gaussian of the same parameters. Given that, the updated Lie algebraic error  $\varepsilon_{k+1}^-$  will be Gaussian distributed with natural parameters

$$\begin{aligned} Y_{k+1}^- &= \mathcal{H}_{k+1}^\top R_{k+1}^{-1} Z_{k+1}, \\ Y_{k+1}^- &= Y_{k+1|k} + \mathcal{H}_{k+1}^\top R_{k+1}^{-1} \mathcal{H}_{k+1}. \end{aligned} \quad (16)$$

However, we have not completed the update step for the following reasons. Namely, from the definition of  $\varepsilon_{k+1}^-$ , the conditional random variable  $X_{k+1|k+1} := X_{k+1|k} \{Z_1, \dots, Z_{k+1}\}$  has the form

$$X_{k+1|k+1} = M_{k+1|k} \exp(\varepsilon_{k+1}^-), \quad (17)$$

but, the mean value of  $\varepsilon_{k+1}^-$  now equals  $m_{k+1}^- = (Y_{k+1}^-)^{-1} Y_{k+1}^-$ , which in general differs from the zero vector, and (17) is not in the form suitable for description by the concentrated Gaussian distribution. To overcome that issue, the state reparametrization, as proposed in Bourmaud et al. (2015), is performed. Let us define  $\xi_{k+1} = \varepsilon_{k+1}^- - m_{k+1}^-$ , then  $\mathbb{E}(\xi_{k+1}) = 0$  and using formula (A.3) from Appendix A we obtain (up to  $\mathcal{O}(|\xi_{k+1}|^2)$  terms)

$$\begin{aligned} X_{k+1|k+1} &= M_{k+1|k} \exp(m_{k+1}^- + \xi_{k+1}^\wedge) \\ &= M_{k+1|k} \exp(m_{k+1}^-) \exp(\Psi(m_{k+1}^-) \xi_{k+1}^\wedge). \end{aligned}$$

Now defining  $M_{k+1} = M_{k+1|k} \exp(m_{k+1}^-)$  and  $\varepsilon_{k+1} = \Psi(m_{k+1}^-) \xi_{k+1}$ , we have  $X_{k+1|k+1}$  in a more suitable form

$$X_{k+1|k+1} = M_{k+1} \exp(\varepsilon_{k+1}^\wedge), \quad (18)$$

from which the posterior distribution can be plainly read off. By definition

$$\begin{aligned} \Sigma_{k+1} &= \mathbb{E}[\varepsilon_{k+1} \varepsilon_{k+1}^\top] = \mathbb{E}[\Psi(m_{k+1}^-) \xi_{k+1} \xi_{k+1}^\top \Psi(m_{k+1}^-)^\top] \\ &= \Psi(m_{k+1}^-) (Y_{k+1}^-)^{-1} \Psi(m_{k+1}^-)^\top, \end{aligned}$$

and therefore, the finally updated information matrix equals

$$Y_{k+1} = \Psi(m_{k+1}^-)^\top Y_{k+1}^- \Psi(m_{k+1}^-)^{-1}. \quad (19)$$

Concerning the information vector, we find

$$\begin{aligned} y_{k+1} &= Y_{k+1} (\log M_{k+1})^\vee \\ &= Y_{k+1} \left( \log \left( \exp((Y_k^{-1} y_k)^\wedge) \exp(\Omega_k^\wedge) \exp(m_{k+1}^-) \right) \right)^\vee. \end{aligned} \quad (20)$$

#### Algorithm 1 The pseudocode of the LG-EIF

**Require:**  $\mathcal{G}_k = \mathcal{G}(y_k, Y_k), \Omega(X), Q_k$

##### Prediction

- 1: Evaluate  $\Omega_k, \mathcal{C}_k$  and  $\tilde{Q}_k$
- 2:  $\mathcal{F}_k = \text{Ad}^\vee \left( \exp(-\Omega_k^\wedge) \right) + \Psi(\Omega_k) \mathcal{C}_k$
- 3:  $Y_{k+1|k} = \tilde{Q}_k^{-1} - \tilde{Q}_k^{-1} \mathcal{F}_k (Y_k + \mathcal{F}_k^\top \tilde{Q}_k^{-1} \mathcal{F}_k)^{-1} \mathcal{F}_k^\top \tilde{Q}_k^{-1}$
- 4:  $y_{k+1|k} = Y_{k+1|k} \log \left( \exp((Y_k^{-1} y_k)^\wedge) \exp(\Omega_k^\wedge) \right)^\vee$

**Require:**  $\mathcal{G}_{k+1|k} = \mathcal{G}(y_{k+1|k}, Y_{k+1|k}), h(X), R_{k+1}$

##### Update

- 5: Evaluate  $\mathcal{H}_{k+1}$
- 6:  $Y_{k+1}^- = Y_{k+1|k} + \mathcal{H}_{k+1}^\top R_{k+1}^{-1} \mathcal{H}_{k+1}$
- 7:  $y_{k+1}^- = \mathcal{H}_{k+1}^\top R_{k+1}^{-1} Z_{k+1}$
- 8:  $m_{k+1}^- = (Y_{k+1}^-)^{-1} y_{k+1}^-$
- 9:  $Y_{k+1} = \Psi(m_{k+1}^-)^\top Y_{k+1}^- \Psi(m_{k+1}^-)^{-1}$
- 10:  $y_{k+1} = Y_{k+1} \left( \log \left( \exp((Y_k^{-1} y_k)^\wedge) \exp(\Omega_k^\wedge) \exp(m_{k+1}^-) \right) \right)^\vee$
- 11: **return**  $\mathcal{G}_{k+1} = \mathcal{G}(y_{k+1}, Y_{k+1})$

The update step is illustratively summarized in Fig. 3. Note that, in comparison to the standard EIF, we cannot calculate the final information vector update in (20) by using just the information form. However, this does not preclude an advantage in computational complexity with respect to the LG-EKF (as shown in Section 4). The pseudocode of the LG-EIF is given in Algorithm 1.

**Remark 2.** Recall that one of the main advantages of the IF lies in the simultaneous update of multiple measurements in the same time step. In case that  $N$  measurements are available at time step  $k+1$  through different measurement models  $h_i$  and measurement noise  $r_{k+1}^i \sim \mathcal{N}_{\mathbb{R}^q}(0, R_{i,k+1})$ , the updated information vector and matrix (prior to the reparametrization step) become

$$\begin{aligned} Y_{k+1}^- &= \sum_{i=1}^N \mathcal{H}_{i,k+1}^\top R_{i,k+1}^{-1} Z_{i,k+1}, \\ Y_{k+1}^- &= Y_{k+1|k} + \sum_{i=1}^N \mathcal{H}_{i,k+1}^\top R_{i,k+1}^{-1} \mathcal{H}_{i,k+1}. \end{aligned} \quad (21)$$

**Remark 3.** Difficulties that could be encountered in the filter design are twofold. First, the evaluation of operators  $\mathcal{C}_k$  and

$\mathcal{H}_k$ , which arise in the linearization of  $\Omega(\cdot)$  and  $h(\cdot)$ , could be mathematically involved. And second,  $\exp(\cdot)$ ,  $\log(\cdot)$ ,  $\text{Ad}(\cdot)$ ,  $\text{ad}(\cdot)$ , and  $\Psi(\cdot)$  might not allow closed-form expressions for some Lie groups. In that case, it is necessary to apply a truncated Taylor series expansion. However, many Lie groups that are significant for engineering applications allow for closed form expressions for the majority of aforementioned maps.

#### 4. Experiments

In this section we demonstrate the effectiveness and applicability of the LG-EIF on the problem of rigid body attitude tracking in 3D. We pose the experiment as a multisensor estimation problem of a state residing on the group  $G = \text{SO}(3) \times \mathbb{R}^3$ , where the first group,  $\text{SO}(3)$ , represents the rigid body orientation in 3D, while the second group,  $\mathbb{R}^3$ , represents pertaining angular rates. This is a slight abuse of notation intended for clarity, since when talking about  $\mathbb{R}^p$  in the framework of groups, we are actually referring to their matrix representation.  $\mathbb{R}^3$  can be thought of as a three-dimensional matrix Lie group through the following identification

$$\mathbb{R}^3 \ni (a_1, a_2, a_3) \mapsto \begin{pmatrix} 1 & 0 & 0 & a_1 \\ 0 & 1 & 0 & a_2 \\ 0 & 0 & 1 & a_3 \\ 0 & 0 & 0 & 1 \end{pmatrix} \in \text{GL}(4; \mathbb{R}), \quad (22)$$

which transfers the addition of vectors, as the group operation in  $\mathbb{R}^3$ , to the multiplication of matrices. Hence,  $G$  can be thought of as a subgroup of  $\text{GL}(7; \mathbb{R})$ , whose elements are block diagonal matrices where the first  $3 \times 3$  block belongs to  $\text{SO}(3)$ , while the second  $4 \times 4$  block is of the form (22). In that setting  $G$  is a unimodular matrix Lie group with the Haar measure being the tensor product of the Haar measure on  $\text{SO}(3)$  and essentially the Lebesgue measure on  $\mathbb{R}^3$ . Thus, the LG-EIF methodology developed in previous sections is applicable on  $G$ .

##### 4.1. Filtering on $\text{SO}(3) \times \mathbb{R}^3$

Note that we designate the system state as  $X_k \in \text{SO}(3) \times \mathbb{R}^3$  which consists of the orientation component  $\Phi_k \in \text{SO}(3)$  and the angular rate component  $\dot{\Phi}_k \in \mathbb{R}^3$ .

##### 4.1.1. Prediction

We propose to model the motion (6) by a constant angular rate motion model

$$\begin{aligned} \Omega(X_k) &= [T\dot{\phi}_{1,k} \quad T\dot{\phi}_{2,k} \quad T\dot{\phi}_{3,k} \quad 0 \quad 0 \quad 0]^T \\ n_k &= \begin{bmatrix} \frac{T^2}{2}n_{1,k} & \frac{T^2}{2}n_{2,k} & \frac{T^2}{2}n_{3,k} & Tn_{1,k} & Tn_{2,k} & Tn_{3,k} \end{bmatrix}^T, \end{aligned} \quad (23)$$

where  $T$  is the discretization time. With such a defined motion model, the system is corrupted with white noise over three separated components, i.e.,  $n_{1,k}$  the noise in local  $\phi_1$  direction,  $n_{2,k}$  the noise in local  $\phi_2$  direction and  $n_{3,k}$  the noise in local  $\phi_3$  direction. Given that, the components can be seen as resembling a Wiener process over the associated axes.

The uncertainty propagation can be challenging, since it requires the calculation of (11), which needs to be patiently evaluated for each considered problem. However, for the Lie algebraic error  $\varepsilon = [\varepsilon_1 \ \varepsilon_2 \ \varepsilon_3 \ \dot{\varepsilon}_1 \ \dot{\varepsilon}_2 \ \dot{\varepsilon}_3]^T$ , and the motion model given by (23), which extracts only the Euclidean part of the state, we obtain

$$\mathcal{C}_k = \begin{bmatrix} 0_{3 \times 3} & T \cdot I_3 \\ 0_{3 \times 3} & 0_{3 \times 3} \end{bmatrix}. \quad (24)$$

Now, we have all the ingredients for applying the motion model to predict the state in an LG-EIF manner.

##### 4.1.2. Update

The measurement function is the map  $h : \text{SO}(3) \times \mathbb{R}^3 \rightarrow \text{SO}(3)$ , and although we have  $N$  measurements we use the expression (21) for the update, hence mapping dimensions correspond as if having a single measurement. The element that specifically needs to be derived is the measurement matrix  $\mathcal{H}_{k+1}$ , which in the vein of (15) requires evaluating partial derivatives and multivariate limits. With having the Lie algebraic error defined, the function to be partially derived is

$$[\log(h(M_{k+1|k})^{-1}h(M_{k+1|k} \exp(\varepsilon^\wedge)))]^\vee = [\varepsilon_1 \ \varepsilon_2 \ \varepsilon_3]^T. \quad (25)$$

The final measurement matrix, for this case, is obtained by taking the partial derivatives of (25) with respect to the Lie algebraic error. Finally, the measurement matrix evaluates to  $\mathcal{H}_{k+1} = [I_3 \ 0_{3 \times 3}]$ . Now, we have all the ingredients to update the filter in the LG-EIF manner.

##### 4.2. Evaluation

In order to demonstrate the performance of the proposed filter we have simulated a rotating rigid body with the constant angular rate model. First, the initial orientation of the rigid body in  $\text{SO}(3)$  and initial angular rates are defined. Note that the angular rates are defined in the  $\mathbb{R}^p$  isomorphic to the  $\mathfrak{so}(3)$ , i.e., the Euler axes representation (see Appendix B). Then, under the assumption of the constant angular rate model, random disturbances are added via accelerations in the pertaining Euclidean space  $\mathbb{R}^p$ . Measurements are generated by corrupting the true orientation of the body in  $\mathbb{R}^p$  with white Gaussian noise, and then mapping the result via the exponential map back to the  $\text{SO}(3)$ .

In Fig. 4 we can see the result of LG-EIF and Euler angles EIF comparison on 100 randomly generated trajectories measured with  $N = 5$  sensors for  $k = 100$  steps. The initial state of the system was set to  $[\log X_0]^\vee = [0_{1 \times 6}]^T$ , the standard deviation of random accelerations over the three axes acting as disturbances was  $\sigma_p = 10^\circ/\text{s}^2$  and standard deviation of measurement noise over the three axes ranged from  $\sigma_m = 0.1^\circ$  to  $\sigma_m = 20^\circ$ . The estimated orientation of the LG-EIF is defined in  $\text{SO}(3)$ , and in Fig. 4 we show the attitude error calculated as the cosine angle between two rotation matrices

$$\Phi_{\text{err}} = \arccos\left(\frac{1}{2}(\text{Tr}[\Phi_t^T \Phi_e] - 1)\right), \quad (26)$$

where  $\Phi_t$  is the true orientation and  $\Phi_e$  is estimated orientation. We can see from Fig. 4 that for measurement noise standard deviation larger than  $2^\circ$  on average the LG-EIF achieves smaller attitude root-mean-square-error (RMSE) and has significantly smaller variation (not noticeable in the figure) in the results compared to the Euler angles EIF. In Fig. 5 we show three examples (with different measurement noise intensity) of time behavior of the attitude estimation error for different filters, where the smaller variation for LG-EIF can be noticed. Furthermore, it could be argued that other filtering methods in lieu of EIF could be used which can better handle nonlinearities. However, the EIF system and measurement equations are linear in this case and we assert that the main reason behind larger errors in EIF comes from the suboptimal state space parametrization, rather than linearization errors in state and measurement equations.

The main advantage of the IF form is the computational efficiency of the update step with respect to a large number of measurements. To verify that the same advantage holds also for the Lie group EKF we have compared the execution time of the LG-EKF and LG-EIF on 100 examples of 100 step long simulated trajectories. Fig. 6 shows the execution time ratio of the LG-EKF and LG-EIF. We can see that for a large number of sensors or features this difference is prominent.

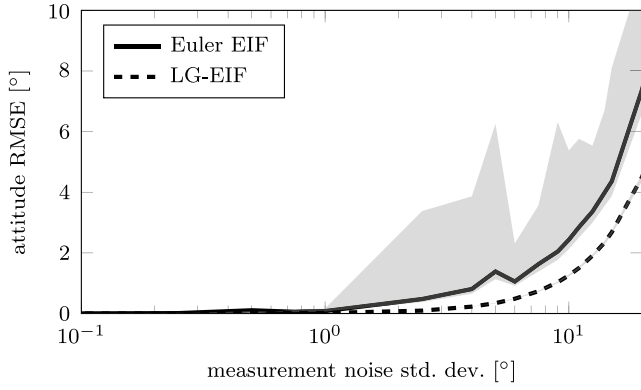


**Fig. 4.** Comparison of attitude RMSE with respect to increase in measurement noise standard deviation. The results represent the mean value of the RMSE and one standard deviation of 100 MC runs. We can see that the LG-EIF exhibits smaller error and has more consistent performance over various trajectories.

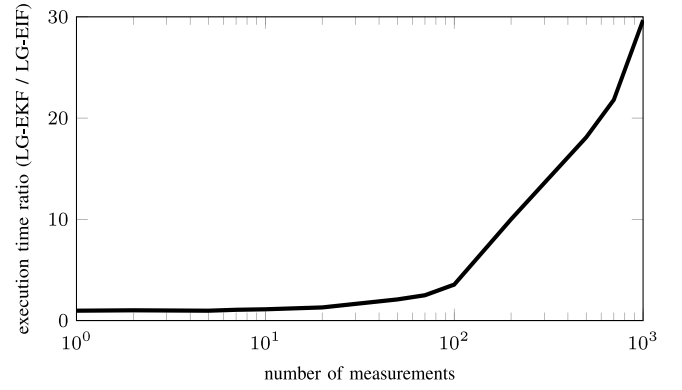


**Fig. 6.** Comparison of LG-EKF and LG-EIF time execution with respect to the number of measurements in the update step. We can see that after 100 measurements the difference becomes extremely prominent. The figure represents mean value of the execution time ratio for 50 Monte Carlo runs.

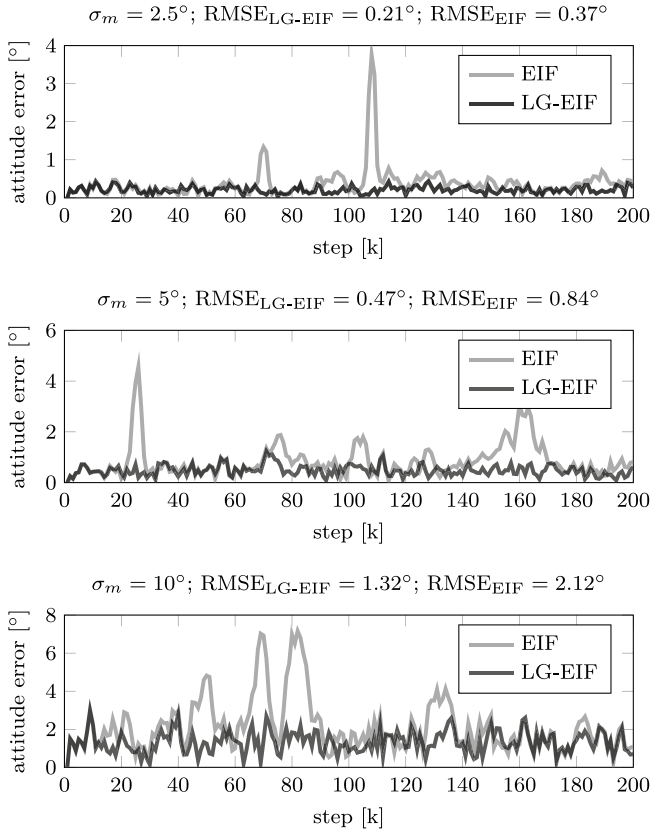


**Fig. 5.** Three examples of time behavior of the attitude estimation error through 200 steps. The standard deviation for measurement noise was set to  $\sigma_m = 2.5^\circ$  (top),  $\sigma_m = 5^\circ$  (middle),  $\sigma_m = 10^\circ$  (bottom). The attitude RMSE for each filter is given in the subfigure titles.

## 5. Conclusion

In this paper we have proposed a new state estimation algorithm on Lie groups. We have embedded the LG-EKF with an EIF form for non-linear systems, thus endowing the filter with the information forms advantages with regard to multisensor update and decentralization, while keeping the accuracy of the LG-EKF for stochastic inference on Lie groups. The theoretical development of the LG-EIF recursion equations was presented and the applicability of the proposed approach demonstrated on the problem of rigid body attitude tracking with multiple sensors by setting the state on the Lie group  $SO(3) \times \mathbb{R}^3$ . The first component of the state

represented the rigid body orientation in 3D, while the second component represented the pertaining angular rates. The system model was then set as a constant angular rate model acting on the state space  $SO(3) \times \mathbb{R}^3$ . The results have shown that the filter can accurately track the rigid body attitude and that on average it exhibits lower RMSE and more consistent performance than the Euler angles based EIF. Furthermore, the information form of the LG-EIF keeps the multisensor or decentralization computational advantage of the update step with respect to the LG-EKF.

## Acknowledgments

This work has been supported from the Unity Through Knowledge Fund under Grant 24/15 (Cooperative Cloud based Simultaneous Localization and Mapping in Dynamic Environments, cloud-SLAM) and the research has also been carried out within the activities of the Centre of Research Excellence for Data Science and Cooperative Systems supported by the Ministry of Science, Education and Sports of the Republic of Croatia under Grant 533-19-15-0007.

## Appendix A. Lie algebraic error prediction

**Proposition 4** (Baker–Campbell–Hausdorff). *Given a Lie algebra  $\mathfrak{g}$ , for all  $a, b \in \mathfrak{g}$  such that  $|a^\vee|$  and  $|b^\vee|$  are sufficiently small, the following identity holds (Hall, 2003):*

$$\log(\exp(a)\exp(b)) = a + \int_0^1 \psi(\exp(\text{ad}(a))\exp(t\text{ad}(b)))b dt, \quad (\text{A.1})$$

where  $\psi(z) = z \log z / (z - 1)$ .

This is an integral version of the famous Baker–Campbell–Hausdorff (BCH) formula, which is better known in an expanded form

$$\begin{aligned} \log(\exp(a)\exp(b)) = & a + b + \frac{1}{2}[a, b] \\ & + \frac{1}{12}([a, [a, b]] + [b, [b, a]]) + \dots \end{aligned} \quad (\text{A.2})$$

Another useful identity used in the derivation of the predicted Lie algebraic error is a first-order approximation relation between additive and multiplicative perturbations on matrix Lie groups. Namely, for every  $a, \delta \in \mathfrak{g}$  and  $|\delta^\vee|$  small, i.e., neglecting the second-order terms in  $|\delta^\vee|$ , it holds

$$\exp(a + \delta) \approx \exp(a) \exp(\Psi(a)\delta), \quad (\text{A.3})$$

where  $\Psi(a)$  denotes the right Jacobian of the Lie group defined by (9). The latter identity implies the approximation formula

$$\log(\exp(-a) \exp(a + \delta)) = \Psi(a)\delta. \quad (\text{A.4})$$

Now we proceed with the derivation of the Lie algebraic error prediction. In Section 3.2 we computed the exponential of the predicted Lie algebraic error  $\varepsilon_{k+1|k}$  at time step  $k$

$$\begin{aligned} \exp(\varepsilon_{k+1|k}^\wedge) &= \exp(-\Omega_k^\wedge) \exp(\varepsilon_k^\wedge) \exp(\Omega(X_k)^\wedge + n_k^\wedge), \\ \text{where we recall } \Omega_k &= \Omega(M_k) \text{ and } \varepsilon_k \text{ is the Lie algebraic error at} \\ \text{time step } k. \text{ Linearizing the map } \Omega \text{ at } M_k \text{ we have} \\ \exp(\varepsilon_{k+1|k}^\wedge) &= \exp(-\Omega_k^\wedge) \exp(\varepsilon_k^\wedge) \exp(\Omega_k^\wedge + (\mathcal{C}_k \varepsilon_k)^\wedge + n_k^\wedge), \end{aligned} \quad (\text{A.5})$$

where

$$\mathcal{C}_k = \frac{\partial}{\partial \varepsilon} \Omega(M_k \exp(\varepsilon^\wedge))|_{\varepsilon=0}.$$

Using the BCH formula (A.2) by considering only the first four members from the expansion and neglecting  $\mathcal{O}(|\varepsilon_k^\wedge, n_k^\wedge|^2)$  terms, we obtain

$$\begin{aligned} z_k^\wedge &= \log(\exp(\varepsilon_k^\wedge) \exp(\Omega_k^\wedge + (\mathcal{C}_k \varepsilon_k)^\wedge + n_k^\wedge)) \\ &= \varepsilon_k^\wedge + \Omega_k^\wedge + (\mathcal{C}_k \varepsilon_k)^\wedge + n_k^\wedge + \frac{1}{2}[\varepsilon_k^\wedge, \Omega_k^\wedge] \\ &\quad + \frac{1}{12}[\Omega_k^\wedge, [\Omega_k^\wedge, \varepsilon_k^\wedge]]. \end{aligned} \quad (\text{A.6})$$

Inserting (A.6) into (A.5) one has

$$\exp(\varepsilon_{k+1|k}^\wedge) = \exp(-\Omega_k^\wedge) \exp(z_k^\wedge),$$

thus, using the approximation identity (A.4), the following expression holds

$$\begin{aligned} \varepsilon_{k+1|k}^\wedge &= \Psi(\Omega_k) \left( \varepsilon_k^\wedge + (\mathcal{C}_k \varepsilon_k)^\wedge + n_k^\wedge + \frac{1}{2}[\varepsilon_k^\wedge, \Omega_k^\wedge] \right. \\ &\quad \left. + \frac{1}{12}[\Omega_k^\wedge, [\Omega_k^\wedge, \varepsilon_k^\wedge]] \right). \end{aligned}$$

Recognizing terms  $\Psi(\Omega_k)(\mathcal{C}_k \varepsilon_k)^\wedge$  and  $\Psi(\Omega_k)n_k^\wedge$  in the prediction formula (8), it remains to discuss terms

$$\Psi(\Omega_k) \left( \varepsilon_k^\wedge + \frac{1}{2}[\varepsilon_k^\wedge, \Omega_k^\wedge] + \frac{1}{12}[\Omega_k^\wedge, [\Omega_k^\wedge, \varepsilon_k^\wedge]] \right). \quad (\text{A.7})$$

Evaluating (A.7):

$$\begin{aligned} \varepsilon_k^\wedge &+ \frac{1}{2}[\varepsilon_k^\wedge, \Omega_k^\wedge] + \frac{1}{12}[\Omega_k^\wedge, [\Omega_k^\wedge, \varepsilon_k^\wedge]] \\ &- \frac{1}{2} \left[ \Omega_k^\wedge, \varepsilon_k^\wedge + \frac{1}{2}[\varepsilon_k^\wedge, \Omega_k^\wedge] + \frac{1}{12}[\Omega_k^\wedge, [\Omega_k^\wedge, \varepsilon_k^\wedge]] \right] \\ &+ \frac{1}{6} \left[ \Omega_k^\wedge, \left[ \Omega_k^\wedge, \varepsilon_k^\wedge + \frac{1}{2}[\varepsilon_k^\wedge, \Omega_k^\wedge] + \frac{1}{12}[\Omega_k^\wedge, [\Omega_k^\wedge, \varepsilon_k^\wedge]] \right] \right] \\ &- \frac{1}{24} \left[ \Omega_k^\wedge, \left[ \Omega_k^\wedge, \left[ \Omega_k^\wedge, \varepsilon_k^\wedge + \frac{1}{2}[\varepsilon_k^\wedge, \Omega_k^\wedge] \right. \right. \right. \\ &\quad \left. \left. \left. + \frac{1}{12}[\Omega_k^\wedge, [\Omega_k^\wedge, \varepsilon_k^\wedge]] \right] \right] \right] \\ &+ \dots \end{aligned}$$

leads to the expression

$$\begin{aligned} \varepsilon_k^\wedge &+ [-\Omega_k^\wedge, \varepsilon_k^\wedge] + \frac{1}{2}[-\Omega_k^\wedge, [-\Omega_k^\wedge, \varepsilon_k^\wedge]] \\ &+ \frac{1}{6}[-\Omega_k^\wedge, [-\Omega_k^\wedge, [-\Omega_k^\wedge, \varepsilon_k^\wedge]]] \\ &+ \frac{5}{144}[-\Omega_k^\wedge, [-\Omega_k^\wedge, [-\Omega_k^\wedge, [-\Omega_k^\wedge, \varepsilon_k^\wedge]]]] \\ &+ \frac{1}{288}[-\Omega_k^\wedge, [-\Omega_k^\wedge, [-\Omega_k^\wedge, [-\Omega_k^\wedge, [-\Omega_k^\wedge, \varepsilon_k^\wedge]]]]] + \dots, \end{aligned}$$

which can be finally recognized as an approximation of

$$\exp(\text{ad}(-\Omega_k^\wedge))\varepsilon_k^\wedge = \text{Ad}(\exp(-\Omega_k^\wedge))\varepsilon_k^\wedge.$$

This finishes the derivation of the Lie algebraic error prediction.

## Appendix B. The special orthogonal group SO(3)

The SO(3) group is a set of orthogonal matrices with determinant one, whose elements geometrically represent rotations. Rotations in 3D can also be represented with an Euler vector (also called the axis-angle notation), where a vector  $\phi = [\phi_1 \ \phi_2 \ \phi_3]^T \in \mathbb{R}^3$  denotes a rotation about the unit vector  $\phi/|\phi|$  by the angle  $|\phi|$ . An interesting notion is that the Lie algebra  $\mathfrak{so}(3)$  is given as the skew symmetric matrix of the Euler vector

$$\phi^\wedge = \begin{bmatrix} 0 & -\phi_3 & \phi_2 \\ \phi_3 & 0 & -\phi_1 \\ -\phi_2 & \phi_1 & 0 \end{bmatrix} \in \mathfrak{so}(3), \quad (\text{B.1})$$

where  $(\cdot)^\wedge : \mathbb{R}^3 \rightarrow \mathfrak{so}(3)$  and its inverse,  $(\cdot)^\vee : \mathfrak{so}(3) \rightarrow \mathbb{R}^3$ , follow trivially. The exponential map  $\exp : \mathfrak{so}(3) \rightarrow \text{SO}(3)$  is given as Barfoot and Furgale (2014)

$$\exp(\phi^\wedge) = \cos(|\phi|)I^3 + (1 - \cos(|\phi|))\frac{\phi\phi^T}{|\phi|^2} + \sin(|\phi|)\frac{\phi^\wedge}{|\phi|}. \quad (\text{B.2})$$

Furthermore, for an  $\Phi \in \text{SO}(3)$ , the matrix logarithm, performing mapping  $\log : \text{SO}(3) \rightarrow \mathfrak{so}(3)$ , is given as

$$\log(\Phi) = \begin{cases} \frac{\gamma}{2 \sin(\gamma)}(\Phi - \Phi^T), & \text{if } \gamma \neq 0 \\ 0, & \text{if } \gamma = 0, \end{cases} \quad (\text{B.3})$$

where  $1 + 2 \cos \gamma = \text{Tr}(\Phi)$  and  $\text{Tr}(\cdot)$  designates the matrix trace. The adjoint operators  $\text{Ad}$  and  $\text{ad}$  for SO(3) are respectively given as

$$\text{Ad}(\Phi) = \Phi \quad \text{and} \quad \text{ad}(\phi^\wedge) = \phi^\wedge. \quad (\text{B.4})$$

Given the above definitions, we have all the needed ingredients to use the SO(3) group within the LG-EIF.

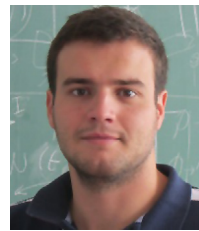
## References

- Bailey, T., Upcroft, B., & Durrant-Whyte, H. (2006). Validation gating for non-linear non-Gaussian target tracking. In *International conference on information fusion*, (pp. 1–6).
- Barfoot, T. D., & Furgale, P. T. (2014). Associating uncertainty with three-dimensional poses for use in estimation problems. *IEEE Transactions on Robotics*, 30(3), 679–693.
- Battistelli, G., & Chisci, L. (2016). Stability of consensus extended Kalman filter for distributed state estimation. *Automatica*, 68, 169–178.
- Bourmaud, G., Mégret, R., Arnaudon, M., & Giremus, A. (2015). Continuous-discrete extended Kalman filter on matrix Lie groups using concentrated Gaussian distributions. *Journal of Mathematical Imaging and Vision*, 51(1), 209–228.
- Bourmaud, G., Mégret, R., Giremus, A., & Berthoumieu, Y. (2013). Discrete extended Kalman filter on Lie groups. In *European signal processing conference, EUSIPCO*, (pp. 1–5).
- Campbell, M. E., & Whitacre, W. W. (2007). Cooperative tracking using vision measurements on SeaScan UAVs. *IEEE Transactions on Control Systems Technology*, 15(4), 613–626.
- Česić, J., Joukov, V., Petrović, I., & Kulić, D. (2016). Full body human motion estimation on Lie groups using 3D marker position measurements. In *IEEE-RAS international conference on humanoid robots, Humanoids*.
- Česić, J., Marković, I., Cvišić, I., & Petrović, I. (2016). Radar and stereo vision fusion for multitarget tracking on the special Euclidean group. *Robotics and Autonomous Systems*.
- Chirikjian, G. S., & Kyatkin, A. B. (2000). *Engineering applications of noncommutative Harmonic analysis: With emphasis on rotation and motion groups*. CRC Press.
- Engel, J., Sch, T., & Cremers, D. (2014). LSD-SLAM: Direct monocular SLAM. In *European conference on computer vision, ECCV*, (pp. 834–849).
- Eustice, R. M., Singh, H., & Leonard, J. J. (2006). Exactly sparse delayed-state filters for view-based SLAM. *IEEE Transactions on Robotics*, 22(6), 1100–1114.
- Forster, C., Carlone, L., Dellaert, F., & Scaramuzza, D. (2015). IMU preintegration on manifold for efficient visual-inertial maximum-a-posteriori estimation. In *Robotics: Science and systems* (p. 9).



- Fu, Y., Ling, Q., & Tian, Z. (2012). Distributed sensor allocation for multi-target tracking in wireless sensor networks. *IEEE Transactions on Aerospace and Electronic Systems*, 48(4), 3538–3553.
- Gilitschenski, I., Kurz, G., Julier, S.J., & Hanebeck, U.D. (2014). A new probability distribution for simultaneous representation of uncertain position and orientation. In *International conference on information fusion, FUSION*, (p. 7).
- Grocholsky, B., Makarenko, A., & Durrant-Whyte, H. (2003). Information-theoretic coordinated control of multiple sensor platforms. In *International conference on robotics and automation, Vol. 1, (ICRA)*, (pp. 1521–1526). IEEE.
- Hall, B. C. (2003). *Lie groups, Lie algebras, and representations: An elementary introduction*. Springer-Verlag.
- Hertzberg, C., Wagner, R., Frese, U., & Schröder, L. (2013). Integrating generic sensor fusion algorithms with sound state representations through encapsulation of manifolds. *Information Fusion*, 14(1), 57–77.
- Khosravian, A., Trumpf, J., Mahony, R., & Hamel, T. (2015). State estimation for invariant systems on Lie groups with delayed output measurements. *Automatica*, 68, 254–265.
- Kümmerle, R., Grisetti, G., Rainer, K., Strasdat, H., Konolige, K., & Burgard, W. (2011). g2o: A general framework for graph optimization. In *IEEE international conference on robotics and automation, ICRA*, (pp. 3607–3613).
- Kurz, G., Gilitschenski, I., & Hanebeck, U.D. (2014). The partially wrapped normal distribution for SE(2) estimation. In *International conference on multisensor fusion and information integration for intelligent systems*, no. 2, (p. 8).
- Lee, D.-J. (2008). Nonlinear estimation and multiple sensor fusion using unscented information filtering. *IEEE Signal Processing Letters*, 15(2), 861–864.
- Liu, G., Wörgötter, F., & Markelić, I. (2012). Square-root sigma-point information filtering. *IEEE Transactions on Automatic Control*, 57(11), 2945–2950.
- Maybeck, P. S. (1979). In A. Press (Ed.), *Stochastic models, estimation and control. Volume I*.
- Mur-Artal, R., Montiel, J. M. M., & Tardos, J. D. (2015). ORB-SLAM: a versatile and accurate monocular slam system. *IEEE Transactions on Robotics*, 31(5), 1147–1163.
- Murray, R. M., Li, Z., & Sastry, S. S. (1994). *A mathematical introduction to robotic manipulation*. Ann Arbor, MI: CRC.
- Nettleton, E., Durrant-Whyte, H.F., & Sukkarieh, S. (2003). A robust architecture for decentralised data fusion. In *International conference on advanced robotics, ICAR*.
- Nielsen, F., & Garcia, V. (2009). Statistical exponential families: A digest with flash cards. *Computing Research Repository*. arXiv:0911.4863.
- Onel, T., Ersoy, C., & Delic, H. (2009). Information content-based sensor selection and transmission power adjustment for collaborative target tracking. *IEEE Transactions on Mobile Computing*, 8(8), 1103–1116.
- Pakki, R., Chandra, B., & Postlethwaite, I. (2013). Square root cubature information filter. *IEEE Sensors Journal*, 13(2), 750–758.
- Rao, B. S. Y., Durrant-Whyte, H. F., & Sheen, J. A. (1993). A fully decentralized multi-sensor system for tracking and surveillance. *International Journal of Robotics Research*, 12(1), 20–44.
- Ros, G., Guerrero, J., Sappa, A. D., Ponsa, D., & Lopez, A. M. (2013). VSLAM pose initialization via Lie groups and Lie algebras optimization. In *International conference on robotics and automation, (ICRA)*, (pp. 5740–5747). IEEE.
- Selig, J. M. (1996). *Geometrical methods in robotics*. New York: Springer-Verlag.
- Thrun, S., Burgard, W., & Fox, D. (2006). *Probabilistic robotics*. The MIT Press.
- Thrun, S., Liu, Y., Koller, D., Ng, A. Y., Ghahramani, Z., & Durrant-Whyte, H. (2004). Simultaneous localization and mapping with sparse extended information filters. *International Journal of Robotics Research*, 23(7–8), 693–716.
- Vercauteren, T., & Wang, X. (2005). Decentralized sigma-point information filters for target tracking in collaborative sensor networks. *IEEE Transactions on Signal Processing*, 53(8), 2997–3009.
- Wang, Y., & Chirikjian, G. S. (2006a). Error propagation on the Euclidean group with applications to manipulator kinematics. *IEEE Transactions on Robotics*, 22(4), 591–602.
- Wang, Y., & Chirikjian, G. (2006b). Error propagation on the Euclidean group with applications to manipulator kinematics. *IEEE Transactions on Robotics*, 22(4), 591–602.
- Wang, S., Feng, J., & Tse, C. K. (2014). A class of stable square-root nonlinear information filters. *IEEE Transactions on Automatic Control*, 59(7), 1893–1898.
- Wolfe, K. C., Mashner, M., & Chirikjian, G. S. (2011). Bayesian fusion on Lie groups. *Journal of Algebraic Statistics*, 2(1), 75–97.
- Woodbury, M. A. (1950). *Inverting Modified Matrices, ser. Statistical Research Group Memorandum Reports*. Princeton, NJ: Princeton University, no. 42.

- Zhang, Y., Chai Soh, Y., & Chen, W. (2005). Robust information filter for decentralized estimation. *Automatica*, 41(12), 2141–2146.



**Josip Česić** has received his B.Sc. and M.Sc. degrees (Magna Cum Laude) in Electrical Engineering and Information Technology from University of Zagreb Faculty of Electrical Engineering and Computing (UNIZG-FER) in 2011 and 2013, respectively. He finished part of the master studies at Chalmers University of Technology, Sweden. He is employed as a research assistant at the Department of Control and Computer Engineering at UNIZG-FER since April 2013. During the undergraduate studies he received Dean's Award and Special Dean's Award for achievements on the first year of studies and the overall B.Sc. level, respectively. During the graduate studies he received the Rector's Award and Special Rector's Award for practical applications in the fields of robotics and control systems, and was awarded with several scholarships. His main research interests are in the areas of autonomous systems, mobile robotics, estimation theory and sensor processing.



**Ivan Marković** is an Assistant Professor at the University of Zagreb Faculty of Electrical Engineering and Computing, Croatia (UNIZG-FER). He received the M.Sc. and Ph.D. degrees in Electrical Engineering from the UNIZG-FER in 2008 and 2014, respectively. During his undergraduate and graduate studies he was awarded with the "INETEC" award (2007), "Josip Lončar" faculty award (2008), and with scholarship from the Croatian Ministry of Science and Education for the best students (2003–2008). In 2014 for his Ph.D. thesis he was awarded with the Silver Plaque "Josip Lončar" faculty award for outstanding doctoral dissertation and particularly successful scientific research. He is a member of the Institute of Electrical and Electronics Engineers (IEEE). He was a visiting researcher at INRIA Rennes-Bretagne Atlantique, Rennes, France, Lagadic group (Prof. François Chaumette). His research interests are mobile robotics, especially detection and tracking of moving objects and speaker localization.



tems.

**Mario Bukal** received the M.S. degree in Applied Mathematics from the University of Zagreb in 2008 and the Ph.D. in Applied Mathematics from the Vienna University of Technology in 2012. From 2012 he is with the University of Zagreb Faculty of Electrical Engineering and Computing, where he is currently an Assistant Professor. His research focus is in applied mathematics, in particular, mathematical and numerical analysis of higher-order diffusion equations, and homogenizations and dimension reduction in nonlinear elasticity theory. His research interests also include information fusion with application to robotic systems.



**Ivan Petrović** ([www.unizg.hr/hr/ivan.petrovic](http://www.unizg.hr/hr/ivan.petrovic)) is the Head of the Laboratory for Autonomous Systems and Mobile Robotics (<http://lamor.fer.hr>) and the Centre of Research Excellence for Advance Cooperative Systems-ACROSS (<http://across.fer.unizg.hr>). He has more than 30 years of professional experience in R&D of automatic control theory and its applications. In the last fifteen years his research is focused on the advanced control and estimation techniques and their application in control and navigation of autonomous mobile robots and vehicles. He published about 50 journal papers and more than 180 conference papers. Results of his research effort have been implemented in several industrial products. He is a member of IEEE, IFAC-Vice Chair of TC on Robotics and FIRA-Executive committee. He is a member of the Croatian Academy of Engineering.

## PUBLICATION 7

J. Ćesić, I. Marković, I. Cvišić and I. Petrović. Radar and stereo vision fusion for multitarget tracking on the special Euclidean group. *Robotics and autonomous systems*, 83:338–348, 2016.



# Radar and stereo vision fusion for multitarget tracking on the special Euclidean group<sup>☆</sup>



Josip Ćesić<sup>\*</sup>, Ivan Marković, Igor Cvišić, Ivan Petrović

University of Zagreb, Faculty of Electrical Engineering and Computing, Department of Control and Computer Engineering, Unska 3, 10000 Zagreb, Croatia

## HIGHLIGHTS

- Radar and stereo camera integration for tracking in ADAS.
- Detection and tracking of moving objects by filtering on matrix Lie groups.
- State space formed as a product of two special Euclidean groups.
- Employed banana-shaped uncertainties typical for range-bearing sensors and vehicles in motion.
- JIPDA filter for multitarget tracking on matrix Lie groups.

## ARTICLE INFO

### Article history:

Available online 12 May 2016

### Keywords:

Advanced driver assistance systems  
Detection and tracking of moving objects  
Joint integrated probabilistic data  
association  
Radar  
Stereo camera

## ABSTRACT

Reliable scene analysis, under varying conditions, is an essential task in nearly any assistance or autonomous system application, and advanced driver assistance systems (ADAS) are no exception. ADAS commonly involve adaptive cruise control, collision avoidance, lane change assistance, traffic sign recognition, and parking assistance—with the ultimate goal of producing a fully autonomous vehicle. The present paper addresses detection and tracking of moving objects within the context of ADAS. We use a multisensor setup consisting of a radar and a stereo camera mounted on top of a vehicle. We propose to model the sensors uncertainty in polar coordinates on Lie Groups and perform the objects state filtering on Lie groups, specifically, on the product of two special Euclidean groups, i.e.,  $SE(2)^2$ . To this end, we derive the designed filter within the framework of the extended Kalman filter on Lie groups. We assert that the proposed approach results with more accurate uncertainty modeling, since used sensors exhibit contrasting measurement uncertainty characteristics and the predicted target motions result with *banana-shaped* uncertainty contours. We believe that accurate uncertainty modeling is an important ADAS topic, especially when safety applications are concerned. To solve the multitarget tracking problem, we use the joint integrated probabilistic data association filter and present necessary modifications in order to use it on Lie groups. The proposed approach is tested on a real-world dataset collected with the described multisensor setup in urban traffic scenarios.

© 2016 Elsevier B.V. All rights reserved.

## 1. Introduction

Reliable comprehension of the surrounding environment, under varying conditions, is an essential task in nearly any assistance or autonomous system application. Since the advent

of autonomous vehicle research, scientific community has been actively engaged in developing advanced driver assistance systems (ADAS). ADAS commonly involve adaptive cruise control, collision avoidance, lane change assistance, traffic sign recognition, and parking assistance—with the final goal being a fully autonomous vehicle. ADAS have been in the focus of research for a few decades, intended to enhance the safety and reduce the possibility of a human error as a cause of road accidents [1]. An essential task in numerous ADAS applications is the detection and tracking of moving objects (DATMO), since it allows the vehicle to be aware of dynamic objects in its immanent surrounding and predict their future behavior. Since the robustness of such an application under varying environmental conditions represents a complex challenge,

<sup>☆</sup> This work has been supported by the Unity Through Knowledge Fund under the project *Cooperative Cloud based Simultaneous Localization and Mapping in Dynamic Environments* and the European Regional Development Fund under the project *Advanced Technologies in Power Plants and Rail Vehicles*.

<sup>\*</sup> Corresponding author.

E-mail addresses: [josip.cesic@fer.hr](mailto:josip.cesic@fer.hr) (J. Ćesić), [ivan.markovic@fer.hr](mailto:ivan.markovic@fer.hr) (I. Marković), [igor.cvisic@fer.hr](mailto:igor.cvisic@fer.hr) (I. Cvišić), [ivan.petrovic@fer.hr](mailto:ivan.petrovic@fer.hr) (I. Petrović).

<http://dx.doi.org/10.1016/j.robot.2016.05.001>

0921-8890/© 2016 Elsevier B.V. All rights reserved.

it has become clear that there does not exist such a sensing system that could solely deliver full information required for adequate quality of ADAS applications [2].

Given that, ADAS commonly rely on using complementary sensing systems: vision, millimeter-wave radars, laser range finder (LRF) or combinations thereof. Radar units are able to produce accurate measurements of the relative speed and distance to the objects. LRF have higher lateral resolution than the radars and, besides accurate object distance, they can detect the occupancy area of an object and provide detailed scene representation [3]. Regarding the robustness, radar units are more robust to rain, fog, snow, and similar conditions that may cause inconveniences for LRF; but, they produce significant amount of clutter as a drawback. Vision-based sensing systems can also provide accurate lateral measurements and wealth of other information from images, thus provide an effective supplement to ranging-based sensor road scene analysis. As an example, a stereo vision sensor can provide target detection with high lateral resolution and less certain range, while usually bringing enough information for identification and classification of objects, whereas radar can provide accurate measurements of range and relative speed. Given the complementarity of radars and vision systems, this combination is commonly used in research for ADAS applications. For example, works based on a monocular camera use radar for finding regions of interest in the image [4–7], process separately image and radar data [8–10], use motion stereo to reconstruct object boundaries [11,12], while [13,14] use directly stereo cameras. Employing multiple sensors, and consequently exploiting their different modalities, requires fusion of the sensing systems at appropriate levels. Depending on the approach, fusion can roughly take place at three levels: before objects detection (low level) [13, 14], at the objects' detection level (fused list of objects) [12,10], or at the state level (updating the states of objects in the list for each sensor system) [9,8,15].

Since in ADAS applications sensors with very different characteristics are used; e.g. radar with higher lateral uncertainty, but precise range estimation, and stereo camera with low lateral uncertainty but higher range imprecision, question arises on how to faithfully model the uncertainty of the state, estimated asynchronously with such sensors. Moreover, since in urban scenarios targets can exhibit varying dynamic behavior, a flexible motion model, capable of capturing the maneuvering diversity, should be used.

In the present paper, which is a continuation of our previous work presented in [16], we use a combination of a radar and a stereo vision system to perform the target tracking task. Our previous work focused on developing an appearance-based detection approach, while this paper deals with the tracking part of the DATMO procedure and uses a motion-based detection technique. Given the previous discussion, our first contribution is in modeling radar and stereo measurements arising in polar coordinates as members of Lie Groups  $SO(2) \times \mathbb{R}^1$ , and in estimating the target state as the product of two special Euclidean motion groups  $SE(2) \times SE(2) = SE(2)^2$ . This is performed within the framework of the extended Kalman filter on Lie groups, which we derive for the proposed system design. Furthermore, the target motion model also resides on the same group product and as such will yield the required model flexibility. This will not only enable us to correctly model sensor uncertainties, but also to have higher diversity in the uncertainty representation of the state estimates. For example, besides the standard Gaussian elliptically shaped uncertainty, proposed representation also supports the so called *banana-shaped* uncertainties. The second contribution of the paper is the adaptation of the joint integrated probabilistic data association (JIPDA) filter for multitarget on the  $SE(2)^2$ . To the best of the author's knowledge, this is the first use of a filtering on Lie Groups for a multitarget tracking application.

The rest of the paper is organized as follows. Section 2 presents related work and the present paper's contributions. Section 3 presents mathematical background of the LG-EKF, while Section 4 derives the proposed asynchronous LG-EKF on  $SE(2)^2$  with polar measurements. The multitarget tracking with JIPDA filter on  $SE(2)^2$  is described in Sections 5 and 6 presents the real-world experimental results. In the end, Section 7 concludes the paper.

## 2. Related work and progress beyond

Several distinct research fields relate to the study presented in this paper. These include the state estimation on Lie groups, multitarget tracking, stereo vision- and radar-based signal processing. We focus our overview of related work in the pertinent fields by considering results relevant to the present application.

To detect objects of interest, vision algorithms can resort to (i) appearances at a single time step, and (ii) motion over several frames [2]. In [17] authors employ detection procedure based on appearances in the disparity space, where clustering and extraction of moving objects are performed. The work in [18] focuses on ego-motion estimation, while moving objects stem from clustering the estimated motions in the filtered point cloud. Scene flow, i.e., the motion in 3D from stereo sequences, was used in [19,20], where adjacent points describing similar flow are considered to belong to a single rigid object. In [21] objects are also extracted from the scene flow, after which clustering is performed, and the iterative closest point algorithm is used to determine the vehicles' pose. Approach in [22] combines depth and optical flow-based clustering with an active learning-based method. In [23] pedestrians were isolated from the stereo point cloud and their pose estimated using a visibility-based 3D model, which is capable of predicting occlusions and using them in the detection process.

Concerning radar and stereo vision integration, in [14] approach based on fitting the model of a vehicle contour to both stereo depth image and radar readings was presented. First, the algorithm fits the contour from stereo depth information and finds the closest point of the contour with respect to the vision sensor. Second, it determines the closest point of the radar observation and fuses radar's and vision's closest points. By translating the initially fitted contour to the fused closest point, the resulting contour is obtained and located. Another low level integration approach was presented in [13]. In particular, the edge map of the stereo image is split into layers corresponding to different target depths so that the layers contain edge pixels of targets at different depth ranges. Hence, the original multitarget segmentation task is decomposed into several single target segmentation tasks on each depth-based layer, thus lowering the computational costs of the segmentation.

In the present paper each sensor reports its detections independently. To estimate the interim vehicle displacement, we use our visual stereo odometry algorithm (named SOFT) presented in [24]. Features not conforming to the computed displacement are considered as moving objects and are grouped together to yield measurements which are then fed to the tracking algorithm. In that respect our approach would fall within the motion-based detection approaches. The radar sensor complements detections from the stereo camera, and reports to the tracking algorithm a list of possible obstacle detections.

Irrespective of the used sensor setup, in traffic scenarios one must address the problem of multitarget tracking. This entails estimation (tracking) of each target's state and dealing with the problem of associating correct measurements to the tracked targets in cluttered environments, i.e. solving the data association problem. Commonly, for state estimation the Kalman filter and its non-linear variants are used. However, in order to achieve the proposed state uncertainty representation and motion model flexibility, in the present paper we use the extended Kalman filter



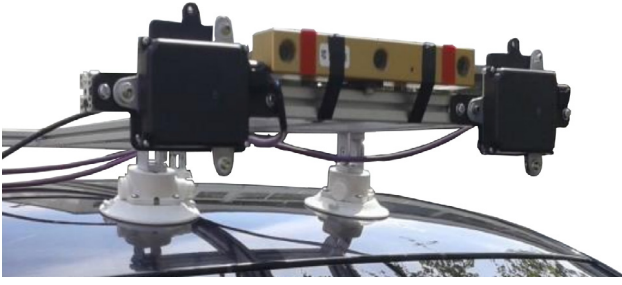


**Fig. 1.** The experimental platform mounted on top of a vehicle, consisting of a stereo camera system and two radar units.

on Lie groups (LG-EKF) [25]. This way we can track targets with the Kalman filter directly on the  $SE(2)^2$ . Considering multitarget tracking, a lot of attention has been devoted to tractable random finite sets (RFS)-based approximations of the multitarget Bayes filter: probability hypothesis density (PHD) [26–28], cardinalized PHD [29,30], and multitarget multi-Bernoulli filters [31–34]. On the other hand, data association-based algorithms, such as multiple hypothesis tracker (MHT) [35] and joint probabilistic data association (JPDA) filter [36], approach the problem by considering explicit measurement-to-target associations. In [37] the JPDA was extended to include the probability of target existence in order to alleviate the assumption of the constant and known number of targets in the scene. The two approaches are not orthogonal; filters very similar to the JIPDA and MHT can be derived from the RFS theory [38,39].

Detection results often serve as inputs to the tracking algorithm and the ADAS works most similar to the present paper are [8, 9]. In [8], the authors fuse the data from radar and image sensor to estimate the position, direction and width of objects in front of the vehicle. Therein, an ego-motion compensated tracking approach is presented which combines radar observations with the results of the contour-based image processing algorithm. The filtering aspect relies on the unscented Kalman filter and the constant turn rate and acceleration model. In [9] authors propose asynchronous independent processing of radar and vision data and use the interacting multiple model Kalman filter to cope with the changing dynamics, associating the observations via probability data association scheme. In particular, the combined motion models are the constant velocity and constant acceleration models.

Since both the stereo camera and the radar work at different frequencies, we use asynchronous filtering; in that respect our approach performs fusion at the state level. We propose to model radar and stereo measurements in polar coordinates within the LG-EKF scheme and we derive the required filter on the product of special Euclidean groups,  $SE(2)^2$ . We also provide an in-depth discussion on the behavior of the state uncertainty when fusing measurements from the used sensors. We believe that faithful uncertainty representation is an important aspect of ADAS, especially when safety applications are concerned. To handle varying dynamic behavior, our motion model will reside on  $SE(2)^2$ , since it can capture well a wide range of behavior [40]. To handle the multitarget scenario, we propose to use the JIPDA filter, which, to the best of the authors' knowledge, is its first use within the Kalman filtering on Lie groups. The proposed approach is validated in real-life experiments, where the dataset was taken in urban scenarios with the sensor setup mounted on a moving vehicle (Fig. 1).

### 3. Mathematical preliminaries

#### 3.1. Lie groups, Lie algebra and the concentrated Gaussian distribution

In this section, we provide notations and properties for matrix Lie groups and the associated Lie algebras which will be

used for the  $SE(2)^2$  filter. Lie group  $G'$  is a group which has the structure of a smooth manifold (i.e. it is sufficiently often differentiable [41]) such that group composition and inversion are smooth operations. Furthermore, for a matrix Lie group  $G$ , of which  $SE(2)$  is an example, these operations are simply matrix multiplication and inversion, with the identity matrix  $I^{n \times n}$  being the identity element [42].

Another important term is the Lie algebra  $\mathfrak{g}$  which is associated to a Lie group  $G$ . It is an open neighborhood of  $\mathbf{0}^{n \times n}$  in the tangent space of  $G$  at the identity  $I^{n \times n}$ . The matrix exponential  $\exp_G$  and matrix logarithm  $\log_G$  establish a local diffeomorphism

$$\exp_G : \mathfrak{g} \rightarrow G \quad \text{and} \quad \log_G : G \rightarrow \mathfrak{g}. \quad (1)$$

The Lie algebra  $\mathfrak{g}$  associated to a  $p$ -dimensional matrix Lie group  $G \subset \mathbb{R}^{n \times n}$  is a  $p$ -dimensional vector space defined by a basis consisting of  $p$  real matrices  $E_i, i = 1, \dots, p$  [43]. A linear isomorphism between  $\mathfrak{g}$  and  $\mathbb{R}^p$  is given by

$$[\cdot]_G^\vee : \mathfrak{g} \rightarrow \mathbb{R}^p \quad \text{and} \quad [\cdot]_G^\wedge : \mathbb{R}^p \rightarrow \mathfrak{g}. \quad (2)$$

Lie groups are generally non-commutative and require the use of two operators which enable the adjoint representation of (i)  $G$  on  $\mathbb{R}^p$  denoted as  $\text{Ad}_G$  and (ii)  $\mathbb{R}^p$  on  $\mathbb{R}^p$  denoted as  $\text{ad}_G$  [42,44].

In order to define the concept of the concentrated Gaussian distribution on Lie groups, necessary for introduction of the LG-EKF, the considered Lie group needs to be a connected unimodular matrix Lie group [45], which is the case of the majority of Lie groups used in robotics.

Let the pdf of  $X$  be defined as [46]

$$p(X) = \beta \exp \left( -\frac{1}{2} [\log_G(X)]_G^\vee P^{-1} [\log_G(X)]_G^\vee \right), \quad (3)$$

where  $\beta$  is a normalizing constant. Let  $\epsilon$  be defined as  $\epsilon \triangleq [\log_G(X)]_G^\vee$ . Under the assumption that the entire mass of probability is contained inside  $G$ , i.e.,  $\int_{\mathbb{R}^{n \times n} \setminus G} p(X) = 0$ ,  $\epsilon$  can be described with  $\epsilon \sim \mathcal{N}_{\mathbb{R}^p}(\mathbf{0}^{p \times 1}, P)$ . This concept is called a concentrated Gaussian distribution (CGD) on  $G$  around the identity [25]. Furthermore, it is a unique parametrization space where the bijection between  $\exp_G$  and  $\log_G$  exists. Now, the distribution of  $X$  can be translated over  $G$  by using left action of the Lie group

$$X = \mu \exp_G([\epsilon]_G^\wedge), \quad \text{with } X \sim \mathcal{G}(\mu, P), \quad (4)$$

where  $\mathcal{G}$  denotes the CGD [46,25]. By this, we have introduced the distribution forming the base for the LG-EKF.

#### 3.2. The Special Euclidean group $SE(2)$

The group  $SE(2)$  describes rigid body motion in 2D and is formed as a semi-direct product of the plane  $\mathbb{R}^2$  and the special orthogonal group  $SO(2)$  corresponding to translational and rotational elements. It is defined as

$$SE(2) = \left\{ \begin{pmatrix} R & \mathbf{t} \\ \mathbf{0}_{1 \times 1} & 1 \end{pmatrix} \in \mathbb{R}^{3 \times 3} \mid \{R, \mathbf{t}\} \in SO(2) \times \mathbb{R}^2 \right\}. \quad (5)$$

Now, we continue with providing the basic ingredients for working with  $SE(2)$ , giving relations for operators presented in Section 3.1, needed for manipulations within the triplet: Lie group  $G$ , Lie algebra  $\mathfrak{g}$ , and Euclidean space  $\mathbb{R}^p$ .

For a Euclidean space vector  $\mathbf{x} = [x \ y \ \theta]^T$ , the most often associated element of the Lie algebra  $\mathfrak{se}(2)$  is given as

$$[\mathbf{x}]_{SE(2)}^\wedge = \begin{bmatrix} [\mathbf{x}]_{SO(2)}^\wedge & x \\ \mathbf{0}_{1 \times 2} & y \end{bmatrix} \in \mathfrak{se}(2) \quad (6)$$

$$[\mathbf{x}]_{SO(2)}^\wedge = \begin{bmatrix} 0 & -\theta \\ \theta & 0 \end{bmatrix} \in \mathfrak{so}(2). \quad (7)$$

Their inverses,  $[\cdot]_{SE(2)}^\vee$  and  $[\cdot]_{SO(2)}^\vee$ , follow trivially from the relations (6) and (7), respectively.

The exponential map for the SE(2) group is given as

$$\exp_{SE(2)}([\mathbf{x}]_{SE(2)}^\wedge) = \begin{bmatrix} \exp_{SO(2)}([\theta]_{SO(2)}^\wedge) & \begin{bmatrix} t_x \\ t_y \end{bmatrix} \\ \mathbf{0}_{1 \times 2} & 1 \end{bmatrix} \in SE(2) \quad (8)$$

$$\exp_{SO(2)}([\theta]_{SO(2)}^\wedge) = \begin{bmatrix} \cos \theta & -\sin \theta \\ \sin \theta & \cos \theta \end{bmatrix} \in SO(2) \quad (9)$$

$$t_x = \frac{1}{\theta} [x \sin \theta + y(-1 + \cos \theta)] \quad (10)$$

$$t_y = \frac{1}{\theta} [x(1 - \cos \theta) + y \sin \theta]. \quad (11)$$

For  $T = \{R, \mathbf{t}\} \in SE(2)$ , the logarithmic map is

$$\log_{SE(2)}(T) = \begin{bmatrix} \mathbf{v} \\ \theta \end{bmatrix}_{SE(2)}^\wedge \in \mathfrak{se}(2) \quad (12)$$

$$\theta = \log_{SO(2)}(R) = \text{atan2}(R_{21}, R_{11}) \quad (13)$$

$$\mathbf{v} = \frac{\theta}{2(1 - \cos \theta)} \begin{bmatrix} \sin \theta & 1 - \cos \theta \\ \cos \theta - 1 & \sin \theta \end{bmatrix} \mathbf{t}. \quad (14)$$

The Adjoint operator  $\text{Ad}_G$  used for representing  $T \in SE(2)$  on  $\mathbb{R}^3$  is given as

$$\text{Ad}_{SE(2)}(T) = \begin{bmatrix} R & J\mathbf{t} \\ \mathbf{0}_{1 \times 2} & 1 \end{bmatrix} \quad \text{with } J = \begin{bmatrix} 0 & 1 \\ -1 & 0 \end{bmatrix}, \quad (15)$$

while the adjoint operator  $\text{ad}_G$  for representing  $\mathbf{x} \in \mathbb{R}^3$  on  $\mathbb{R}^3$  is given by

$$\text{ad}_{SE(2)}(\mathbf{x}) = \begin{bmatrix} -\theta J & J\mathbf{v} \\ \mathbf{0}_{1 \times 2} & 1 \end{bmatrix}, \quad (16)$$

where  $\mathbf{v} = [x \ y]^T \in \mathbb{R}^2$ . Given the definitions above, we have all the needed ingredients for using the SE(2) motion group within the proposed approach.

## 4. Second order rigid body motion estimation

### 4.1. State space construction

As a rigid body, vehicle's state can be well described employing the rigid body motion group. Furthermore, when considering velocities of such an object, we can also represent these higher order moments by using the same motion group. Following the rigid body equivalent of the constant velocity motion model [47], here we model the vehicle by constructing the state space  $G$  as the Cartesian (direct) product of the two matrix Lie group SE(2) members [40]

$$SE(2) \times SE(2) = SE(2)^2. \quad (17)$$

The first SE(2) member is the position component, while the second one contributes the velocity components. This can be regarded as a white noise acceleration model [47] on the SE(2) group. Considering vehicle tracking applications, in contrast to other well established motion models—constant velocity, constant turn rate and velocity, constant curvature and velocity [48,49]—the  $SE(2)^2$  motion model provides more artificial flexibility. This flexibility is manifested through including the holonomic behavior over all three velocity components, i.e., the longitudinal, lateral, and rotational velocities, which have Wiener process characterization [47]. Such flexibility provides the ability to describe motion of objects appearing in ADAS, e.g., vehicles, motorcycles and pedestrians, and hence is appropriate for usage in our particular DATMO focused application.

Matrix Lie group composition and inversion are simple matrix multiplication and inversion, hence for all the calculations dealing with operations on  $G$ , we can use the symbolic representation constructed by placing the two SE(2) members of  $G$  block diagonally. The Lie algebra associated to the Lie group  $G$  is denoted as  $\mathfrak{g} = \mathfrak{se}(2) \times \mathfrak{se}(2)$ . The term  $[\mathbf{x}]_G^\wedge$  is also constructed by placing both  $\mathfrak{se}(2)$  members on the main diagonal, and correspondingly the exponential map on such  $G$  is as well formed block diagonally. For more details on the construction and symbolical representation of the groups of interest, please confer [40] where the state model was first proposed.

### 4.2. Motion model and prediction

The motion model satisfies the following equation

$$X_{k+1} = f(X_k, n_k) = X_k \exp_G([\hat{\Omega}_k + n_k]_G^\wedge), \quad (18)$$

where  $X_k \in G$  is the state of the system at time  $k$ ,  $G$  is a  $p$ -dimensional Lie group,  $n_k \sim \mathcal{N}_{\mathbb{R}^p}(\mathbf{0}^{p \times 1}, Q_k)$  is white Gaussian noise and  $\hat{\Omega}_k = \Omega(X_k) : G \rightarrow \mathbb{R}^p$  is a non-linear  $\mathcal{C}^2$  function. If the posterior distribution at step  $k - 1$  follows the concentrated Gaussian distribution on matrix Lie Groups as  $\mathcal{G}(\mu_{k-1}, P_{k-1})$ . The predicted mean is given by [25]

$$\mu_{k+1|k} = \mu_k \exp_G([\hat{\Omega}_k]_G^\wedge). \quad (19)$$

We model the motion (18) by [40]

$$\Omega(X_k) = [T v_{x_k} \ T v_{y_k} \ T \omega_k \ 0 \ 0 \ 0]^T \in \mathbb{R}^6, \quad (20)$$

$$n_k = \left[ \frac{T^2}{2} n_{x_k} \ \frac{T^2}{2} n_{y_k} \ \frac{T^2}{2} n_{\omega_k} \ T n_{x_k} \ T n_{y_k} \ T n_{\omega_k} \right]^T \in \mathbb{R}^6.$$

With this model, the system is corrupted with white noise over three components, i.e.  $n_x$  is the noise in the local  $x$  direction,  $n_y$  is the noise in local  $y$  direction and  $n_w$  is the noise in the rotational component.

Formula for propagating the covariance of  $\epsilon_{k+1|k}$  through the general motion model (18) is given as in [25]

$$P_{k+1|k} = \mathcal{F}_k P_k \mathcal{F}_k^T + \Phi_G(\hat{\Omega}_k) Q_k \Phi_G(\hat{\Omega}_k)^T, \quad (21)$$

where the operator  $\mathcal{F}_k$ , a matrix Lie group equivalent to the Jacobian of  $f(X_k, n_k)$ , and  $\Phi_G$ , are evaluated as

$$\mathcal{F}_k = \text{Ad}_G \left( \exp_G([\hat{\Omega}_k]_G^\wedge) \right) + \Phi_G(\hat{\Omega}_k) \mathcal{E}_k$$

$$\Phi_G(\mathbf{v}) = \sum_{m=0}^{\infty} \frac{(-1)^m}{(m+1)!} \text{ad}_G(\mathbf{v})^m, \ \mathbf{v} \in \mathbb{R}^p \quad (22)$$

$$\mathcal{E}_k = \frac{\partial}{\partial \epsilon} \Omega(\mu_k \exp_G([\epsilon]_G^\wedge))|_{\epsilon=0}.$$

The covariance propagation is challenging since it requires calculation of (22). The final expression for  $\mathcal{E}_k$  is thus given as

$$\mathcal{E}_k = \begin{bmatrix} \mathbf{0}_{3 \times 3} & T \cos \omega_k & -T \sin \omega_k & 0 \\ & T \sin \omega_k & T \cos \omega_k & 0 \\ & 0 & 0 & T \\ \mathbf{0}_{3 \times 3} & & \mathbf{0}_{3 \times 3} & \end{bmatrix}. \quad (23)$$

The complete derivation of  $\mathcal{E}_k$  is given in [40]. The adjoint operators  $\text{Ad}_G$  and  $\text{ad}_G$  are also formed block diagonally.

The last needed ingredient is the process noise covariance matrix  $Q_k$ . In the present paper, we perform sensor fusion in an asynchronous manner with the arrival of each measurement. Hence, we proceed by defining the process to follow continuous white noise acceleration model (CWNA) over the three components discussed

previously. In the sequel, we derive the discrete time process noise by relating it to the continuous one [47]. Let  $\tilde{q}_x$ ,  $\tilde{q}_y$  and  $\tilde{q}_\omega$  denote the time-invariant continuous time process noise intensities reflecting power spectral density over all three components. Then, the process noise covariance matrix  $Q$  evaluates to

$$Q = \begin{bmatrix} \frac{T^3}{3}\tilde{q}_x & 0 & 0 & \frac{T^2}{2}\tilde{q}_x & 0 & 0 \\ 0 & \frac{T^3}{3}\tilde{q}_y & 0 & 0 & \frac{T^2}{2}\tilde{q}_y & 0 \\ 0 & 0 & \frac{T^3}{3}\tilde{q}_\omega & 0 & 0 & \frac{T^2}{2}\tilde{q}_\omega \\ \frac{T^2}{2}\tilde{q}_x & 0 & 0 & T\tilde{q}_x & 0 & 0 \\ 0 & \frac{T^2}{2}\tilde{q}_y & 0 & 0 & T\tilde{q}_y & 0 \\ 0 & 0 & \frac{T^2}{2}\tilde{q}_\omega & 0 & 0 & T\tilde{q}_\omega \end{bmatrix}. \quad (24)$$

At this point, we have defined all the necessary ingredients for the asynchronous prediction step of the LG-EKF filter.

#### 4.3. Measurement model and correction

The discrete measurement model on the matrix Lie group is defined as

$$Z_{k+1} = h(X_{k+1}) \exp_{G'}([m_{k+1}]_{G'}^\wedge), \quad (25)$$

where  $Z_{k+1} \in G'$ ,  $h: G \rightarrow G'$  is a  $\mathcal{C}^1$  function and  $m_{k+1} \sim \mathcal{N}_{\mathbb{R}^q}(\mathbf{0}^{q \times 1}, R_{k+1})$  is white Gaussian noise.

The predicted system state is described with  $X_{k+1|k} \sim \mathcal{G}(\mu_{k+1|k}, P_{k+1|k})$  and now we proceed to updating the state by incorporating the newly arrived measurement  $Z_{k+1} \in G'$ . In this case, we propose the measurements to arise in the space of a Lie group constructed as  $G' = \text{SO}(2) \times \mathbb{R}^1$ , measuring the current position of the tracked object in 2D in polar coordinates. The radar and the stereo camera, as well as many other widely spread on-board sensing systems, perceive the surrounding from a single point, and hence perform the measurement in polar coordinates. Thus the uncertainty of such measurements, i.e. the measurement likelihood, resembles *banana-shaped* contours rather than the elliptical ones. In order to integrate such sensing modalities into the LG-EKF, we now introduce necessary ingredients for the update step of the filter.

The measurement function is mapping  $h: \text{SE}(2) \times \text{SE}(2) \rightarrow \text{SO}(2) \times \mathbb{R}^1$ . It is given as

$$h(X_{k+1}) = \begin{bmatrix} \exp_{\text{SO}(2)} \left( \left[ \arctan \frac{y_{k+1}}{x_{k+1}} \right]_{\text{SO}(2)}^\wedge \right) \\ \exp_{\mathbb{R}^1} \left( \left[ \sqrt{x_{k+1}^2 + y_{k+1}^2} \right]_{\mathbb{R}^1}^\wedge \right) \end{bmatrix}. \quad (26)$$

The exponential and logarithm on  $\mathbb{R}^p$  follows a mapping procedure and is only a matter of representation. Hence we introduce  $\exp_{\mathbb{R}}$  for implementation purposes only, to follow the matrix representation of the procedure, hence each composition and inversion follow matrix multiplication and inversion procedures, even when working with Euclidean space. In particular, the Euclidean space is a trivial example of a matrix Lie group, so the representation of  $v \in \mathbb{R}^p$  in the form of a Lie algebra  $[v]_{\mathbb{R}^p}^\wedge \subset \mathbb{R}^{p+1 \times p+1}$  and matrix Lie group  $\exp_{\mathbb{R}^p}([v]_{\mathbb{R}^p}^\wedge) \subset \mathbb{R}^{p+1 \times p+1}$  is given as

$$[v]_{\mathbb{R}^p}^\wedge = \begin{bmatrix} \mathbf{0}^{p \times p} & v \\ \mathbf{0}^{1 \times p} & 0 \end{bmatrix} \quad \text{and} \quad \exp_{\mathbb{R}^p}([v]_{\mathbb{R}^p}^\wedge) = \begin{bmatrix} \mathbf{I}^{p \times p} & v \\ \mathbf{0}^{1 \times p} & 1 \end{bmatrix}. \quad (27)$$

One should note that there exists a trivial mapping between the members of the triplet  $v$ ,  $[v]_{\mathbb{R}^p}^\wedge$  and  $\exp_{\mathbb{R}^p}([v]_{\mathbb{R}^p}^\wedge)$ , hence the formal inverses of the terms from (27) are omitted here.

Let us now define the following innovation term

$$\begin{aligned} \tilde{Z}_{k+1} &= [\log_{G'}(h(\mu_{k+1|k})^{-1}Z_{k+1})]_{G'}^\vee \\ &= \mathcal{H}_{k+1}\epsilon_{k+1|k} + m_{k+1} + \mathcal{O}(\|\epsilon_{k+1|k}\|^2, \|m_{k+1}\|^2) \end{aligned} \quad (28)$$

which is linear in the lie algebraic error  $\epsilon_{k+1|k} \sim \mathcal{N}_{\mathbb{R}^p}(\mathbf{0}^{p \times 1}, P_{k+1|k})$ . Now, we can apply the classical update equations employing the measurement model to update the Lie algebraic mean and covariance, such that  $\epsilon_{k+1}^- \sim \mathcal{N}_{\mathbb{R}^p}(\mu_{k+1}^-, P_{k+1}^-)$ . The update step of the filter, based on the measurement model (25), strongly resembles the standard EKF update procedure [48], relying on the Kalman gain  $K_{k+1}$  and innovation vector  $v_{k+1}$ , and is calculated as

$$\begin{aligned} K_{k+1} &= P_{k+1|k} \mathcal{H}_{k+1}^T (\mathcal{H}_{k+1} P_{k+1|k} \mathcal{H}_{k+1}^T + R_{k+1})^{-1} \\ v_{k+1} &= [\log_{G'}(h(\mu_{k+1|k})^{-1}Z_{k+1})]_{G'}^\vee. \end{aligned} \quad (29)$$

Hence the updated Lie algebraic error  $\epsilon_{k+1}^-$  is given as

$$\begin{aligned} \mu_{k+1}^- &= K_{k+1} v_{k+1} \\ P_{k+1}^- &= (\mathbf{I}^{p \times p} - K_{k+1} \mathcal{H}_{k+1}) P_{k+1|k}. \end{aligned} \quad (30)$$

The matrix  $\mathcal{H}_k$  can be seen as the measurement matrix of the system, i.e. a matrix Lie group equivalent to the Jacobian of  $h(X_k)$ , and is given as

$$\mathcal{H}_{k+1} = \frac{\partial}{\partial \epsilon} [\log_{G'}(h(\mu_{k+1|k})^{-1}h(\mu_{k+1|k} \exp_G([\epsilon]_G^\wedge)))]_{G|\epsilon=0}^\vee. \quad (31)$$

The final expression of the measurement matrix  $\mathcal{H}_{k+1}$  is given as follows

$$\mathcal{H}_{k+1} = \begin{bmatrix} \frac{-y \cos \theta + x \sin \theta}{x^2 + y^2} & \frac{x \cos \theta + y \sin \theta}{y^2} \\ \frac{x \cos \theta + y \sin \theta}{\sqrt{x^2 + y^2}} & \frac{y \cos \theta - x \sin \theta}{\sqrt{x^2 + y^2}} \mathbf{0}^{2 \times 4} \end{bmatrix}. \quad (32)$$

Note that the subscript indices determining the time step of the filter have been omitted in the previous expression due to clarity, i.e.  $\theta_{k+1|k} \triangleq \theta$ ,  $x_{k+1|k} \triangleq x$  and  $y_{k+1|k} \triangleq y$ . Detailed derivation of the matrix  $\mathcal{H}_{k+1}$  is given in the Appendix.

The update procedure is expected to deliver the concentrated Gaussian distribution such that  $X = \mu \exp_G([\epsilon]_G^\wedge)$ , with expectation  $\mathbb{E}[\epsilon] = \mathbf{0}^{p \times 1}$ . However, since operating with generally non-Euclidean spaces, we have  $\mathbb{E}[\epsilon_{k+1}^-] = \mu_{k+1}^- \neq \mathbf{0}^{p \times 1}$  which is resolved by state reparametrization [25]. The mean and the covariance are updated as

$$\begin{aligned} \mu_{k+1} &= \mu_{k+1|k} \exp_G([\mu_{k+1}^-]_G^\wedge) \\ P_{k+1} &= \Phi_G(\mu_{k+1}^-) P_{k+1}^- \Phi_G(\mu_{k+1}^-)^T. \end{aligned} \quad (33)$$

As in the case of the prediction step, the state  $X_{k+1} \sim \mathcal{G}(\mu_{k+1}, P_{k+1})$  has remained  $\mathcal{G}$ -distributed after correction. Now we have all the means for updating the filter by calculating the Kalman gain  $K_{k+1}$  and the innovation vector  $v_{k+1}$  (29), and finally correcting the mean  $\mu_{k+1}$  and the covariance matrix  $P_{k+1}$  (33).

Fig. 2 shows examples of LG-EKF filter state uncertainties updated with three different sensors types. In all the examples the filter prediction follows the  $\text{SE}(2)^2$  motion model and yields *banana-shaped* state uncertainties. In Fig. 2(a) we show an example of updating the filter with a sensor having elliptical measurement uncertainty; this resembles ‘classical’ Gaussian like uncertainty. In Fig. 2(b) we depict update with a sensor that has larger uncertainty in the bearing than in the range and the update of the filter acts as ‘intersecting’ the two *banana-shaped* distributions.

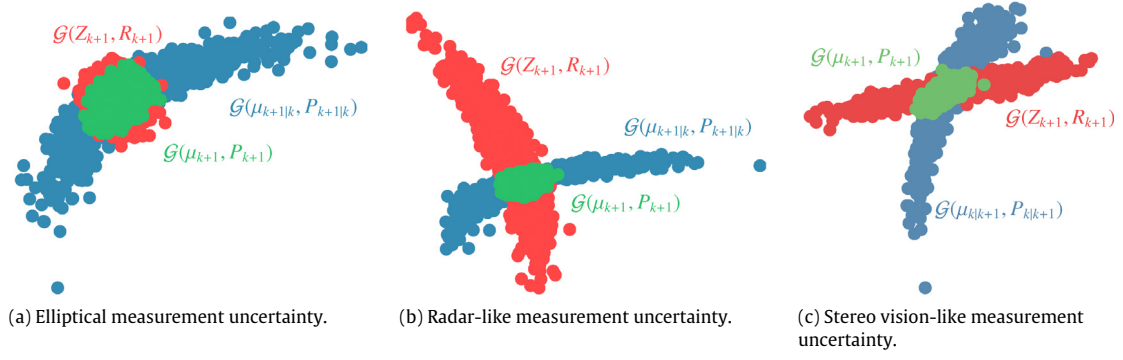


**Fig. 2.** Examples of LG-EKF state uncertainties when updated with sensors having different measurement characteristics. The filter prediction in blue follows the SE(2)<sup>2</sup> motion model, measurement is depicted in red, and the updated state is depicted in green. We can notice that the LG-EKF filter can capture a wide range of uncertainty contours; from Gaussian elliptical uncertainties to *banana-shaped* uncertainties typical for range-bearing sensors and vehicles in motion with non-zero turn rate deviation.

This example resembles update performed with a radar unit. Finally, Fig. 2(c) shows the example with sensor having larger uncertainty in the range than in the bearing. Notice how the prediction uncertainty skews to the right indicating that the vehicle had higher probability of turning right than left. This example resembles update performed with the stereo vision sensor. From the above examples we can see how the filter can handle diverse measurement uncertainties and efficiently fuse them with the information from the prediction step. Having finished with the single target filtering, what is left is to resolve the LG-EKF tracking with multiple targets in the scene.

## 5. Joint integrated probabilistic data association

Assume that we are tracking multiple targets,  $\{\mathcal{T}_1, \dots, \mathcal{T}_{t_k}\}$ , with the number of targets,  $t_k$ , varying with time, i.e., targets can appear and disappear from the sensors' field-of-view. Let  $Z_k$  denote the set of all measurements at time step  $k$

$$Z_k = \{Z_k^j : j = 1, \dots, m_k\},$$

and  $Z_{1:k} = \{Z_1, \dots, Z_k\}$  the history of all the measurements. The vector  $Z_k$ , besides target originating measurements, also contains clutter which is a Poisson distributed random variable. The main issue at hand is how to appropriately assign the received measurement set to the targets in track, and how to manage the target appearance and disappearance.

The JIPDA [37] approaches this problem by estimating the following a posteriori density for each  $\mathcal{T}_i$

$$p(X_k^i, \chi_k^i | Z_{1:k}) = p(X_k^i | \chi_k^i, Z_{1:k})p(\chi_k^i | Z_{1:k}), \quad (34)$$

i.e., the density of the target's state  $X_k^i$  and its existence  $\chi_k^i$  given all the measurements up to and including  $k$ . Note that in the present paper,  $X_k^i$  is distributed according to  $\mathcal{G}(\mu_k^i, P_k^i)$  as in the case of (4). For the probability of target existence, we adopt the Markov Chain One model [37]

$$p(\chi_k^i | Z_{1:k-1}) = p_s p(\chi_{k-1}^i | Z_{1:k-1}), \quad (35)$$

where  $p_s$  denotes the probability that target will continue to exist at step  $k$  given that it existed at step  $k-1$ .

In order to alleviate computational complexity, at each scan tracks are separated into clusters which share selected measurements. As a criteria for measurement-to-track validation, the gating principle is used where based on the innovation uncertainty (29) a gating volume is defined, and measurements falling within are accepted as cluster members. For notation clarity we will not differentiate measurements belonging to the cluster from those outside of the clusters. The former will participate in the data association operations, while the latter

will be treated as candidates for new tracks initialization. For filtering on LG, validation gate is defined in the algebra where measurements are associated to targets, and if multiple targets share the same measurements they are formed into a cluster. The ensuing formulae will pertain to a single cluster and all the measurements and targets are assumed to belong to the cluster.

Upon availability of a set of new measurements  $Z_k = \{Z_k^j : j = 1, \dots, m_k\}$ , the following set of hypotheses is built:

$$\theta_k^{ij} = \{Z_k^j \text{ is caused by } \mathcal{T}_i\}, \quad j = 1, \dots, m_k, \quad \text{and}$$

$$\theta_k^{i0} = \{\text{none of the measurements is caused by } \mathcal{T}_i\}.$$

The total probability formula implies that the posterior density for object  $\mathcal{T}_i$  at scan  $k$  is given by [37]

$$\begin{aligned} p(X_k^i, \chi_k^i | Z_{1:k}) &= p(\chi_k^i | Z_{1:k}) \sum_{j=0}^{m_k} p(X_k^i | \theta_k^{ij}, \chi_k^i, Z_{1:k}) p(\theta_k^{ij} | \chi_k^i, Z_{1:k}) \\ &= p(\chi_k^i | Z_{1:k}) \sum_{j=0}^{m_k} \beta_k^{ij} p(X_k^i | \theta_k^{ij}, \chi_k^i, Z_{1:k}), \end{aligned} \quad (36)$$

where  $\beta_k^{ij} = p(\theta_k^{ij} | \chi_k^i, Z_{1:k})$  represent a posteriori *data association probabilities* conditioned on object existence. Explicitly,  $\beta_k^{ij}$  is the probability that measurement  $z_k^j$  is caused by  $\mathcal{T}_i$  and  $\beta_k^{i0}$  is the probability that none of the measurements is caused by  $\mathcal{T}_i$ . The densities  $p(X_k^i | \theta_k^{ij}, \chi_k^i, Z_{1:k})$  represent 'classically' updated LG-EKF (30) for  $j = 1, \dots, m_k$ , while for  $j = 0$  the density is just the prediction calculated via (18) and (21). Parameters of the mixture components are denoted by  $\mu_{k+1}^{ij,-}$  and  $P_{k+1}^{ij,-}$ , specifically, when  $j = 0$ ,  $\mu_{k+1}^{i0,-} = \mu_{k+1|k}^i$  and  $P_{k+1}^{i0,-} = P_{k+1|k}^i$ .

In order to calculate  $\beta_k^{ij}$  we need to take into account measurement-to-object associations events jointly across the set of objects in the cluster. This means that hypothesis  $\theta_k^{ij}$  consists of all *feasible joint events*  $\mathcal{E}$  where each track is assigned zero or one measurement and each measurement is allocated to zero or one track; thus, they partition the hypothesis  $\theta_k^{ij}$  and

$$p(\theta_k^{ij}, \chi_k^i | Z_{1:k}) = \sum_{\mathcal{E} \in \theta_k^{ij}} P(\mathcal{E} | Z_{1:k}), \quad j > 1, \quad (37)$$

$$p(\theta_k^{i0} | Z_{1:k}) = 1 - p(\theta_k^{ij}, \chi_k^i | Z_{1:k}). \quad (38)$$

Furthermore, probability that  $\mathcal{T}_i$  exists and that no measurement in the cluster is its detection, is given by [37]

$$p(\theta_k^{i0}, \chi_k^i | Z_{1:k}) = \frac{(1 - P_G^i P_G^i) p(\chi_k^i | Z_{1:k})}{1 - P_G^i P_G^i p(\chi_k^i | Z_{1:k})} p(\theta_k^{i0} | Z_{1:k}). \quad (39)$$



To calculate  $P(\mathcal{E} \mid Z^{1:k})$ , for each joint event  $\mathcal{E}$  we define: set of targets allocated no measurement,  $T_0(\mathcal{E})$ , and set of tracks allocated one measurement,  $T_1(\mathcal{E})$ . Following [37,38] we obtain

$$P(\mathcal{E} \mid Z^{1:k}) = C_k^{-1} \prod_{i \in T_0(\mathcal{E})} (1 - P_d^i P_G^i P(\chi_k^i \mid Z^{1:k-1})) \cdot \prod_{i \in T_1(\mathcal{E})} P_d^i P_G^i P(\chi_k^i \mid Z^{1:k-1}) \frac{p_k^i(\tau(\mathcal{E}, i))}{\rho_k(\tau(\mathcal{E}, i))}, \quad (40)$$

where  $P_d^i$  is the probability of  $\mathcal{T}_i$  being detected,  $P_G^i$  is the probability that the correct measurement will be inside the validation gate of  $\mathcal{T}_i$ ,  $\tau(\mathcal{E}, i)$  is the index of measurement allocated to  $\mathcal{T}_i$  under joint event  $\mathcal{E}$ ,  $\rho_k(\tau(\mathcal{E}, i))$  denotes a priori clutter measurement density at  $\mathbf{z}_k^{\tau(\mathcal{E}, i)}$ , and  $C_k^{-1}$  is the normalization constant calculated from the fact that  $\mathcal{E}$  are mutually exclusive and form an exhaustive set, i.e.,  $\sum_{\mathcal{E}} P(\mathcal{E} \mid Z^{1:k}) = 1$ . The innovation is calculated by using results from (29)

$$p_k^i(\tau(\mathcal{E}, i)) = \frac{1}{P_G} p_k^i(v_k^{\tau(\mathcal{E}, i)}; 0, \mathcal{H}_{k+1} P_{k+1|k} \mathcal{H}_{k+1}^T + R_{k+1}). \quad (41)$$

The innovation in (41) is normalized by  $P_G$  in order to account for the validation gating, i.e., since it is truncated to integrate to unity. Finally, we have all the elements to determine the probability of target existence

$$p(\chi_k^i \mid Z^{1:k}) = \sum_{j=0}^{m_k} p(\theta_k^{ij}, \chi_k^i \mid Z^{1:k}), \quad (42)$$

and to calculate the data association probabilities

$$\beta_k^{ij} = \frac{p(\theta_k^{ij}, \chi_k^i \mid Z^{1:k})}{p(\chi_k^i \mid Z^{1:k})}, \quad j = 0, \dots, m_k. \quad (43)$$

Note that all the operations concerning a specific target  $\mathcal{T}_i$ , described so far in the section, are carried out in the pertaining algebra of  $\mu_{k+1|k}^i$ , since, we are still at the update stage of the LG-EKF. To calculate the final a posteriori state estimate the JIPDA logic dictates reducing the mixture in (36) to a single density with the following parameters [50,38]

$$\mu_{k+1}^{i,-} = \sum_{j=0}^{m_k} \beta_k^{ij} \mu_{k+1}^{ij,-}, \quad (44)$$

$$P_{k+1}^{i,-} = \sum_{j=0}^{m_k} (\beta_k^{ij} + \mu_{k+1}^{ij,-} (\mu_{k+1}^{ij,-})^T) - \mu_{k+1}^{i,-} (\mu_{k+1}^{i,-})^T. \quad (45)$$

As in the case of the LG-EKF update,  $\mathbb{E}[\epsilon_{k+1}^-] = \mu_{k+1}^{i,-} \neq 0^{p \times 1}$ ; thus, before mapping the updated state and covariance to G we have to perform reparametrization [40]

$$\mu_{k+1}^i = \mu_{k+1|k}^i \exp_G \left( [\mu_{k+1}^{i,-}]_G^\wedge \right) \quad (46)$$

$$P_{k+1}^i = \Phi_G(\mu_{k+1}^i) P_{k+1}^{i,-} \Phi_G(\mu_{k+1}^i)^T.$$

## 6. Experimental results

### 6.1. System overview

The experiments were carried out using two radar units and a stereo camera system, mounted on a sensor platform on top of a vehicle. The sensor platform was constructed so that the stereo camera is placed in-between the two radar units as shown in Fig. 1.

In the present paper we used the Continental Short Range Radar 209–2 units (measurement range of 50 m) configured to operate in the cluster mode, at a rate of 15 Hz. The field of view

is 150° horizontally and 12° vertically, with the resolution in the horizontal direction of 1°, while there is no discrimination of the angle in vertical direction, and hence the radar cluster data can be considered as 2D measurements. After each scanning cycle the radar can deliver a cluster consisting of up to 128 detections. In the prefiltering stage we dismissed all the cluster measurements whose radar cross section, i.e., the measure of the reflective strength, did not exceed −5 dBm.

The stereo images were recorded with the monochrome Point Grey Bumblebee XB3 camera system. This system is a 3-sensor multi-baseline stereo camera with 1.3 mega-pixel global shutter sensors. The image resolution is 1280 × 960 pixels, with horizontal field of view of 66°. The experiments were carried out at the maximum frame rate of 16 Hz, and by using the largest, 24 cm long baseline, since the expected target measurement range is up to 50 m. The stereo image synchronization was executed internally, while the experiment was recorded in the auto-exposure mode of the camera.

Given that the sensors are closely spaced, mechanically aligned using custom-made plates on the same rail, and since we perform sensor fusion at the state level, the inter-sensor calibration was done by measuring the mounting position displacements by hand. Moreover, due to the coarse nature of radar measurements we find the current rail-mounting sufficiently precise to assert that differences in the orientation of the sensor coordinate frames can be neglected for case of the present sensor setup. However, for arbitrary radar and stereo vision setups a closer inspection of the calibration problem might be required [7]. Furthermore, special attention was taken to assure the clock synchronization, since our approach relies on state estimation performed in an asynchronous manner. Although both sensors work at close frequencies, generally this might not be the case, and the approach of asynchronous filtering is kept for the sake of generality. The prediction step directly depends on the time period  $T$ , i.e., the time passed between the two consecutive steps  $k$  and  $k + 1$ . Therefore, a clock drift or large delay in data acquisition could significantly affect the performance of the algorithm.

### 6.2. Stereo detection procedure

The main goal of the stereo image processing part of the algorithm is to detect moving objects in the scene, while the motion of the observer makes this task especially challenging. However, this work focuses on the estimation procedure and the fusion of two sensor modalities, hence the sole stereo based detection of moving objects is only briefly described.

The first part of the algorithm works on the ego-motion estimation, which results in transformation matrix between the previous and the current camera frame. Regarding this issue, we employed our SOFT algorithm [24], which has proven to be very robust on the appearance of moving objects in the scene, illumination changes, various specularities, sensor overexposure etc. However, SOFT uses very sparse set of salient feature points, which are not sufficient to reliably detect objects in the scene. Therefore, we employ the corner detector from [51] for detection of semi-dense set of feature points. Position and velocity of each detected feature is estimated in 3D Euclidean space. Now we need to determine the correspondences between features in the left and the right image of the current and previous frame. For this purpose we have used the optical flow procedure presented in [52], and have computed the correspondences by using the stereo block matching algorithm from [53].

Since the images are rectified, all the feature points from the previous frame are projected into 3D world frame through a standard pinhole camera model, and then are back-projected into the current camera frame by compounding the position with

the motion matrix obtained from the ego-motion algorithm. Such transformed 3D points from the previous frame connected to corresponding 3D points from the current frame form a vector field, with each vector representing a motion of corresponding 3D point relative to the world frame. Since the measurement uncertainties are highly anisotropic in 3D space, it is difficult to accurately determine the motion intensity along the optical axis direction. Hence, we project the vectors into the image plane where the uncertainties are more evenly distributed, and apply the threshold on the magnitude of motion of each point. The remaining vectors are then connected into clusters by respecting both translational and rotational parameters. Finally, we consider each clusters corresponds to a moving object if at least 3 vectors appear within it, and describe it with the centroid point of all the corresponding points. The positions of the moving objects detected with the stereo camera system are finally projected into the radar plane and passed to the multitarget tracking algorithm presented in Section 5.

The projection of raw detections of the stereo vision based detection (red circles) and radar readings (green circles) onto the image plane along with filter tracks (yellow circles) is shown in Fig. 3. The images represent four snapshots of the experiment which illustrates the drawbacks of using just a single sensing technology. For example, in the top-most snapshot within Fig. 3 the radar did not capture the two motorcycles, while the stereo camera managed to detect their motion. The second snapshot gives an example of a busy intersection, while the third snapshot shows an example where the vehicle right in front of the ego-vehicle was not detected by the stereo camera due to moving along the camera's optical axis whereas the radar provided consistent detections and the vehicle was tracked by the filter. The final snapshot shows an example where the radar did not detect a vehicle and a pedestrian, while the stereo camera managed to consistently detect their motion and respective filter tracks were obtained.

### 6.3. Real-world experiments

The experiments were conducted with the sensor platform equipped vehicle driving through an urban environment. The algorithm was tested in several highly dynamic scenarios, involving cars, trams and pedestrians. The process noise intensities for the asynchronous filter were set to  $\tilde{q}_x = \tilde{q}_y = 1$  and  $\tilde{q}_\omega = (2\frac{\pi}{180})^2$ . The clutter size and the probability of detection were set to  $c^{\text{radar}} = 10$  and  $p_d^{\text{radar}} = 0.7$ , respectively. The radar unit likelihood was configured such that the measurement uncertainty in the bearing component was  $m_{k+1}^{\phi, \text{radar}} \sim \mathcal{N}_{\mathbb{R}^1}(0, 2^\circ)$ , while the measurement uncertainty in the range component was  $m_{k+1}^{r, \text{radar}} \sim \mathcal{N}_{\mathbb{R}^1}(0, 0.25^2)$ . The clutter size related to the stereo vision system was set to  $c^{\text{stereo}} = 2$ , while the detection probability was  $p_d^{\text{stereo}} = 0.75$ . The stereo vision likelihood was configured so that the measurement uncertainty in the bearing component was  $m_{k+1}^{\phi, \text{stereo}} \sim \mathcal{N}_{\mathbb{R}^1}(0, 0.5^\circ)$ , while the measurement uncertainty in the range component was  $m_{k+1}^{r, \text{stereo}} \sim \mathcal{N}_{\mathbb{R}^1}(0, 1^2)$ . The JIPDA filter gating probability was  $P_G = 0.9$ , and the survival probability was  $p_S = 0.95$ . We have implemented an approach where the tracks are confirmed to be truly existing objects once the probability of object existence exceeded the value of  $p(\chi_k^i | Z_{1:k}) = 0.9$ . The tracks were deleted once the probability of existence fell below  $p(\chi_k^i | Z_{1:k}) = 0.1$ .

The first experiment, lasting about 60 s, involved a scenario in which the vehicle turned right and kept driving down an avenue. The results of this experiment are shown in Fig. 4. In this example it is important to note the very dense traffic on the left-hand side of the vehicle during the turn, which represents a very busy intersection (see the most bottom image in Fig. 3). However, due to



**Fig. 3.** Four snapshots of experiments illustrating detections of the stereo camera (red circles) and radar readings (green circles), which serve as the input for the tracking algorithm (yellow circles). The red lines depict optical flow vectors of the detected motion. An accompanying video is available at <https://youtu.be/Br-qwez1L18>. (For interpretation of the references to color in this figure legend, the reader is referred to the web version of this article.)

high radar clutter, it occasionally happened that the clutter caused false tracks. Such an example can be seen on the right-hand image of Fig. 4. Even though the algorithm manages to track the vehicles on the road (in both directions), some objects, like the roadside hedges next to the road and the pertaining radar clutter, have caused the algorithm to detect them too as true targets. In this experiment, after raw sensor data preprocessing, on average there were 6.46 radar detections and 1.69 stereo camera detections per frame which yielded 3560 filter initializations and 228 confirmed tracks.

In the second experiment, lasting about 85 s, the vehicle drove in one direction along a three lane avenue, performed a u-turn (at the same busy intersection as in Fig. 4) and kept driving forward. The results of this experiment are shown in Fig. 5. The dataset was collected on a three lane road, where the vehicle drove in the middle lane, and detected vehicles in both the left and right lane. It can be noticed that again some radar measurements have caused the algorithm to believe that roadside objects corresponds to true targets. By analyzing the

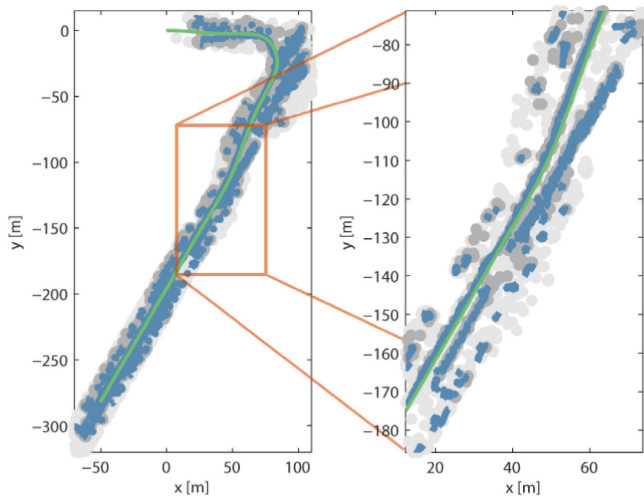


**Fig. 4.** The experimental scenario in which the platform vehicle turned right and kept driving down an avenue. The left part shows the entire 2D projection of the experiment where light and dark gray dots correspond to stereo and radar measurements, blue lines correspond to existing moving objects in the surrounding, and green line represents the ego motion of the vehicle (starting from (0, 0)). (For interpretation of the references to color in this figure legend, the reader is referred to the web version of this article.)

results we have noticed the occasional appearance of false positive trajectories, i.e. the ones that correspond to roadside hedges. In this experiment, after raw sensor data preprocessing, on average there were 12.19 radar detections and 3.0 stereo camera detections per frame which yielded 6935 filter initializations and 450 confirmed tracks. It is also important to mention that we have conducted the experiments during a foggy day, which presented challenging conditions for the stereo image processing.

#### 6.4. Discussion

The presented experimental results illustrate the ability of the proposed approach to track moving objects in the context of ADAS with sensing systems of different modalities, i.e., the radar unit and the stereo camera system—a combination of sensing technologies that has recently been adopted by many car manufacturers. However, to the best of the authors' knowledge, none of the available datasets using these sensors contain ground truth data, hence it is difficult to ensure a quantitative real-world experimental evaluation of the proposed approach. Still, in our previous work [40] we have performed an in-depth evaluation of

filtering on Lie Groups in simulations, and proven the advantages of using  $SE(2)^2$  state space for tracking whenever the characteristics of the system are such that the Euclidean space cannot fully account for the geometry of the state space, while in this work we have applied the mentioned results for multitarget tracking in an ADAS application, and particularly for the sensors whose measurements arise in polar coordinates. Hence, in the present paper we omit an in-depth simulation based evaluation of the LG-EKF procedure.

From the viewpoint of estimation, the advantages of the proposed approach lie in the flexibility of modeling the sensors' and the tracked object's uncertainty and motion. This can prove advantageous in projecting the object's future motion and uncertainty thereof for applications such as collision avoidance or motion planning of autonomous vehicles. The detection procedure of the stereo camera does not rely on a specific appearance of objects and can detect arbitrary motion, including that of cars, vans, motorcycles, and pedestrians as shown in Fig. 3. However, therein lies also the disadvantage of being able to detect only objects exhibiting relative motion with respect to the ego-motion. Objects moving in parallel to the car with the exact same velocity, thus in the image appearing as static, and objects moving along the optical axis can be difficult to detect with the stereo camera. This necessitates then the need for fusing data with other sensors, such as the radar, which can then complement these situations and yield better range measurements for objects further away from the ego-vehicle.

Also, as mentioned in Section 2, the JIPDA filter in its basic Kalman filter-like form represents a well-established approach for multitarget tracking problems. By performing the presented experiments, we have verified the approach of joining the two fundamental multitarget tracking building blocks: the state estimation and probabilistic data association scheme, both based on the geometry of Lie Groups. Given the above, we believe this work will not only serve as a DATMO reference, but also as a guideline for using the LG-EKF in various ADAS aspects.

#### 7. Conclusion

In this paper we have addressed the detection and tracking problem, within the context of advanced driver assistance systems, with a multisensor setup consisting of a radar unit and a stereo camera. The stereo camera estimated relative displacement of the vehicle, using stereo visual odometry, generating measurements as cluster centers of optical flow vectors not conforming to the estimated motion. The radar directly reported its measurements to

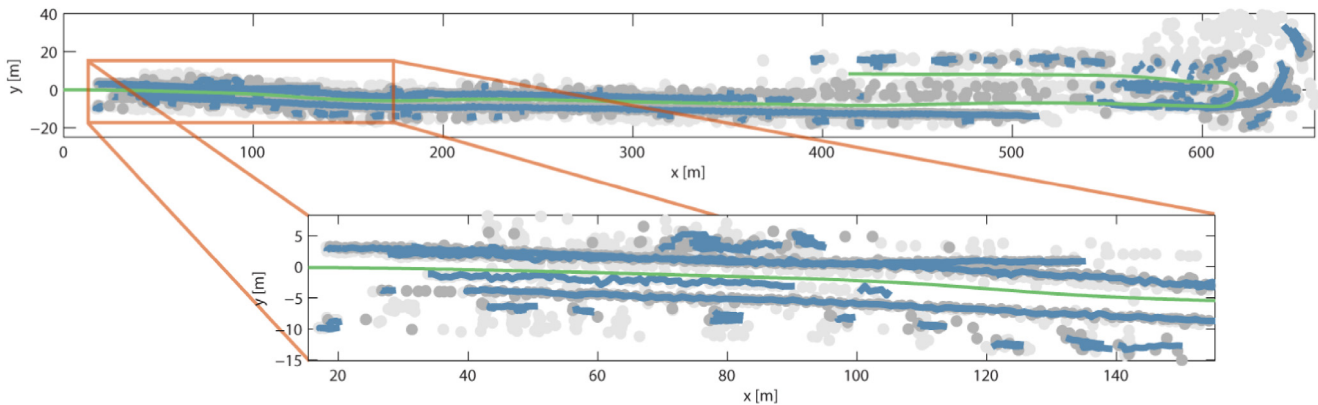


**Fig. 5.** The experimental scenario in which the vehicle drove in direction, performed a u-turn, and kept driving forward. The upper part shows the entire 2D projection of the experiment where light and dark gray dots correspond to stereo and radar measurements, blue lines correspond to existing moving objects in the environment, and green line represents the ego motion of the vehicle starting from (0, 0). (For interpretation of the references to color in this figure legend, the reader is referred to the web version of this article.)



the filter, thus complementing the stereo camera measurements. Since the two sensors worked at different frequencies, sensor measurements were fused using an asynchronous Kalman filter on Lie groups.

This particular representation was proposed so as to most faithfully model the uncertainties of both the sensor measurements and the vehicle's state. Concretely, the radar and the stereo camera were modeled as polar sensors, while the vehicle's state resided on the Lie group  $SE(2)^2$ . This enabled us to reliably model the uncertainties as having *banana-shaped* contours, when such a situation arises, in contrast to elliptical uncertainty contours given by the 'classical' Gaussian distribution. To solve the multitarget tracking problem we adapted the JIPDA filter to work with the Kalman filter on Lie groups. In the end, the proposed filter performance was presented on a real-world dataset recorded in urban traffic scenarios.

## Appendix. Derivation of $\mathcal{H}$

As part of the update step we need to derive the matrix  $\mathcal{H}_{k+1}$  denoting the LG-EKF equivalent to the Kalman filter measurement Jacobian. Before proceeding with explicit derivation, we define the measurement function  $h(X_{k+1})$  as

$$h(X_{k+1}) = \begin{bmatrix} \exp_{SO(2)} \left( \left[ \arctan \frac{y_{k+1}}{x_{k+1}} \right]_{SO(2)}^\wedge \right) \\ \exp_{\mathbb{R}^1} \left( \left[ \sqrt{x_{k+1}^2 + y_{k+1}^2} \right]_{\mathbb{R}^1}^\wedge \right) \end{bmatrix}. \quad (A.1)$$

For this purpose we start with the definition of the Lie algebraic error  $\epsilon = [\epsilon_x \ \epsilon_y \ \epsilon_\theta \ \epsilon_{v_x} \ \epsilon_{v_y} \ \epsilon_\omega]^\top$ . We further provide the prerequisites for deriving  $\mathcal{H}$ . We firstly give the expression which is an argument for evaluating  $\mathcal{H}$

$$\begin{aligned} h(\mu_{k+1|k})^{-1} h(\mu_{k+1|k} \exp_G([\epsilon]_G^\wedge)) &= \begin{bmatrix} h_c^1 & h_c^2 \end{bmatrix} \\ &= \begin{bmatrix} \exp_{SO(2)}^{-1} \left( \left[ \arctan 2 \frac{y_{k+1}}{x_{k+1}} \right]_{SO(2)}^\wedge \right) \exp_{SO(2)} \left( \left[ \arctan 2 \frac{y_{k+1}^\epsilon}{x_{k+1}^\epsilon} \right]_{SO(2)}^\wedge \right) \\ \exp_{\mathbb{R}^1}^{-1} \left( \left[ \sqrt{x_{k+1}^2 + y_{k+1}^2} \right]_{\mathbb{R}^1}^\wedge \right) \exp_{\mathbb{R}^1} \left( \left[ \sqrt{x_{k+1}^{\epsilon 2} + y_{k+1}^{\epsilon 2}} \right]_{\mathbb{R}^1}^\wedge \right) \end{bmatrix}, \end{aligned} \quad (A.2)$$

where  $x_{k+1}^\epsilon$  and  $y_{k+1}^\epsilon$  denote variables extracted from the current matrix Lie group system state  $X_{k+1}$ , compound with the Lie algebraic error mapped via the  $\exp_G$ . These two variables are hence given as

$$\begin{aligned} x_{k+1}^\epsilon &= x_{k+1} + \cos \theta_{k+1} f - \sin \theta_{k+1} g \\ y_{k+1}^\epsilon &= y_{k+1} + \sin \theta_{k+1} f + \cos \theta_{k+1} g. \end{aligned} \quad (A.3)$$

where the terms  $f$  and  $g$  follow terms

$$\begin{aligned} f &= [\epsilon_x \sin \epsilon_\theta + \epsilon_y (-1 + \cos \epsilon_\theta)] \epsilon_\theta^{-1} \\ g &= [\epsilon_x (1 - \cos \epsilon_\theta) + \epsilon_y \sin \epsilon_\theta] \epsilon_\theta^{-1}. \end{aligned} \quad (A.4)$$

The function to be partially derived is obtained by taking the logarithm on  $G'$  as follows

$$\left[ \log_{G'} \left( \begin{bmatrix} h_c^1 \\ h_c^2 \end{bmatrix} \right) \right]_{G'}^\vee = \begin{bmatrix} \left[ \log_{SO(2)} (h_c^1) \right]_{SO(2)}^\vee \\ \left[ \log_{\mathbb{R}^1} (h_c^2) \right]_{\mathbb{R}^1}^\vee \end{bmatrix}. \quad (A.5)$$

Let  $\mathcal{H}_{k+1}^1$  and  $\mathcal{H}_{k+1}^2$  denote the two rows of (A.5). In order to derive (31), we need to determine partial derivatives and multivariate limits over all directions of the Lie algebraic error vector. This result is given as

$$\begin{aligned} \frac{\partial \mathcal{H}_{k+1}^1}{\partial \epsilon_x} \Big|_0 &= \frac{-y_{k+1|k} \cos \theta_{k+1|k} + x_{k+1|k} \sin \theta_{k+1|k}}{x_{k+1|k}^2 + y_{k+1|k}^2} \\ \frac{\partial \mathcal{H}_{k+1}^1}{\partial \epsilon_y} \Big|_0 &= \frac{x_{k+1|k} \cos \theta_{k+1|k} + y_{k+1|k} \sin \theta_{k+1|k}}{x_{k+1|k}^2 + y_{k+1|k}^2} \\ \frac{\partial \mathcal{H}_{k+1}^2}{\partial \epsilon_x} \Big|_0 &= \frac{x_{k+1|k} \cos \theta_{k+1|k} + y_{k+1|k} \sin \theta_{k+1|k}}{\sqrt{x_{k+1|k}^2 + y_{k+1|k}^2}} \\ \frac{\partial \mathcal{H}_{k+1}^2}{\partial \epsilon_y} \Big|_0 &= \frac{y_{k+1|k} \cos \theta_{k+1|k} - x_{k+1|k} \sin \theta_{k+1|k}}{\sqrt{x_{k+1|k}^2 + y_{k+1|k}^2}} \\ \frac{\partial \mathcal{H}_{k+1}^1}{\partial \epsilon_\theta} \Big|_0 &= 0 \quad \frac{\partial \mathcal{H}_{k+1}^2}{\partial \epsilon_\theta} \Big|_0 = 0 \\ \frac{\partial \mathcal{H}_{k+1}^1}{\partial \epsilon_{v_x}} \Big|_0 &= 0 \quad \frac{\partial \mathcal{H}_{k+1}^1}{\partial \epsilon_{v_y}} \Big|_0 = 0 \quad \frac{\partial \mathcal{H}_{k+1}^1}{\partial \epsilon_\omega} \Big|_0 = 0 \\ \frac{\partial \mathcal{H}_{k+1}^2}{\partial \epsilon_{v_x}} \Big|_0 &= 0 \quad \frac{\partial \mathcal{H}_{k+1}^2}{\partial \epsilon_{v_y}} \Big|_0 = 0 \quad \frac{\partial \mathcal{H}_{k+1}^2}{\partial \epsilon_\omega} \Big|_0 = 0. \end{aligned} \quad (A.6)$$

The final measurement matrix  $\mathcal{H}_{k+1}$  is given as

$$\mathcal{H}_{k+1} = \begin{bmatrix} \frac{\partial \mathcal{H}_{k+1}^1}{\partial \epsilon_x} \Big|_0 & \frac{\partial \mathcal{H}_{k+1}^1}{\partial \epsilon_y} \Big|_0 & \frac{\partial \mathcal{H}_{k+1}^1}{\partial \epsilon_\theta} \Big|_0 & \mathbf{0}^{2 \times 3} \\ \frac{\partial \mathcal{H}_{k+1}^2}{\partial \epsilon_x} \Big|_0 & \frac{\partial \mathcal{H}_{k+1}^2}{\partial \epsilon_y} \Big|_0 & \frac{\partial \mathcal{H}_{k+1}^2}{\partial \epsilon_\theta} \Big|_0 & \mathbf{0}^{2 \times 3} \end{bmatrix}. \quad (A.7)$$

Even though the term (A.5) appears involved, the relations (A.6) are actually obtained by patient algebraic manipulations and hence the detailed derivation is not shown here.

## References

- [1] E. Dickmanns, The development of machine vision for road vehicles in the last decade, in: *Intelligent Vehicle Symposium (IV)*, IEEE, 2002, pp. 268–281.
- [2] S. Sivaraman, M.M. Trivedi, Looking at vehicles on the road: A survey of vision-based vehicle detection, tracking, and behavior analysis, *IEEE Trans. Intell. Transp. Syst.* 14 (4) (2013) 1773–1795.
- [3] M. Oliveira, V. Santos, A. Sappa, P. Dias, Scene representations for autonomous driving: An approach based on polygonal primitives, in: *Robot 2015: Second Iberian Robotics Conference*, Vol. 417, Springer, 2016, pp. 503–515.
- [4] B. Steux, C. Laureau, L. Salesse, D. Wautier, Fade: a vehicle detection and tracking system featuring monocular color vision and radar data fusion, in: *Intelligent Vehicle Symposium (IV)*, 2002, pp. 632–639.
- [5] G. Alessandretti, A. Broggi, P. Cerri, Vehicle and guard rail detection using radar and vision data fusion, *IEEE Trans. Intell. Transp. Syst.* 8 (1) (2007) 95–105.
- [6] Z. Ji, D. Prokhorov, Radar-vision fusion for object classification, in: *International Conference on Information Fusion, FUSION*, IEEE, 2008, pp. 1–6.
- [7] T. Wang, N. Zheng, J. Xin, Z. Ma, Integrating millimeter wave radar with a monocular vision sensor for on-road obstacle detection applications, *Sensors* 11 (9) (2011) 8992–9008.
- [8] E. Richter, R. Schubert, G. Wanielik, Radar and vision-based data fusion – advanced filtering techniques for a multi-object vehicle tracking system, in: *Intelligent Vehicles Symposium (IV)*, IEEE, 2008, pp. 120–125.
- [9] F. Liu, J. Sparbert, C. Stiller, IMMPPDA vehicle tracking system using asynchronous sensor fusion of radar and vision, in: *Intelligent Vehicles Symposium (IV)*, IEEE, 2008, pp. 168–173.
- [10] R.O. Chavez-Garcia, T.-D. Vu, J. Burlet, O. Aycard, Frontal object perception using radar and mono-vision, in: *Intelligent Vehicles Symposium (IV)*, IEEE, 2012, pp. 159–164.
- [11] T. Kato, Y. Ninomiya, I. Masaki, An obstacle detection method by fusion of radar and motion stereo, *IEEE Trans. Intell. Transp. Syst.* 3 (3) (2002) 182–187.
- [12] M. Bertozzi, L. Bombini, P. Cerri, P. Medici, P.C. Antonello, M. Miglietta, Obstacle detection and classification fusing radar and vision, in: *Intelligent Vehicles Symposium (IV)*, IEEE, 2008, pp. 608–613.
- [13] Y. Fang, I. Masaki, B. Horn, Depth-based target segmentation for intelligent vehicles: fusion of radar and binocular stereo, *IEEE Trans. Intell. Transp. Syst.* 3 (3) (2002) 196–202.
- [14] S. Wu, S. Decker, P. Chang, T. Camus, J. Eledath, Collision sensing by stereo vision and radar sensor fusion, *IEEE Trans. Intell. Transp. Syst.* 10 (4) (2009) 606–614.
- [15] I. Marković, I. Petrović, Bayesian sensor fusion methods for dynamic object tracking – a comparative study, *Automatika* 55 (4) (2014) 386–398.
- [16] M. Obrvan, J. Česić, I. Petrović, Appearance based vehicle detection by radar-stereo vision integration, in: *Second Iberian Robotics Conference*, Vol. 417, Robot 2015, Springer, 2016, pp. 437–449.



- [17] A. Broggi, A. Cappelunga, C. Caraffi, S. Cattani, S. Ghidoni, P. Grisleri, P.P. Porta, M. Posterli, P. Zani, TerraMax vision at the urban challenge 2007, *IEEE Trans. Intell. Transp. Syst.* 11 (1) (2010) 194–205.
- [18] B. Lefaudoux, F. Nashashibi, Real-time visual perception: Detection and localisation of static and moving objects from a moving stereo rig, in: *Intelligent Transportation Systems Conference, ITSC, 2012*, pp. 522–527.
- [19] P. Lenz, J. Ziegler, A. Geiger, M. Roser, Sparse scene flow segmentation for moving object detection in urban environments, in: *Intelligent Vehicles Symposium (IV)*, 2011, pp. 926–932.
- [20] A. Wedel, T. Brox, T. Vaudrey, C. Rabe, U. Franke, D. Cremers, Stereoscopic scene flow computation for 3D motion understanding, *Int. J. Comput. Vis.* 95 (1) (2011) 29–51.
- [21] B. Barrois, S. Hristova, C. Wohler, F. Kummert, C. Hermes, 3D pose estimation of vehicles using a stereo camera, in: *Intelligent Vehicles Symposium (IV)*, 2009, pp. 267–272.
- [22] E. Ohn-bar, S. Sivaraman, M. Trivedi, Partially occluded vehicle recognition and tracking in 3D, in: *Intell. Veh. Symposium (IV)*, 2013, pp. 1350–1355.
- [23] J. Almeida, V. Santos, Pedestrian pose estimation using stereo perception, in: *Second Iberian Robotics Conference*, Vol. 417, Robot 2015, Springer, 2016, pp. 491–502.
- [24] I. Cvišić, I. Petrović, Stereo odometry based on careful feature selection and tracking, in: *European Conference on Mobile Robots, ECMR, 2015*.
- [25] G. Bourmaud, R. Mégret, M. Arnaudon, A. Giremus, Continuous-discrete extended kalman filter on matrix lie groups using concentrated Gaussian distributions, *J. Math. Imaging Vision* 51 (1) (2014) 209–228.
- [26] R.P.S. Mahler, Multitarget Bayes filtering via first-order multitarget moments, *IEEE Trans. Aerosp. Electron. Syst.* 39 (4) (2003) 1152–1178.
- [27] B.-N. Vo, S. Singh, A. Doucet, Sequential monte carlo methods for multi-target filtering with random finite sets, *IEEE Trans. Aerosp. Electron. Syst.* 41 (4) (2005) 1224–1245.
- [28] B.-N. Vo, W.-K. Ma, The Gaussian mixture probability hypothesis density filter, *IEEE Trans. Signal Process.* 54 (11) (2006) 4091–4104.
- [29] R. Mahler, PHD filters of higher order in target number, *IEEE Trans. Aerosp. Electron. Syst.* 43 (4) (2007) 1523–1543.
- [30] B.-T. Vo, B.-N. Vo, A. Cantoni, Analytic implementations of the cardinalized probability hypothesis density filter, *IEEE Trans. Signal Process.* 55 (7) (2007) 3553–3567.
- [31] R. Mahler, *Statistical Multisource-Multitarget Information Fusion*, Artech House, 2007.
- [32] B.T. Vo, B.N. Vo, A. Cantoni, The cardinality balanced multi-target multi-Bernoulli filter and its implementations, *IEEE Trans. Signal Process.* 57 (2) (2009) 409–423.
- [33] S. Reuter, B.T. Vo, B.N. Vo, K. Dietmayer, The labeled multi-Bernoulli filter, *IEEE Trans. Signal Process.* 62 (12) (2014) 3246–3260.
- [34] H. Deusch, S. Reuter, K. Dietmayer, The labeled multi-Bernoulli SLAM filter, *IEEE Signal Process. Lett.* 22 (10) (2015) 1561–1565.
- [35] D. Reid, An algorithm for tracking multiple targets, *IEEE Trans. Automat. Control* 24 (6) (1979) 843–854.
- [36] Y. Bar-Shalom, E. Tse, Sonar tracking of multiple targets using joint probabilistic data association filter, *Automatica* 11 (1975) 451–460.
- [37] D. Mušicki, R. Evans, Joint integrated probabilistic data association – JIPDA, *IEEE Trans. Aerosp. Electron. Syst.* 40 (3) (2004) 1093–1099.
- [38] S. Challa, M.R. Morelande, D. Mušicki, R.J. Evans, *Fundamentals of object tracking*, 2011.
- [39] J.L. Williams, Marginal multi-Bernoulli filters: RFS derivation of MHT, JIPDA and association-based MeMBer, *IEEE Trans. Aerosp. Electron. Syst.* 51 (3) (2015) 1664–1687.
- [40] J. Č. I. Marković, I. Petrović, Moving object tracking employing rigid body dynamics on matrix Lie groups, in: *Submitted to International Conference on Information Fusion, FUSION, 2016*.
- [41] C. Hertzberg, R. Wagner, U. Frese, L. Schröder, Integrating generic sensor fusion algorithms with sound state representations through encapsulation of manifolds, *Inf. Fusion* 14 (1) (2013) 57–77.
- [42] G.S. Chirikjian, *Stochastic Models, Information Theory, and Lie Groups, Volume 2: Analytic Methods and Modern Applications*, Springer, 2012.
- [43] W. Park, Y. Wang, G.S. Chirikjian, The path-of-probability algorithm for steering and feedback control of flexible needles, *Int. J. Robot. Res.* 29 (7) (2010) 813–830.
- [44] T.D. Barfoot, P.T. Furgale, Associating uncertainty with three-dimensional poses for use in estimation problems, *IEEE Trans. Robot.* 30 (3) (2014) 679–693.
- [45] Y. Wang, G.S. Chirikjian, Nonparametric second-order theory of error propagation on motion groups, *Int. J. Robot. Res.* 27 (11) (2008) 1258–1273.
- [46] K.C. Wolfe, M. Mashner, G.S. Chirikjian, Bayesian fusion on Lie groups, *J. Algebr. Stat.* 2 (1) (2011) 75–97.
- [47] Y. Bar-Shalom, T. Kirubarajan, X.-R. Li, *Estimation with Applications to Tracking and Navigation*, John Wiley & Sons, Inc., 2002.
- [48] S. Thrun, W. Burgard, D. Fox, *Probabilistic Robotics*, The MIT Press, 2006.
- [49] R. Schubert, C. Adam, M. Obst, N. Mattern, V. Leonhardt, G. Wanielik, Empirical evaluation of vehicular models for ego motion estimation, in: *Intelligent Vehicles Symposium, IEEE, 2011*, pp. 534–539.

- [50] D. Salmond, Mixture reduction algorithms for point and extended object tracking in clutter, *IEEE Trans. Aerosp. Electron. Syst.* 45 (2) (2009) 667–686.
- [51] J. Shi, C. Tomasi, Good features to track, in: *1994 IEEE Computer Society Conference on Computer Vision and Pattern Recognition, 1994. Proceedings CVPR '94, 1994*, pp. 593–600.
- [52] J.-Y. Bouguet, *Pyramidal implementation of the Lucas Kanade feature tracker description of the algorithm*, Tech. Rep. 2, Intel Corporation, Microsoft Research Labs, 2000.
- [53] K. Konolige, *Small vision systems: Hardware and implementation*, in: *Robotics Research*, Springer, London, 1998, pp. 203–212.



**Josip Česić** has received his B.Sc. and M.Sc. degree (Magna Cum Laude) in electrical engineering and information technology from University of Zagreb, Faculty of Electrical Engineering and Computing (UNIZG-FER) in 2011 and 2013, respectively. He finished part of his master studies at Chalmers University of Technology, Sweden. He is employed as a research assistant at the Department of Control and Computer Engineering at FER Zagreb since April 2013. During the undergraduate studies he received Dean's Award and Special Dean's Award for outstanding achievements on the first year of studies and the overall B.Sc. level, respectively. During the graduate studies he received Rector's Award and Special Rector's Award for practical applications in the fields of robotics and control systems. He was also awarded with Scholarship from the Croatian Ministry of Science, Scholarship of the University of Zagreb and Scholarship of the City of Zagreb. His main research interests are in the areas of autonomous systems and mobile robotics, estimation theory and sensor processing.



**Ivan Marković** received the B.Sc. and the Ph.D. degree in Electrical Engineering from the University of Zagreb, Faculty of Electrical Engineering and Computing (FER), Croatia in 2008 and 2014, respectively. He is currently employed at the FER, Zagreb, as a Research and Teaching Assistant funded by the Ministry of Science, Education and Sport, Republic of Croatia. During his undergraduate studies, for outstanding academic achievements, he received the "Institute for Nuclear Technology Award" and the "Josip Lončar Award" in 2007 and 2006, respectively. In 2013 and 2014 he was a visiting researcher at Inria Rennes—Bretagne Atlantique in the Lagadic group directed by Prof. François Chaumette, Ph.D. He also serves as the coordinator of the technical editing team of the *Automatika* journal. His main research interests are in mobile robotics, estimation theory and human–robot interaction.



**Igor Cvišić** received diploma degree in Electrical Engineering from the Faculty of Electrical Engineering and Computing (FER Zagreb), University of Zagreb, Croatia in 2001. He is currently employed at the FER, Department of Control and Computer Engineering, as a researcher on the EU FP7 ACROSS project, and he is pursuing his Ph.D. degree. Previously, he worked at DAMCO as an R&D Engineer, where he successfully coordinated and developed more than 10 different custom made industrial automated systems based on manipulation guided by computer vision. His research interests include robotics vision, system control and automation, electronics and autonomous flying vehicles. For his work, he was awarded with the Best Student Paper Award at the RAAD Workshop 2013, Portorož, Slovenia.



**Ivan Petrović** received B.Sc. degree in 1983, M.Sc. degree in 1989 and Ph.D. degree in 1998, all in Electrical Engineering from the Faculty of Electrical Engineering and Computing (FER Zagreb), University of Zagreb, Croatia. He had been employed as an R&D engineer at the Institute of Electrical Engineering of the Končar Corporation in Zagreb from 1985 to 1994. Since 1994 he has been with FER Zagreb, where he is currently a full professor. He teaches a number of undergraduate and graduate courses in the field of control systems and mobile robotics. His research interests include various advanced control strategies and their applications to control of complex systems and mobile robots navigation. He has published more than 40 journals and 160 conference papers, and results of his research have been implemented in several industrial products. He is a member of IEEE, IFAC – TC on Robotics and FIRA – Executive committee. He is a member of the Croatian Academy of Engineering and Editor-in-Chief of the *Automatika* journal.

## PUBLICATION 8

J. Ćesić, I. Marković, and I. Petrović. Mixture Reduction on Matrix Lie Groups. *IEEE Signal Processing Letters*, 24(11):1719–1723, 2017.

# Mixture Reduction on Matrix Lie Groups

Josip Česić, *Member, IEEE*, Ivan Marković, *Member, IEEE*, and Ivan Petrović, *Member, IEEE*

**Abstract**—Many physical systems evolved on matrix Lie groups and mixture filtering designed for such manifolds represent an inevitable tool for challenging estimation problems. However, mixture filtering faces the issue of a constantly growing number of components, hence requiring appropriate mixture reduction techniques. In this letter, we propose a mixture reduction approach for distributions on matrix Lie groups, called the concentrated Gaussian distributions (CGDs). This entails appropriate reparameterization of CGD parameters to compute the KL divergence, pick and merge the mixture components. Furthermore, we also introduce a multitarget tracking filter on Lie groups as a mixture filtering study example for the proposed reduction method. In particular, we implemented the probability hypothesis density filter on matrix Lie groups. We validate the filter performance using the optimal subpattern assignment metric on a synthetic dataset consisting of 100 randomly generated multitarget scenarios.

**Index Terms**—Estimation on matrix lie groups, mixture reduction, multitarget tracking, probability hypothesis density filter.

## I. INTRODUCTION

MANY statistical and engineering problems require modeling of complex multimodal data, wherein mixture distributions became an inevitable tool [1], [2], primarily in traditional application domains like radar and sonar tracking [3], and later in different modern fields such as computer vision [4], speech recognition [5], or multimedia processing [6]. Approaches relying on mixture distributions often face the problem of large or an ever increasing number of mixture components; hence, the growth of components must be controlled by approximating the original mixture with a mixture of a reduced size [7]–[9]. For example, in the case of multitarget tracking applications, by employing conventional Gaussian mixture based filters [10], [11], during the recursion process, the number of components inevitably increases. This appears first due to appearance of newly birthed or spawned components, and second, due to inclusion of multiple measurements, which results in a geometrical increase in the number of components.

Another important aspect of estimation is the state space geometry; hence, many works have been dedicated to appropriate uncertainty modeling and estimation techniques for a wide range

of applications [12]–[15], motivated by theoretical and implementation difficulties caused by treating a constrained problem naively with Euclidean tools. For example, Lie groups are natural ambient (state) spaces for description of the dynamics of rigid body mechanical systems. In [16], it has been observed that the distribution of the pose of a differential drive mobile robot is not a Gaussian distribution in Cartesian coordinates, but rather a distribution on the special Euclidean group  $SE(2)$ . Similarly, in [17], it was discussed the uncertainty association with three-dimensional (3-D) pose employing the  $SE(3)$  group. Furthermore, attitude estimation arises naturally on the  $SO(3)$  group [15]. In [18], a feedback particle filter on matrix Lie groups was proposed, while in [19], [20], the authors proposed an extended Kalman filter on matrix Lie groups (LG-EKF), building the theory upon the concentrated Gaussian distribution (CGD) on matrix Lie groups [21].

In this letter, we address finite mixtures of distributions on matrix Lie groups. We propose a novel approach to CGD mixture reduction, which required finding solutions for computing Kullback–Leibler divergence of CGD components and CGD component merging. Furthermore, since previous methods require choosing the appropriate tangent space, we also provide an extensive analysis on the choice thereof. As a study example, we use the proposed reduction method in a multitarget tracking scenario. We introduce the probability hypothesis density filter (PHD) on matrix Lie groups with approximation based on a finite mixture of CGDs.

## II. MATHEMATICAL PRELIMINARIES

We now introduce theoretical preliminaries concerning Lie groups; however, for a more rigorous introduction, the reader is directed to [22]. A Lie group  $G$  is a group that has the structure of a smooth manifold; moreover, a tangent space  $T_X(G)$  is associated to  $X \in G$  such that the tangent space placed at the group identity, called Lie algebra  $\mathfrak{g}$ , is transferred by applying corresponding action to  $X$ . In this letter, we are interested in matrix Lie groups that are usually the ones considered in engineering and physical sciences.

The Lie algebra  $\mathfrak{g} \subset \mathbb{R}^{n \times n}$  associated to a  $p$ -dimensional matrix Lie group  $G \subset \mathbb{R}^{n \times n}$  is a  $p$ -dimensional vector space. The matrix exponential  $\exp_G$  and matrix logarithm  $\log_G$  establish a local diffeomorphism between the two

$$\exp_G : \mathfrak{g} \rightarrow G \quad \text{and} \quad \log_G : G \rightarrow \mathfrak{g}. \quad (1)$$

Furthermore, a natural relation exists between  $\mathfrak{g}$  and the Euclidean space  $\mathbb{R}^p$  given through a linear isomorphism

$$[\cdot]_G^\vee : \mathfrak{g} \rightarrow \mathbb{R}^p \quad \text{and} \quad [\cdot]_G^\wedge : \mathbb{R}^p \rightarrow \mathfrak{g}. \quad (2)$$

For  $x \in \mathbb{R}^p$  and  $X \in G$ , we use the following notation [23]:

$$\exp_G^\wedge(x) = \exp_G([\cdot]_G^\wedge x) \quad \text{and} \quad \log_G^\vee(X) = [\log_G(X)]_G^\vee. \quad (3)$$

Manuscript received May 3, 2017; revised June 23, 2017; accepted July 2, 2017. Date of publication July 5, 2017; date of current version October 11, 2017. This work has been supported from the Unity Through Knowledge Fund (no. 24/15) under the project Cooperative Cloud based Simultaneous Localization and Mapping in Dynamic Environments (cloudSLAM) and the European Union's Horizon 2020 research and innovation programme under grant agreement No 688117 (SafeLog). The associate editor coordinating the review of this manuscript and approving it for publication was Prof. Marco Felipe Duarte. (*Corresponding Author: Ivan Marković.*)

The authors are with the Faculty of Electrical Engineering and Computing, University of Zagreb, Zagreb 10000, Croatia (e-mail: josip.cesic@fer.hr; ivan.markovic@fer.hr; ivan.petrovic@fer.hr).

Digital Object Identifier 10.1109/LSP.2017.2723765

Lie groups are generally noncommutative, i.e.,  $XY \neq YX$ . However, the noncommutativity can be captured by the so-called adjoint representation of  $G$  on  $\mathfrak{g}$  [24]

$$X \exp_G^\wedge(y) = \exp_G^\wedge(\text{Ad}_G(X)y)X \quad (4)$$

which can be seen as a way of representing the elements of the group as a linear transformation of the group's algebra. The adjoint representation of  $\mathfrak{g}$ ,  $\text{ad}_G$ , is in fact the differential of  $\text{Ad}_G$  at the identity. Another important result for working with Lie group elements is the Baker–Campbell–Hausdorff (BCH) formula, which enables representing the product of Lie group members as a sum in the Lie algebra. We will use the following BCH formulae [24], [25]:

$$\log_G^\vee(\exp_G^\wedge(x) \exp_G^\wedge(y)) = y + \varphi_G(y)x + O(\|y\|^2) \quad (5)$$

$$\log_G^\vee(\exp_G^\wedge(x+y) \exp_G^\wedge(-x)) = \Phi_G(x)y + O(\|y\|^2) \quad (6)$$

where  $\varphi_G(y) = \sum_{n=0}^{\infty} \frac{B_n \text{ad}_G(y)^n}{n!}$ ,  $B_n$  are Bernoulli numbers, and  $\Phi_G(x) = \varphi_G(x)^{-1}$ . For many common groups used in engineering and physical sciences, closed-form expressions for  $\varphi_G(\cdot)$  and  $\Phi_G(\cdot)$  can be found [17], [24]; otherwise, a truncated series expansion is used.

#### A. Concentrated Gaussian Distribution

Herein, we introduce the concept of the concentrated Gaussian distribution that is used to define random variables on matrix Lie group. A random variable  $X \in G$  has a CGD with the mean  $\mu$  and covariance  $\Sigma$ , i.e.,  $X \sim \mathcal{G}(X; \mu, \Sigma)$ , if

$$X = \exp_G^\wedge(\xi)\mu \quad (7)$$

where  $\mu \in G$ , and  $\xi \sim \mathcal{N}(\xi; \mathbf{0}_{p \times 1}, \Sigma)$  is a zero-mean “classical” Gaussian random variable with the covariance  $\Sigma \subset \mathbb{R}^{p \times p}$  [17], [20]. Note that in this way, we are directly defining the CGD covariance in the pertaining Lie algebra  $\mathfrak{g}$ , while the mean is defined on the group  $G$ .

Given that the previous definition (7) then induces a probability density function (pdf) of  $X$  over  $G$  as follows [17], [20]:

$$\begin{aligned} 1 &= \int_{\mathbb{R}^p} \frac{1}{\sqrt{(2\pi)^p |\Sigma|}} \exp_G^\wedge \left( -\frac{1}{2} \|\xi\|_\Sigma^2 \right) d\xi \\ &= \int_G \beta \exp_G^\wedge \left( -\frac{1}{2} \|\log_G^\vee(X\mu^{-1})\|_\Sigma^2 \right) dX \end{aligned} \quad (8)$$

where  $\|x\|_\Sigma^2 = x^T \Sigma^{-1} x$ . Therein, the change of coordinates  $\xi = \log_G^\vee(X\mu^{-1})$ , with the pertaining differentials  $dX = |\Phi(\xi)| d\xi$ , resulted with the CGD normalizing constant

$$\beta = 1/\sqrt{(2\pi)^p |\Phi(\log_G^\vee(X\mu^{-1})) \Sigma \Phi(\log_G^\vee(X\mu^{-1}))^T|}. \quad (9)$$

Note that this change of variables is valid if all eigenvalues of  $\Sigma$  are small, i.e., almost all the mass of the distribution is concentrated in a small neighborhood around the mean value [20]. The pdf over  $X$  is now fully determined by (8) and (9).

### III. CGD MIXTURE REDUCTION

With the theoretical preliminaries setup, we continue with mixture reduction on matrix Lie groups. A finite mixture of our present interest is given as the weighted sum of CGDs

$$\sum_{i=1}^N w_i \mathcal{G}(X; \mu_i, \Sigma_i) \quad (10)$$

where  $w_i$  are component weights and  $N$  is the total number of mixture components. An illustration of (10) is given in Fig. 1. Component reduction procedures typically require three building blocks: (i) component distance measure, (ii) component picking algorithm, and (iii) component merging. While various solutions exist for “classical” Gaussian mixtures [7]–[9], questions remain on how to approach the component number reduction for CGD mixtures on matrix Lie groups. Therefore, first, we focus on the fundamental question of how to measure the distance between two CGD components.

#### A. Component Distance Measure

Our aim is to use a standard information-theoretic measure between two CGD components, and we propose to use the Kullback–Leibler (KL) divergence [26]. Let  $\mathcal{G}_i = \mathcal{G}(X; \mu_i, \Sigma_i)$  and  $\mathcal{G}_j = \mathcal{G}(X; \mu_j, \Sigma_j)$  be two mixture components with  $p_i(X)$  and  $p_j(X)$  as their respective pdfs. Since there is nothing intrinsic in the definition of KL divergence that requires the underlying space to be Euclidean, by definition

$$\mathcal{D}_{\text{KL}}(\mathcal{G}_i, \mathcal{G}_j) = \int_G p_i(X) \log \left( \frac{p_i(X)}{p_j(X)} \right) dX. \quad (11)$$

In order to evaluate the integral (11), we need to employ the change of coordinates as in (8), but this time from the direction of the group  $G$ , i.e., from  $X \in G$  to  $\xi \in \mathbb{R}^p$ . Note that in (8) the change evolved around the distribution mean  $\mu$ ; however, since in (11) generally  $\mu_i \neq \mu_j$ , we cannot apply the same approach. Hence, before evaluating (11), we first discuss how to change the coordinates on the level of a single distribution.

Let  $\mathcal{G}(X; \mu, \Sigma)$  be a CGD, and if we change the coordinates using  $X = \exp_G^\wedge(\xi)\mu_t$ ,  $\mu_t \in G$ , where  $\mu_t \neq \mu$ , we get

$$\begin{aligned} 1 &= \int_G \beta \exp_G^\wedge \left( -\frac{1}{2} \|\log_G^\vee(X\mu^{-1})\|_\Sigma^2 \right) dX \\ &\stackrel{\text{CoC}}{\approx} \int_{\mathbb{R}^p} \eta \exp_G^\wedge \left( -\frac{1}{2} \|\log_G^\vee(\exp_G^\wedge(\xi)\mu_t\mu^{-1})\|_\Sigma^2 \right) d\xi \\ &\stackrel{(6)}{\approx} \int_{\mathbb{R}^p} \eta \exp_G^\wedge \left( -\frac{1}{2} \|\Phi_G(r_t)(\xi - r_t)\|_\Sigma^2 \right) d\xi \\ &= \int_{\mathbb{R}^p} \eta \exp_G^\wedge \left( -\frac{1}{2} \|\xi - r_t\|_{\varphi_G(r_t)\Sigma\varphi_G(r_t)^T}^2 \right) d\xi \end{aligned} \quad (12)$$

where  $r_t = \log_G^\wedge(\mu\mu_t^{-1})$ ,  $\eta$  approximately evaluates to

$$\begin{aligned} \eta &= \beta |\Phi(\xi)| = \frac{|\Phi(\xi)|}{\sqrt{(2\pi)^p |\Sigma|} \cdot |\Phi(\log_G^\vee(\exp_G^\wedge(\xi)\mu_t\mu^{-1}))|} \\ &\approx \frac{1}{\sqrt{(2\pi)^p |\varphi_G(r_t)\Sigma\varphi_G(r_t)^T|}} \end{aligned} \quad (13)$$

and we obtain  $\xi \sim \mathcal{N}(\xi; r_t, \varphi_G(r_t)\Sigma\varphi_G(r_t)^T)$ .

*Remark 1:* Covariance of a CGD represents the uncertainty relevant only to the tangent space of its own mean. In [24], the authors studied how the covariance changes if looked at from the perspective of a value that is different than the distribution mean. They dubbed this procedure “distribution unfolding.” For example, if we unfold  $\mathcal{G}(X; \mu, \Sigma)$  around an arbitrary  $\mu_t \in G$ , using (5) and following [24], we get

$$\begin{aligned} \xi_t &= \log_G^\vee(\exp_G^\wedge(\xi)\mu\mu_t^{-1}) \\ &\approx \log_G^\vee(\mu\mu_t^{-1}) + \varphi_G(\log_G^\vee(\mu\mu_t^{-1}))\xi. \end{aligned} \quad (14)$$



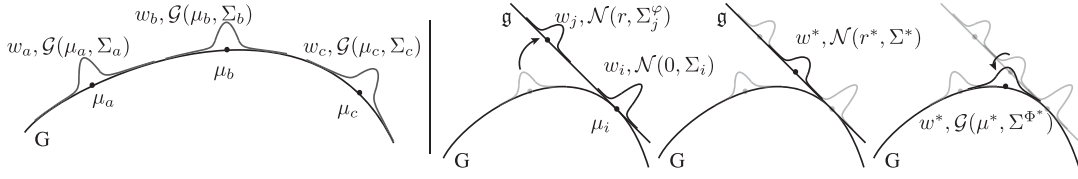


Fig. 1. Illustration of a finite mixture of CGDs (left) and the component merging procedure (right).

By computing the expectation and covariance of (14), we obtain a reparameterized distribution,  $\xi_t \sim \mathcal{N}(\xi_t; r_t, \Sigma^\varphi)$ , where

$$r_t = \log_G^\vee(\mu \mu_t^{-1}) \quad (15)$$

$$\Sigma^\varphi = \varphi_G(r_t) \Sigma \varphi_G^T(r_t). \quad (16)$$

This pdf is equal to the one obtained through the change of coordinates in (12). However, obtaining this result by using the procedure of coordinates change through a pdf is important from the perspective of KL divergence evaluation. An illustration of unfolding a component  $j$  around  $\mu_i$ , using (15) and (16), is given in Fig. 1.

The KL divergence between two CGDs  $\mathcal{G}_i = \mathcal{G}(\mu_i, \Sigma_i)$  and  $\mathcal{G}_j = \mathcal{G}(\mu_j, \Sigma_j)$  can now be evaluated as

$$\begin{aligned} \mathcal{D}_{\text{KL}}(\mathcal{G}_i, \mathcal{G}_j) &\approx \int_{\mathbb{R}^p} p_i(\xi) \log \left( \frac{p_i(\xi)}{p_j(\xi)} \right) d\xi = D_{\text{KL}}(\mathcal{N}_i, \mathcal{N}_j) \\ p_i(\xi) &\sim \mathcal{N}_i = \mathcal{N}(\xi; r_i, \Sigma_i^\varphi), \quad r_i = \log_G^\wedge(\mu_i \mu_t^{-1}) \\ p_j(\xi) &\sim \mathcal{N}_j = \mathcal{N}(\xi; r_j, \Sigma_j^\varphi), \quad r_j = \log_G^\wedge(\mu_j \mu_t^{-1}) \end{aligned} \quad (17)$$

and  $\Sigma^\varphi = \varphi_G(r) \Sigma \varphi_G^T(r)$ . By employing the change of coordinates, we can evaluate the KL divergence of two CGDs similarly as in the case of “classical” Gaussian distributions, but with reparameterized means and covariances. The KL divergence is then equal to

$$\begin{aligned} \mathcal{D}_{\text{KL}}(\mathcal{N}_i, \mathcal{N}_j) &= \frac{1}{2} \left( \text{tr}(\Sigma_j^{-1} \Sigma_i^\varphi) - K + \log_{\mathbb{R}} \frac{|\Sigma_j^\varphi|}{|\Sigma_i^\varphi|} \right. \\ &\quad \left. + (r_j - r_i)^T (\Sigma_j^\varphi)^{-1} (r_j - r_i) \right) \end{aligned} \quad (18)$$

where  $\text{tr}(\cdot)$  and  $|\cdot|$  designate matrix trace and determinant, respectively, while  $K$  is the mean vector dimension. Finally, for mixture components, it is necessary to use the scaled symmetrized KL divergence [27], which also takes component weights into account

$$\begin{aligned} \mathcal{D}_{s\text{KL}}(w_i \mathcal{N}_i, w_j \mathcal{N}_j) &= \frac{1}{2} \left( (w_i - w_j) \log_{\mathbb{R}} \frac{w_i}{w_j} \right. \\ &\quad \left. + w_i \mathcal{D}_{\text{KL}}(\mathcal{N}_i, \mathcal{N}_j) + w_j \mathcal{D}_{\text{KL}}(\mathcal{N}_j, \mathcal{N}_i) \right). \end{aligned} \quad (19)$$

### B. Component Picking Algorithm

Now that we know how to compute a distance measure between two CGD mixture components, we need to choose an appropriate component picking algorithm that will tell us how to screen the whole mixture and which components to pick for merging. However, with CGD mixtures, there is also another momentum. If we have  $N$  components in the mixture with different weights, how should we approach the problem of measuring distance, i.e., choosing  $\mu_t$  for the change of coordinates? Should all the distances be calculated with respect to the mean of the component with the highest weight or the lowest weight? Or should we “reparameterize” each component

on a pairwise basis? In this letter, we study the following five scenarios: (i/ii) all components are reparameterized about the mean of the component with the highest/lowest weight, (iii) the reparameterization about the identity element, and (iv/v) components are reparameterized on a pairwise basis by choosing the mean of the component pair with the higher/lower weight. For analyzing the five scenarios, we use two common component picking strategies; (i) Exhaustive pairwise [28] and (ii) West’s [29] algorithms. The Exhaustive pairwise algorithm determines distances between all components and merges the closest pair, while West’s algorithm sorts the components according to their respective weights, then finds and merges the component most similar to the first one.

### C. Merging the Components

A component-merging algorithm for Gaussian components in  $\mathbb{R}^p$  was proposed in [28]

$$r^* = \frac{1}{w^*} \sum_i w_i r_i, \quad \Sigma^* = \frac{1}{w^*} \sum_i \left( w_i (\Sigma_i + r_i r_i^T) \right) - r^* (r^*)^T$$

where  $w^* = \sum_i w_i$ ,  $w_i \mathcal{N}(r_i, \Sigma_i)$  represents the  $i$ th component, and  $w^* \mathcal{N}(r^*, \Sigma^*)$  is the resulting component. Although merging works for an arbitrary number of components, in our case, we will always merge two.

However, the previous expressions are defined for Gaussians in  $\mathbb{R}^p$ , and the question arises how to apply the same approach for CGD mixtures? We propose to use the same principle as for computing the KL divergence described in Section III-A, i.e., the components to be merged need to be first reparameterized about the tangent space of the same mean, since covariances are only relevant with respect to their own mean. Once we compute the resulting component,  $w^* \mathcal{N}(r^*, \Sigma^*)$ , we need to map it back to the group  $G$ . Given a lemma from [20] and following convention (7), the procedure evaluates to

$$\mu^* = \exp_G^\wedge(r^*) \mu_t, \quad \Sigma^{\Phi^*} = \text{Ad}_G^{r^*} \Phi_G(r^*) \Sigma^* (\text{Ad}_G^{r^*} \Phi_G(r^*))^T \quad (20)$$

where  $\text{Ad}_G^{r^*} = \text{Ad}_G(\exp_G^\wedge(r^*))$ . We can notice that covariance reparameterization was necessary to make it relevant from the perspective of the tangent space of the newly computed  $\mu^*$ . An illustration of merging and reparameterization (20) of component  $j$  with respect to  $\mu_i$  is given in Fig. 1.

## IV. STUDY EXAMPLE—PHD FILTER ON LIE GROUPS

Multitarget tracking (MTT) is a complex problem consisting of many challenges, and PHD filter presents itself as one of the solutions to MTT. The reason why PHD filter is interesting for the present letter is because one of its implementations is based on Gaussian mixtures (GM-PHD) [10]. Besides Gaussians, other distributions can be used, and in our previous work [30], we proposed a mixture approximation of the PHD filter based on the von Mises distribution on the unit circle. In this

letter, as a study example, we implement a PHD filter tailored for Lie groups (LG-PHD), based on the mixture of CGDs and the reduction schemes presented in the previous section. The LG-PHD can be potentially applied in MTT scenarios where the target state is modeled as a pose in  $SE(2)$  or  $SE(3)$ .

The PHD filter propagates the *intensity function*  $D_{k-1}$ , and operates by evaluating two steps—prediction and update. By assuming  $D_{k-1}$  and birth intensity being Gaussian mixtures [10], the GM-PHD prediction results with another Gaussian mixture [10, Proposition 1]. Similarly, if  $D_{k-1}$  and birth intensity are given with CGD mixtures, the LG-PHD prediction results with another CGD mixture, relying on the LG-EKF prediction applied to each mixture component [23].

The product of two Gaussians evaluates to a scaled Gaussian; hence, the update step of GM-PHD can be calculated analytically [10, Proposition 2]. In contrary, the product of two CGDs, occurring in LG-PHD update, cannot be evaluated directly. Hence, we apply approximations following the same train of thought as in LG-EKF prediction [23], where given posterior  $p(X_{k-1}|Z_{1:k-1})$  and motion model  $p(X_k|X_{k-1})$ , it approximates the joint distribution  $p(X_k, X_{k-1}|Z_{1:k-1})$ , and then marginalizes obtaining  $p(X_k|Z_{1:k-1})$ . Similarly, given  $p(X_k|Z_{1:k-1})$  and likelihood  $p(Z_k|X_k)$ , we approximate the joint distribution  $p(X_k, Z_k|Z_{1:k-1})$ , and then marginalize obtaining  $p(X_k|Z_k)$ . Final LG-PHD formulae are nearly identical to GM-PHD, except for Jacobian matrices.

### A. Experiments

In order to validate the performance of the proposed LG-PHD filter, and compare different reduction approaches that are applied after update steps, we devised appropriate Monte Carlo simulation scenarios. We applied two component picking strategies, namely West's algorithm and the pairwise component picking algorithm. For each, we applied the reparameterization approaches as discussed in Section III-B, including the mapping to tangent space of (i) pairwise larger component  $\mathcal{T}_L$ , (ii) pairwise smaller component  $\mathcal{T}_S$ , (iii) identity element  $\mathcal{T}_{Id}$ , (iv) largest component  $\mathcal{T}_{Max}$ , and (v) smallest component  $\mathcal{T}_{Min}$  (West's algorithm always merges the smallest component; hence, (ii) and (v) are the same). We generated 100 examples of an MTT scenario and compared the performance of the approaches. The initial number of targets in the scene was a random integer  $N_{0|0} \in [5, 7]$ , while the probability of survival was  $p_S = 0.975$  and birth rate was  $\lambda_b = 0.25$ . All measurements were corrupted with white noise variance  $\sigma_{xy}^2 = 0.5^2 \text{ m}^2$  in distance and  $\sigma_\phi = 0.1 \text{ rad/s}$  in orientation, while clutter was governed by the Poisson distribution with intensity  $\lambda_Z = 5$ . The state  $X = (X^{\text{pos}}, X^{\text{vel}}) \in SE(2) \times \mathbb{R}^3$  contains position and velocity components. Here, we apply the constant velocity motion model [31] given as

$$f(X_{k-1}) = X_{k-1} \exp_G^\wedge \begin{bmatrix} T X_{k-1}^{\text{vel}} \\ \mathbf{0} \end{bmatrix}. \quad (21)$$

We derive the pertaining Jacobian

$$\begin{aligned} F_{k-1} &= -\frac{d}{ds} \left( \log_G^\vee \left( f(\mu_{k-1}) f(\exp_G^\wedge(s) \mu_{k-1})^{-1} \right) \right) \Big|_{s=0} \\ &= \begin{bmatrix} \mathbf{I} & T \Phi_{SE(2)} \left( T \text{Ad}_{SE(2)} (\mu_{k-1}^{\text{pos}}) \mu_{k-1}^{\text{vel}} \right) \text{Ad}_{SE(2)} (\mu_{k-1}^{\text{pos}}) \\ \mathbf{0} & \mathbf{I} \end{bmatrix} \end{aligned} \quad (22)$$

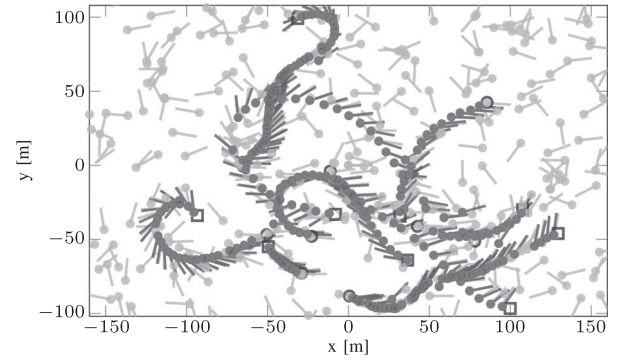


Fig. 2. Example of a multitarget tracking scenario, involving 10 objects, out of which 5 appeared at the beginning, and 5 more were born during the 100 steps long sequence (gray arrows—measurements including false alarms, black arrows—estimated states, black circles—true object birth place, black square—true object death place).

TABLE I  
AVERAGE OSPA OVER 100 MULTITARGET SCENARIOS (BOLDED NUMBERS REPRESENT THE SMALLEST ERROR)

	Exhaustive pairwise					West			
	$\mathcal{T}_L$	$\mathcal{T}_S$	$\mathcal{T}_{Id}$	$\mathcal{T}_{Max}$	$\mathcal{T}_{Min}$	$\mathcal{T}_L$	$\mathcal{T}_S$	$\mathcal{T}_{Id}$	$\mathcal{T}_{Max}$
$\mathcal{D}_t$	<b>2.445</b>	2.515	2.764	2.912	3.082	<b>1.910</b>	1.924	2.060	2.125
$\mathcal{D}_d$	<b>2.100</b>	2.163	2.419	2.558	2.695	<b>1.415</b>	1.420	1.537	1.605
$\mathcal{D}_c$	<b>0.594</b>	0.613	0.627	0.653	0.745	<b>0.737</b>	0.746	0.797	0.792

Boldd numbers represent the smallest error.

where  $\mu_{k-1} = (\mu_{k-1}^{\text{pos}}, \mu_{k-1}^{\text{vel}}) \in SE(2) \times \mathbb{R}^3$  is the mean value, and  $T$  is discretization time. The probability of measurement detection was  $p_D = 0.975$  and the measurements were arising as  $SE(2)$ ; hence,  $h(X_k) = X_k^{\text{pos}}$  and the measurement Jacobian was  $H_k = [\mathbf{I} \ \mathbf{0}]$ . For illustration purposes, an example of a multitarget scenario with tracking in total 10 targets on  $SE(2)$  is given in Fig. 2 together with LG-PHD results.

As a performance metric, we used the optimal subpattern assignment (OSPA) metric [32]. In Table I, we present the results where for each of the 100 multitarget trajectories the cumulative OSPA  $\mathcal{D}_t$ , and its localization component  $\mathcal{D}_d$  and cardinality component  $\mathcal{D}_c$  were calculated.

For both Exhaustive pairwise and West's picking strategies, relying on mapping to the tangent space of pairwise larger components  $\mathcal{T}_L$  generally outperformed the other approaches.

### V. CONCLUSION

In this letter, we have studied the problem of mixture reduction on matrix Lie groups. We have particularly dealt with the manipulation of CGD components to compute the KL divergence, pick and merge the mixture components. As a study example, we implemented the LG-PHD filter, a mixture approximation of the PHD filter tailored for MTT with states evolving on matrix Lie groups. Using the OSPA metric, we analyzed the performance of the LG-PHD filter with respect to mixture component number reduction.

### REFERENCES

- [1] D. Alspach and H. Sorenson, "Nonlinear Bayesian estimation using Gaussian sum approximations," *IEEE Trans. Autom. Control*, vol. 17, no. 4, pp. 439–448, Aug. 1972.

- [2] R. Chen and J. S. Liu, "Mixture Kalman filters," *J. Roy. Statist. Soc.: Series B (Statist. Methodol.)*, vol. 62, no. 3, pp. 493–508, 2000.
- [3] S. S. Blackman, *Multiple-Target Tracking with Radar Applications*. Norwood, MA, USA: Artech House, 1986.
- [4] C. Stauffer and W. E. L. Grimson, "Learning patterns of activity using real-time tracking," *IEEE Trans. Pattern Anal. Mach. Intell.*, vol. 22, no. 8, pp. 747–757, Aug. 2000.
- [5] J. Goldberger and H. Aronowitz, "A distance measure between GMMs based on the unscented transform and its application to speaker recognition," in *Proc. Interspeech*, 2005, pp. 1985–1989.
- [6] A. Nikseresht and M. Gelgon, "Gossip-based computation of a gaussian mixture model for distributed multimedia indexing," *IEEE Trans. Multimedia*, vol. 10, no. 3, pp. 385–392, Apr. 2008.
- [7] D. Salmond, "Mixture reduction algorithms for target tracking," in *Proc. IEEE Colloq. State Estimation Aerosp. State Estimation*, 1989, pp. 1–4.
- [8] A. Runnalls, "Kullback-Leibler approach to Gaussian mixture reduction," *IEEE Trans. Aerosp. Electron. Syst.*, vol. 43, no. 3, pp. 989–999, Jul. 2007.
- [9] M. Bukal, I. Marković, and I. Petrović, "Composite distance based approach to von Mises mixture reduction," *Inf. Fusion*, vol. 20, no. 1, pp. 136–145, 2014.
- [10] B.-N. Vo and W.-K. Ma, "The Gaussian mixture probability hypothesis density filter," *IEEE Trans. Signal Process.*, vol. 54, no. 11, pp. 4091–4104, Nov. 2006.
- [11] B.-T. Vo, B.-N. Vo, and A. Cantoni, "Analytic implementations of the cardinalized probability hypothesis density filter," *IEEE Trans. Signal Process.*, vol. 55, no. 7, pp. 3553–3567, Jul. 2007.
- [12] Y. M. Lui, "Advances in matrix manifolds for computer vision," *Image Vis. Comput.*, vol. 30, no. 6/7, pp. 380–388, 2012.
- [13] G. Loianno, M. Watterson, and V. Kumar, "Visual inertial odometry for quadrotors on SE(3)," in *Proc. IEEE Int. Conf. Robot. Autom.*, 2016, pp. 1544–1551.
- [14] J. Česić, V. Joukov, I. Petrović, and D. Kulić, "Full body human motion estimation on Lie groups using 3D marker position measurements," in *Proc. IEEE-RAS Int. Conf. Humanoid Robots*, 2016, pp. 826–833.
- [15] A. Barrau and S. Bonnabel, "Intrinsic filtering on Lie groups with applications to attitude estimation," *IEEE Trans. Autom. Control*, vol. 60, no. 2, pp. 436–449, Feb. 2015.
- [16] A. W. Long, K. C. Wolfe, M. J. Mashner, and G. S. Chirikjian, "The banana distribution is Gaussian: A localization study with exponential coordinates," in *Proc. Robot.: Sci. Syst.*, Sydney, Australia, 2012.
- [17] T. D. Barfoot and P. T. Furgale, "Associating uncertainty with three-dimensional poses for use in estimation problems," *IEEE Trans. Robot.*, vol. 30, no. 3, pp. 679–693, Jun. 2014.
- [18] C. Zhang, A. Taghvaei, and P. G. Mehta, "Feedback particle filter on matrix Lie groups," in *Proc. Am. Control Conf.*, 2016, pp. 2723–2728.
- [19] G. Bourmaud, R. Mégret, A. Giremus, and Y. Berthoumieu, "Discrete extended Kalman filter on Lie groups," in *Proc. Eur. Signal Process. Conf.*, 2013, pp. 1–5.
- [20] G. Bourmaud, R. Mégret, M. Arnaudon, and A. Giremus, "Continuous-discrete extended Kalman filter on matrix Lie groups using concentrated Gaussian distributions," *J. Math. Imaging Vis.*, vol. 51, no. 1, pp. 209–228, 2015.
- [21] K. C. Wolfe, M. Mashner, and G. S. Chirikjian, "Bayesian fusion on Lie groups," *J. Algebr. Statist.*, vol. 2, no. 1, pp. 75–97, 2011.
- [22] G. S. Chirikjian, *Stochastic Models, Information Theory, and Lie Groups*. Basel, Switzerland: Birkhäuser, 2012, vol. 2.
- [23] G. Bourmaud, R. Mégret, A. Giremus, and Y. Berthoumieu, "From intrinsic optimization to iterated extended Kalman filtering on Lie groups," *J. Math. Imaging Vis.*, vol. 55, no. 3, pp. 284–303, 2016.
- [24] G. Bourmaud, "Estimation de paramètres évoluant sur des groupes de Lie: Application à la cartographie et à la localisation d'une caméra monoculaire," Ph.D. dissertation, Univ. Bordeaux, Bordeaux, France, 2015.
- [25] W. Miller, *Symmetry Groups and Their Applications*. New York, NY, USA: Academic, 1972.
- [26] S. Kullback, *Information Theory and Statistics*. New York, NY, USA: Dover, 1997.
- [27] S. Amari, "Alpha-divergence is unique, belonging to both f-divergence and Bregman divergence classes," *IEEE Trans. Inf. Theory*, vol. 55, no. 11, pp. 4925–4931, Nov. 2009.
- [28] D. J. Salmond, "Mixture reduction algorithms for point and extended object tracking in clutter," *IEEE Trans. Aerosp. Electron. Syst.*, vol. 45, no. 2, pp. 667–686, Apr. 2009.
- [29] M. West, "Approximating posterior distributions by mixtures," *J. Royal Statist. Soc., Series B*, vol. 55, no. 2, pp. 409–442, 1993.
- [30] I. Marković, J. Česić, and I. Petrović, "Von Mises Mixture PHD Filter," *IEEE Signal Process. Lett.*, vol. 20, no. 12, pp. 2229–2233, Dec. 2015.
- [31] J. Česić, I. Marković, and I. Petrović, "Moving object tracking employing rigid body motion on matrix Lie groups," in *Proc. Int. Conf. Inf. Fusion*, 2016, p. 7.
- [32] D. Schuhmacher, B. T. Vo, and B. N. Vo, "A consistent metric for performance evaluation of multi-object filters," *IEEE Trans. Signal Process.*, vol. 56, pp. 3447–3457, Aug. 2008.

**PUBLICATION 8 - SUPPLEMENTARY MATERIAL**

J. Ćesić, I. Marković, and I. Petrović. Supplementary material to Mixture Reduction on Matrix Lie Groups. *IEEE Signal Processing Letters*, 24(11):1719–1723, 2017.



# Supplementary material to Mixture Reduction on Matrix Lie Groups

Josip Česić, Ivan Marković, and Ivan Petrović,\*

## I. THE EXTENDED KALMAN FILTER ON LIE GROUPS

In the letter entitled *Mixture Reduction on Matrix Lie Groups*, we have used the definition of a concentrated Gaussian distribution (CGD) [1] with mean  $\mu$  and covariance  $P$  similarly as is presented in [2]

$$X = \exp_G^\wedge(\epsilon)\mu, \quad X \sim \mathcal{G}(\mu, P), \quad (1)$$

where  $\epsilon \sim \mathcal{N}_{\mathbb{R}^p}(\mathbf{0}^p, P)$  is a zero-mean Gaussian distribution with covariance  $P \subset \mathbb{R}^{p \times p}$  defined in the Lie algebra, i.e., the Euclidean space  $\mathbb{R}^p$ .

When it comes to general Bayes filter, the estimation usually consists of the prediction step governed by the following integral

$$P(X_k|Z_{1:k-1}) = \int p(X_k|X_{k-1})p(X_{k-1}|Z_{1:k-1})dX_{k-1}, \quad (2)$$

where  $p(X_{k-1}|Z_{1:k-1})$  is the posterior at  $k-1$  and  $p(X_k|X_{k-1})$  is the transition density. The correction step is the solution to the Bayes rule and the posterior at  $k$  is obtained as

$$p(X_k|Z_{1:k}) = \frac{p(Z_k|X_k)p(X_k|Z_{1:k-1})}{\int p(Z_k|X_k)p(X_k|Z_{1:k-1})dX_k}, \quad (3)$$

where  $p(Z_k|X_k)$  is the measurement likelihood.

The LG-EKF used in the letter follows the convention presented in [2], but without the iterated part, as used in [3]. By assuming that the distributions in (2) follow the CGD assumption and the following motion model

$$X_k = \exp_G^\wedge(w_k)f(X_{k-1}), \quad w_k \sim \mathcal{N}_{\mathbb{R}^p}(\mathbf{0}^p, Q_k), \quad (4)$$

i.e.,  $p(X_k|X_{k-1}) = \mathcal{G}(X_k; f(\mu_{k-1}), Q_k)$  and  $p(X_{k-1}|Z_{1:k-1}) = \mathcal{G}(X_{k-1}; \mu_{k-1}, P_{k-1})$ , the prediction step in [2] was solved by approximating the integrand in (2) with a joint distribution  $p(X_k, X_{k-1}|Z_{1:k-1})$  by way of Gauss-Newton minimization in  $\mu_{k-1}$  and  $f(\mu_{k-1})$ . The resulting covariance had the following form

$$P = \begin{bmatrix} F_k P_{k-1} F_k^T + Q_k & F_k P_{k-1} \\ P_{k-1} F_k^T & P_{k-1} \end{bmatrix}, \quad F_k = - \left. \frac{d \log_G^\vee(f(\mu_{k-1})f(\exp_G^\wedge(s)\mu_{k-1})^{-1})}{ds} \right|_{s=0}. \quad (5)$$

To obtain  $p(X_k|Z_{1:k-1})$ , the augmented CGD was marginalized yielding formula for the covariance prediction  $P_{k|k-1} = F_k P_{k-1} F_k^T + Q_k$ , while the mean is predicted applying the propagation function, hence  $\mu_{k|k-1} = f(\mu_{k-1})$ .

By assuming that the measurement likelihood followed the CGD assumption and the measurement model

$$Z_k = \exp_G^\wedge(v_k)h(X_k), \quad v_k \sim \mathcal{N}_{\mathbb{R}^p}(\mathbf{0}^p, R_k), \quad (6)$$

i.e.,  $p(Z_k|X_k) = \mathcal{G}(Z_k; h(X_k), R_k)$ , the correction step was solved in [2] by approximating the numerator in (3) up to a proportion with a single CGD which yields parameters for  $p(X_k|Z_{1:k})$  by using an iterated Gauss-Newton method. This is correct since the denominator in (3) assures proper scaling of the distribution and would cancel any scaling parameter. However, in this letter we are not using the iterated version, but the extended one as in [3], hence the update step of the LG-EKF has the following formulae

$$\begin{aligned} H_k &= - \left. \frac{d \log_G^\vee(Z_k h(\exp_G^\wedge(s)\mu_{k|k-1})^{-1})}{ds} \right|_{s=0} \\ K_k &= P_{k|k-1} H_k^T (H_k P_{k|k-1} H_k^T + R_k)^{-1} \\ m_k &= K \log_G^\vee(Z_k h(\mu_{k|k-1})^{-1}) \\ \mu_k &= \exp_G^\wedge(m_k)\mu_{k|k-1} \\ P_k &= \Phi_G(m_k)(I - K_k H_k)P_{k|k-1}\Phi_G(m_k). \end{aligned} \quad (7)$$

\* Authors are with the University of Zagreb, Faculty of Electrical Engineering and Computing, Department of Control and Computer Engineering, Unska 3, 10000 Zagreb, Croatia. E-mail: {name.surname@fer.hr}

## II. THE CGD MIXTURE PHD FILTER ON LIE GROUPS

As elaborated in the letter, the prediction step of the Gaussian mixture PHD filter evaluates to solving (2) on a mixture component basis. Therefore, if we are working with a CGD mixture, as in the case of the CGD mixture PHD filter on Lie groups (LG-PHD), given the result from [2] we can assert that (5) can equally be applied to LG-PHD prediction. However, the update step of the PHD filter requires direct evaluation of the product  $p(Z_k|X_k)P(X_k|Z_{1:k-1})$ , as well as the integral thereof. We propose to follow the same train of thought as in [4] and evaluate first the joint distribution  $p(Z_k, X_k|Z_{1:k-1})$ , which can be obtained by using the same procedure as for  $p(X_k, X_{k-1}|Z_{1:k-1})$  in the prediction step given in previous section. In other words, by augmenting  $p(X_k|Z_{1:k-1})$  with  $Z_k$  and linearizing in  $\mu_{k|k-1}$  and  $h(\mu_{k|k-1})$ , the joint distribution will have the following parameters

$$\mu = \begin{bmatrix} \log_G^\vee(Z_k h(\mu_{k|k-1})^{-1}) & \log_G^\vee(X_k \mu_{k|k-1}^{-1}) \end{bmatrix} \quad (8)$$

$$P = \begin{bmatrix} H_k P_{k|k-1} H_k^T + R_k & H_k P_{k|k-1} \\ P_{k|k-1} H_k^T & P_{k|k-1} \end{bmatrix} = \begin{bmatrix} P_{11} & P_{12} \\ P_{21} & P_{22} \end{bmatrix}, \quad (9)$$

where  $H_k$  is given in (7). Note that for the clarity we have denoted that both means belong to the same group  $G$ , which is, however, not a requirement.

In [4] it was shown that under the CGD assumption a distribution with parameters as in (8) can be factorized to the following product of two distributions

$$p(Z_k, X_k|Z_{1:k-1}) = \mathcal{N}_G(Z_k; h(\mu_{k|k-1}), P_{11}) \mathcal{N}_G^*(X_k; \exp_G^\wedge(P_{12}^T P_{11}^{-1} \log_G^\vee(Z_k h(\mu_{k|k-1})^{-1})) \mu_{k|k-1}, P_{22} - P_{12}^T P_{11}^{-1} P_{12}). \quad (10)$$

If we insert for  $P_{11}$ ,  $P_{12}$  and  $P_{22}$  corresponding values we obtain the following

$$\begin{aligned} \exp_G^\wedge(P_{12}^T P_{11}^{-1} \log_G^\vee(Z_k h(\mu_{k|k-1})^{-1})) \mu_{k|k-1} \\ = \exp_G^\wedge(P_{k|k-1} H_k^T (H_k P_{k|k-1} H_k^T + R_k)^{-1} \log_G^\vee(Z_k h(\mu_{k|k-1})^{-1})) \mu_{k|k-1} \\ = \exp_G^\wedge(K_k \log_G^\vee(Z_k h(\mu_{k|k-1})^{-1})) \mu_{k|k-1} = \exp_G^\wedge(m_k) \mu_{k|k-1} \end{aligned} \quad (11)$$

$$\begin{aligned} P_{22} - P_{12}^T P_{11}^{-1} P_{12} &= P_{k|k-1} - P_{k|k-1} H_k^T (H_k P_{k|k-1} H_k^T + R_k)^{-1} H_k P_{k|k-1} \\ &= P_{k|k-1} - K_k H_k P_{k|k-1} = (I - K_k H_k) P_{k|k-1}. \end{aligned}$$

By inspecting (10) and (11) we can notice that for the second factor (denoted by  $\mathcal{N}_G^*$ ) the covariance is defined in the algebra of the prediction  $\mu_{k|k-1}$ , while we need it to be defined in the algebra associated to  $\mu_k$ , i.e., after the correction step we expect to have  $X_k = \exp_G^\wedge(\epsilon_k) \mu_k$ , where  $\mathbb{E}[\epsilon_k] = 0$  [5]. For this reason we need to additionally reparametrize the covariance as follows

$$\mu_k = \exp_G^\wedge(m_k) \mu_{k|k-1} \quad (12)$$

$$P_k = \Phi_G(m_k) (I - K_k H_k) P_{k|k-1} \Phi_G(m_k)^T, \quad (13)$$

thus (10) factorizes as follows:

$$\begin{aligned} p(Z_k, X_k|Z_{1:k-1}) &= \mathcal{N}_G(Z_k; h(\mu_{k|k-1}), H_k P_{k|k-1} H_k^T + R_k) \mathcal{N}_G(X_k; \mu_k, P_k) \\ &= \mathcal{N}_G(Z_k; h(\mu_{k|k-1}), S_k) \mathcal{N}_G(X_k; \mu_k, P_k). \end{aligned} \quad (14)$$

If group  $G$  would be Euclidean space then (14) would yield the same results as was obtained for the Gaussian mixture PHD [6]. In order to complete the update step of the PHD filter, we also need to compute the integral  $\int_{\mathcal{X}} p(Z_k | X_k) p(X_k | Z_{1:k-1}) dX_k$ , which similarly to the LG-EKF prediction step [3] yields  $\mathcal{N}_G(Z_k; h(\mu_{k|k-1}), S_k)$ . Note that in this supplementary material, we have omitted discussion on the choice of the integration measure and for more formal elaboration the interested reader is directed to [3]. Furthermore, note that with the previous reasoning we have also demonstrated how LG-EKF can be seen as a Bayes filter on Lie groups.

Now we have all the means for performing the two successive steps of the LG-PHD filter for the application described in the letter. The pseudocode for the prediction step is given in Alg. 1, where the  $\text{PRED}_G(\cdot)$  function follows the equations given for determining  $p(X_k|Z_{1:k-1})$  as

- $\text{PRED}_G(\cdot)$  - using  $P_{k|k-1} = F_k P_{k-1} F_k^T + Q_k$  and  $\mu_{k|k-1} = f(\mu_{k-1})$ .

---

**Algorithm 1** The prediction step of the LG-PHD filter
 

---

**Require:**  $\{w_{k-1}^i, \mathcal{G}_{k-1}^i\}_{i=1}^{J_{k-1}}, \{w_k^{b,i}, \mathcal{G}_k^{b,i}\}_{i=1}^{J_k^b}, p_S$

```

1:  $j \leftarrow 0$  (initialization)
2: for  $i := 1$  to  $J_k^b$  (# of newly born components) do
3:    $w_{k|k-1}^j \leftarrow w_k^{b,i}; \mathcal{G}_{k|k-1}^j \leftarrow \mathcal{G}_k^{b,i}; j \leftarrow j + 1$ 
4: end for
5: for  $i := 1$  to  $J_{k-1}$  (# of components existing at  $k-1$ ) do
6:    $w_{k|k-1}^j \leftarrow p_S w_{k-1}^i; \mathcal{G}_{k|k-1}^j \leftarrow \text{PRED}_G(\mathcal{G}_{k-1}^i); j \leftarrow j + 1$ 
7: end for
8:  $J_{k|k-1} \leftarrow j$  (# of predicted components)
9: return  $\{w_{k|k-1}^i, \mathcal{G}_{k|k-1}^i\}_{i=1}^{J_{k|k-1}}$ 

```

---

In the particular application presented in the letter, where we assume that the objects were following the constant velocity  $\text{SE}(2) \times \mathbb{R}^3$  motion model assumption [7], the motion model  $f(\mu_{k-1})$  and the Jacobian  $F$  are given as

$$\begin{aligned}
 f(\mu_{k-1}) &= \mu_{k-1} \exp_G^\wedge \begin{bmatrix} T v_{k-1} \\ \mathbf{0} \end{bmatrix}, \\
 F &= -\frac{d}{ds} \left( \log_G^\vee \left( f(\mu_{k-1}) f(\exp_G^\wedge(s) \mu_{k-1})^{-1} \right) \right) \Big|_{s=0} \\
 &= -\frac{d}{ds} \left( \log_G^\vee \left( \mu_{k-1} \exp_G^\wedge \begin{bmatrix} T v_{k-1} \\ \mathbf{0} \end{bmatrix} \left( \exp_G^\wedge(s) \mu_{k-1} \exp_G^\wedge \begin{bmatrix} T(s^{\text{vel}} + v_{k-1}) \\ \mathbf{0} \end{bmatrix} \right)^{-1} \right) \right) \Big|_{s=0} \\
 &= -\frac{d}{ds} \left( \log_G^\vee \left( \mu_{k-1} \exp_G^\wedge \begin{bmatrix} T v_{k-1} \\ \mathbf{0} \end{bmatrix} \exp_G^\wedge \begin{bmatrix} T(s^{\text{vel}} + v_{k-1}) \\ \mathbf{0} \end{bmatrix}^{-1} \mu_{k-1}^{-1} \exp_G^\wedge(s)^{-1} \right) \right) \Big|_{s=0} \\
 &= -\frac{d}{ds} \left( \log_G^\vee \left( \exp_G^\wedge \left( \text{Ad}_G(\mu_{k-1}) \begin{bmatrix} T v_{k-1} \\ \mathbf{0} \end{bmatrix} \right) \mu_{k-1}^{-1} \exp_G^\wedge \left( \text{Ad}_G(\mu_{k-1}) \begin{bmatrix} T(s^{\text{vel}} + v_{k-1}) \\ \mathbf{0} \end{bmatrix} \right)^{-1} \exp_G^\wedge(s)^{-1} \right) \right) \Big|_{s=0} \\
 &\approx -\frac{d}{ds} \left( \log_G^\vee \left( \exp_G^\wedge \left( \Phi_G \left( \text{Ad}_G(\mu_{k-1}) \begin{bmatrix} T v_{k-1} \\ \mathbf{0} \end{bmatrix} \right) \text{Ad}_G(\mu_{k-1}) \begin{bmatrix} -T s^{\text{vel}} \\ \mathbf{0} \end{bmatrix} \right) \exp_G^\wedge(s)^{-1} \right) \right) \Big|_{s=0} \\
 &\approx -\frac{d}{ds} \left( \Phi_G \left( \text{Ad}_G(\mu_{k-1}) \begin{bmatrix} T v_{k-1} \\ \mathbf{0} \end{bmatrix} \right) \text{Ad}_G(\mu_{k-1}) \begin{bmatrix} -T s^{\text{vel}} \\ \mathbf{0} \end{bmatrix} - s \right) \Big|_{s=0} \\
 &= \begin{bmatrix} \mathbf{I} & T \Phi_{\text{SE}(2)} \left( T \text{Ad}_{\text{SE}(2)}(\mu_{k-1}^{\text{pos}}) v_{k-1} \right) \text{Ad}_{\text{SE}(2)}(\mu_{k-1}^{\text{pos}}) \\ \mathbf{0} & \mathbf{I} \end{bmatrix},
 \end{aligned} \tag{16}$$

where  $\mu_{k-1}$  consists of positional and velocity part constructed by placing the  $\text{SE}(2)$  and  $\mathbb{R}^3$  components block-diagonally, such that  $\mu_{k-1} = \text{blkdiag}(\mu_{k-1}^{\text{pos}}, \mu_{k-1}^{\text{vel}})$ ,  $v_{k-1} = \log_{\mathbb{R}^3}^\vee(\mu_{k-1}^{\text{vel}})$ , and accordingly  $s = [s^{\text{pos}} \ s^{\text{vel}}]^T$  and  $\text{Ad}_G(\mu) = \text{blkdiag}(\text{Ad}_{\text{SE}(2)}(\mu^{\text{pos}}), \text{Ad}_{\mathbb{R}^3}(\mu^{\text{vel}}))$ . The parameter  $T$  represents the discretization time. To obtain the second-to-last step, the following Baker-Campbell-Hausdorff formula was used

$$\log_G^\vee(\exp^\wedge(-x) \exp^\wedge(x+y)) = \Phi_G(-x)y + O(\|y\|^2). \tag{17}$$

The pseudocode for the update step is given in Alg. 2. The algorithm employs several outlying functions including:

- $\text{INNOV}_{G'}(\cdot, \cdot)$  - using  $\nu_k^{i,j} = \left[ \log_{G'} \left( Z_k^j h(\mu_{k|k-1}^i)^{-1} \right) \right]_{G'}^\vee$ ,  $S_k^{i,j} = H_k^{i,j} P_{k|k-1}^{i,j} H_k^{i,jT} + R_k$ ,
- $\text{CORRECT}_{\mathbb{R}}(\cdot, \cdot)$  - using  $w_k^{i,j} = \frac{p_D w_{k|k-1}^i q_k^{i,j}(Z)}{\lambda_{ZC}(Z) + p_D \sum_{l=1}^{J_{k|k-1}} w_{k|k-1}^l q_k^{l,j}(Z)}$ , where  $q_k^{i,j}(Z) = \mathcal{N}(Z_k^j, h(\mu_{k|k-1}^i), S_k^{i,j})$ ,
- $\text{REPARAM}_G(\cdot, \cdot)$  - using (12) and (13),
- $\text{REDUCTION}_G(\cdot)$  - employing reduction schemes as described in the letter.

For the multitarget tracking application given in the letter, since the measurement arises as a  $\text{SE}(2)$  member, i.e.,  $h(X_k) = X_k$  and the measurement Jacobian  $H_k$  evaluates to  $H_k = [\mathbf{I} \ \mathbf{0}]$ .

---

**Algorithm 2** The correction step of the LG-PHD filter
 

---

**Require:**  $\{w_{k|k-1}^i, \mathcal{G}_{k|k-1}^i\}_{i=1}^{J_{k|k-1}}, \{Z_k^j \in \mathcal{Z}_k\}_{j=1}^{M_k}, p_D$

- 1: **for**  $i := 1$  to  $J_{k|k-1}$  (*non-detected components*) **do**
- 2:    $w_k^i \leftarrow (1 - p_D) w_{k|k-1}^i$ ;  $\mathcal{G}_k^i \leftarrow \mathcal{G}_{k|k-1}^i$
- 3: **end for**
- 4:  $j \leftarrow 0$  (*measurement designator*)
- 5: **for all**  $Z_k \in \mathcal{Z}_k$  **do**
- 6:    $j \leftarrow j + 1, s^j \leftarrow 0$  (*per measurement intensity*)
- 7:   **for**  $i := 1$  to  $J_{k|k-1}$  (*detected components*) **do**
- 8:      $l \leftarrow i + j J_{k|k-1}$
- 9:      $[\nu_k^{i,j}, \mathcal{S}_k^{i,j}] \leftarrow \text{INNOV}_{G'}(\mathcal{G}_{k|k-1}^i, Z_k^j)$
- 10:      $w_k^l \leftarrow p_D w_{k|k-1}^i \mathcal{N}(\nu_k^{i,j}; \mathbf{0}, \mathcal{S}_k^{i,j}), s^j \leftarrow s^j + w_k^l$
- 11:      $\mathcal{N}_k^{l-} \leftarrow \text{CORRECT}_{\mathbb{R}}(\mathcal{G}_{k|k-1}^i, Z_k^j)$
- 12:      $\mathcal{G}_k^l \leftarrow \text{REPARAM}_G(\mathcal{G}_{k|k-1}^i, \mathcal{N}_k^{l-})$
- 13:   **end for**
- 14:   **for**  $i := 1$  to  $J_{k|k-1}$  (*re-weighting*) **do**
- 15:      $w_k^{i+j J_{k|k-1}} \leftarrow w_k^{i+j J_{k|k-1}} / (\lambda_{ZC}(Z) + s^j)$
- 16:   **end for**
- 17: **end for**
- 18:  $J_k \leftarrow (j + 1) J_{k|k-1}$  (*# of components existing at k*)
- 19:  $\{w_k^{i,R}, \mathcal{G}_k^{i,R}\}_{i=1}^{J_k^R} \leftarrow \text{REDUCTION}_G(\{w_k^i, \mathcal{G}_k^i\}_{i=1}^{J_k})$
- 20: **return**  $\{w_{k+1}^{i,R}, \mathcal{G}_{k+1}^{i,R}\}_{i=1}^{J_{k+1}^R}$

---

## REFERENCES

- [1] K. C. Wolfe, M. Mashner, and G. S. Chirikjian, “Bayesian Fusion on Lie Groups,” *Journal of Algebraic Statistics*, vol. 2, no. 1, pp. 75–97, 2011.
- [2] G. Bourmaud, R. Megret, A. Giremus, and Y. Berthoumieu, “From Intrinsic Optimization to Iterated Extended Kalman Filtering on Lie Groups,” *Journal of Mathematical Imaging and Vision*, vol. 55, no. 3, pp. 284–303, 2016.
- [3] G. Bourmaud and A. Giremus, “Robust Wearable Camera Localization as a Target Tracking Problem on  $\text{SE}(3)$ ,” in *British Machine Vision Conference*, 2015, pp. 39.1–39.12.
- [4] G. Bourmaud, R. M  gret, M. Arnaudon, and A. Giremus, “Continuous-Discrete Extended Kalman Filter on Matrix Lie Groups Using Concentrated Gaussian Distributions,” *Journal of Mathematical Imaging and Vision*, vol. 51, no. 1, pp. 209–228, 2015.
- [5] G. Bourmaud, R. M  gret, A. Giremus, and Y. Berthoumieu, “Discrete Extended Kalman Filter on Lie Groups,” in *European Signal Processing Conference (EUSIPCO)*, 2013, pp. 1–5.
- [6] B.-N. Vo and W.-K. Ma, “The Gaussian mixture probability hypothesis density filter,” *IEEE Transactions on Signal Processing*, vol. 54, no. 11, pp. 4091–4104, 2006.
- [7] J.   esi  , I. Markovi  , and I. Petrovi  , “Moving object tracking employing rigid body motion on matrix Lie groups,” in *19th International Conference on Information Fusion (FUSION), Special Session on Directional Estimation*, 2016, p. 7.

---

## CURRICULUM VITAE

JOSIP ĆESIĆ was born in Zagreb, Croatia in 1989. He finished XV Gymnasium (MIOC) in Zagreb in 2008 and received his BSc and MSc degree (Magna Cum Laude) in electrical engineering and information technology from the University of Zagreb, Faculty of Electrical Engineering and Computing (UNIZG-FER) in 2011 and 2013, respectively. He finished the third semester of his master program at Chalmers University of Technology, Sweden, as an exchange student.

During the undergraduate studies he received Dean's Award Josip Lončar and Special Dean's Award Josip Lončar for outstanding achievements on the first year of studies and the overall BSc level, respectively. During the graduate studies he received Rector's Award and Special Rector's Award for practical applications in the fields of robotics and control systems. He was also awarded with scholarships from the Croatian Ministry of Science (2008-2009), Scholarship of the University of Zagreb (2009-2010) and Scholarship of the City of Zagreb (2010-2013).

He is employed as a research assistant at the Department of Control and Computer Engineering at FER Zagreb since April 2013. Since then, he was actively participating in several international scientific projects, i.e., Computer Vision Innovations for Safe Traffic (VISTA), Advanced Technologies in Power Plants and Rail Vehicles (FER-KIET) and Cooperative cloud based simultaneous localization and mapping in dynamic environments (cloudSLAM). His main research interests are in the areas of autonomous systems and mobile robotics, estimation theory and sensor processing, particularly employing radar, lidar and stereo systems. He is an author or co-author of a book chapter, 7 papers published in peer-reviewed journals and 13 papers presented at international conferences. The full list of publications is given below.

## FULL LIST OF PUBLICATIONS

### BOOK CHAPTERS:

1. J. Ćesić, I. Marković, S. Jurić-Kavelj and I. Petrović. Short-Term Map Based Detection and Tracking of Moving Objects with 3D Laser on a Vehicle. *Informatics in Control, Automation and Robotics*, Lecture Notes in Electrical Engineering, Vol. 370, Joaquim Filipe, Oleg Gusikhin, Kurosh Madani, Jurek Sasiadek (ed.), Cham, Switzerland : Springer International Publishing, 205–222, 2016.

### JOURNAL PUBLICATIONS:

1. J. Ćesić, I. Marković and I. Petrović. Mixture Reduction on Matrix Lie Groups. *IEEE Signal Processing Letters*, 24(11):1719–1723, 2017, IF: 2.528 (Q2).
2. I. Cvišić, J. Ćesić, I. Marković and I. Petrović. SOFT-SLAM: Computationally Efficient Stereo Visual SLAM for Autonomous UAVs. *Journal of Field Robotics*, (accepted for publication), DOI: 10.1002/rob.21762, 2017, IF: 4.882 (Q1).
3. J. Ćesić, I. Marković, M. Bukal and I. Petrović. Extended Information Filter on Matrix Lie Groups. *Automatica*, 53(9):226–234, 2017, IF: 5.451 (Q1).
4. I. Marković, M. Bukal, J. Ćesić and I. Petrović. Multitarget tracking with the von Mises-Fisher filter and probabilistic data association. *Journal of Advances in Information Fusion*, (accepted for publication) 2017.
5. J. Ćesić, I. Marković, I. Cvišić and I. Petrović. Radar and stereo vision fusion for multitarget tracking on the special Euclidean group. *Robotics and autonomous systems*, 83:338–348, 2016, IF: 1.950 (Q2).
6. I. Marković, J. Ćesić and I. Petrović. Von Mises Mixture PHD Filter. *IEEE Signal Processing Letters*, 22(12):2229–2233, 2015, IF: 1.661 (Q2).
7. M. Orsag, J. Ćesić, T. Haus and S. Bogdan. Spincopter Wing Design and Flight Control. *Journal of intelligent & robotic systems*, 70(1/4):165–179, 2013, IF: 0.932 (Q3).

### CONFERENCE PUBLICATIONS:

1. K. Lenac, J. Ćesić, I. Marković and I. Petrović. Cooperative Cloud SLAM on Matrix Lie Groups. *Third Iberian Robotics Conference (Robot2017)* Sevilla, Spain, (accepted for publication) 2017.
2. K. Lenac, J. Ćesić, I. Marković, I. Cvišić and I. Petrović. Revival of filtering based SLAM? Exactly sparse delayed state filter on Lie groups. *IEEE/RSJ International Conference on Intelligent Robots and Systems (IROS)* Vancouver, Canada, pages 1012–1018, 2017.

3. V. Joukov, J. Ćesić, K. Westermann, I. Marković, D. Kulić and I. Petrović. Human motion estimation on Lie groups using IMU measurements. *IEEE/RSJ International Conference on Intelligent Robots and Systems (IROS)* Vancouver, Canada, pages 1965–1972, 2017.
4. J. Ćesić, V. Joukov, I. Petrović and D. Kulić. Full Body Human Motion Estimation on Lie Groups Using 3D Marker Position Measurements. *IEEE-RAS International Conference on Humanoid Robotics (Humanoids2016)*. Cancun, Mexico, pages 826–833, 2016.
5. J. Ćesić, I. Marković and I. Petrović. Moving object tracking employing rigid body motion on matrix Lie groups. *International Conference on Information Fusion (FUSION), Special Session on Directional Estimation*. Heidelberg, Germany, pages 2109–2115, 2016.
6. I. Marković, J. Ćesić and I. Petrović. On wrapping the Kalman filter and estimating with the  $SO(2)$  group. *International Conference on Information Fusion (FUSION), Special Session on Directional Estimation*. Heidelberg, Germany, pages 2245–2250, 2016.
7. M. Obrvan, J. Ćesić and I. Petrović. Appearance based vehicle detection by radar-stereo vision integration. *Second Iberian Robotics Conference ((Robot2015))*. Lisbon, Portugal, pages 437–449, 2015.
8. B. Novoselnik, J. Ćesić, M. Baotić and I. Petrović. Nonlinear Model Predictive Control for Energy Efficient Housing with Modern Construction Materials. *IEEE Sensors Applications Symposium (SAS)*. Zadar, Croatia, pages 266–271, 2015.
9. I. Marković, M. Bukal, J. Ćesić and I. Petrović. Direction-only tracking of moving objects on the unit sphere via probabilistic data association. *International Conference on Information Fusion (FUSION), Special Session on Directional Estimation*. Salamanca, Spain, 2014.
10. J. Ćesić, I. Marković, S. Jurić-Kavelj and I. Petrović. Detection and tracking of dynamic objects using 3D laser range sensor on a mobile platform. *International Conference on Informatics in Control, Automation and Robotics (ICINCO)*. Wien, Austria, 2014.
11. J. Ćesić, I. Marković and I. Petrović. Tracking of multiple moving objects on the unit sphere using a multiple-camera system on a mobile robot. *International Conference on Intelligent Autonomous Systems (IAS)*. Padua, Italy, pages 899–911, 2014.
12. N. Skeledžija, J. Ćesić, E. Kočo, V. Bachler, H. N. Vučemilo and H. Džapo. Smart Home Automation System for Energy Efficient Housing. *International Convention on Information and Communication Technology, Electronics and Microelectronics (MIPRO2014)*. Opatija, Croatia, pages 166–171, 2014.
13. J. Ćesić, M. Orsag and S. Bogdan. Spincopter wing design and flight control. *International Conference on Unmanned Aircraft Systems (ICUAS12)*. Philadelphia, PA, USA, 2012.



---

## ŽIVOTOPIS

JOSIP ĆESIĆ rođen je u Zagrebu, Hrvatska, 1989. godine. Završio je XV. gimnaziju (MIOC) u Zagrebu 2008. godine, dok je zvanje prvostupnika, odnosno magistra elektrotehnike i informacijske tehnologije Sveučilišta u Zagrebu, Fakulteta elektrotehnike i računarstva (UNIZG-FER) uz visoke počasti (Magna Cum Laude) stekao 2011., odnosno 2013. godine. Treći semestar diplomskoga studija završio je na Tehničkom Sveučilištu Chalmers, Švedska, u sklopu studentske razmjene.

U sklopu preddiplomskoga studija dobitnik je Dekanove nagrade Josip Lončar i Posebne dekanove nagrade Josip Lončar za istaknuti uspjeh na prvoj godini studija, odnosno tijekom cjelokupnog preddiplomskoga studija. Tijekom diplomskoga studija dobio je Rektorovu nagradu te Posebnu Rektorovu nagradu za praktične primjene u području robotike i sustava upravljanja. Također je nagrađen Stipendijom Ministarstva znanosti i obrazovanja (2008.-2009.), Stipendijom Sveučilišta u Zagrebu (2009.-2010.) i Stipendijom Grada Zagreba (2010.-2013.).

Zaposlen je na mjestu asistenta na Zavodu za automatiku i računalno inženjerstvo na UNIZG-FER od travnja 2013. godine. Od tada je aktivno sudjelovao u nekoliko međunarodnih istraživačkih projekata, i.e., Inovativni sustavi računalnog vida za siguran promet (VISTA), Napredne tehnologije u elektroenergetskim postrojenjima i tračničkim vozilima (FER-KIET) te Kooperativno simultano lokaliziranje i kartiranje dinamičkog prostora zasnovano na uslugama u oblaku (cloudSLAM). Njegovi istraživački interesi uključuju autonomne sustave i mobilnu robotiku, teoriju estimacije, obradu senzora s naglaskom na radare, lidare i stereovizijske sustave. Autor je ili suautor poglavlja u knjizi, 7 znanstvenih radova u časopisima i 13 radova prezentiranih na međunarodnim konferencijama.

## COLOPHON

This document was typeset and inspired by the typographical look-and-feel classicthesis developed by André Miede, which was based on Robert Bringhurst's book on typography *The Elements of Typographic Style*, and by the FERElemental developed by Ivan Marković whose design was based on FERBook developed by Jadranko Matuško.